

**UNIVERSIDADE FEDERAL DO RIO GRANDE DO SUL
INSTITUTO DE GEOCIÊNCIAS
PROGRAMA DE PÓS-GRADUAÇÃO EM GEOCIÊNCIAS**

**ASSOCIAÇÃO DE LITOFAÇÕES, INTERAÇÃO LAVA-SEDIMENTO E
CARACTERIZAÇÃO SÍSMICA DO MAGMATISMO SERRA GERAL NA
REGIÃO DE UBERLÂNDIA E ARAGUARI (MG)**

NATÁLIA FAMELLI PEREIRA

ORIENTADOR: Prof. Dr. Evandro Fernandes de Lima

CO-ORIENTADOR: Dra. Isabela de Oliveira Carmo

Porto Alegre, 2020

**UNIVERSIDADE FEDERAL DO RIO GRANDE DO SUL
INSTITUTO DE GEOCIÊNCIAS
PROGRAMA DE PÓS-GRADUAÇÃO EM GEOCIÊNCIAS**

**ASSOCIAÇÃO DE LITOFAÇIES, INTERAÇÃO LAVA-SEDIMENTO E
CARACTERIZAÇÃO SÍSMICA DO MAGMATISMO SERRA GERAL NA
REGIÃO DE UBERLÂNDIA E ARAGUARI (MG)**

NATÁLIA FAMELLI PEREIRA

ORIENTADOR: Prof. Dr. Evandro Fernandes de Lima

CO-ORIENTADOR: Dra. Isabela de Oliveira Carmo

BANCA EXAMINADORA

Prof. Dr. Breno Leitão Waichel – Departamento de Geociências, Universidade de Santa Catarina

Prof. Dr. Carlos Augusto Sommer – Instituto de Geociências, Universidade Federal do Rio Grande do Sul

Dr. João Marinho de Moraes Neto – Petróleo Brasileiro S.A. – PETROBRAS/EXP/AEXP-T

Tese de doutorado apresentada como requisito parcial para a obtenção do Título de Doutor em Ciências

Porto Alegre, 2020

CIP - Catalogação na Publicação

PEREIRA, NATÁLIA FAMELLI
ASSOCIAÇÃO DE LITOFAÇIES, INTERAÇÃO LAVA-SEDIMENTO
E CARACTERIZAÇÃO SÍSMICA DO MAGMATISMO SERRA GERAL NA
REGIÃO DE UBERLÂNDIA E ARAGUARI (MG) / NATÁLIA FAMELLI
PEREIRA. -- 2020.

212 f.

Orientador: EVANDRO FERNANDES DE LIMA.

Coorientadora: Isabela de Oliveira CARMO.

Tese (Doutorado) -- Universidade Federal do Rio
Grande do Sul, Instituto de Geociências, Programa de
Pós-Graduação em Geociências, Porto Alegre, BR-RS,
2020.

1. pillow lava. 2. magmatismo Serra Geral. 3.
petrofísica de rochas vulcânicas. I. LIMA, EVANDRO
FERNANDES DE, orient. II. CARMO, Isabela de Oliveira,
coorient. III. Título.

Dedico esse trabalho ao meu pai Waldir (in memoriam), à minha mãe Terezinha por terem me ensinado a seguir sempre em frente independente das adversidades, e a todos os professores que ainda acreditam no poder transformador da educação.

AGRADECIMENTOS

Agradeço a essa força maior, conhecidas por uns como Deus, Olorum, Guaraci, Alá, Viracocha, dentre outros, por estar viva e por ter tido a oportunidade de desenvolver este trabalho e conhecer um pouquinho mais deste mundo;

Agradeço aos meus pais (Waldir Martins Pereira e Terezinha Famelli) que, por muitas vezes, abdicaram de seus sonhos para que eu pudesse dar continuidade aos meus estudos. Por compreenderam minha ausência durante o desenvolvimento deste trabalho, por todos os conselhos e ensinamentos dados, meus mais sinceros agradecimentos;

Muito obrigada aos meus orientadores Evandro Lima e Isabela Carmo os quais deram total suporte para o desenvolvimento desta pesquisa e forneceram valiosas orientações. Obrigada à Lucia Moraes e Hildor Seer por nos apresentarem a área de estudo. Agradeço também aos professores John Millett, Malcolm Hole, Dougal Jerram, Sverre Planke, David Jolley e John Howell por todos os ensinamentos e auxílio durante o desenvolvimento deste trabalho;

Agradeço ao suporte da Petróleo Brasileiro S.A. (PETROBRAS) pelo financiamento desta tese através do Programa de Pós-Graduação (CENPES), Projetos PT-166.01.11923 e PT-166.01.13484, e CNPq (442812/2015-9). Muito obrigada à Universidade Federal do Rio Grande do Sul e University of Aberdeen pela infraestrutura disponibilizada. Obrigada às minhas ex-gerentes Maria José Oliveira e Monica Pequeno acreditarem na minha capacidade em desenvolver esse trabalho;

Um agradecimento especial ao meu amigo Gabriel Marins que me ergueu por várias vezes durante essa caminhada, seja com palavra amiga durante os momentos difíceis ou com seu auxílio durante as atividades de campo e discussões geológicas.

Obrigada também aos geólogos Jonas Weschenfelder e Rodrigo Ré pelo imprescindível suporte durante as atividades de campo, e aos pesquisadores Vitor Savastano e Luis Felipe Andrade pelo auxílio com a obtenção das imagens de drone feitos em Uberlândia. Obrigada também à Magda Chmielewska e Jessica Pugsley pelo auxílio com as atividades de campo e modelos digitais feitos na Escócia;

Sou grata a todos os amigos da Petrobras, em especial aos geólogos Fernanda Lourenço, Leandro Bevílaqua, Bruno Carvalho e Ivan Loutfi que muitas vezes cederam seus tempos para me auxiliar com questões geológicas ou suporte com softwares, e à Heloisa Martins por seu profissionalismo e alegria contagiante. Gostaria de agradecer ao André Bulcão, Guilherme Vasquez, Yaro Parizek e todos os outros pesquisadores do CENPES pelo suporte durante as análises.

Obrigada a todos os amigos que fizeram com que essa caminhada se tornasse menos árdua. Agradeço, em especial, à amizade da Nadia Couto que esteve comigo durante a situação mais triste e difícil da minha vida e por todas as palavras amigas que me fortaleceram durante esses últimos meses. Obrigada também Maria Alice Fernandes, Lisa Ribeiro, Mellissa Bahiense, Marcelo Feitoza pela amizade, conversas, conselhos e momentos de descontração, vocês foram fundamentais durante essa minha trajetória. Obrigada Denise e Márcio por me ajudarem a manter a sanidade e a clareza durante esses últimos anos.

RESUMO

Esta tese apresenta os estudos realizados na porção norte da Província Ígnea Paraná-Etendeka (PIPE), com enfoque na estratigrafia, nas interações lava-sedimento e na caracterização em imagem sísmica de diferentes cenários de transição basalto-sedimento envolvendo sucessões vulcânicas. Os resultados são apresentados sob a forma de três artigos científicos submetidos a revistas internacionais. No primeiro artigo são definidas quatro associações de litofácies: pillow lavas, derrames pahoehoe compostos e simples, peperito e brecha vulcânica com matriz infiltrada. Derrames pahoehoe simples, compostos e pillow lavas caracterizam o início do magmatismo, enquanto peperito e derrames espessos ocorrem nas porções superiores da estratigrafia da área. Essas lavas correspondem a magmas de alto-TiO₂ do tipo Pitanga. Na área de estudo, a ocorrência de feições formadas em condições úmidas reflete condições ambientais diferentes daquelas previamente descritas como áridas em outras porções da PIPE. No segundo artigo são apresentados e discutidos alguns dos produtos de interação entre lava e sedimento estudados nesta tese como, por exemplo, peperito, estrutura de carga, lavas invasivas, peperito do tipo pillow e pseudocrateras (rootless cones). Em geral, esses produtos afetam poucos metros além do contato lava-sedimento. Entretanto, lavas invasivas podem estender esses impactos para uma área maior. O terceiro artigo combina modelo digital de afloramento obtido na Província Ígnea do Atlântico Norte e dados petrofísicos da área estudada na PIPE, para a construção de modelos sísmicos sintéticos envolvendo quatro cenários geológicos diferentes. Essas imagens sísmicas foram geradas utilizando fontes com diferentes conteúdos de frequência com o objetivo de avaliar as variações da detectabilidade e características das reflexões sísmicas ao longo da transição basalto-sedimento. Foi possível observar como a variabilidade geológica associada à transição basalto-sedimento pode influenciar o imageamento sísmico e complicar a interpretação. Em particular, feições como lavas invasivas podem ser difíceis de diferenciar de soleiras em dados sísmicos e, portanto, os potenciais impactos nas propriedades e conectividade do reservatório devem ser avaliados cuidadosamente.

ABSTRACT

This thesis presents the study made in the northern portion of the Paraná-Etendeka Igneous Province, focusing on the stratigraphy, lava-sediment interaction and seismic characterization of different basalt-sediment transition scenarios involving volcanic successions. The results are presented in three scientific manuscripts submitted to international journals. In the first manuscript four lithofacies association were defined: pillow lavas, compound and simple pahoehoe, peperite and sedimentary-infill basalt breccia. The onset of the volcanic activity is characterized by pillow lavas, simple and compound pahoehoe, whereas peperite and thick lava flows occur at the upper stratigraphic levels of the study area. These studied lavas are compatible with high-TiO₂ Pitanga magma type. In the study area, the presence of features formed in wet conditions reflect different environmental conditions from those previously described as arid in other portions of the PEIP. The second manuscript present and discuss some products of lava-sediment interactions such as peperite, loading, invasive flows, pillow-like peperite and rootless cones. These interactions are generally restricted to a few meters from the lava-sediment contact. However, lava invasion may extend this impact further. The third manuscript combines 3D virtual outcrop model from the North Atlantic Igneous Province with laboratory petrophysical measurements from Paraná-Etendeka Igneous Province field outcrop analogues to develop synthetic seismic forward models for four different base-basalt transition scenarios. The models were run using source wavelets with different frequency spectrums in order to assess variations in seismic reflection character and detectability of the volcanic features along with the basalt-sediment transition. The results demonstrate how geological variability associated with the basalt-sediment transition can influence seismic imaging and complicate interpretation. In particular, features such as invasive lava flows may be challenging to differentiate from sill intrusions in seismic data, and therefore their potentially very different impacts on reservoir properties and connectivity must be appraised carefully.

LISTA DE TABELAS

Tab. 1: Fácies dos derrames, características físicas e petrográficas das lavas das Formações do Grupo Serra Geral (Modificado de Rossetti et al., 2018).....	24
Tab. 2: Description and interpretation of the Uberlândia-Araguari volcanic lithofacies.....	66
Tab. 3: Lithofacies association of the Uberlândia-Araguari region (modified from Barreto et al., 2014; Duraiswami et al., 2013).	72
Tab. 4: Representative geochemical data of subaerial lava flows and pillow lava samples of Uberlândia-Araguari region. The table includes samples with lower, intermediate and upper end of silica contents, all with low LOI values.....	85
Tab. 5: Lava-sediment interactions observed in the study areas. Emp.Type = Emplacement types; Loc. = Location; P = Paraná Basin, M = Isle of Mull; S = St. Cyrus.....	127
Tab. 6: Statistics of petrophysical data collected from the study area in Uberlândia area (Brazil). The wave velocities present in this table were acquired under a confining stress of 6.9 MPa.....	166
Tab. 7: Velocity and density data for the representative facies used for the seismic forward modeling. Velocities and densities used for the heterogeneous sedimentary sequence were compiled from Rabbel et al. (2018).	169

LISTA DE FIGURAS

- Fig. 1: Localização da área de estudo. A) Mapa do Brasil com o estado de Minas Gerais (MG) em destaque; B) Detalhe do retângulo marcado em A com a área de estudo delimitada pelo retângulo tracejado; C) Imagem do Google Maps da área de estudo.....17
- Fig. 2: Distribuição global das grandes províncias ígneas (*LIPs*) de acordo com a configuração do *Pangea* há cerca de 320 Ma. As idades indicadas referem-se ao início da fase principal ou ao primeiro pulso do magmatismo dessas *LIPs*. Linhas verdes conectam grandes províncias ígneas oceânicas separadas por espraiamento oceânico. Abreviações: CAMP – Província Magmática do Atlântico Central; EUNWA – Européia, noroeste da África; HALIP – Grande Província Ígnea do Ártico; NAIP – Província Ígnea do Atlântico Norte; OJP – Platô Ontong Java; RT-ST – Rajmahal Traps-Sylhet Traps; SRP – Planície Snake River; KCA – Kennedy-Connors-Auburn. Legenda: áreas vermelhas - Províncias basálticas continentais/Margens vulcânicas rifteadas; áreas amarelas - *LIPs* félscicas; áreas azuis - Platôs oceânicos/Províncias basálticas oceânicas. Extraído de Bryan and Ferrari (2013).20
- Fig. 3: Mapa geológico das principais unidades da PIPE (modificado de Peate et al., 1992; Stewart et al., 1996; Hawkesworth et al., 2000; Rossetti et al., 2018). Enxame de diques: 1 – Ponta Grossa; 2 – Santos-Rio de Janeiro; 3 – Florianópolis; 4 – Paraguai; 5 – Skeleton Coast. Estrelas representam ocorrência de pillow lavas e peperitos.....23
- Fig. 4: Mapa de localização da Província do Atlântico Norte. Quadrado vermelho indica a localização da Província Ígnea Britânica. Modificado de Ganerød et al. (2008).26
- Fig. 5: Mapa de localização de St Cyrus. A) Mapa da Escócia com as principais falhas marcadas; B) Mapa geológico da porção oeste da Bacia Midland Valley (área entre Stonehaven e Arbroath). Modificado de Hole et al. (2013) e Rawcliffe (2016). MVF = Formação Vulcânica Montrose (em marrom escuro no mapa B), o qual está incluído no Grupo Arbuthnott.28
- Fig. 6: Os membros finais do espectro de morfologias de lavas subaéreas. A) Lobo pahoehoe ativo com superfície lisa e cordada. Foto de Bernard M.Gunn, retirada de http://www.discoverlife.org/IM/I_AMC/0107/mx/; B) Derrame a'ā sendo colocado sobre campo de lavas pahoehoe. Extraído de <http://planet-terre.ens-lyon.fr/image-de-la-semaine/Img228-2008-03-17.xml>.....30
- Fig. 7: Diagrama da taxa de deformação por cisalhamento vs. viscosidade Newtoniana aparente, mostrando as relações aproximadas dos campos de estabilidade para as lavas pahoehoe havaianas e os fluxos a'ā, e os limites aproximados da zona de transição (TTZ). Modificado de Loock et al. (2010).32
- Fig. 8: Seção esquemática de colocação de um derrame de lava pahoehoe por inflação. Escala vertical varia de 1 a 5 m para derrames havaianos a 5 a 50 m para derrames do CRB. Extraído do de (Waichel et al., 2006).33
- Fig. 9: Afloramentos de derrames a'ā com núcleo maciço (setas amarelas) e brechas de base e topo. A) Empilhamento de derrames a'ā mostrando características do núcleo denso (10-20 cm de espessura) e margens brechadas. Extraído de Cashman and Mangan, 2014; B) Afloramento de lavas a'ā de La Palma (Ilhas Canárias). Extraído de <https://www.sandatlas.org/types-lava-flows/>.35

Fig. 10: Lavas platy-ridge. (a) margem de lavas platy-ridge definidas por uma profunda ranhura (seta vermelha) limitando esse tipo de derrame. (b) Imagem aérea onde é possível observar lava platy-ridge onde a placa pahoehoe plana (Pp) é limitada por ranhuras de aspecto áspido e rugoso (seta vermelha). Extraído de Stevenson et al. (2012)	36
Fig. 11: Afloramento de derrame <i>rubbly pahoehoe</i> (A) e derrame do tipo pasta de dente (B). A) Contato entre dois derrames <i>rubbly pahoehoe</i> . Abreviações: Bam - basalto maciço hipocristalino e afírico; Brt – brecha de topo de derrame. Extraído de Barreto et al. (2014). B) superfície de derrame do tipo pasta de dente. Extraído de Waichel et al. (2006).	37
Fig. 12: A) Exemplos das morfologias de derrames subaquosos: derrames em almofadas (<i>pillow lavas</i>), lobados e tabulares; B) Mapas batimétricos de alta resolução (em mesma escala) de áreas dominadas por <i>pillow lavas</i> (à esquerda) e áreas dominadas por derrames lobados e tabulares (à direita). A área com <i>pillow lavas</i> é caracterizada por relevo com montículos formados por empilhamento de <i>pillows</i> de 500 m de diâmetro e 50-100 m de altura. A área dominada por derrames lobados e tabulares é caracterizada por relevos não muito altos que podem se estender por 1-4 km a partir da cratera ou fissura eruptiva. Modificado de White et al. (2015)	39
Fig. 13: Estruturas características de superfícies de lobos de <i>pillows</i> e modelo de crescimento de <i>pillow lavas</i> . Extraído de Mcphie et al. (1993).....	40
Fig. 14: Padrão da distribuição de vesículas em <i>pillows</i> da Islândia, desenhadas numa mesma escala. Vesículas <i>pipe</i> podem ocorrer principalmente na base ou ao redor da circunferência de <i>pillows</i> de águas rasas. Extraído de Walker (1992).....	41
Fig. 15: Sumário com as características dos domínios de peperitos (a); (b) morfologia dos clastos juvenis; (c) evidências para a natureza não consolidada dos sedimentos hospedeiros; (d) geração de clastos juvenis; e (e) mistura de clastos juvenis e sedimentos hospedeiros. Modificado de Skilling et al., (2002).....	45
Fig. 16: Peperitos da Bacia do Paraná com diferentes proporções relativas de clastos juvenis e sedimento hospedeiro. A) Exemplo de peperito clasto-suportado; B) Peperito matriz suportado. Extraído de Waichel et al. (2007).....	46
Fig. 17: A) Figura esquemática ilustrando arquitetura de juntas observada no derrame da figura B. B) Seção do derrame de Búrfell, próximo a Gjain, com colunado superior e inferior, e um domínio de entablamento na porção central do derrame. Escala tem 1m. Modificado de Forbes et al., (2014).....	48
Fig. 18: Face de uma coluna com estrias marcadas pela repetição de porções lisas e rugosas representando início e interrupção de juntas, respectivamente. Direção do crescimento da junta é indicado pela seta. A lapiseira tem 15 cm de comprimento. Extraído de Lyle (2000).	49
Fig. 19: Geological map of the major volcanic units of the Paraná-Etendeka Igneous Province (modified after Hawkesworth et al., 2000; Peate et al., 1992; Rossetti et al., 2017; Stewart et al., 1996). Dyke swarms: 1 – Ponta Grossa; 2 – Santos-Rio de Janeiro; 3 – Florianópolis; 4 – Paraguay; 5 – Skeleton Coast. Pillow lava occurrences: A – Study area (yellow square); Uberlândia-Araguari (Ferreira, 1985; Moraes et al., 2018; Moraes and Seer, 2017); B – São Paulo State (Mano, 1987); C – Rio Iguaçu (Marques Filho et al., 1981); Peperite occurrences involving basaltic lavas: D – West of Mato Grosso do Sul (Machado et al., 2015); E – West of Paraná (Waichel et al., 2007); F – Torres Syncline (Barreto et al., 2014; Rossetti	

et al., 2014); Peperite occurrences involving silicic lavas (Luchetti et al., 2014): G – São Jerônimo da Serra; H – Mangueirinhas and Palmas; I – Bento Gonçalves region; J – Santa Maria. Dashed lines correspond to an inferred contact between the northern (high TiO ₂) and southern (low TiO ₂) lava chemical groups as suggested by Hawkesworth et al. (2000).	60
Fig. 20: A) Geological map of the Uberlândia-Araguari region with samples location (modified from Pacheco et al., 2017). B) Detail of the central portion of the study area. The red lines in figures A and B represent locations of the main stratigraphic logs across the study area.....	63
Fig. 21: Volcanic lithofacies of Uberlândia-Araguari region: A) Pillowed basalts (Bp, white dashed line) and glassy basaltic breccias (Bgp). The yellow arrows indicate flame structures of the underlying sedimentary rock; B) Detail of glassy basaltic breccia with glassy basaltic fragments (red arrows) and sedimentary matrix (black arrows); C) Aphanitic massive basalt with sparse vesicles (yellow arrows) and amygdales (white arrows) filled with zeolite; D) Basalt with pods filled by segregation vesicles at the base of the unit; E) Aphanitic vesicular basalt flow top; F) Basalt with proto-cylinder vesicles.	69
Fig. 22: Volcanic lithofacies of Uberlândia-Araguari region: A) Basalt with giant amygdales (< 40 cm, yellow arrow) filled with silica; B) Upper portion of basaltic lava with sheet vesicles (dashed lines); C) Basalt with ropy surface; D) Basalt with smooth billowy surface (yellow arrows). Dashed line shows the contact between two lavas; E) Columnar basalt with rectilinear faces; F) Columnar basalt with undulatory faces.....	70
Fig. 23: Lithofacies of Uberlândia-Araguari region: A) Laminated sediment-matrix basalt breccia occurring on the top of a basalt unit from the central portion of the study area; B) Dispersed sediment-matrix basalt breccia occurring on the top of a basalt unit from the central portion of the study area. Basalt fragments (black arrows) are dispersed within a silty sandstone; C) Close-packed sediment-matrix basalt breccia occurring on the top of a basalt unit in the central portion of the study area. Basalt fragments are closely packed within a tight framework (black arrows); D) Peperitic domain with close-packed and dispersed sediment-matrix basalt breccia (yellow dashed lines) and large coherent basaltic domain (Blcd) lithofacies (white dashed lines).	71
Fig. 24: Summary of stratigraphic cross-section with composite logs showing the lithofacies associations of each study site (see Fig 2A and 2B for the vertical profiles location). Elevation is used as the reference point for correlation (see discussion in the text).	73
Fig. 25: Pillow lavas from the central portion of the study area. A) Highly-altered pillow lavas from the upper interval. Close-packed pillows superposed by glassy basaltic breccias and subaerial pahoehoe lobe; B) Pillow lavas with varied shapes and radial cracks; C) Contact between subaerial and pillow lavas from the lower interval; D) Contact between subaerial lava flows and pillow lavas from the upper interval.....	74
Fig. 26: Photomicrographs of the basaltic lavas: A) Amygdaloidal basalt from the margins of a pillow lava: vitrophyric basalt with plagioclase and augite microphenocrysts and large amygdales are filled with calcite and smectite, PP; B) Pillow lava central portion: basalt with plagioclase microphenocrysts and vesicles. Note a higher crystallinity when compared with the pillow margins in (A), PP. C) Vitreous clast with curviplanar edges (red arrow) and greenish mudstone clasts in	

a sandy matrix, PP; D) Detail of augite (Aug - yellow arrow), plagioclase (Plg - red arrow), and olivine (Olv - green arrow) phenocrysts. Olivine crystal is partially altered to iddingsite, PP; E) High glass content in basalt with undulatory columns. Dashed yellow circle highlights plagioclase and augite phenocrysts, PP; F) Lower glass content in basalt with rectilinear columns. Dashed yellow circle highlights plagioclase and augite phenocrysts, PP. PP= plane polarizer, blue color represents the resin color used in the slides preparation. 75

Fig. 27: Features of the subaerial flows in the study area. A) Panoramic view of simple pahoehoe lava flows separated by a thick peperite layer in the inactive Arpasa quarry (log D); B) Dome-like features filled by peperitic breccia at the top of the simple pahoehoe flow (yellow solid line) in the active Arpasa quarry (log D); the undulatory columns converge towards the dome-like features (yellow arrows) and the horizontal layer of columnar basalt with rectilinear faces (yellow dashed line) dips adjacent to this area; C) Basaltic breccia occurring locally on top of a simple pahoehoe in the inactive Arpasa quarry (log D). 77

Fig. 28: General aspects of sedimentary-matrix igneous breccia intervals. A) Peperite layer on the base of a basaltic flow at Arpasa inactive quarry (yellow dashed line delimits the base of the lava flow and the top of the peperite, whereas the base of the peperite is covered by talus deposits); coherent igneous domains (Blcd) in the form of lobe and sill are represented by the white solid lines; B) Basaltic dark gray fragments with irregular blocky morphology; C) Basaltic reddish fragments with irregular fluidal morphology. 79

Fig. 29: Photomicrographs of sedimentary and peperitic levels. A) General aspects of peperite with irregular angular juvenile fragments with augite (Aug - red arrows) and plagioclase phenocrysts (Plg - yellow arrows). Dominant curvilinear to sub-planar margins, PP; B) Basalt fragments with dominant crenulate margins in contact with a silty sandstone matrix. Finger-like bulbous projection indicated by the yellow arrow, PP; C) Sedimentary portion of peperitic domain with vesicle rims partially filled by microcrystalline silica (yellow arrows), PP; D) Matrix-supported conglomerate with crystalline basement pebbles (indicated by letter X) occurring below the volcanic sequence (corresponding to pre-volcanic sedimentary rocks). Moldic porosity given by dissolution of lithic fragments is indicated by the orange arrows, PP; E) Bimodal sandstone composed of rounded quartz grains and subordinate alkali feldspars and mudstones lithoclasts (Lmud - red arrow). Moldic porosity given by the dissolution of the lithoclasts is indicated by the orange arrows (Mpor). Sample from sandstone layer occurring between the pillow lava and the compound pahoehoe lava flows, PP; F) Calcrete layer with sand levels and planar lamination occurring below the pillow lavas, PP. PP= parallel polarizer, blue color represents the resin color used in the slides preparation. 81

Fig. 30: Geochemical data of the Uberlândia-Araguari lava flows. Major oxide contents are recalculated to 100% on an anhydrous basis. A) Total-Alkalies vs. Sílica diagram (modified from Le Bas et al., 1986); B) $\text{Fe}_2\text{O}_3^{(\text{t})}$ vs. TiO_2 diagram for discriminating the different PEIP magmas type (Peate et al., 1992); C) Winchester and Floyd (1977) classification diagram; D) Zr/Y vs Sr diagram for discriminating the different PEIP magmas type (Peate et al., 1992); E) Multi-element diagram normalized to primitive mantle (Sun and McDonough, 1989) for the distinct lavas recognized in the studied area in comparison with the general composition of the Pitanga Magma type from Peate et al. (1992); F) REE profiles normalized to primitive mantle (Sun and McDonough, 1989) for the distinct lavas recognized in the studied area. 84

- Fig. 31: f Diagram showing the lava flows emplacement in Uberlândia-Araguari area considering the invasive lava flow/shallow intrusion hypothesis. A) Beginning of volcanic activity characterized by thin simple and compound pahoehoe overlying pre-existing sediments of a peridesert environment; B) Topographic irregularities allowed the accumulation of small lakes where the subaerial lava flows became subaqueous resulting in pillow lavas; C) Thick simple pahoehoe lava flows covered the subaerial and subaqueous deposits; D) Sediments of peridesert environment covering the thick pahoehoe flows; E) Simple pahoehoe start to invade pre-existing sediments giving rise to thick invasive flows. The interaction between the invasive lava flow and pre-existing sediments resulted in thick (up to 7 m) of lower and upper peperite deposits; F) Thick pahoehoe lava flows covered the upper peperite related to the previous invasive flow. G) Profile X – X' of the figure 31E.....91
- Fig. 32: Geological map of the Paraná Basin (modified after Hawkesworth et al., 2000; Peate et al., 1992; Rossetti et al., 2018; Stewart et al., 1996). Dike swarms: 1 – Ponta Grossa; 2 – Santos-Rio de Janeiro; 3 – Florianópolis; 4 – Paraguay; 5 – Skeleton Coast. Stars represent pillow lava and peperite occurrences. The black star highlights the location of the study area.112
- Fig. 33: Lava and sediment features from Uberlândia-Araguari; A) Irregular upper contact (yellow line) of an invasive lava flow overlain by peperites; B) Disperse peperite with irregular juvenile clasts (JC - red arrows) and host sediment (S - green arrows); C) Juvenile clasts (JC - red arrows) and vesiculated host sediment (Vs - yellow arrows); D) Coherent igneous domains from peperitic interval; lobes morphologies delimited by white dashed line, and sill morphologies highlighted by yellow dashed line; E) Detail of the conglomeratic sandstone with metamorphic basement lithoclasts; F) Sharp contact between subaerial lava flow and underlying sediment; G) Pillow lavas (dashed lines) with different sizes and shapes.....114
- Fig. 34: A) Map of Scotland showing the location of the study area in St. Cyrus; B) Geological map of Old Red Sandstone age strata of the area between Stonehaven and Arbroath (modified after Hole et al., 2013; Rawcliffe, 2016). MVF = Montrose Volcanic Formation (in brown on map B) which is part of the Arbuthnott Group.116
- Fig. 35: Lava and sediment features from St. Cyrus area. A) Virtual outcrop of the study area in St. Cyrus. Red squares represent the location of studied outcrops and the yellow arrow indicates the Woodston Fishery location; B) Irregular morphology of peperite; C) Irregular juvenile clasts and host sediment with distinct colors - green (Gs - green arrow) and red (Rs - red arrows); D) Invasive lobes with irregular contacts and related peperites; E) Pillow-like peperites. Depending on the cross-section direction it is possible to observe elongated lobe or pillow morphologies; F) Detail of the figure 35E (white square) where it is possible to observe pillow-like peperites of decimeter size; G) Invasive lobes with sharp contacts.118
- Fig. 36: A) Location map of Scotland, indicating the position of the Isle of Mull (in red); B) Simplified geological map of the Isle of Mull with the location of the study area in Carraig Mhór (black star) (Modified after Brown and Bell, 2007).....121
- Fig. 37: Lava and sediment features from Carraig Mhór (Isle of Mull); A) Virtual outcrop of the study area in Carraig Mhór. Red squares represent the location of the studied outcrops; B) Vesicle cylinders in the lava core; C) Vesicle sheets (yellow arrows) on the upper crust of a pahoehoe lava flow; D) Pipe vesicle (yellow arrow) at the basal portion of the flow; E) Ropy structure at the surface of the lava flow; F) Loading structure at the basal contact of a subaerial lava flow; G) Blocky peperite with juvenile clasts of a few centimeters size; H) Close-up of the white square in figure 6F showing juvenile clasts (JC – red arrows) with curviplanar to planar

surfaces and jigsaw-fit texture embedded in mudstone (S – red arrow); I) Fluidal juvenile clast (yellow arrow) and bulbous lava lobe invading the underlying sediment (dashed red line); J) Preferential zone of fluid scape of volatile with a major concentration of vesicles and cylinders occurring between the two red lines; K) Agglutinate deposit; L) Detail of the agglutinate deposit with rounded to flatten fragments of lava (red arrows).....	122
Fig. 38: Geological map of the major volcanic units of the Paraná-Etendeka Igneous Province (modified after Peate et al., 1992; Stewart et al., 1996; Hawkesworth et al., 2000). Dyke swarms: 1 – Ponta Grossa; 2 – Santos-Rio de Janeiro; 3 – Florianópolis; 4 – Paraguay; 5 – Skeleton Coast. The study area location is highlighted by the black star.....	151
Fig. 39: A) Outline of the North Atlantic Igneous Province (modified after Ganerød et al., 2008). B) Location map of Scotland, indicating the position of the Isle of Mull (in pink). C) Simplified geological map of the Isle of Mull with the location of the study area (black star) between Carsaig Bay and Carsaig Arches (modified after Brown and Bell, 2007).	153
Fig. 40: Virtual outcrop model of Carsaig Arches area subdivided in three main sections. A) Northeastern section of the studied area. The sedimentary outcrop is evidenced in the black square a. The area selected for the seismic forward modelling is delimited by the dashed black square. B) Central section of the studied area. Black squares b and c show the occurrence of an intrusion and compounded flows, respectively. C) Southwestern section of the studied area. The location with the best exposure simple lava flows is highlighted in the square d.	158
Fig. 41: Detailed view of the virtual outcrop model of Carsaig Arches. Non-interpreted (on left) and interpreted (on right) images showing the facies recognized in the virtual outcrop model (black squares in Fig. 40). A) Sandstone exposure with intrusion. B) Intrusive rock. C) Image of compound lava flows. D) Image of simple lava flows.....	160
Fig. 42: Juvenile clasts geometries of a peperitic deposit from PEIP (Uberlândia, Brazil). A) Picture of a peperite outcrop with juvenile clasts delimited by the white line. B) Geological model for a peperitic interval based on the PEIP outcrop. Black arrows highlight juvenile clasts. S = sedimentary matrix.	161
Fig. 43: Interpretation of the virtual outcrop model and construction of the geological model, along Carsaig Arches cliff: A) 2D projection of the area selected for the seismic forward modeling. B) Interpretation of the geological features in areas with good exposures. C) Geological model interpreted for the selected area. The covered areas were populated with compounded lobe morphologies.....	162
Fig. 44: Geological models used for the seismic forward modeling. All models were simulated at water depth of 100 m. A) Model 1: Volcanic succession occurring between sandstone layers. B) Model 2: Volcanic succession superposed by sandstone and overlying heterogeneous sedimentary sequence. C) Model 3: Similar to model 2, but an intrusive rock with peperite at its contacts occur cross cutting the heterogeneous sedimentary sequence. D) Similar to model 2, but an invasive flow with peperite occurring on its contacts occur invading the heterogeneous sedimentary sequence. Sw = Sea water; Sed = Sediments; Int = Intrusions; Lco = Lobe core; Lcr = Lobe crust; Sint = Sheet intrusion; Pep = Peperite; Ilf = Invasive lava flow.	164
Fig. 45: Outcrops exemplifying the type of material where plugs were taken. A) Exposure of sandstone. B) Mudstone outcrop. C) Core and upper crust of a lava	

flow superposed by a layer of peperite related to the base of the superposed lava flow.....	165
Fig. 46: Petrophysical variations of the PEIP samples (Uberlândia area, Brazil). A) Density plotted against porosity for all studied samples. B) Detail of the dashed square in diagram A showing only volcanic samples. C) Permeability plotted against porosity for all studied samples. D) Relationship between permeability and porosity of volcanic samples (detail of the dashed square in the diagram C). E) V_p and V_s plotted against porosity for all the studied samples. F) Variation of V_p and V_s against porosity for volcanic rocks (detail of the dashed square in the diagram E). G) V_p and V_s against density for all samples. H) V_p and V_s against density showing only volcanic samples.	168
Fig. 47: Models 1 and 2. A, B) Velocity model. C, D) Seismic forward modelling, dominant frequency of 30 Hz. E, F) Seismic forward modelling, dominant frequency of 50 Hz. G, H) Seismic forward modelling, dominant frequency of 70 Hz.	171
Fig. 48: Models 3 and 4. A, B) Velocity model. C, D) Seismic forward modelling, dominant frequency of 30 Hz. E, F) Seismic forward modelling, dominant frequency of 50 Hz. G, H) Seismic forward modelling, dominant frequency of 70 Hz.	172
Fig. 49: Model 2 (30 Hz dominant frequency). A) Non-interpreted seismic model. B) Igneous features interpreted in the seismic model. D = dyke; F = Fault; T = Top of the volcanic sequence; R = Discontinuous reflectors; A = Artefact. 1 = Water layer; 2 = Homogeneous sedimentary rock; 3 = Volcanic succession; 4 = Layered sedimentary rock.	174
Fig. 50: Model 3 (50 Hz dominant frequency). A) Non-interpreted seismic model. B) Igneous features interpreted in the seismic model. D = dyke; F = Fault; T = Top of the volcanic sequence; R = Discontinuous reflectors; S = Sheet intrusion; Orange square with letter C = Area dominated by compound lava flows; Orange square with letter P = Area dominated by simple lava flows. 1 = Water layer; 2 = Homogeneous sedimentary rock; 3 = Volcanic succession; 4 = Layered sedimentary rock intruded by a sheet intrusion.	175
Fig. 51: Model 4 (70 Hz dominant frequency). A) Non-interpreted seismic model. B) Igneous features interpreted in the seismic model. D = dyke; F = Fault; T = Top of the volcanic sequence; R = Discontinuous reflectors; I = Invasive lava flow; Orange square with letter C = Area dominated by compound lava flows; Orange square with letter P = Area dominated by simple lava flows. 1 = Water layer; 2 = Homogeneous sedimentary rock; 3 = Volcanic succession; 4 = Layered sedimentary rock invaded by an invasive flow.....	176

Sumário

CAPÍTULO I	16
1. INTRODUÇÃO	16
1.1 JUSTIFICATIVA	17
1.2 OBJETIVOS	18
CAPÍTULO II	19
2. CONTEXTO GEOLÓGICO	19
2.1 GRANDES PROVÍNCIAS ÍGNEAS	19
2.2 PROVÍNCIAS BASÁLTICAS CONTINENTAIS	21
2.3 PROVÍNCIA ÍGNEA PARANÁ-ETENDEKA	22
2.4 PROVÍNCIA ÍGNEA DO ATLÂNTICO NORTE	25
2.5 BACIA <i>MIDLAND VALLEY</i> NA ESCÓCIA.....	27
CAPÍTULO III	29
3. ESTADO DA ARTE.....	29
3.1 DEPÓSITOS VULCÂNICOS DAS PROVÍNCIAS BASÁLTICAS CONTINENTAIS	29
CAPÍTULO VI	51
4. METODOLOGIA.....	51
4.1 REVISÃO BIBLIOGRÁFICA.....	51
4.2 ATIVIDADES DE CAMPO.....	51
4.3 PETROGRAFIA.....	52
4.5 QUÍMICA DE ROCHA TOTAL	52
4.6 ENSAIOS PETROFÍSICOS.....	53
4.7 MODELO DIGITAL DE AFLORAMENTO.....	55
4.8 MODELO SÍSMICO SINTÉTICO	55
CAPÍTULO V	57
5. APRESENTAÇÃO DOS ARTIGOS CIENTÍFICOS.....	57
5.1 ARTIGO A	57
5.2 ARTIGO B	107
5.3 ARTIGO C	146
CAPÍTULO VI	195
6. SÍNTESE E CONCLUSÕES.....	195
REFERÊNCIAS	198

ESTRUTURA DA TESE

Esta tese é requisito para a obtenção do título de doutor no programa de pós-graduação em Geociências da Universidade Federal do Rio Grande do Sul e está estruturada sob a forma de artigos científicos. Sendo assim, sua organização compreende os seguintes capítulos:

Capítulo I: Apresenta uma introdução, com as justificativas que motivaram o desenvolvimento desta tese e os objetivos propostos para este estudo.

Capítulo II: Apresenta uma breve discussão sobre Grandes Províncias Ígneas e o contexto geológico da Província Ígnea Paraná-Etendeka e apresentação do contexto geológico de outras áreas visitadas durante o desenvolvimento desta tese (Província do Atlântico Norte e Bacia *Midland Valley*).

Capítulo III: Revisão bibliográfica sobre os depósitos vulcânicos de Províncias Basálticas Continentais.

Capítulo IV: Os métodos e técnicas utilizados para atingir os objetivos propostos.

Capítulo V: Os resultados desta tese são apresentados sob a forma de três artigos científicos submetidos a periódicos internacionais, conforme as normas estabelecidas pelo Programa de Pós-Graduação em Geociências da Universidade Federal do Rio Grande do Sul.

Capítulo VI: Síntese dos principais resultados alcançados durante a realização deste projeto de doutorado. As cartas de submissão dos artigos científicos, bem como os dados analíticos de litogegeoquímica e petrofísica gerados por este trabalho são apresentados sob a forma de Anexos.

CAPÍTULO I

Neste capítulo são apresentadas as principais questões que levaram ao desenvolvimento deste trabalho, bem como as justificativas, objetivos gerais e específicos.

1. INTRODUÇÃO

Na porção meridional do Brasil afloram rochas vulcânicas da Província Ígnea Paraná-Etendeka (PIPE), formadas por um megaevento vulcânico relacionado à fragmentação do supercontinente *Gondwana* e abertura do Oceano Atlântico Sul, há cerca de 135 Ma (p.ex. Deckart *et al.*, 1998; Thiede and Vasconcelos, 2010; Renne, 2015). Muito embora a porção mais significativa da PIPE esteja localizada na América do Sul (Brasil, Paraguai, Uruguai e Argentina), volumes subordinados deste vulcanismo também afloram na África (Etendeka – Namíbia) (Melfi *et al.*, 1988; White and McKenzie, 1989). Além de exposições em área continental (*onshore*), as lavas da PIPE parecem ter se estendido para bacias sedimentares localizadas na costa sul e sudeste brasileira (*offshore*) (Stica *et al.*, 2014), onde podem ocorrer como reservatório de hidrocarbonetos (p.ex. Mizusaki, 1988; Mizusaki *et al.*, 2008). Desta forma, sucessões vulcânicas encontradas na porção *onshore* podem representar bons análogos para sistemas vulcânicos encontrados nas porções *offshore*.

Este trabalho visa o reconhecimento das fácies vulcânicas, do arcabouço estratigráfico e das propriedades petrofísicas das lavas aflorantes em uma região pouco explorada da PIPE, mais especificamente, na região entre Uberlândia e Araguari (Minas Gerais, Brasil) (Fig. 1). O reconhecimento das fácies e arquitetura de fácies em sucessões vulcânicas são fundamentais para a compreensão da evolução do vulcanismo, bem como reconstrução paleoambiental das áreas afetadas por este vulcanismo. Por outro lado, a investigação das propriedades físicas, como porosidade e permeabilidade, associada à distribuição espacial das litofácies identificadas, permite o melhor entendimento do potencial reservatório dessas sucessões vulcânicas e a forma como o vulcanismo interage com os sedimentos subjacentes. Adicionalmente, a integração dos dados de petrofísica (p.ex. velocidade acústica e densidade) e distribuição das litofácies vulcânicas tem como objetivo a construção de imagens sísmicas sintéticas, simulando diferentes configurações geológicas, para o entendimento de como as reais geometrias observadas nas sequências vulcânicas são imageadas em subsuperfície. Esse tipo de informação é importante, visto que

dados de reflexão sísmica são, geralmente, a primeira base de dados utilizada para mapear feições geológicas em áreas prospectivas (p.ex. Planke *et al.* 2005; Jackson *et al.* 2013; Magee *et al.* 2013; Schofield *et al.* 2015; Schmiedel *et al.* 2017).

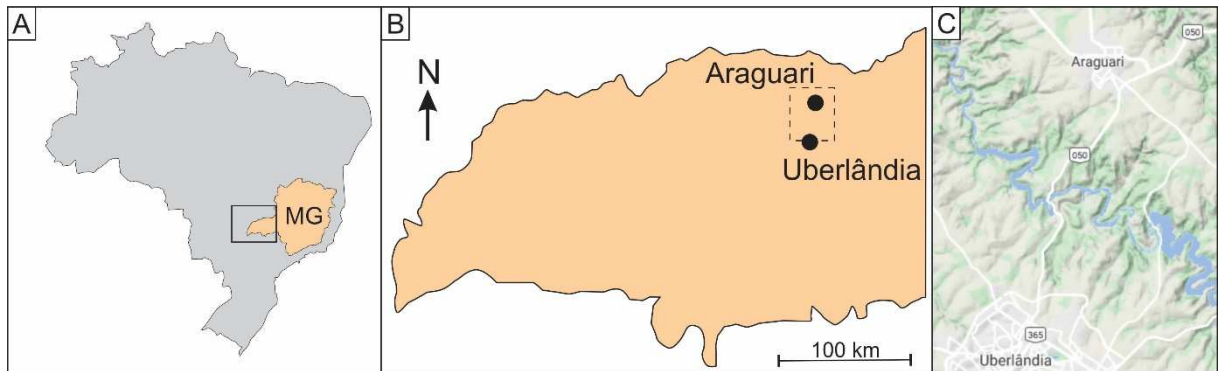


Fig. 1: Localização da área de estudo. A) Mapa do Brasil com o estado de Minas Gerais (MG) em destaque; B) Detalhe do retângulo marcado em A com a área de estudo delimitada pelo retângulo tracejado; C) Imagem do Google Maps da área de estudo.

1.1 JUSTIFICATIVA

A presença de produtos vulcânicos associados às descobertas recentes de grandes campos petrolíferos na sucessão sedimentar pré-sal das bacias marginais brasileiras aumentou o interesse no entendimento da evolução do vulcanismo nas províncias ígneas. Essas descobertas incentivaram consideravelmente a investigação de sistemas vulcânicos em ambientes bacinais, tanto no que diz respeito a distribuição espacial e geométrica dos elementos arquiteturais, quanto na definição de características petrofísicas, como porosidade e permeabilidade.

O entendimento das arquiteturas de fácies pode melhorar a previsibilidade de ocorrência de fácies, como por exemplo, a distribuição e proporção de núcleo e crosta vesiculada em derrames tabulares clássicos e derrames compostos, auxiliando o planejamento de projetos de perfuração de poços de petróleo. Além de fornecer informações a respeito do potencial dessas rochas para atuar como reservatório de hidrocarbonetos, os dados petrofísicos são utilizados como dados de entrada para a confecção de imagens sísmicas sintéticas, estas consideradas fundamentais para caracterização da assinatura sísmica de pacotes rochosos.

A principal motivação para o desenvolvimento deste trabalho foi compreender a estratigrafia e a evolução do vulcanismo na área de estudo, além de identificar as respostas petrofísicas (porosidade e permeabilidade) e assinaturas em sísmica de sucessões vulcânicas.

1.2 OBJETIVOS

Este projeto de doutorado objetiva a caracterização das litofácies para a construção da arquitetura da sucessão vulcânica na região de Araguari (porção norte da Província Ígnea Paraná-Etendeka), assim como sua caracterização petrofísica e sua assinatura sísmica, de forma a avaliar seu potencial como reservatório de fluidos e definir uma assinatura sísmica para sucessões vulcânicas, respectivamente.

Os objetivos específicos consistem em:

- 1) Definir o arcabouço estratigráfico da área entre Uberlândia e Araguari através da caracterização dos tipos de lavas e da arquitetura de fácies dos depósitos vulcânicos;
- 2) Compreender os efeitos do início do vulcanismo em bacias sedimentares através da identificação dos produtos de interação entre lava e sedimento, processos atuantes e possíveis efeitos nos sedimentos subjacentes;
- 3) Avaliar o potencial como reservatórios das rochas dos intervalos subaéreos e subaquosos através da quantificação da sua porosidade e permeabilidade;
- 4) Apresentar a assinatura de sucessões vulcânicas em imagens sísmicas sintéticas compostas por variadas frequências dominantes (30, 50 e 70 Hz).

CAPÍTULO II

Este capítulo apresenta uma breve definição do que são as Grandes Províncias Ígneas e Províncias Basálticas Continentais, e descreve o contexto geológico das áreas visitadas durante o desenvolvimento deste trabalho.

2. CONTEXTO GEOLÓGICO

2.1 GRANDES PROVÍNCIAS ÍGNEAS

Algumas regiões do planeta preservam grandes volumes de rochas ígneas intrusivas e extrusivas que ocupam áreas maiores que $0,1 \times 10^6 \text{ km}^2$ e volumes maiores que $0,1 \times 10^6 \text{ km}^3$. Quando ocorrem em ambiente intraplaca, e uma grande proporção do total de volume íneo ($> 75\%$) é expelida em um curto período de tempo (1-5 Ma), esses eventos vulcânicos são caracterizados como Grandes Províncias Ígneas (*Large Igneous Provinces – LIPs*) (Bryan and Ernest, 2008). Em geral, *LIPs* são predominantemente compostas por rochas magmáticas maficas, com subordinada presença de componentes ácidos e ultramáficos e ocorrem em diferentes contextos crustais, sendo agrupadas em *LIPs* continentais e *LIPs* oceânicas (Coffin and Eldholm, 1992, 1994; Bryan and Ernest, 2008). As *LIPs* continentais incluem províncias basálticas continentais, margens vulcânicas rifteadas, enxames de diques gigantes e complexos intrusivos máfico- ultramáficos; *greenstone belts* arqueanos, e grandes províncias ígneas ácidas. Por outro lado, *LIPs* oceânicas são compostas por platôs oceânicos e basaltos de fundo oceânico (Bryan and Ernest, 2008). Vale ressaltar que muitos dos estudos, que levaram ao desenvolvimento dos conceitos chaves para a definição de *LIPs*, foram desenvolvidos em registros relativamente bem preservados do Mesozoico e Cenozoico (Fig. 2).

Além da extensão, volume, contexto crustal e duração da colocação desses magmas, as *LIPs* podem ser caracterizadas pela idade, sendo os *greenstone belts* toleíticos-komatiíticos classificados como *LIPs* arqueanas; sistema de alimentação (*plumbing system*) de *LIPs* erodidas, caracterizado por diques, soleiras, caldeiras, intrusões acamadas ou batólitos, correspondem às *LIPs* proterozóicas-paleozóicas; e as províncias basálticas continentais, margens vulcânicas rifteadas, grandes províncias ígneas ácidas e platôs oceânicos, representantes das *LIPs* mesozoicas e cenozoicas (Bryan and Ernest, 2008).

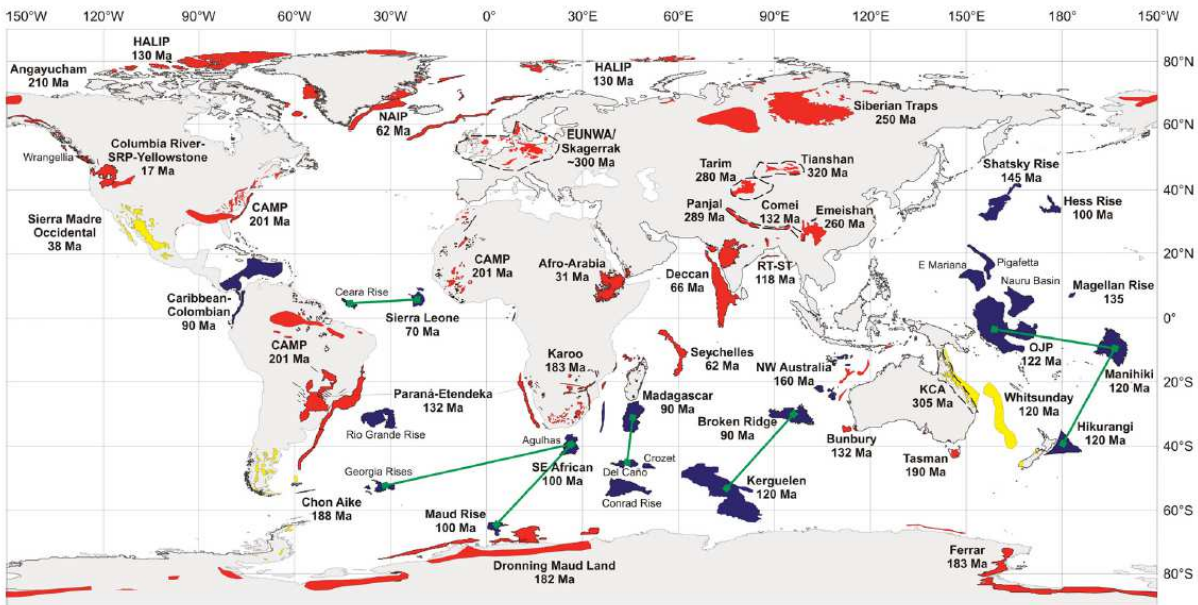


Fig. 2: Distribuição global das grandes províncias ígneas (*LIPs*) de acordo com a configuração do *Pangea* há cerca de 320 Ma. As idades indicadas referem-se ao início da fase principal ou ao primeiro pulso do magmatismo dessas *LIPs*. Linhas verdes conectam grandes províncias ígneas oceânicas separadas por espraiaimento oceânico. Abreviações: CAMP – Província Magmática do Atlântico Central; EUNWA – Européia, noroeste da África; HALIP – Grande Província Ígnea do Ártico; NAIP – Província Ígnea do Atlântico Norte; OJP – Platô Ontong Java; RT-ST – Rajmahal Traps-Sylhet Traps; SRP – Planície Snake River; KCA – Kennedy-Connors-Auburn. Legenda: áreas vermelhas - Províncias basálticas continentais/Margens vulcânicas rifteadas; áreas amarelas - *LIPs* félscicas; áreas azuis - Platôs oceânicos/Províncias basálticas oceânicas. Extraído de Bryan and Ferrari (2013).

Os eventos que originaram *LIPs* são considerados excepcionais na história da Terra devido à quantidade de magma liberado e frequência das erupções. Muitas vezes esses eventos são associados a impactos ambientais (mudanças climáticas e extinções em massa) (Coffin and Eldholm, 1994; Bryan and Ferrari, 2013) e a formação de recursos minerais e energéticos, seja como alvos exploratórios para minérios ortomagmáticos ou hidrocarbonetos (quando atuam como rochas reservatório, fonte de calor para a geração de hidrocarbonetos, constituindo selos, ou gerando estruturas) (Bryan and Ferrari, 2013; Caineng *et al.*, 2013).

Como esta tese tem como foco principal o estudo da Província Paraná-Etendeka, que representa uma importante província basáltica continental, os próximos itens focam em introduzir e sumarizar as principais características deste tipo específico de *LIP*.

2.2 PROVÍNCIAS BASÁLTICAS CONTINENTAIS

As Províncias Basálticas Continentais (PBCs) representam um tipo específico de *LIP* onde as grandes quantidades de lava são colocadas sobre crosta continental (Jerram and Widdowson, 2005). A facilidade de acesso a essas províncias faz com que essas manifestações magmáticas sejam muito investigadas. Entretanto, devido às elevadas taxas de erosão subaérea, as incertezas sobre a extensão e volume original do vulcanismo são um limitador especialmente em províncias muito antigas (Coffin and Eldholm, 1992, 1994). Uma alternativa para estimar o volume de províncias antigas que foram significativamente erodidas e que tiveram preservados apenas os componentes intrusivos (enxames de diques continentais) é considerar a razão extrusão-intrusão de 1:10 sugerida para PBCs através de estudos geofísicos (Bryan and Ferrari, 2013).

A maioria das PBCs são composicionalmente bimodais, com magmatismo predominantemente toleítico (Bryan and Ernst, 2008; Coffin and Eldholm, 1992, 1994). O estudo geoquímico detalhado das últimas décadas reconheceu nessas províncias a ocorrência de dois tipos de magma com distintos teores de TiO_2 e de elementos incompatíveis, basaltos de baixo e alto-Ti (Bellieni *et al.*, 1984; Peate *et al.*, 1992; Bryan *et al.*, 2010). Basaltos de alto-Ti são moderadamente alcalinos enquanto que basaltos de baixo-Ti são de composição toleítica.

Nas últimas décadas, o estudo de modelos e processos associados à colocação de magma, a caracterização de fácies dos depósitos vulcânicos e associação e arquitetura de fácies em PBCs deslocaram o foco da investigação da evolução, tradicionalmente geoquímica e geocronológica, e mudaram a concepção de que estas são sucessões basálticas monótonas com uma estratigrafia do *tipo layer cake* (Single and Jerram, 2004; Jerram and Widdowson, 2005). No estudo de sucessões vulcânicas, Single and Jerram (2004) adotaram um esquema de intrafácies para descrever as variações litológicas internas dos derrames, que são equivalentes às litofácies utilizadas tanto na estratigrafia de sucessões sedimentares e vulcânicas. No campo da vulcanologia, litofácies são definidas através da identificação, em escala de afloramento, de características como estrutura, textura, organização interna e geometria (McPhie *et al.*, 1993; Németh and Martin, 2007), fortemente controladas pelo estilo eruptivo e processos de colocação (Jerram, 2002).

2.3 PROVÍNCIA ÍGNEA PARANÁ-ETENDEKA

A Província Ígnea Paraná-Etendeka (PIPE), que é uma das maiores províncias basálticas continentais do mundo, tem sua porção mais significativa abrangendo a região meridional do Brasil, oriental do Paraguai e ocidental do Uruguai, e a porção norte da Argentina (Nardy *et al.*, 2008) (Fig. 3). Parte subordinada dos registros desse vulcanismo encontra-se na Namíbia, sudoeste da África (White and McKenzie, 1989). No continente Sul Americano, essa província ocorre sob a forma de enxames de diques e derrames que atingem volumes da ordem de $\sim 0,8 \times 10^6 \text{ km}^3$, ocupam uma área de $1,2 \times 10^6 \text{ km}^2$ em sequências com espessuras que podem atingir 1.530 m (Fig. 3) (Bellieni *et al.*, 1984). No lado africano, em especial na região de Etendeka, as lavas recobriram uma área aproximada de $0,78 \times 10^6 \text{ km}^2$, e foram acumuladas em uma pilha de até 1 km de espessura (Peate, 1997).

No Brasil, esses derrames ocorrem sobre a Bacia do Paraná que é uma bacia intracratônica com uma sucessão sedimentar formada essencialmente por rochas siliciclásticas relacionadas a sucessivos ciclos transgressivo-regressivo paleozóicos (Milani and Zalán, 1999; Milani and Thomaz Filho, 2000), e por rochas ígneas da PIPE. A parte mais significativa desta bacia encontra-se na região sul do Brasil, estendendo-se para o Paraguai, Argentina e Uruguai, com uma área total de cerca de 1,5 milhões de km^2 (Fig. 3). O registro estratigráfico da Bacia do Paraná inclui seis supersequências deposicionais: Rio Ivaí (Ordoviciano-Siluriano), Paraná (Devoniano), Gondwana I (Carbonífero-Eotriássico), Gondwana II (Meso a Nesotriássico), Gondwana III (Neojurássico-Eocretáceo) e Bauru (Neocretáceo) (Milani *et al.*, 2007). A supersequência Gondwana III compreende os sedimentos da Formação Botucatu e as lavas da Formação Serra Geral, as quais representam o foco desta tese.

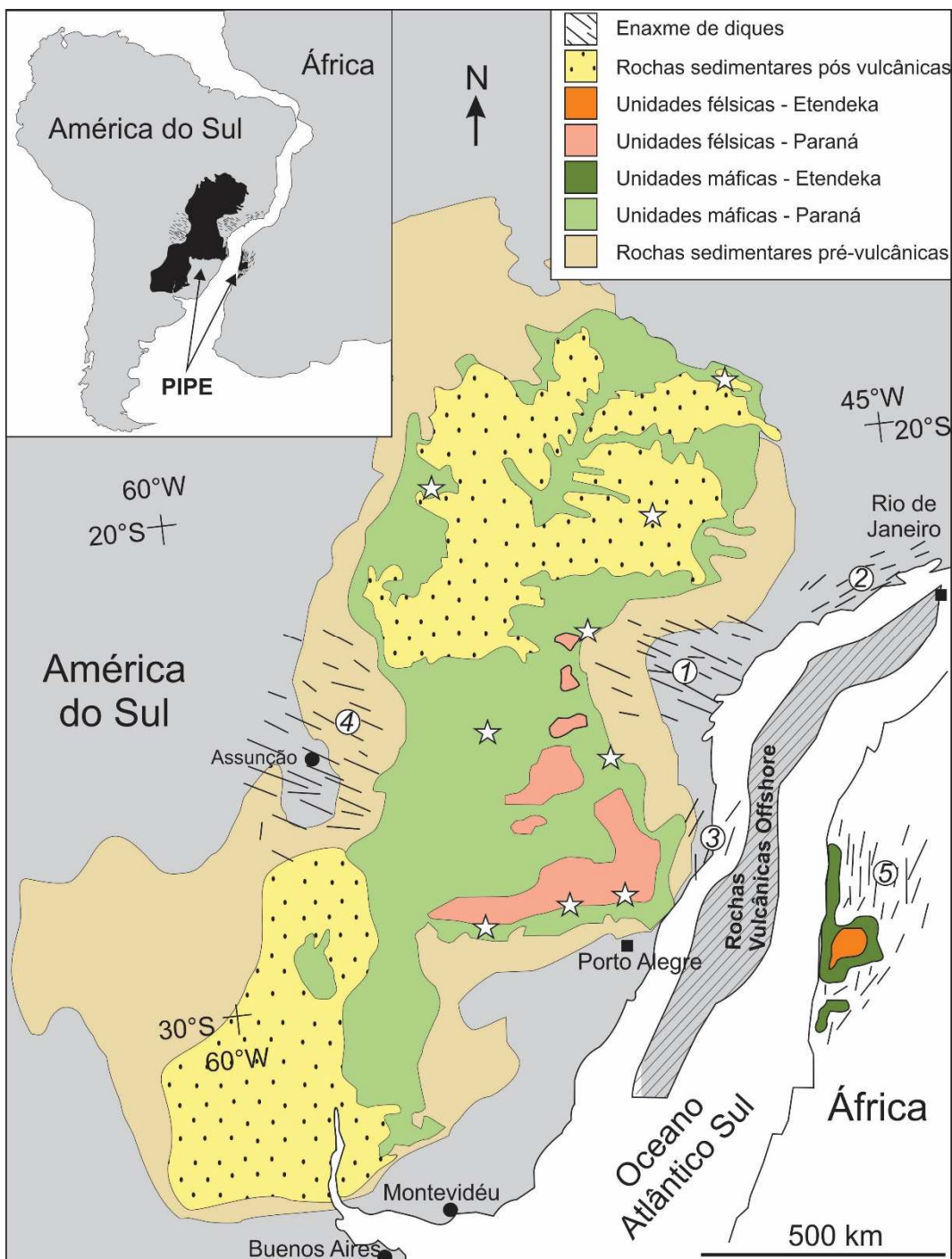


Fig. 3: Mapa geológico das principais unidades da PIPE (modificado de Peate *et al.*, 1992; Stewart *et al.*, 1996; Hawkesworth *et al.*, 2000; Rossetti *et al.*, 2018). Enxame de diques: 1 – Ponta Grossa; 2 – Santos-Rio de Janeiro; 3 – Florianópolis; 4 – Paraguai; 5 – Skeleton Coast. Estrelas representam ocorrência de *pillow* lavas e peperitos.

A formação da PIPE é atribuída a separação do supercontinente Gondwana e formação do Oceano Atlântico Sul. Datações obtidas pelo método $^{40}\text{Ar}/^{39}\text{Ar}$ mostram que a maior parte da PIPE foi formada em $\sim 135 \pm 1$ Ma e que esse magmatismo durou menos que $\sim 1,2$ Ma (Renne *et al.*, 1992; Thiede and Vasconcelos, 2010; Baksi, 2017).

Os estudos geoquímicos revelaram a existência de dois grupos de rochas quimicamente distintos, com diferentes teores de TiO_2 e elementos incompatíveis, denominados alto titânio ($TiO_2 > 2\%$) e baixo titânio ($TiO_2 < 2\%$) (Bellieni *et al.*, 1984; Mantovani *et al.*, 1985). Eses diferentes grupos geoquímicos ocupam regiões geográficas distintas; enquanto basaltos de alto- TiO_2 dominam as regiões norte, os basaltos de baixo TiO_2 prevalecem nas áreas sul da Bacia do Paraná. Peate *et al.* (1992), com base nas concentrações de Ti e elementos traços incompatíveis (Sr, Y e Zr), dividiram os magmas basálticos em seis subgrupos, sendo quatro tipos de alto- TiO_2 (Urubici, Pitanga, Paranapanema e Ribeira), e tipos de baixo TiO_2 (Gramado e Esmeralda).

A evolução dos estudos do vulcanismo na PIPE, sob a perspectiva da vulcanologia física, mostrou que as sucessões basálticas dessa província são compostas por arquiteturas externas e internas complexas (p.ex.: Waichel *et al.*, 2012; Barreto *et al.*, 2014; Rossetti *et al.*, 2014, 2018). Estudos recentes sobre os derrames da porção sul da Província Paraná-Etendeka identificaram quatro pacotes de lavas que diferem na arquitetura, estrutura interna do campo de lava, texturas e composições. Rossetti *et al.* (2018) propuseram a elevação hierárquica da Formação Serra Geral para Grupo Serra Geral e a classificação desses 4 pacotes morfológicamente diferentes como Formação Torres (derrames tabulares espessos, lobos e lava *toes*), Formação Vale do Sol (derrames tabulares do tipo *rubbly pahoehoe*), Formação Palmas (derrames tabulares, domos de lavas e sistemas complexos de conduto) e Formação Esmeralda (pequenos lobos *pahoehoe* do tipo-S). As principais características de cada pacote vulcânico são apresentadas na tabela AA.

Tab. 1: Fácies dos derrames, características físicas e petrográficas das lavas das Formações do Grupo Serra Geral (Modificado de Rossetti *et al.*, 2018).

Formação	Espessura unidade/derrame	Fácies	Característica física principal	Feições petrográficas
Esmeralda	25-300 m 0.2-3 m	Composta anastomosada	Lobos métricos com estruturas <i>pahoehoe</i> típicas: crosta inferior vesiculada, núcleo maciço, e crosta superior vesiculada	Basalto preto afírico e afanítico. Micrólitos de plagioclásio aciculares a esqueletais, augita e óxidos de ferro. Matriz vítreia.
Palmas	40-400 m ?	Tabular clássico	Derrames tabulares de dacito, riolito e obsidiana. Terminações lobadas, porções autobrechadas, camadas de vesículas e megavesículas	Textura vitrofírica, fenocristais de plagioclásio e augita, textura granofírica com intercrescimento de k-feldspato e quartzo é comum.
Vale do Sol	40-500 m 20-60 m	Tabular clássico	Lavas <i>rubbly pahoehoe</i> com geometria tabular simples. Estrutura em quatro partes: crosta inferior vesiculada, núcleo maciço, crosta vesicular coerente, superfície brechada	Basaltos andesíticos afíricos a finamente granulados, com raros fenocristais de plagioclásio. Plagioclásio de granulação fina com augita e óxido de ferro intergranular.
Torres	100-290 m 0.2-18 m	Composta anastomosada	Lobos de lava, <i>toes</i> , e lobos tabulares. Estruturas <i>pahoehoe</i> típicas: crosta inferior com vesículas do tipo <i>pipe</i> , núcleo maciço, e crosta superior vesiculada.	Basaltos de granulação média e com fenocristais de plagioclásio ou olivina. Porfiríticos a glomeroporfiríticos, com plagioclásio, augita, óxidos de ferro ± olivina.

Derrames *ponded*, também identificados na PIPE, (p.ex.: Waichel *et al.*, 2012; Barreto *et al.*, 2014; Rossetti *et al.*, 2014; Moraes and Seer, 2017) podem ter até 50 m de espessura, são formadas pelo confinamento da lava em áreas de interduna, e correspondem aos derrames iniciais em algumas porções da Sinclinal de Torres (Waichel *et al.*, 2012; Barreto *et al.*, 2014; Rossetti *et al.*, 2014).

Pillow lavas e peperitos associados a sedimentos com água também foram descritos nesta província evidenciando a presença de ambiente úmido como rios e lagos efêmeros formados em regiões de paleobaixos (p. ex. Marques Filho *et al.*, 1981; Ferreira, 1985; Mano, 1987; Waichel *et al.*, 2007; Moraes and Seer, 2017), em diferentes partes da PIPE. As *pillow* lavas descritas nesta província variam de 0,2 a 2 m de largura e contém vesículas variando de 1 a 5 mm. Algumas *pillows* podem ter fraturas radiais e margens resfriadas de 0,5 a 2,5 cm de espessura. O material *interpillow* é composto por sedimentos arenoargilosos, flúvio lacustres e hialoclastitos. Os peperitos identificados na região oeste do Paraná, na Sinclinal de Torres e na região de Araguari (MG) formam pacotes de até 4 m de espessura, estendem-se por até 80 m e são compostos por clastos juvenis fluidais formados em regime dúctil (p. ex.: Waichel *et al.*, 2007; Costa, 2015).

2.4 PROVÍNCIA ÍGNEA DO ATLÂNTICO NORTE

A Província Ígnea do Atlântico Norte (*North Atlantic Igneous Province - NAIP*) é uma Província Basáltica Continental localizada na região do Atlântico Norte, relacionada à abertura do Oceano Atlântico Norte por volta de 62-61 Ma (p.ex. Saunders *et al.*, 1997; Jerram and Widdowson, 2005; Hansen *et al.*, 2009). As lavas da NAIP cobrem uma área de $1,3 \times 10^6$ km², volumes de $1,8 \times 10^6$ km³ (Eldholm and Grue, 1994), e seus remanescentes estão agora expostos em afloramentos no Leste e Oeste da Groelândia, na Província ígnea Britânica (British Paleogene Igneous Province – BPIP; p.ex. Ilhas Hebridas Interiores da Escócia, e Antrim na Irlanda do Norte), e Ilhas Faroe (Fig. 4) (Saunders *et al.*, 1997; Jerram and Widdowson, 2005). Significativas quantidades de sequencias vulcânicas são encontradas em regiões *offshore*, sob a forma de diversas fácies sísmicas nas margens vulcânicas da Eurásia e Groelândia (Saunders *et al.*, 1997; Planke *et al.*, 2000; Abdelmalak *et al.*, 2019).

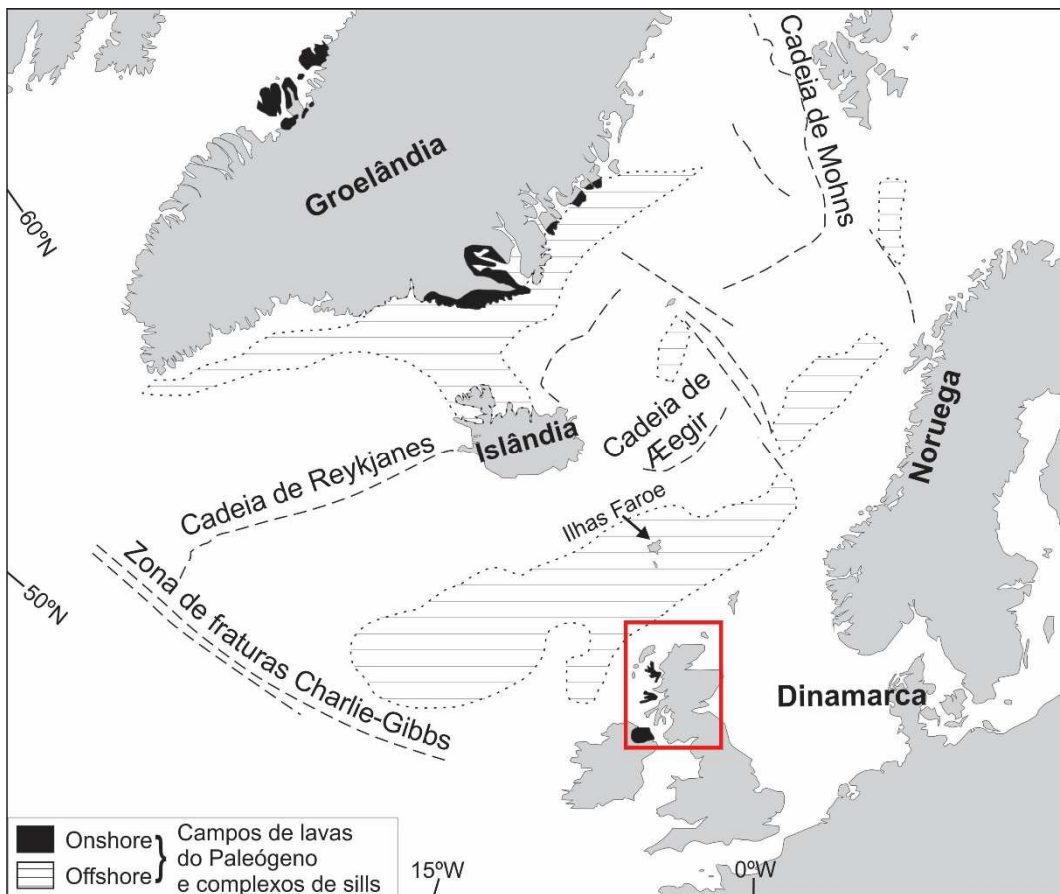


Fig. 4: Mapa de localização da Província do Atlântico Norte. Quadrado vermelho indica a localização da Província Ígnea Britânica. Modificado de Ganerød *et al.* (2008).

Basaltos toleíticos são os principais produtos do vulcanismo de NAIP, muito embora basaltos alcalinos sejam comuns. Subordinadamente, diferentes tipos de rochas podem ser encontrados nas porções continentais e ao longo das margens rifteadas (Saunders *et al.*, 1997). Uma grande variedade de morfologias de lavas subaéreas foi descrita nesta província, como por exemplo, derrames tabulares, *pahoehoe* compostas, com subordinados derrames do tipo a'ā (p.ex. Kent *et al.*, 1998; Jerram 2002; Single and Jerram, 2004; Jerram and Widdowson, 2005; Williamson and Bell, 2012). Apesar da dominância de produtos formados em ambiente subaéreo, *pillow* lavas e hialoclastitos são frequentemente encontrados nas porções basais da estratigrafia (p.ex. Jerram and Widdowson, 2005; Williamson and Bell, 2012), evidenciando que os primeiros derrames interagiram com corpos aquosos em algumas porções de NAIP. Em alguns casos, esta interação resultou em significantes fácies de deltas de lava (Jerram *et al.*, 2009; Wright *et al.*, 2012; Abdelmalak *et al.*, 2018).

O Campo de Lavas de Mull (Mull Lava Field – MLF), preservadas no oeste da Escócia na Ilha de Mull, compõe a BPIP, e representa uma das áreas contempladas por este estudo. Este campo de lavas tem entre 1800 a 2200 m de espessura (p.ex. Walker, 1970), e foram depositadas em um intervalo de 2.52 ± 0.36 Ma (Chambers and Pringle, 2001). Essas lavas cobrem uma área de cerca de 840 km^2 (Emeleus, 1991) e sua estratigrafia inclui as Formações Staffa (mais antiga), Mull Plateau Lava, e Mull Central Lava (mais nova) (Emeleus and Bell, 2005). Muitos estudos com foco em geoquímica e petrologia das lavas de Mull mostram uma predominância de basaltos com composições transicionais alcalinas e seus derivados, e subordinados basaltos toleíticos e seus derivados (Bailey *et al.*, 1924; Beckinsale *et al.*, 1978; Kerr, 1995a, 1995b; Kerr *et al.*, 1999; Morrison *et al.*, 1985; Thompson *et al.*, 1986).

A sucessão vulcânica do MLF é predominantemente formada por derrames subaéreos relacionados a erupções fissurais, com hialoclastitos e *pillow* lavas ocorrendo na porção basal da Formação Staffa. Localmente, significantes atividades eruptivas deram origem a depósitos de *spatter* e tefra, e ignimbritos composicionalmente mais evoluídos, que também compõem o MLF (Williamson and Bell, 2012).

2.5 BACIA MIDLAND VALLEY NA ESCÓCIA

A Bacia *Midland Valley* na Escócia (*Midland Valley Basin – MVB*) é uma bacia do Paleozóico Inferior preenchida por uma variedade de rochas sedimentares, vulcânicas e plutônicas. Esta bacia é limitada a norte pela falha *Highland Boundary* e a sul pela falha *Southern Uplands* (Fig. 5). O fechamento e sutura do Oceano Iapetus no sul da Escócia por volta de 420 Ma originou as Montanhas *Caledonian*. Essa cadeia de montanhas foi posteriormente erodida e deformada simultaneamente à formação e desenvolvimento da Bacia *Midland Valley* (Oliver *et al.*, 2008).

A área contemplada por esta tese está localizada na porção norte da MVB e é dominada por sedimentos do Supergrupo Lower Old Red Sandstone (ORS). Esta sucessão é caracterizada por seis Grupos denominados Stonehaven, Dunnottar, Crawton, Arbuthnott, Garvoch e Strathmore, com idades desde o Devoniano ao Siluriano Médio. O ORS é composto predominantemente por conglomerados, arenitos e lamitos, com rochas vulcânicas intercaladas (Hole *et al.*, 2013). A Formação Vulcânica Montrose (MVF), que integra o Grupo Arbuthnott, é dominado por basaltos e basaltos

andesíticos (Thirlwall, 1981), e aflora desde o Norte de Crawton até Arbroath. Não há dados de idades absolutas disponíveis para MVF, mas esses basaltos devem ser mais novos que $415,5 \pm 5,8$ Ma (idade encontrada para as rochas da Formação vulcânica Crawton que ocorrem abaixo) (Thirlwall, 1988).

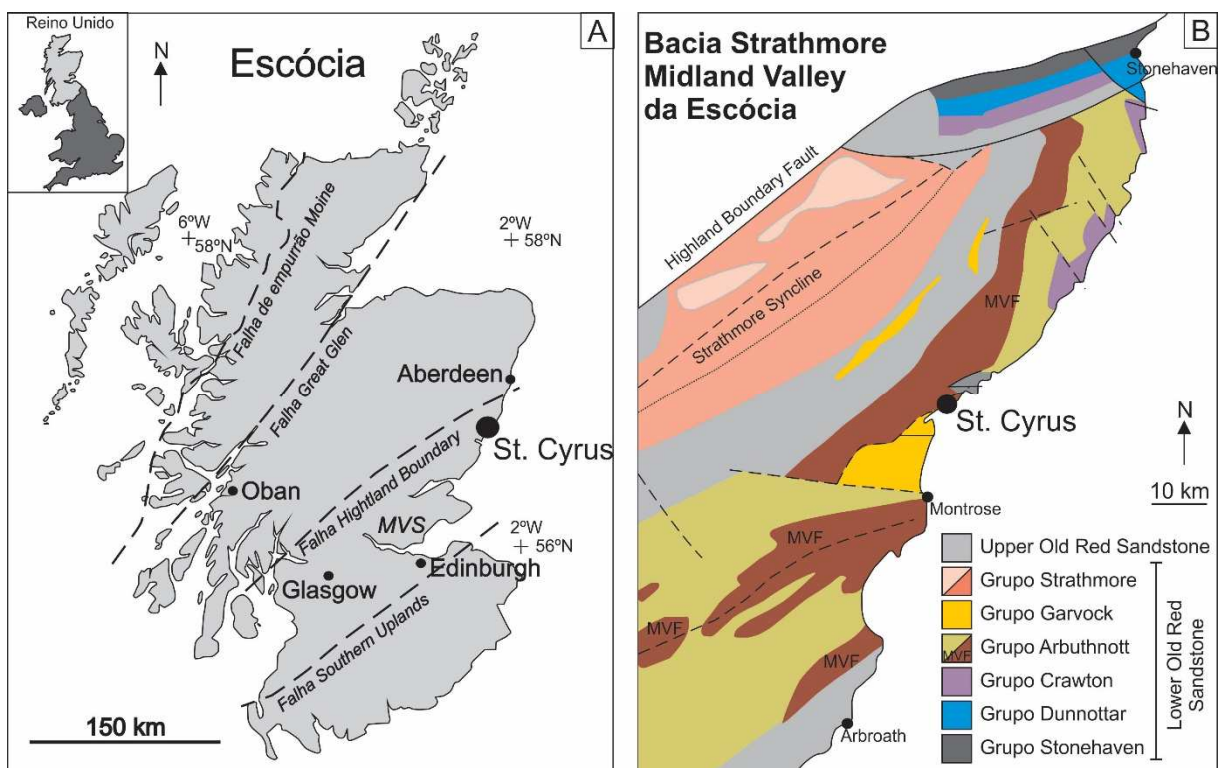


Fig. 5: Mapa de localização de St Cyrus. A) Mapa da Escócia com as principais falhas marcadas; B) Mapa geológico da porção oeste da Bacia Midland Valley (área entre Stonehaven e Arbroath). Modificado de Hole *et al.* (2013) e Rawcliffe (2016). MVF = Formação Vulcânica Montrose (em marrom escuro no mapa B), o qual está incluído no Grupo Arbuthnott.

A área de estudo, localizada no litoral de St. Cyrus, é composta por uma sucessão de lavas e sedimentos intercalados da MVF (Hole *et al.*, 2013). Nesta área, túneis de lava alimentaram o campo de lavas *pahoehoe* resultado em lobos de até 5 m de espessura. Hole *et al.* (2013) descreveram ocorrências localizadas de depósitos de *spatter* intercalados com finas lentes de sedimentos e sugerem ocorrência de atividade explosiva em uma superfície localizada, potencialmente favorecida por interação da lava com sedimento saturado em água localizado próximo a superfície. Depósitos similares foram descritos em pseudo-crateras (*rootless cone*) na Islândia (Hamilton *et al.*, 2017), sugerindo que os depósitos descritos em St Cyrus possam ser produtos de pseudo-crateras.

CAPÍTULO III

Neste capítulo são apresentados, de forma sintética, as principais características de depósitos vulcânicos relacionados à colocação de lavas em ambiente subaéreo, subaquoso e os produtos de interação entre lava e sedimento descritos em Províncias Basálticas Continentais.

3. ESTADO DA ARTE

3.1 DEPÓSITOS VULCÂNICOS DAS PROVÍNCIAS BASÁLTICAS CONTINENTAIS

Os depósitos vulcânicos apresentam morfologias variadas que podem refletir tanto o ambiente de deposição (ambiente subaéreo ou subaquoso) quanto o estilo eruptivo e características da lava expelida (p.ex: viscosidade e temperatura da lava, taxa de efusão, sustentação da taxa de efusão). Os derrames que compõem PBCs são predominantemente formados por campos de lava *pahoehoe*, *a'a* e *rubbly* (Self *et al.*, 1996; Brown *et al.*, 2011; Bryan and Ferrari, 2013; Duraiswami *et al.*, 2014; Rossetti *et al.*, 2014, 2018). Entretanto, outras morfologias mais complexas (p.ex.: lava deltas, lavas almofadadas - *pillow lavas*), resultantes da interação da lava com água (oceanos ou lagos), podem estar presentes nessas províncias magmáticas (p. ex.: Larsen *et al.*, 2006). Os parâmetros que controlam as morfologias dos derrames, os diferentes tipos de derrames, bem como feições que evidenciam a interação entre lava e água serão apresentados a seguir.

3.1.1. Derrames subaéreos

Lavas formadas em ambiente subaéreo podem apresentar uma série de feições de superfície que permitem classificar diferentes morfotipos. Os membros finais do espectro de morfologias são representados por derrames de lavas *pahoehoe* e *a'a* (Macdonald, 1953; Rowland and Walker, 1990) (Fig. 6). Derrames *pahoehoe* têm superfícies lisas, onduladas ou em cordas, enquanto que os derrames *a'a* possuem superfícies brechadas. Um derrame *pahoehoe* pode eventualmente evoluir para derrames *a'a* (Macdonald, 1953) e vice-versa (Hon *et al.*, 2003). Essa transição é controlada principalmente por viscosidade e taxa de deformação por cisalhamento (que pode estar relacionado à velocidade do derrame) (Peterson and Tilling, 1980; Loock *et al.*, 2010). A relação entre estes parâmetros pode ser demonstrada

qualitativamente por um gráfico onde os campos de derrames *pahoehoe* e *a'ā* são separados por uma zona de transição (TTZ) (Fig. 6) (Peterson and Tilling, 1980; Loock *et al.*, 2010).



Fig. 6: Os membros finais do espectro de morfologias de lavas subaéreas. A) Lobo *pahoehoe* ativo com superfície lisa e cordada. Foto de Bernard M.Gunn, retirada de http://www.discoverlife.org/IM/I_AMC/0107/mx/; B) Derrame *a'ā* sendo colocado sobre campo de lavas *pahoehoe*. Extraído de <http://planet-terre.ens-lyon.fr/image-de-la-semaine/Img228-2008-03-17.xml>.

Derrames do tipo *pahoehoe* comportam-se como um líquido newtoniano e são formados por lavas de baixa viscosidade colocadas sob uma baixa taxa de deformação por cisalhamento, enquanto que os derrames *a'ā* resultam de lavas de alta viscosidade colocadas a uma alta taxa de deformação por cisalhamento (Loock *et al.*, 2010; Gregg, 2017). O aumento da viscosidade ou da taxa de deformação por

cisalhamento pode levar um sistema de comportamento newtoniano transformar-se em um sistema de comportamento tipo Bingham, cruzando a TTZ e, consequentemente, gerando lavas do tipo *a'ā* (Peterson and Tilling, 1980; Loock *et al.*, 2010) (Fig. 7). Um exemplo dessa transição pode ser observada no caso em que uma lava *pahoehoe*, colocada sob taxa de deformação por cisalhamento constante, passa para *a'ā* devido ao aumento da sua viscosidade (pela cristalização, resfriamento e perda de gás, conteúdo de bolhas). Similarmente, se a viscosidade se mantiver relativamente constante, o aumento das taxas de deformação por cisalhamento (pelo avanço da lava em um terreno inclinado ou irregular, por exemplo) pode levar a transição de lavas *pahoehoe* para *a'ā*. Nos casos em que essa transição for gerada por um incremento da taxa de deformação por cisalhamento, a lava pode voltar a se comportar como *pahoehoe* quando a taxa de deformação por cisalhamento decrescer. Isso ocorre com lavas *pahoehoe* que se transformam em *a'ā* conforme o derrame é colocado sobre um terreno íngreme e então volta para *pahoehoe* quando as taxas de deformação por cisalhamento diminuem conforme a lava flui em uma superfície plana, por exemplo (Peterson and Tilling, 1980; Rowland and Walker, 1990; Hon *et al.*, 2003). Nos casos onde a transição de *pahoehoe* para *a'ā* é causada por mudanças na viscosidade, a morfologia não se reverterá (Peterson and Tilling, 1980). No caso onde essa transição se dá de forma progressiva, lavas transicionais podem ser formadas (Loock *et al.*, 2010).

Os tipos morfológicos de lavas básicas se diferenciam especialmente por feições de superfície, porém possuem também diferenças na sua estruturação interna (Macdonald, 1953; Duraiswami *et al.*, 2014), esta última, útil no reconhecimento de derrames cuja superfície não é observada, seja por não ter sido amostrada ou por ter sido erodida, como podem ser os casos de amostragem em poços exploratórios ou de derrames de terrenos antigos (Macdonald, 1953; Harris *et al.*, 2017). As características gerais dos membros finais, bem como de alguns derrames transicionais são descritas a seguir.

Derrames *pahoehoe* - Derrames *pahoehoe* são reconhecidos em campo por apresentarem superfície lisa, com ondas amplas, ou com cordas (Macdonald, 1953) (Fig. 6A) e estrutura interna composta por crosta superior vesiculada, núcleo e zona basal vesiculada (Aubele *et al.*, 1988). Tanto as características de superfície quanto à estruturação interna de derrames *pahoehoe* sugerem espessamento do lobo por processo de inflação (Self *et al.*, 1996, 1998).

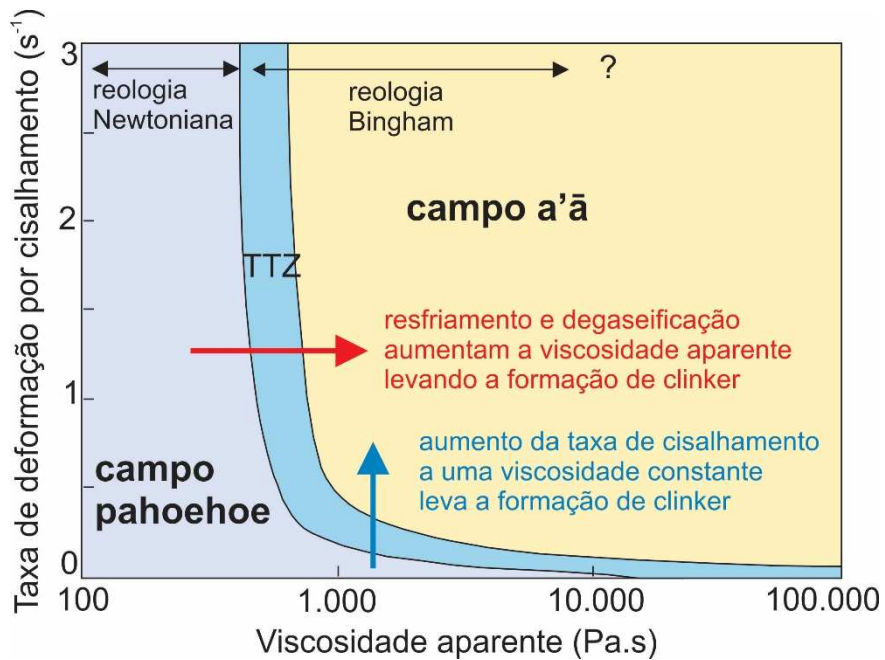


Fig. 7: Diagrama da taxa de deformação por cisalhamento vs. viscosidade Newtoniana aparente, mostrando as relações aproximadas dos campos de estabilidade para as lavas *pahoehoe* havaianas e os fluxos *a'a*, e os limites aproximados da zona de transição (TTZ). Modificado de Loock *et al.* (2010).

A inflação ou crescimento endógeno é um mecanismo contínuo no qual lobos, inicialmente com poucos centímetros de espessura, inflam para dimensões maiores que podem alcançar algumas dezenas de metros em um período de tempo que pode levar dias, meses ou até anos (Self *et al.*, 1996, 1998; Hon *et al.*, 2003). Num estágio inicial, bolhas são inicialmente retidas nas crostas superior e inferior (Fig. 8A). Vesículas esféricas ficam retidas no material visco-elástico da base da crosta superior formando uma zona horizontal de vesículas (HVZ) enquanto que vesículas do tipo *pipe* se formam na crosta inferior. Após a estagnação, diápiros de vesículas residuais formam cilindros verticais e lençóis horizontais de vesículas dentro do núcleo de lava que está começando a cristalizar (Fig. 8C). O resultado da história de colocação de um derrame fica registrado na rocha e é evidenciado pela distribuição das vesículas e padrão de juntas que nele se encontram (Fig. 8D) (Self *et al.*, 1996). Assim, a crosta superior de derrames *pahoehoe* inflados que compreende, quase que invariavelmente, 40-60% do total da espessura do derrame é caracterizada por bandamento de vesículas, bolhas de gás (*gas blister*) e fraturas causadas por inflação (*inflation clefs*) (Self *et al.*, 1998); enquanto que o núcleo maciço poderá ter algumas juntas e poderá conter lençóis de vesículas horizontais e cilindros de vesículas. A zona

basal vesicular será geralmente marcada por vesículas do tipo *pipe* (Philpotts and Lewis, 1987; Walker, 1987).

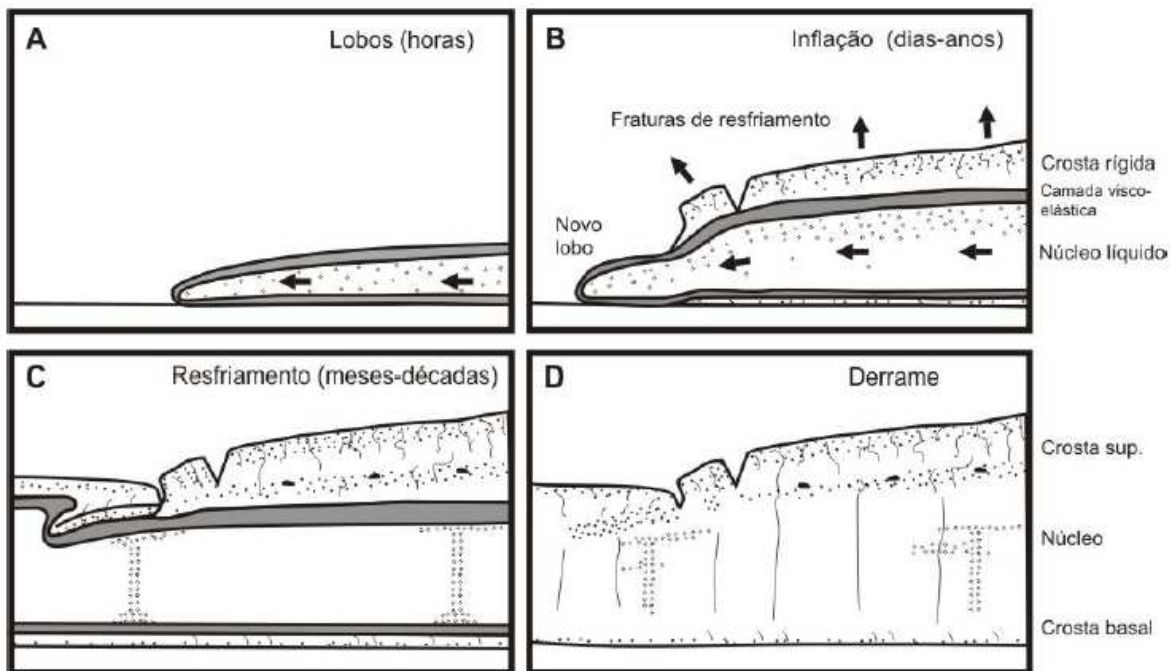


Fig. 8: Seção esquemática de colocação de um derrame de lava *pahoehoe* por inflação. Escala vertical varia de 1 a 5 m para derrames havaianos a 5 a 50 m para derrames do CRB. Extraído do de (Waichel *et al.*, 2006).

Os derrames *pahoehoe*, como dito anteriormente, são formados por lavas de baixa viscosidade e sob baixas taxas de deformação por cisalhamento (Peterson and Tilling, 1980; Loock *et al.*, 2010; Gregg, 2017) (Fig. 7) e, em geral, são associados a fluxos com taxas de efusão baixas e sustentadas (Rowland and Walker, 1990). As taxas de efusão calculadas para lavas *pahoehoe* de área vulcânicas ativas, como no caso dos derrames do vulcão Etna de 1975, bem como para registros históricos de erupções dos vulcões Kilauea e Mauna Loa, mostram valores que variam de 2 a 10 x $10^{-3} \text{ m}^3 \text{ s}^{-1}$, respectivamente (Pinkerton and Sparks, 1976; Rowland and Walker, 1990).

Derrames a'ā - Derrames a'ā são caracterizados por um núcleo maciço envolto por camada brechada composta por fragmentos *clinker* (Macdonald, 1953) (Fig. 9). *Clinker* é um termo utilizado para descrever fragmentos maciços ou escoriáceos comumente associados a derrames a'ā (Loock *et al.*, 2010). Esses fragmentos são extremamente rugosos, irregulares e espinhosos, podem ter tamanho variado e estar

soltos ou soldados ao derrame. *Clinkers* formam-se como resultado da autobrechação da camada vesicular superior, devido ao aumento da taxa de deformação por cisalhamento e/ou aumento da viscosidade aparente, e são transportados para a frente de derrame e incorporados a base por movimentação do tipo *caterpillar* (Macdonald, 1953; Loock *et al.*, 2010; Gregg, 2017). Em geral, as camadas brechadas superiores são mais espessas que as camadas brechadas inferiores e quando somadas essas camadas compõem cerca de 15 a 65% do volume total do derrame. O núcleo desse derrame é maciço, pode conter juntas e algumas vesículas (Macdonald, 1953; Duraiswami *et al.*, 2014). As vesículas em derrames *a'ā* são distribuídas irregularmente e comumente estão muito estiradas (Macdonald, 1953). Zonas vesiculadas também podem ocorrer no interior do derrame segundo um arranjo vertical ou horizontal (Gregg, 2017).

Esses derrames, conforme dito anteriormente, são formados sob altas taxas de deformação por cisalhamento e alta viscosidade (Peterson and Tilling, 1980; Loock *et al.*, 2010) e estão associados a taxas de efusão elevadas (maiores que $5\text{-}10 \text{ m}^3 \text{ s}^{-1}$) (Rowland and Walker, 1990). Alguns autores afirmam que derrames *a'ā* não poderiam viajar longas distâncias, mesmo sob forte canalização e ocorreriam associados apenas a regiões próximas à cratera ou fissura (Macdonald, 1953; Brown *et al.*, 2011). Entretanto, estudos dos derrames da Província do Deccan mostram que esse tipo de derrame pode formar-se em regiões distais em províncias basálticas continentais como resultado do aumento repentino do aporte de lava que atingiram porções distais do campo de lava (Duraiswami *et al.*, 2014).

Derrames transicionais - Derrames do tipo *platy-ridge*, *slabby pahoehoe*, *rubbly pahoehoe* e lavas tipo pasta de dente correspondem aos derrames transicionais, (Harris *et al.*, 2017). Estes derrames são produto da transição progressiva de derrames *pahoehoe* para *a'ā* (Loock *et al.*, 2010) e podem preservar características gradacionais entre os dois tipos (Peterson and Tilling, 1980). Feições típicas de derrames *a'ā*, como crosta superior rugosa e fragmentada, ou típicas de derrames *pahoehoe*, como por exemplo, superfícies lisas, com cordas, crosta basal com vesículas do tipo *pipe* podem estar presentes em um derrame transicional. A distinção entre os diferentes tipos de derrames transicionais, em geral, é feita pelo tamanho dos blocos da crosta superior e pelas características de superfície desses fragmentos (áspera, lisa, com cordas). O tamanho dos blocos parece estar relacionado às taxas

de efusão, onde blocos pequenos são produzidos por faturamento rápido devido às altas taxas de efusão, enquanto que baixas taxas de efusão levam a fragmentação limitada que dá origem a grandes placas de crosta (Anderson *et al.*, 1998).

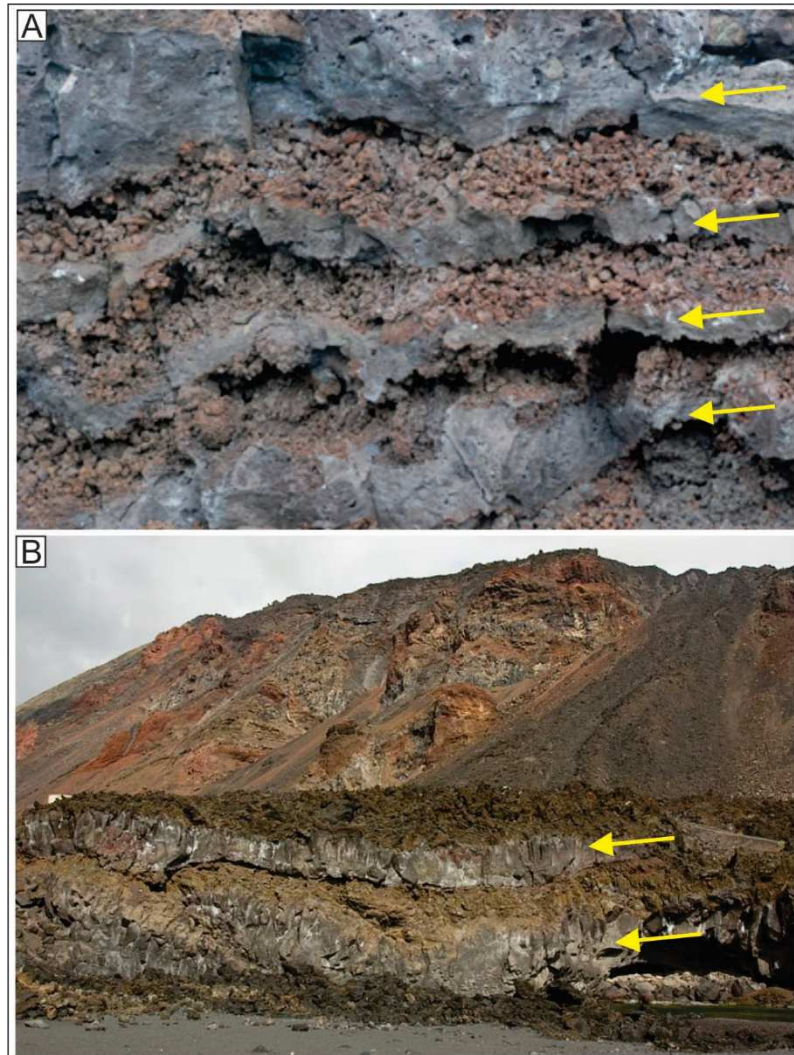


Fig. 9: Afloramentos de derrames a'a com núcleo maciço (setas amarelas) e brechas de base e topo. A) Empilhamento de derrames a'a mostrando características do núcleo denso (10-20 cm de espessura) e margens brechadas. Extraído de Cashman and Mangan, 2014; B) Afloramento de lavas a'a de La Palma (Ilhas Canárias). Extraído de <https://www.sandatlas.org/types-lava-flows/>.

O derrame transicional cuja crosta superior consiste de placas *pahoehoe* planas separadas por uma elevação composta por blocos da superfície *pahoehoe* quebrada é denominado *platy-ridge*. Essas placas podem ter de 30 a 100 m de diâmetro enquanto que as elevações têm de 7 a 12 m de largura e 2 a 5 m de altura (Stevenson *et al.*, 2012). O relevo desses blocos é, em geral, plano, mas fraturas

profundas e estreitas estão presentes (Fig. 10). Derrames *platy-ridge* são formados por inflação instável de *pahoehoe*s tabulares de crosta frágil.

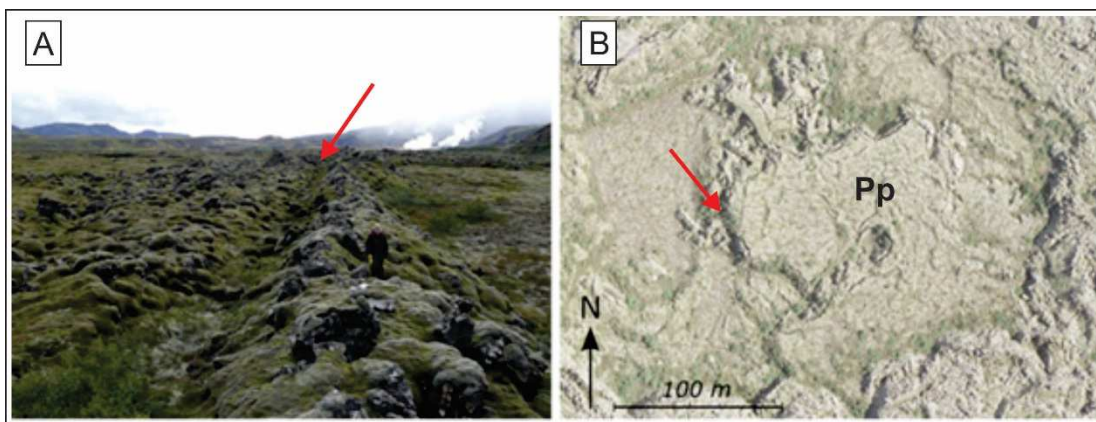


Fig. 10: Lavas *platy-ridge*. (a) margem de lavas *platy-ridge* definidas por uma profunda ranhura (seta vermelha) limitando esse tipo de derrame. (b) Imagem aérea onde é possível observar lava *platy-ridge* onde a placa *pahoehoe* plana (Pp) é limitada por ranhuras de aspecto áspido e rugoso (seta vermelha). Extraído de Stevenson *et al.* (2012).

Outro tipo de derrame transicional, os derrames *slabby pahoehoe*, exibem características predominantes de lavas *pahoehoe*, mas seu topo é marcado por placas quebradas e espaçadas de 2 a 3 m de diâmetro (Peterson and Tilling, 1980; Duraiswami *et al.*, 2014). Essas placas geralmente têm uma superfície lisa ou cordada e uma superfície mais áspera e espinhosa (correspondente a superfície inferior da crosta superior) (Macdonald, 1953; Peterson and Tilling, 1980). Esse tipo de derrame ocorre quando lavas relativamente pouco viscosas são colocadas sob altas taxas de tensão. A quebra da crosta superior ocorre a partir do centro do derrame e é comumente causada por altas taxas de tensão dadas pela chegada repentina de lava, geralmente, em lobos do *pahoehoe* mais espessos (Keszthelyi, 2002).

Os derrames *rubbly pahoehoe* (Fig. 11A), são um tipo de derrame transicional que em seção, tem quatro partes estruturais, passando de autobrecha *rubbly* de topo para crosta superior coerente e vesiculada a núcleo denso com juntas e crosta inferior vesiculada. A autobrecha *rubbly* refere-se a pedaços quebrados de lobos *pahoehoe* que possuem margens vítreas em ambos os lados (Keszthelyi, 2002). Esses pedaços quebrados podem ser irregulares e vesiculados, podem estar soltos ou soldados e terem tamanhos variando de <10 cm a >1 m (Stevenson *et al.*, 2012). Embora esse tipo de derrame tenha características de derrames *a'a*, eles apresentam base similar

a de derrames *pahoehoe* e características internas que indicam inflação (Keszthelyi, 2002). Os três tipos de derrames citados anteriormente são interpretados como sendo formados por processo de transferência endógena de lava, inflação e autobrechação devido à mudança do regime de estresse durante a fase terminal do derrame (Keszthelyi *et al.*, 2004; Guilbaud *et al.*, 2005; Duraiswami *et al.*, 2014).

As lavas tipo “pasta de dente” (*toothpaste lava*, *rough pahoehoe* ou *spiny pahoehoe* - (Peterson and Tilling, 1980; Rowland and Walker, 1987, 1990) são línguas de lavas viscosas que foram comprimidas para fora do derrame através da abertura da crosta localizadas próxima ou na porção inferior do final do derrame (Macdonald, 1953). Elas geralmente mostram feições cordadas formadas em lavas *pahoehoe* típicas, mas com superfície granulada e espinhosa de lavas *a'a* que são marcas de crescimento e de vibração devido à fricção contra os lados da abertura (Macdonald, 1953; Rowland and Walker, 1990) (Fig. 11B). Estes derrames transicionais são originados quando a lava adquire viscosidade típica de derrames *a'a* mas são submetidas a baixas taxas de efusão (Rowland and Walker, 1990).

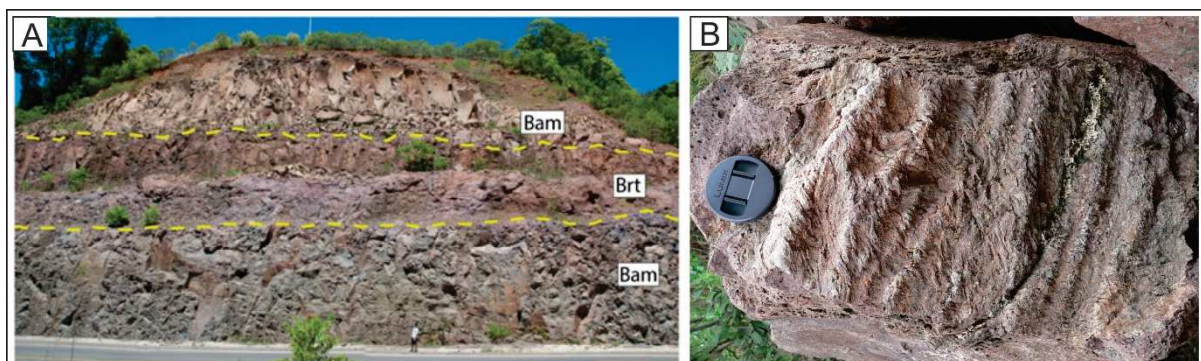


Fig. 11: Afloramento de derrame *rubbly pahoehoe* (A) e derrame do tipo pasta de dente (B). A) Contato entre dois derrames *rubbly pahoehoe*. Abreviações: Bam - basalto maciço hipocristalino e afírico; Brt – brecha de topo de derrame. Extraído de Barreto *et al.* (2014). B) superfície de derrame do tipo pasta de dente. Extraído de Waichel *et al.* (2006).

Muito embora muitos autores (p.ex.: Peterson and Tilling, 1980; Keszthelyi, 2002; Duraiswami *et al.*, 2014) classifiquem os derrames descritos anteriormente (*platy-ridge*, *slabby pahoehoe*, *rubbly pahoehoe*, lavas tipo pasta de dente) como transicionais, Harris *et al.* (2017) criaram um esquema de classificação baseado em elementos descritivos onde classificam estes derrames como sub-tipos de derrames *pahoehoe* e *a'a*. No esquema proposto por esses autores, lavas tipo pasta de dente,

slabby pahoehoe, *blocky* e *shelly* são consideradas subtipos de derrames *pahoehoe*, enquanto que lavas *rubbly*, *clinkery*, a'ā de granulação fina, média ou grossa seriam subtipos de lavas a'ā.

3.1.2 Derrames subaquosos e hialoclastitos

Derrames subaquosos são formados pela colocação de lavas em ambiente subaquoso e, portanto, abundantes ao longo de cadeias meso-oceânicas, montes submarinos e ilhas oceânicas vulcânicas. Assim como derrames subaéreos, os principais tipos de derrames subaquosos – lavas em almofada (*pillow lavas*), lavas lobadas e lavas tabulares – apresentam características morfológicas distintivas que refletem o ambiente deposicional e a taxa de efusão (Gregg and Fink, 2000; White et al. 2015). *Pillows* formam-se sob baixa taxa de efusão, enquanto que as lavas tabulares são produto das taxas mais elevadas dentre os três tipos (Fig. 12). Hialoclastitos são depósitos formados pelo resfriamento abrupto de lava em contato com água, resultado em uma brecha composta por clastos vítreos e fragmentos vulcânicos que podem estar alterados (p.ex. argilominerais e zeólita) (Watton et al., 2013). As características gerais dos três principais tipos de derrames subaquosos e hialoclastitos serão descritos a seguir, com maior enfoque nos derrames do tipo *pillow* (presentes na área de estudo).

Derrames tabulares – Os derrames tabulares têm interior completamente interconectado e sua superfície não apresenta nenhuma indicação de lobos individualizados (Fig. 12). Sua superfície pode ser lisa, apresentar feições cordadas ou lineares (indicando a direção do fluxo de lava), ou ser uma mistura destas feições (*jumbled surface*) (White et al., 2015). Este último tipo de superfície (*jumbled*) é interpretado como produto da contínua deformação de superfícies dobradas ou com feições lineares, resultando em fragmentação da crosta (Gregg and Fink, 1995). Derrames tabulares são formados sob altas taxas de efusão e são comumente restritos às regiões próximas da cratera ou fratura eruptiva e áreas onde o derrame é confinado, por exemplo, por barreiras topográficas ou canalização de derrames (Gregg and Fink, 1995; Soule et al., 2005).

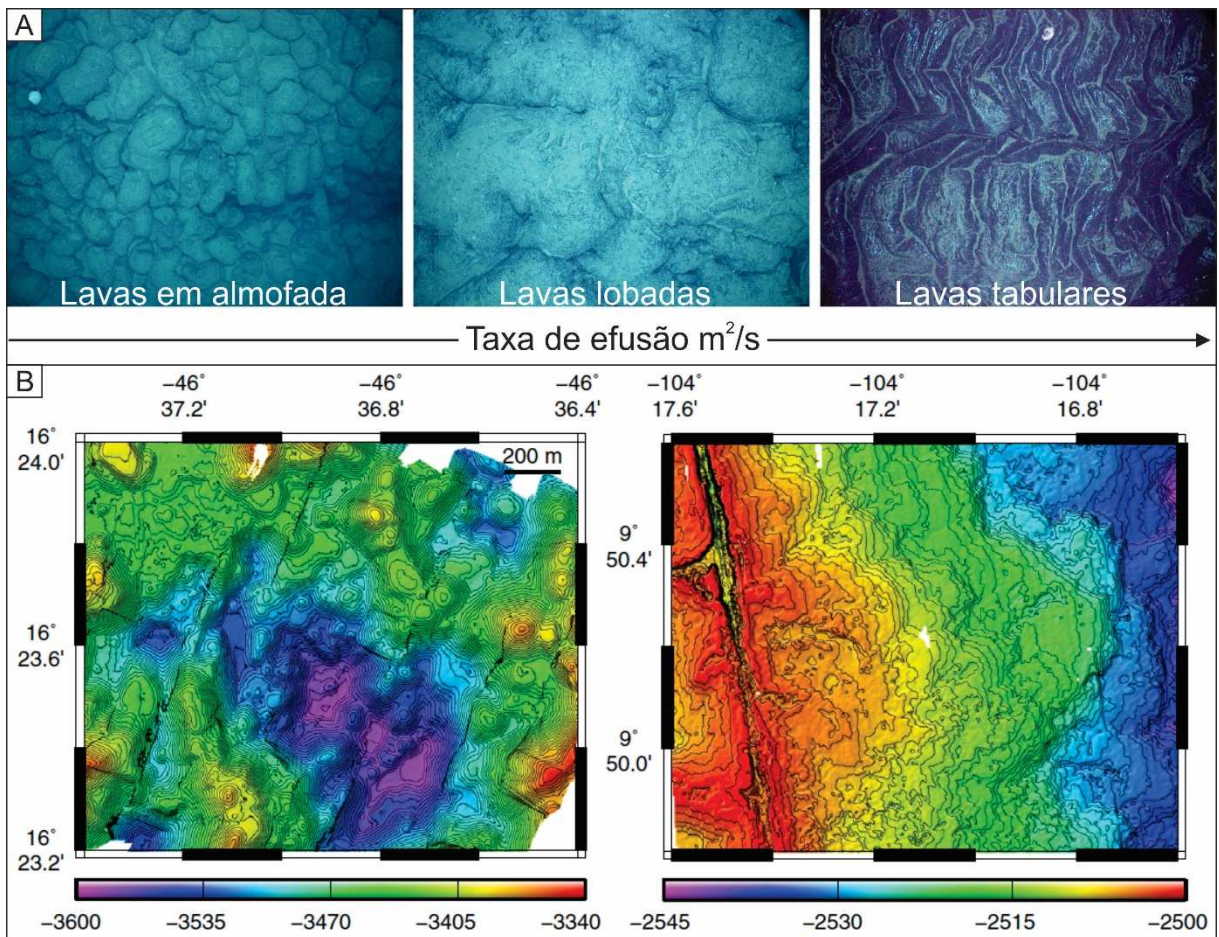


Fig. 12: A) Exemplos das morfologias de derrames subaquosos: derrames em almofadas (*pillow lavas*), lobados e tabulares; B) Mapas batimétricos de alta resolução (em mesma escala) de áreas dominadas por *pillow lavas* (à esquerda) e áreas dominadas por derrames lobados e tabulares (à direita). A área com *pillow lavas* é caracterizada por relevo com montículos formados por empilhamento de *pillows* de 500 m de diâmetro e 50-100 m de altura. A área dominada por derrames lobados e tabulares é caracterizada por relevos não muito altos que podem se estender por 1-4 km a partir da cratera ou fissura eruptiva. Modificado de White *et al.* (2015).

Derrames lobados – Os derrames do tipo lobado são similares às *pillow lavas* no que diz respeito ao reconhecimento da geometria externa dos lobos (Fig. 12), mas com a diferença de que esses limites não são comumente visíveis no interior dos derrames lobados. Os lobos desse tipo de derrame tendem a ser muito mais largos do que espessos, e caracterizados por superfícies lisas. Entretanto, lobos maiores podem conter feições em corda (White *et al.*, 2015). Segundo Gregg and Fornari (1998), o baixo relevo da superfície de lavas lobadas sugere que esses lobos possam ter suas porções interiores completamente interconectadas e infladas até um nível comum. A formação deste tipo de derrame tem sido atribuída a taxas de inflação mais elevadas

do que as que deram origem às *pillow* lavas (Gregg and Fink, 1995, 2000; White *et al.*, 2015).

Derrames do tipo *pillow* – Derrames de *pillow* lavas são caracterizados por lobos tubulares interconectados de lava, separados uns dos outros por uma crosta vítrea (Walker, 1992). Superfície de *pillows* pode conter dobras em corda, enrugamentos, juntas abertas, juntas de contração e juntas de tensão (Yamagishi, 1985) (Fig. 13). A crosta mais externa da *pillow* geralmente é vítrea, tem poucos centímetros de espessura, pode ser múltipla e apresentar fraturas devido ao efeito do choque térmico (*quenching*) (Walker, 1992; Velev and Nedialkov, 2011).

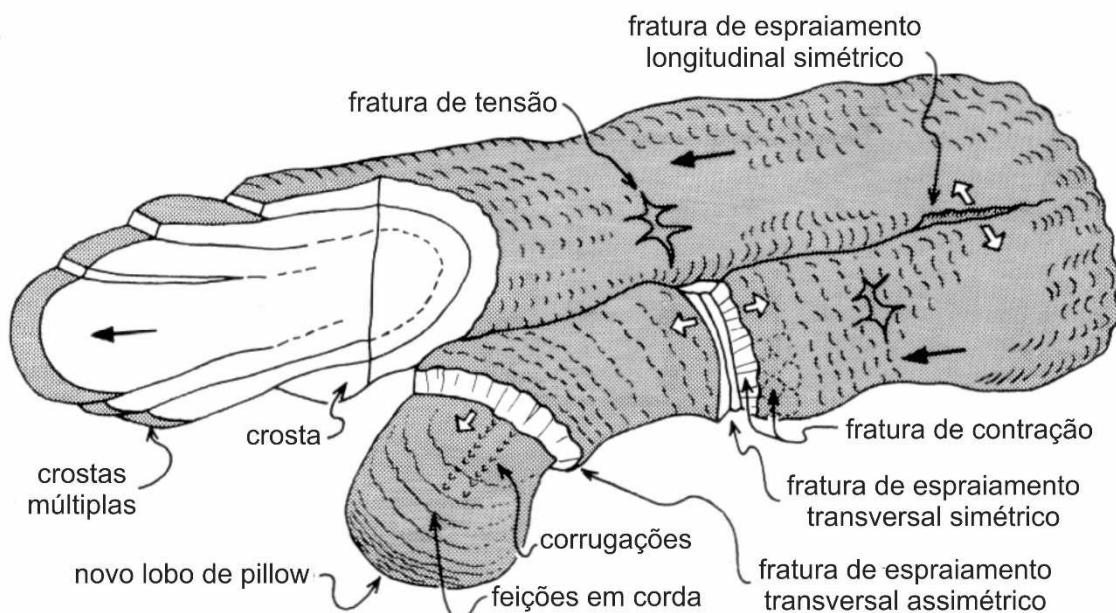


Fig. 13: Estruturas características de superfícies de lobos de *pillows* e modelo de crescimento de *pillow* lavas. Extraído de Mcphie *et al.* (1993).

O interior das *pillows* pode exibir juntas colunares radiais, juntas do tipo carapaça de tartaruga (*tortoise shell joints*), além de juntas concêntricas menos desenvolvidas associadas às juntas colunares radiais (Mcphie *et al.*, 1993). Vesículas em *pillows* tendem a variar em tamanho e abundância concentricamente, enquanto vesículas do tipo *pipe* tendem a ser radiais a partir do centro ou são restritas à parte inferior das *pillows* (Mcphie *et al.*, 1993) (Fig. 14). Muito embora vesículas esféricas e do tipo *pipe* sejam as mais comumente observadas em *pillow* lavas, outros dois tipos

de vesiculação também foram reconhecidos em lobos de *pillows*: cilindros de vesículas e lençóis de vesículas (Merle *et al.*, 2005).

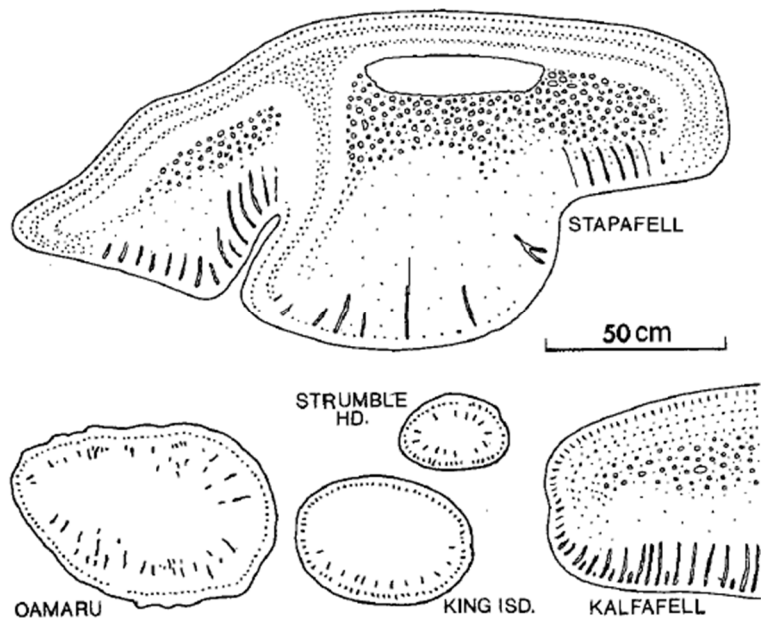


Fig. 14: Padrão da distribuição de vesículas em *pillows* da Islândia, desenhadas numa mesma escala. Vesículas *pipe* podem ocorrer principalmente na base ou ao redor da circunferência de *pillows* de águas rasas. Extraído de Walker (1992).

O estudo das propriedades físicas e morfológicas de *pillow* lavas em afloramento podem fornecer importantes informações a respeito da taxa de efusão e condições ambientais sob as quais essas lavas foram colocadas (p.ex. Jones, 1969; Walker, 1992; Schnur, 2007; Jerram and Petford, 2014). O padrão de vesiculação de *pillows*, por exemplo, pode indicar a profundidade da lâmina d'água na qual essas lavas se colocaram. A pressão hidrostática, relacionada à profundidade da lâmina d'água, atua facilitando ou prevenindo o escape de gás ou água da lava após a extrusão. Alguns estudos mostram uma diminuição do tamanho e abundância das vesículas com o aumento da profundidade da lâmina d'água (Moore, 1965; Jones, 1969). Esse decréscimo parece ser gradual até 1 km, após esse limite de profundidade esse decréscimo é rápido (Moore, 1965).

Jerram and Petford (2014) afirmam que, em profundidades menores que 500 m, as *pillows* apresentam vesicularidade de cerca de 10 a 40%. Enquanto que para profundidades de até 1000 m, a média de porosidade pode ser menor que 5%. Além do tamanho e abundância dessas vesículas, o tipo e a distribuição delas também

parece refletir a profundidade em que essas lavas foram colocadas. Vesículas do tipo *pipe*, alongadas a partir do interior da *pillow* para o exterior, indicam escape de gás e pequenas profundidades de colocação (Walker, 1992) (Fig. 14). Entretanto, quando estas vesículas ocorrem restritas à porção basal das *pillows*, é sugerido que estas lavas foram colocadas em declividades de até 4º (Walker, 1987). Adicionalmente, o zoneamento concêntrico de vesículas no topo das *pillows* indica profundidades pequenas de menos de 350 a 450 metros (Jones, 1969).

As dimensões das *pillows* podem, por sua vez, dar indicações sobre a taxa de efusão. O decréscimo do diâmetro das *pillows* em direção ao topo e a transição na morfologia de um derrame maciço para *pillow*, observados em vários estudos, são relacionados a potencial diminuição da taxa de efusão durante o período de erupção, com decréscimo do volume da extrusão da lava, levando a *pillows* menores (Dimroth *et al.*, 1978; Busby-Spera, 1987; Gillis and Sapp, 1997).

Adicionalmente, o estudo morfométrico de *pillows* feito por Walker (1992) mostra que a declividade do substrato exerce forte controle na morfologia e empacotamento desses depósitos. Segundo esse autor, declives suaves favorecem a formação de *pillows* grandes (até 10 m de largura), mais arredondadas e bulbosas, e um empacotamento mais fechado (*closely packed pillows*), enquanto que declives mais íngremes (maiores que 10º) tendem a gerar *pillows* menores (poucos decímetros) e mais alongadas, e com uma maior quantidade de brechas ricas em clastos vítreos ocorrendo entre os lobos (Walker, 1992; Umino *et al.*, 2000). Walker (1992) chama atenção para a quantidade de brechas em depósitos formados em condições de alta declividade; apenas 25% desse material é composto por *pillows*. Vale ressaltar que, o ambiente de formação de uma *pillow* não necessariamente é o mesmo da erupção que o originou, pois, a entrada de derrames subaéreos em corpos d'água podem, igualmente, resultar na formação de depósitos ricos em *pillows* e hialoclastitos (descritos a seguir), nos chamados deltas de lava (McPhie *et al.*, 1993).

Hialoclastitos - O termo hialoclastito é utilizado para agregados monomíticos de clastos vítreos, que podem estar litificados ou inconsolidados, formados por fraturamento não explosivo e desintegração de lavas e intrusões por choque térmico (Mcphie *et al.*, 1993). Essa fragmentação ocorre em resposta ao estresse térmico, pelo rápido resfriamento, e estresse imposto às partes externas resfriadas de lava e intrusões pelo movimento contínuo do interior dúctil. Os clastos vítreos são blocos poliédricos ou clastos estilhaçados limitados por superfícies curviplanares, são (ou

foram) total ou parcialmente vítreos e podem ser vesiculados. Estes clastos podem ser depositados em qualquer profundidade de lâmina d'água, podem ter tamanhos variados (menos de um milímetro a dezenas de centímetros), estar *in situ* (caracterizado por ausência de estratificação e, em geral, textura *jigsaw-fit*) ou serem resedimentados (Mcphie *et al.*, 1993). Os depósitos formados por estes clastos vítreos têm, em geral, dezenas de metros de espessura, mas podem alcançar ~1 km. O estudo desses depósitos é relevante porque, além de indicadores valiosos de paleoambiente, eles também podem representar importantes alvos exploratórios na indústria do petróleo (Watton *et al.*, 2014).

3.1.3 Produtos de interação entre lava e sedimento

A colocação de lavas subaéreas ou subaquosas sobre sedimentos inconsolidados pode resultar em uma variedade de produtos de interação lava-sedimento como, por exemplo, inclusões sedimentares, formação de estrutura de carga e peperitos com morfologias diversas (p.ex. Busby-Spera and White, 1987; Jerram and Stollhofen, 2002; Brown and Bell, 2007; Ebinghaus *et al.*, 2014; Rawcliffe, 2016). Nesta seção serão apresentadas as principais características de peperitos; o principal produto de interação entre lava e sedimento descrito na área de estudo (região entre Uberlândia e Araguari).

Peperito, segundo White *et al.* (2000) é um termo genérico aplicado à rocha formada essencialmente *in situ* por desintegração do magma que intrudiu e se misturou com sedimento inconsolidado ou pobemente consolidado, tipicamente molhado. Entretanto, alguns exemplos de peperitos formados em ambiente árido foram reportados em algumas áreas da Província Ígnea Paraná-Etendeka (p.ex. Jerram and Stollhofen, 2002; Petry *et al.*, 2007).

A formação de peperitos pode envolver magmas com diferentes composições (magmas andesíticos, traquíticos, dacíticos, riolíticos e basálticos) e pode ocorrer associadas a intrusões rasas, preenchendo crateras em vulcões freatomagmáticos, bem como associados a base de lavas e de fluxos piroclásticos (p.ex. Busby-Spera and White, 1987; Hanson and Wilson, 1993; Jerram and Stollhofen, 2002; Skilling *et al.*, 2002; Waichel *et al.*, 2007; Luchetti *et al.*, 2013).

Os depósitos peperíticos podem variar de poucos m³ a vários km³ e sua morfologia em duas dimensões varia amplamente, passando de irregular a tabular

(Fig. 15). Além da classificação pela forma geral do depósito, os peperitos podem ser classificados de acordo com a proporção relativa de clastos juvenis e sedimento hospedeiro, sendo classificados como peperito clasto suportado (*close-packed peperite*) ou peperitos dispersos (*dispersed peperite*) (Hanson and Wilson, 1993) (Figs. 15 e 16). Vale ressaltar que pode haver gradação de um domínio para outro (por exemplo, peperitos clasto suportado podem gradar para peperitos dispersos) e que, muito embora a distância máxima que clastos individuais possam ser transportados pelo sedimento não seja conhecida, distâncias de mais de 100 m já foram observadas (Hanson and Wilson, 1993; Skilling *et al.*, 2002).

Outra classificação amplamente utilizada em peperitos está relacionada à dominância dos formatos dos clastos juvenis. Peperito pode ser classificado como peperito em bloco, fluidal ou ser uma mistura desses dois tipos (Busby-Spera and White, 1987; McPhie, 1993). Os fragmentos juvenis de peperitos em bloco são poliédricos a tabulares, com superfícies curviplanares a planares, enquanto que em peperitos fluidais, os fragmentos juvenis são caracterizados por uma morfologia fluidal ou globular, geralmente com limites complexos (Skilling *et al.*, 2002). Algumas das formas de fragmentos juvenis são apresentadas na figura 15. Além das formas variadas, fragmentos juvenis descritos em peperitos podem apresentar padrão de vesiculação altamente variável, podendo conter desde fragmentos pouco vesiculados a púmice (Hunns and McPhie, 1999; Gifkins *et al.*, 2002).

Grandes domínios ígneos coerentes podem ocorrem dispersos dentro do peperito ou na rocha sedimentar hospedeira (Fig. 15). Esses corpos ígneos podem ter formas semelhantes a *pillow* lavas ou lobos, ser tabulares ou terem padrão complexo de juntas e fraturas que podem estar preenchidas por sedimento hospedeiro ou peperito (Skilling *et al.*, 2002). Alguns autores sugerem que domínios de rochas ígneas coerentes representam os maiores condutos alimentadores que fornecem magma para desenvolver os domínios de peperito (p.ex. Hanson and Wilson, 1993).

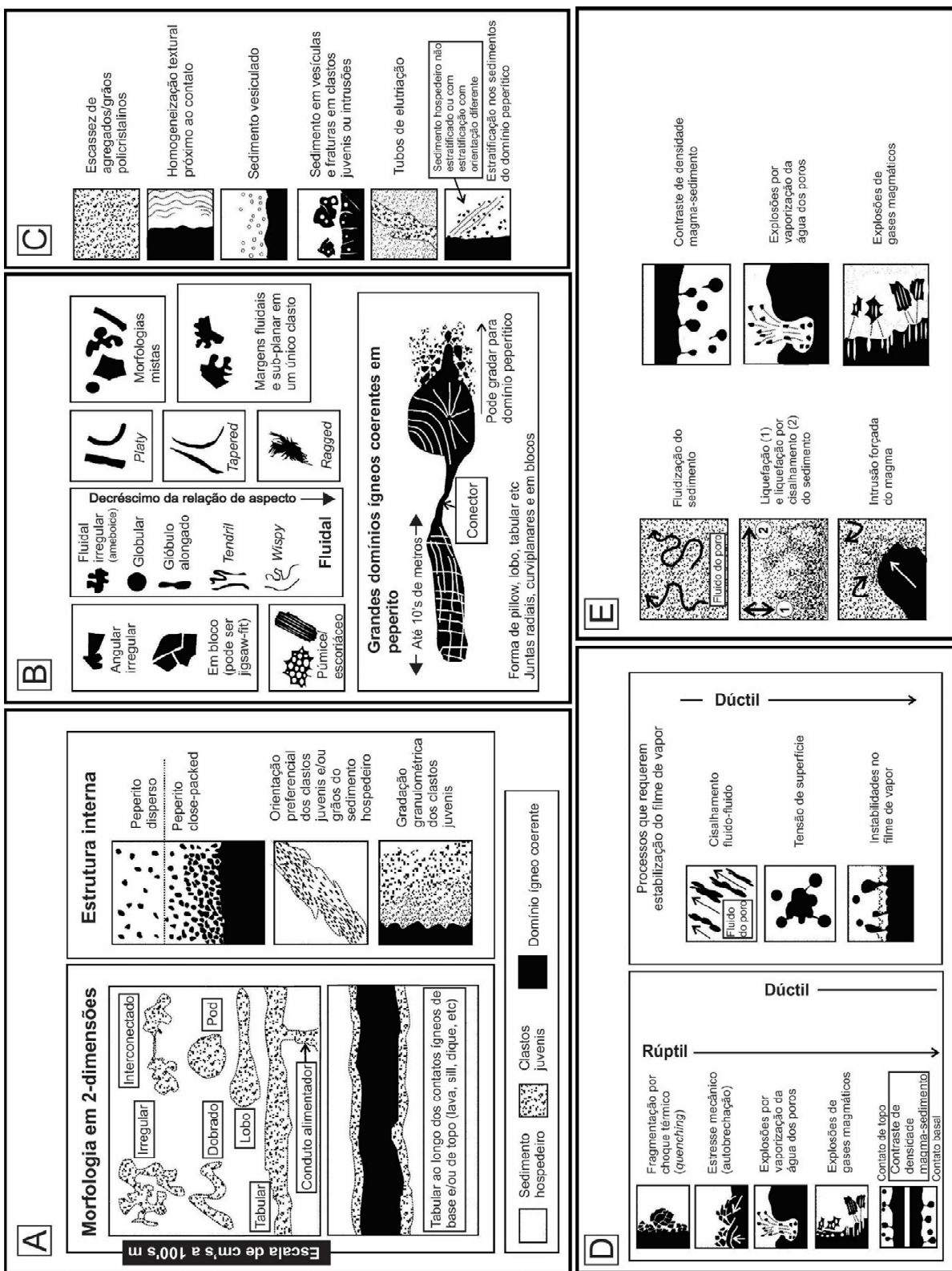


Fig. 15: Sumário com as características dos domínios de peperitos (a); (b) morfologia dos clastos juvenis; (c) evidências para a natureza não consolidada dos sedimentos hospedeiros; (d) geração de clastos juvenis; e (e) mistura de clastos juvenis e sedimentos hospedeiros. Modificado de Skilling *et al.*, (2002).

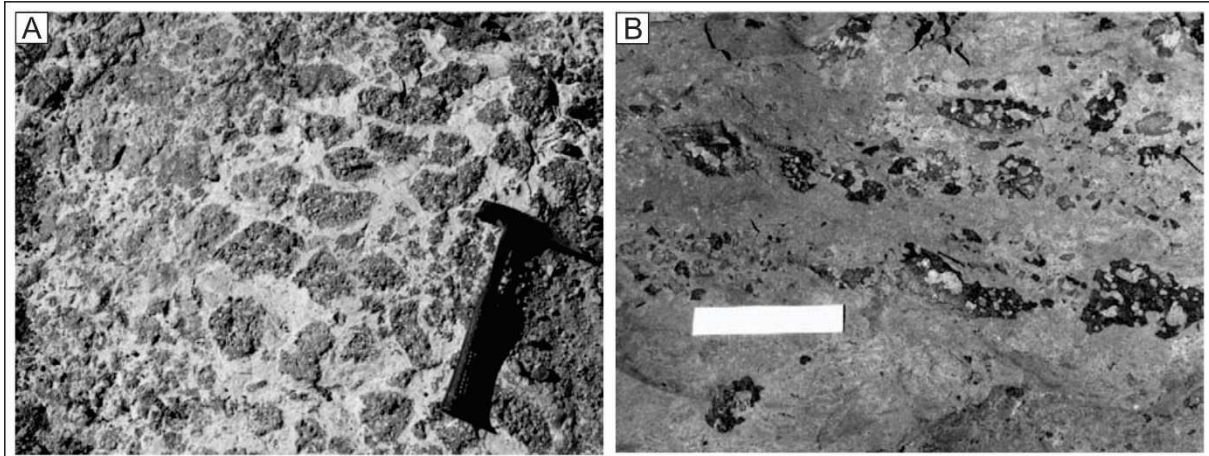


Fig. 16: Peperitos da Bacia do Paraná com diferentes proporções relativas de clastos juvenis e sedimento hospedeiro. A) Exemplo de peperito clasto-suportado; B) Peperito matriz suportado. Extraído de Waichel *et al.* (2007).

A formação de peperitos envolve desintegração ou fragmentação do magma gerando clastos juvenis e mistura desses clastos com um sedimento hospedeiro (Fig. 15). A fragmentação do magma é fortemente influenciada pelas características do sedimento hospedeiro. Em sedimentos úmidos com baixa permeabilidade e granulometria fina, as altas temperaturas da lava favorecem a formação de um filme de vapor na interface clasto juvenil-sedimento, evitando o contato direto do magma com o sedimento molhado e facilitando a formação de peperito fluidal (Busby-Spera and White, 1987). Nos casos onde o sedimento hospedeiro têm granulometria grossa, alta permeabilidade e seleção baixa, a formação do filme de vapor é prejudicada levando a fragmentação do magma por choque térmico (*quenching*) e explosões por vaporização da água dos poros. Essa fragmentação favorece a formação de peperitos em bloco. Embora sedimento molhado seja provavelmente essencial para formar peperito fluidal, isso pode não ter sido essencial para a formação de alguns tipos de peperito em bloco. (p. ex. Jerram and Stollhofen, 2002, Petry *et al.*, 2007).

A mistura dos clastos juvenis e sedimento hospedeiro pode ser dada por fluidização do sedimento, intrusões forçadas de magma, explosões por vaporização da água dos poros, contraste de densidade entre magma e sedimento, e liquefação do sedimento (Fig. 15). Como resultado, o sedimento hospedeiro pode ser cimentado, localmente fundido ou metamorfizado (metamorfismo de contato), apresentar estratificações, dobras, ou vesículas, estas últimas raramente preservadas (Kokelaar, 1982; Hunns and McPhie, 1999; Skilling *et al.*, 2002).

3.1.4 Juntas em rochas vulcânicas

Juntas de resfriamento podem ocorrer em derrames de composições variadas, diques e soleiras, depósitos piroclásticos bem soldados a arenitos silicificados. As juntas podem formar duas fácies distintas: colunados e entablamento, que podem ocorrer em uma variedade de ambientes desde subáreos a subglaciais (Phillips *et al.*, 2013). Os colunados consistem de colunas relativamente bem formadas, comumente perpendiculares à base do derrame e que variam de ~0,3–2 m de largura. Essas estruturas, que são bem definidas em muitos derrames, ocorrem na porção mais inferior ocupando de 10% a 30% do derrame e, quando presentes na porção superior, ocupam de 10% a 20% do derrame (Fig. 17) (Saemundsson, 1970; Long and Wood, 1986; Phillips *et al.*, 2013). O termo entablamento refere-se à porção do derrame composta por colunas irregulares a denteadas, de diâmetro menor (0,2 a 0,5 m de diâmetro) que, em geral, são observados nas porções centrais desses corpos ígneos (60% a 70% do derrame) (Fig. 17). Padrões radiais ou colunas não perpendiculares à base do derrame podem ocorrer neste intervalo. Em alguns casos, pode haver alternância de entablamento e colunados mais de uma vez dentro de um derrame tabular ou, em outros casos, derrames podem não apresentar entablamento (Long and Wood, 1986; Lyle, 2000).

Existe um consenso sobre o principal mecanismo produtor de juntas internas em basaltos ser a contração das lavas durante o resfriamento (Lyle, 2000). Dois mecanismos são considerados para o resfriamento das lavas, condução e convecção, sendo este último o mais eficiente no que diz respeito à perda de calor do derrame quente para o ambiente circundante. A perda de calor por convecção resulta em taxas de resfriamento mais rápidas, comparativamente à perda de calor por condução. Independente do mecanismo de perda de calor, à medida que o derrame vai sendo resfriado, ocorre um estresse termal que causa a contração e formação de fraturas que se formam no limite externo e se propagam para o centro do derrame. Essas fraturas facilitam a transferência de calor do interior do derrame para o ambiente no entorno. O avanço da fratura acompanha o avanço da frente de resfriamento e ocorre quando o estresse dado pela contração excede a resistência da lava à tração (Schaefer and Kattenhorn, 2004; Phillips *et al.*, 2013). Esse avanço cessará quando o material por onde a fratura está se propagando se tornar muito quente para sustentar o faturamento rúptil (Ryan and Sammis, 1978). A propagação das juntas em direção ao centro do derrame se dá por meio de incrementos e terminações das fraturas de

forma cíclica, o que pode ser observado através de estrias existentes nas colunas (Fig. 18) (Forbes *et al.*, 2014).

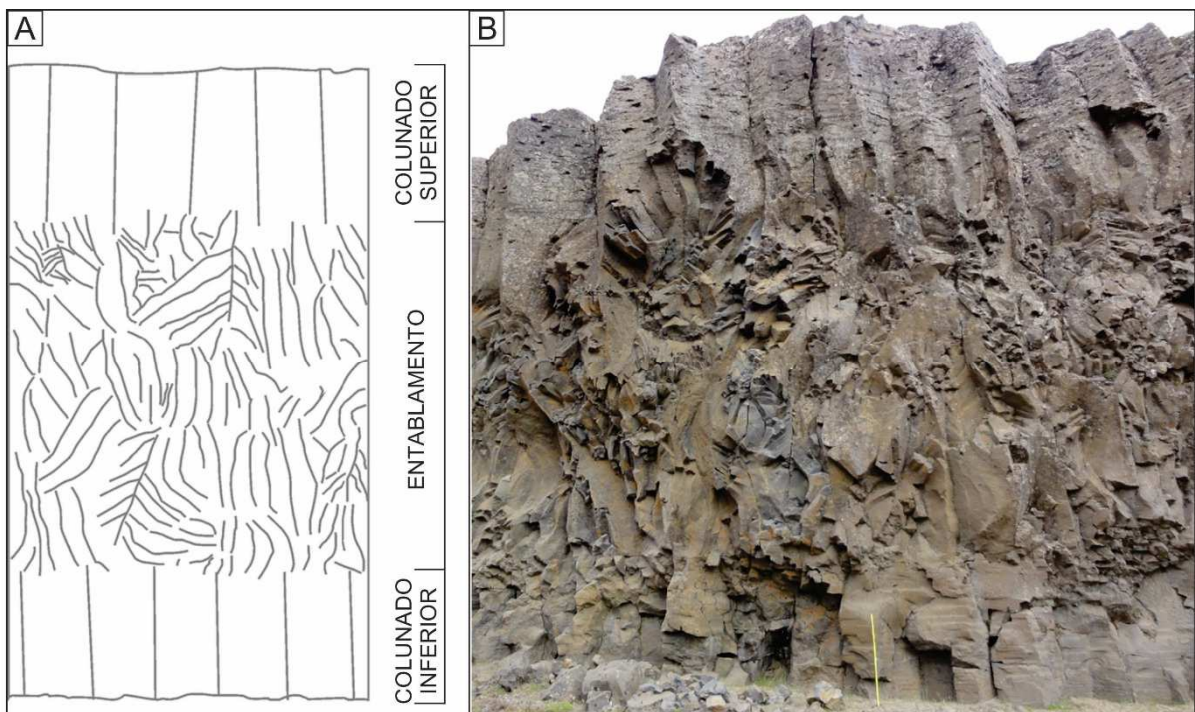


Fig. 17: A) Figura esquemática ilustrando arquitetura de juntas observada no derrame da figura B. B) Seção do derrame de Búrfell, próximo a Gjáin, com colunado superior e inferior, e um domínio de entablamento na porção central do derrame. Escala tem 1m. Modificado de Forbes *et al.*, (2014).

Ryan and Sammis (1978) afirmam que as estrias consistem de porções lisas e porções rugosas que são atribuídas, respectivamente, ao início da fratura em lava relativamente rígida (a porção lisa) e interrupção da fratura em lava mais quente, mais dúctil (a porção rugosa) (Fig. 18). Em geral, estrias são coplanares, tem de 2 a 40 cm (Grossenbacher and McDuffie, 1995) e, segundo Goehring (2008) há uma relação diretamente proporcional entre altura da estria e média da largura das colunas. Em casos onde o resfriamento foi rápido, pequenas pausas na propagação das fraturas individuais resultam em menores topografias de estrias. Portanto, em geral, a topografia de estrias em porções colunadas é maior que a topografia daquelas em entablamento, sugerindo que a taxa de resfriamento em entablamento foi maior do que em colunados (Forbes *et al.*, 2014).

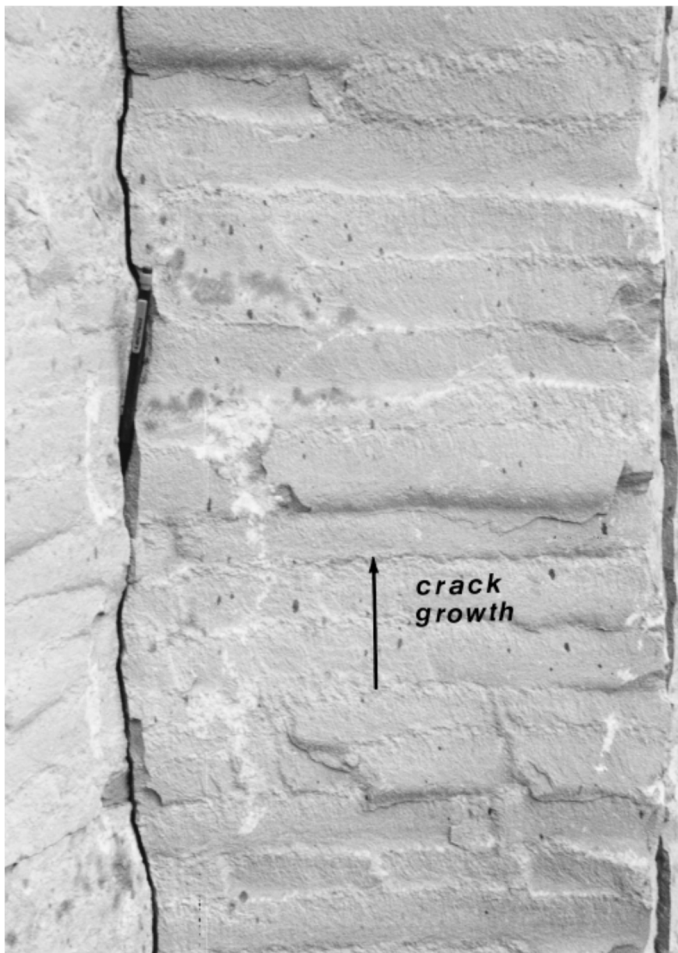


Fig. 18: Face de uma coluna com estrias marcadas pela repetição de porções lisas e rugosas representando início e interrupção de juntas, respectivamente. Direção do crescimento da junta é indicado pela seta. A lapiseira tem 15 cm de comprimento. Extraído de Lyle (2000).

Outro indicador relativo para taxa de resfriamento é o tamanho dos lados das colunas. Como o tamanho dos lados das colunas é controlado pela resposta visco-elástica da lava à taxa de resfriamento (Lore *et al.*, 2000), colunas resfriadas mais rapidamente serão menores que aquelas resfriadas lentamente. Forbes *et al.* (2014) mostram que nas lavas do sudoeste da Islândia, a largura da lateral da coluna é 1,5 a 3 vezes menores em entablamento do que colunados, sugerindo que as taxas de resfriamento foram mais rápidas em porções de entablamento no derrame.

Indícios sobre a taxa de resfriamento também podem vir do estudo petrográfico comparativo de colunados e entablamentos. Long e Wood (1986) observaram que a abundância de mesóstase em entablamentos é substancialmente maior que em colunados, variando de 15% a 25% em colunados e 35% a 65% em entablamento nos derrames da Província Columbia River. Outra feição abundante em entablamento, e

ausente em colunados, é a presença de grãos de óxidos de Fe e Ti com morfologia dendrítica. A abundância de mesóstase, assim como a presença de grãos de óxidos dendríticos são associados a taxas de resfriamento maiores e, portanto, indicam que entablamento e colunados estão associados a altas e baixas taxas de resfriamento, respectivamente (Long e Wood, 1986; Lyle, 2000).

Conforme dito anteriormente, o resfriamento mais lento e mais rápido de porções com colunados e com entablamento está relacionado à perda de calor por condução e convecção, respectivamente (Long and Wood, 1986; Degriff *et al.*, 1989). A perda de calor por convecção, e consequente formação de entablamento, é atribuída a presença de água interagindo com a lava. Durante a colocação dessas lavas, pode haver represamento e transbordamento de rios pré-existentes que podem transpassar e atingir a superfície da lava que o represou (Saemundsson, 1970; Long and Wood, 1986, Lyle, 2000). Essa água atua no resfriamento do derrame, favorecendo a perda de calor por convecção água-vapor, do topo para a base do derrame, conforme mostrado por estudos de estrias em entablamentos (DeGraff *et al.*, 1989). Derrames que não exibem entablamento parecem ter escapado da inundação. Por outro lado, a ocorrência de entablamentos e colunados repetidos mais de uma vez em um único derrame pode ser explicada por múltiplos eventos de inundação com intervenção de períodos de seca (Degriff *et al.*, 1989; Long and Wood, 1986). Diante do exposto, a ocorrência de entablamento é, portanto, um possível indicador paleoambiental (Forbes *et al.*, 2014).

CAPÍTULO VI

Neste capítulo serão apresentados os métodos e técnicas utilizados para atingir os objetivos propostos.

4. METODOLOGIA

4.1 REVISÃO BIBLIOGRÁFICA

A revisão bibliográfica tem por objetivo uma atualização e síntese do conhecimento disponível na literatura sobre assuntos relacionados ao tema dessa tese, tais como características do vulcanismo em ambiente subaéreo e subaquoso, feições de interação entre lava e sedimento, conceito de fácies aplicado a sucessões vulcânicas, Grandes Províncias Ígneas e Províncias Magmáticas Continentais. Esta etapa foi essencial para fundamentar a definição dos tipos de derrames, arquiteturas de fácies e comparação das feições observadas na área de estudo com feições similares presentes em outras províncias.

4.2 ATIVIDADES DE CAMPO

As atividades de campo desenvolvidas neste trabalho contemplaram três regiões distintas no Brasil e na Escócia com exposições de rochas vulcânicas, sedimentares e os mais diversos produtos de interação entre lava e sedimento. O foco principal desta etapa foi a caracterização dos basaltos subaéreos e subaquosos do Grupo Serra Geral na porção norte da PIPE (região de Uberlândia e Araguari – MG). Esta etapa visou à descrição dos afloramentos e à confecção de perfis compostos para identificação das litofácies, associação de litofácies e dos tipos morfológicos dos derrames aflorantes na área de estudo. Amostras pouco alteradas foram coletadas para análises petrográfica, geoquímica e petrofísica.

As campanhas de campo realizadas na Escócia tiveram como foco os basaltos e os produtos de interação entre lavas e sedimentos de afloramentos pertencentes à Província Ígnea do Atlântico Norte e bacia de Midland Valley, que ocorrem na Ilha de Mull e em Saint Cyrus, respectivamente. Nesses lugares, foi realizada a descrição dos afloramentos e o levantamento de imagens feitas por drone (veículo aéreo não

tripulado) para caracterização da interação entre lava e sedimento e a confecção de modelos digitais que permitiram a observação de porções não acessíveis em campo.

4.3 PETROGRAFIA

A caracterização petrográfica foi realizada em um total de 111 amostras (78 vulcânicas e 33 sedimentares), através de microscopia óptica e difração de raios-x. Algumas dessas lâminas delgadas foram confeccionadas nos laboratórios de preparação de amostras do Centro de Pesquisas da Petrobras (CENPES) e da Weatherford, ambos localizados no Rio de Janeiro, enquanto outra parte foi feita no laboratório da PetrografiaBR em Contagem (MG). Todas as lâminas foram polidas e impregnadas com resina azul visando ressaltar os poros e fraturas existentes.

A descrição petrográfica foi feita com auxílio de microscópio óptico com luz transmitida (microscópio da marca Carl Zeiss) visando a caracterização mineralógica e texturas, bem como a identificação dos tipos de poros das rochas ígneas e sedimentares coletadas durante a etapa de campo. Para melhor caracterizar as fases cristalinas mais finas que não puderam ser identificadas com análise de microscópio de luz transmitida utilizou-se a técnica de difratometria de raios-x.

Após a caracterização petrográfica em microscópio óptico, foram selecionadas 50 amostras representativas de rochas vulcânicas e sedimentares para análises de difratometria de raio-X (DRX). Estas amostras incluem, peperitos e material *interpillow*.

A preparação das amostras e as análises foram realizadas no laboratório de difratometria de raio-X do CENPES. O preparo das amostras envolveu pulverização em moinho McCrone, desagregação em ultrassom de ponta e concentração do material por centrifugação. A aquisição dos dados de DRX em rocha total e na fração argila foram feitas através de difratômetro RIGAKU D/MAX - 2200/PC e Bruker D8. A interpretação dos difratogramas foi realizada com auxílio do software Jade 9, EVA (BRUKER AXS GMBH) e banco de dados disponíveis na literatura.

4.5 QUÍMICA DE ROCHA TOTAL

A análise de química de rocha total visa investigar os contrastes químicos existentes entre os derrames da FSG da área de estudo e os derrames da porção sul

da Bacia do Paraná. As diferentes porções do derrame (base, meio e topo) também foram analisadas para investigar possíveis diferenças químicas dentro de um mesmo derrame. Um total de 34 amostras foram selecionadas (evitando-se fragmentos muito alterados e com amígdalas), britadas, e enviadas para o laboratório da Activation Laboratories Ltd. (Actlabs) no Canadá para limpeza, moagem e análise química de rocha total segundo os pacotes S1, B3, RX6 e 4Lithoresearch. A análise de elementos maiores foi feita utilizando a técnica de ICP (Inductively Coupled Plasma), enquanto os elementos traços e terras raras foram determinados por ICP-MS (Inductively Coupled Plasma Microspectrometry). A descrição completa dos procedimentos e os limites de detecção de cada elemento podem ser encontrados no *website* da Actlabs (<https://actlabs.com/geochemistry/lithogeochemistry-and-whole-rock-analysis/lithogeochemistry/> and <https://actlabs.com/downloads/>).

4.6 ENSAIOS PETROFÍSICOS

Um total de 45 amostras representativas da PIPE foram selecionadas para análises de petrofísica convencionais (porosidade, permeabilidade) e medidas de velocidades das ondas acústicas. Essas amostras foram adquiridas com auxílio de uma perfuratriz rotativa com broca diamantada, preferencialmente orientadas (vertical e/ou horizontal), resultando em 81 amostras cilíndricas (plugues) de até 1,5" de diâmetro e 2" de comprimento. Esses plugues foram lavados e, posteriormente, secos a uma temperatura de 60 °C e à umidade relativa de 45% visando eliminar água dos poros e prevenir o colapso das argilas (McPhee *et al.*, 2015). O peso, comprimento e diâmetro de cada plugue foram obtidos através de uma balança e um cípiper de alta precisão, respectivamente. Esses 81 plugues foram analisados para obtenção de suas densidades, porosidade e permeabilidade, enquanto apenas 22 dessas amostras (preferencialmente orientadas verticalmente) foram analisadas para obtenção das velocidades das ondas acústicas (velocidades das ondas compressionais – V_p, e velocidades das ondas cisalhantes – V_s).

4.6.1 Medidas de porosidade

A porosidade efetiva (poros conectados) foi medida usando um porosímetro a gás manufaturado pela empresa Weatherford, seguindo a metodologia descrita pelo Instituto Americano de Petróleo (*American Petroleum Institute* - 1998) e McPhee *et*

al., (2015). Essa análise é baseada em equações da termodinâmica para identificar o volume de grãos de uma amostra e, consequentemente, sua porosidade e densidade. A medida do volume de grãos considera o princípio da Lei de Boyle, através de um experimento que utiliza um aparato com duas câmaras conectadas com volumes conhecidos: a câmara de referência e a câmara da amostra. Primeiro, um volume conhecido de gás hélio a uma pressão de 700 psi é inserido na câmara de referência. Posteriormente, esse gás é expandido a partir da câmara de referência para a câmara que contém a amostra até atingir o equilíbrio. A diferença entre o volume de gás da câmara vazia e da câmara com a amostra representa o volume no qual o gás não acessou durante a expansão, ou seja, o volume de grãos (Gonçalves *et al.*, 2019). A diferença entre o volume total calculado para o plugue e o volume de grãos obtido no porosímetro determina a porosidade dessas amostras.

4.6.2 Medidas de permeabilidade

A permeabilidade das amostras foi medida em um permeâmetro a gás, onde a amostra foi submetida a uma pressão de confinamento de 700 psi. Essa análise envolve um fluxo de gás sendo continuamente aplicado ao eixo axial dessas amostras enquanto a pressão, temperatura e taxa de fluxo são eletronicamente monitoradas pelo equipamento. Quando esses parâmetros estabilizam, a equação modificada de Darcy é usada para obter os valores de permeabilidade (American Petroleum Institute 1998; McPhee *et al.* 2015). Apenas 20 das 81 amostras testadas apresentaram permeabilidade superior ao limite de detecção do permeâmetro ($>0,001$ mD) e, portanto, foram consideradas nesse estudo.

4.6.3 Medidas de velocidades das ondas acústicas

Velocidades de ondas compressionais e cisalhantes (V_p e V_s) foram determinadas no laboratório de física de rocha do CENPES usando um pulsor/receptor ultrassônico. Este equipamento consiste em um transdutor de cerâmica, osciloscópio digital e uma câmara na qual a amostra a ser medida é colocada. Um sinal eletrônico conhecido é gerado e convertido em vibração mecânica (compressional ou cisalhante) no transdutor (operando a 700 kHz). Essa vibração mecânica viaja através da amostra até alcançar o transdutor receptor que a converte em um sinal eletrônico que será analisado pelo osciloscópio. As 22 amostras foram

medidas sob pressões de confinamento variadas e as velocidades das ondas acústicas (V_p e V_s) foram adquiridas a cada 500 psi durante o aumento e a diminuição da pressão de confinamento (1000 - 5000 – 1000 psi). Vale ressaltar que os dados utilizados para discussões e para o modelo de sísmica sintética correspondem àqueles adquiridos sob pressão confinante de 1000 psi (pressão de confinamento ascendente).

4.7 MODELO DIGITAL DE AFLORAMENTO

O modelo digital do afloramento foi construído utilizando fotografias de alta resolução adquiridas por um drone DJI Phantom 4 Pro com uma câmera acoplada do tipo FC6310. O sensor utilizado foi o 1" CMOS com 20 Megapixels, com estabilização dada por GPS/Glonass. O software Agisoft Photoscan 1.4.5 foi utilizado para processar as fotografias de alta resolução, reconstruir a geometria dos afloramentos e criar um modelo digital para o afloramento. As interpretações e medições do modelo digital do afloramento foram feitas com o software LIME 3D viewer (Buckley *et al.*, 2019) na Universidade de Aberdeen (Escócia). Esses modelos foram utilizados para analisar áreas não acessíveis em campo e serviram de base para confecção de modelos geológicos e modelos sísmicos sintéticos.

4.8 MODELO SÍSMICO SINTÉTICO

Os modelos de sísmica sintética foram desenvolvidos em um *software* de modelagem sísmica no CENPES, o qual utiliza como dados de entrada um modelo de refletividade gerado a partir de modelos de velocidade e densidade. Esses modelos consistem em modelos geológicos convertidos em imagem em escala de cinza onde cada cor corresponde a um valor específico de velocidade e de densidade. A geometria de aquisição adotada foi a do tipo *fixed spread*, que consistiu em 100 receptores a cada 10 m e o mesmo número de fontes também colocadas a cada 10 m umas das outras, ambos com profundidades de 6 m. Os dados sísmicos gerados por computador foram utilizados como dados de entrada para um algoritmo de imageamento sísmico que resultou em imagens sísmicas em profundidade migradas. O método de migração utilizado foi o *reverse time migration* que é amplamente utilizado na indústria de óleo e gás devido a sua eficácia em imagear estruturas geológicas complexas e com grande variação lateral de velocidade. Para atenuar

ruídos de retro-espalhamento (*backscattering noise*), foi utilizada a condição de imagem *Inverse Scattering*. As frequências dominantes testadas foram 30, 50 e 70 Hz e o aumento da impedância acústica é caracterizada por refletores pretos.

CAPÍTULO V

Neste capítulo serão apresentados os manuscritos com figuras e tabelas que foram submetidos a periódicos internacionais, conforme as normas estabelecidas pelo Programa de Pós-Graduação em Geociências da Universidade Federal do Rio Grande do Sul serão apresentadas neste capítulo. As cartas de submissão dos três artigos científicos são apresentadas no Anexo A.

5. APRESENTAÇÃO DOS ARTIGOS CIENTÍFICOS

5.1 ARTIGO A

Lithostratigraphy of the Serra Geral Formation in the northern portion of the Paraná-Etendeka Igneous Province: a tool for tracking Early Cretaceous paleoenvironmental changes.

Authors: Natália Famelli^{a,b*}, Evandro F. Lima^a, Isabela de O. Carmo^b.

Filiations, Address:

^a Instituto de Geociências, Universidade Federal do Rio Grande do Sul, Av. Bento Gonçalves, 9500, Prédio 43136, Caixa Postal 15001, Agronomia, 91501-970 Porto Alegre, RS, Brazil

^b Centro de Pesquisas e Desenvolvimento Leopoldo Américo Miguez de Mello – CENPES/PETROBRAS, Av. Horácio Macedo, 950, Cidade Universitária, 21941-915 Rio de Janeiro, RJ, Brazil

^c Departamento de Geociências, Universidade Federal Rural do Rio de Janeiro, BR-465, Km 7, 23897-000 Seropédica, RJ, Brazil

* Corresponding author. E-mail: natfamelli@gmail.com

Abstract

A detailed lithofacies analysis in Continental Flood Basalt Provinces allows the comprehension of their evolution and paleoenvironmental significance. In the northern portion of the Paraná-Etendeka Igneous Province (PEIP), in Brazil (Uberlândia-Araguari area), a volcanological and stratigraphic approach provided evidence that the volcanic succession is not monotonous, involving different lava flow morphologies and architecture. The volcanic succession reaches a thickness of ca. 300 m and includes five lithofacies associations: pillow lavas, compound pahoehoe, simple pahoehoe, peperite, and sediment-infill basalt breccia. Pillow lavas, simple pahoehoe, and compound pahoehoe characterize the onset of volcanic activity in the area. Peperitic intervals and thick simple pahoehoe lavas occur in upper stratigraphic levels. Some of these thick igneous bodies can represent invasive flows or shallow intrusions. In the study area, the common presence of volcanic deposits and structures formed in wet conditions is evidenced by occurrence of pillow lavas, undulatory columns, and interleaved lacustrine and fluvial sedimentary rocks. These deposits reflect different environmental conditions from those previously described as arid in other portions of the PEIP. Low-temperature post-depositional alteration has affected the volcanic and sedimentary rocks of the study area, obliterating many of the primary sedimentary structures. The subaerial and subaqueous lava flows are chemically similar, and compatible with high-TiO₂ Pitanga magma type. The lavas of the Uberlândia-Araguari area and the southern part of the PEIP have a similar evolution, with dominance of compound pahoehoe lava flows at the base, and simple pahoehoe from the middle to the top of the sequence, which interacted with wet alluvial to fluvio-lacustrine sediments at some parts of the study area.

Keywords: Paraná-Etendeka Igneous Province Volcanic Stratigraphy Lava flows and water interaction.

5.1.1 Introduction

Recent studies focusing on the development of facies and facies architecture have changed the idea that Continental Flood Basalt Provinces (CFBPs) are monotonous volcanic successions with layer-cake stratigraphy (Barreto et al., 2014; Jerram and Widdowson, 2005; Nelson et al., 2009; Rossetti et al., 2018, 2014; Single and Jerram, 2004; Waichel et al., 2012). These studies help to define typical lava morphologies, volcanic facies and facies associations in CFBPs, fundamental to the comprehension of the evolution and paleoenvironmental reconstructions of Large Igneous Provinces (LIPs) (e.g. Jerram 2002; Self et al., 1997; Svensen et al., 2019). Understanding CFBPs is important as they form a subset of LIPs which can occur in a variety of environments such as subaerial and subaqueous and transitioning to open marine in rifted volcanic margins, and as such their facies construction through time helps to constrain their evolution in a broader context such as rifting and continental break-up and linking to offshore parts of the provinces (e.g. Abdelmalak et al., 2016; Jerram et al., 2009; Svensen et al., 2017).

A stratigraphic approach has been applied to the southern portion of the Paraná-Etendeka Igneous Province (PEIP) in Brazil (e.g. Barreto et al., 2014; Costa, 2015; Rossetti et al., 2018, 2014; Waichel et al., 2012, 2006), enabling the identification of different lava flow morphologies (e.g. compound pahoehoe, simple pahoehoe, ponded pahoehoe, rubbly pahoehoe, and a'a lavas). The study of lava flow morphology and interlava sedimentary rocks allows the interpretation of lava flow dynamics, determination of paleotopography, mechanisms involved in their emplacement and the related environmental impacts (Ebinghaus et al., 2014; Fantasia et al., 2016). The lithostratigraphy defined for the southern portion of the PEIP provided the model of volcanic evolution, with the effusion of small-volume lava flows at the early stages of volcanism, and thick tabular lava flows representing an increase in the volume of single eruptions and the climax of volcanic activity (Rossetti et al., 2017). In contrast, the northern portion of the province lacks a systematic study of volcanic stratigraphy and lava flow morphologies. Recently, some studies (Fernandes et al., 2010; Moraes et al., 2018; Moraes and Seer, 2017) have focused on the description and distribution of lava morphologies (Fig. 19), documenting different volcanic sequences such as thick and extensive lava flows or pillow lavas. However, the description of lithofacies and their architecture still needs to be detailed in order to understand the internal organization of flood basalt stratigraphy of the northeastern area.

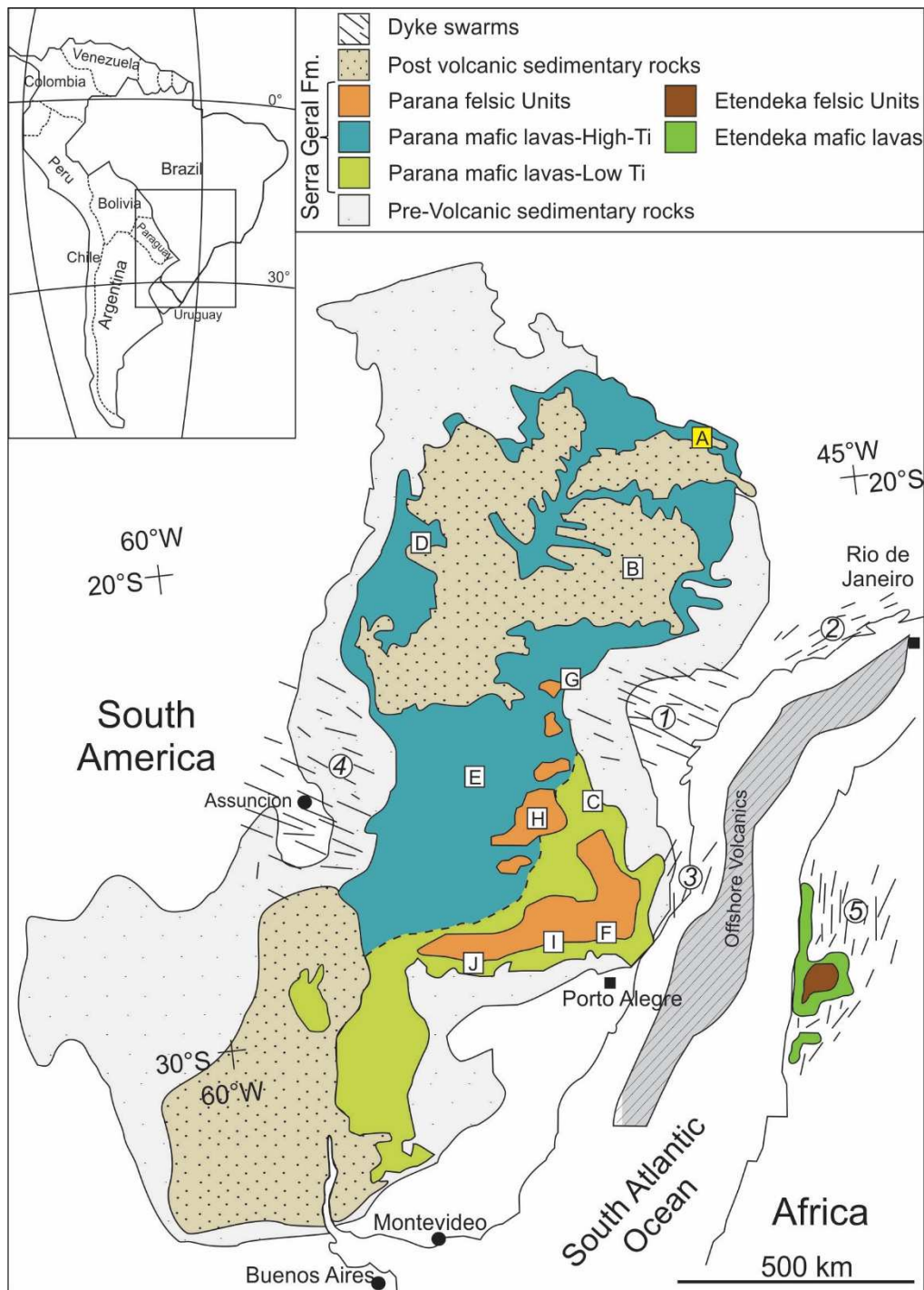


Fig. 19: Geological map of the major volcanic units of the Paraná-Etendeka Igneous Province (modified after Hawkesworth et al., 2000; Peate et al., 1992; Rossetti et al., 2017; Stewart et al., 1996). Dyke swarms: 1 – Ponta Grossa; 2 – Santos-Rio de Janeiro; 3 – Florianópolis; 4 – Paraguay; 5 – Skeleton Coast. Pillow lava occurrences: A – Study area (yellow square); Uberlândia-Araguari (Ferreira, 1985; Moraes et al., 2018; Moraes and Seer, 2017); B – São Paulo State (Mano, 1987); C – Rio Iguaçu (Marques Filho et al., 1981); Peperite occurrences involving basaltic lavas: D – West of Mato Grosso do Sul (Machado et al., 2015); E – West of Paraná (Waichel et al., 2007); F – Torres Syncline (Barreto et al., 2014; Rossetti et al., 2014); Peperite occurrences involving silicic lavas (Luchetti et al., 2014): G – São Jerônimo da Serra; H – Mangueirinhas and Palmas; I – Bento Gonçalves region; J – Santa Maria. Dashed lines correspond to an inferred contact between the northern (high TiO₂) and southern (low TiO₂) lava chemical groups as suggested by Hawkesworth et al. (2000).

Another relevant point of discussion is the interpretation of the paleoenvironmental conditions during the PEIP volcanism. According to Scherer (2000), the environment was hyperarid during the emplacement of these basaltic lavas, evidenced by the absence of wet interdune deposits or any other sedimentary feature that indicates a near surface ground-water level. Pillow lavas and rocks involving interaction between lava flows and wet sediments are described in different parts of the PEIP (Fig. 19), suggesting a wet environment in some portions (Ferreira, 1985; Luchetti et al., 2014; Machado et al., 2015; Mano, 1987; Marques Filho et al., 1981; Moraes and Seer, 2017; Waichel et al., 2007). Pillow lavas are scarce in the PEIP and the existing studies are focused on their descriptive aspects (Ferreira, 1985; Mano, 1987; Marques Filho et al., 1981; Moraes and Seer, 2017). Recently, geochemical aspects and a preliminary stratigraphy of the subaerial and subaqueous lavas of the studied area were addressed (Moraes et al., 2018; Moraes and Seer, 2017).

The aim of this work is to improve the stratigraphic framework of the northeastern part of the PEIP (Fig. 19) through the definition of lithofacies and lithofacies associations, and geochemistry, throughout a larger area than described by previous studies (Moraes and Seer, 2017). Results include the characterization of volcanic episodes, volcano-sedimentary interactions and interlava sedimentary beds, used as paleoenvironmental indicators. The interlava sedimentary rocks present in the PEIP are compared to other Igneous Provinces, evidencing their significance in terms of paleoenvironment and climatic conditions during the development of such impressive volcanic provinces. The interaction between lava and water/wet sediment described in this work underpins our understanding of the relation between the emplacement of the PEIP and climatic changes during the Early Cretaceous.

5.1.2 Regional setting

The PEIP is a CFBP that occupies an area of 1.2×10^6 km², volumes of around 0.8×10^6 km³ (Bellieni et al., 1984) and is associated with the Gondwana supercontinent break-up and to the formation of the South Atlantic Ocean around 135 Ma (Deckart et al., 1998; Renne, 2015; Thiede and Vasconcelos, 2010). The most significant part of the province is in South America (Brazil, Argentina, Paraguay and Uruguay) and nearly 6% of its area is located in the southwestern Africa (Namibia and Angola) (Peate et al., 1992). In South America, these rocks occur as thick volcanic

successions of the Serra Geral Formation and dykes swarms of Serra do Mar, Ponta Grossa, Florianópolis, and Paraguay (Fig. 19), essentially composed of basalts, basaltic andesites and, subordinately, felsic rocks. Geochemical studies allowed the division of this formation into two groups based on their TiO_2 contents and incompatible elements concentrations (Fig. 19). The high- TiO_2 and $\text{Ti/Y} > 310$ group occurs dominantly in the north of the province and is formed by the Pitanga, Paranapanema and Ribeira magma types. The south of the province is composed of the Gramado, Esmeralda (low- TiO_2 and $\text{Ti/Y} < 310$) and Urubici (high- TiO_2 and $\text{Ti/Y} > 310$) magma types (Peate et al., 1992; Peate, 1997).

Physical volcanology studies in the southern portion of the Serra Geral Formation permitted the recognition of different lava flow morphologies and the construction of a preliminary stratigraphy for the area (e.g. Barreto et al., 2014; Rossetti et al., 2014; Waichel et al., 2012). Rossetti et al. (2018) proposed a hierarchical change for the Parana volcanics, from Serra Geral Formation to Serra Geral Group, composed of four morphologically distinct formations (Torres, Vale do Sol, Palmas and Esmeralda formations), which are products of variations in the eruptive dynamics recognized in a vertical stratigraphic sequence. According to these authors, the volcanism onset in southern Brazil was characterized by compound pahoehoe lavas of Torres Formation overlaid by sheet-like rubbly pahoehoe from Vale do Sol Formation. The felsic lava domes and tabular lava flows from Palmas Formation occur covering both Torres and Vale do Sol formations, later covered by the youngest pahoehoe lava flows of the Esmeralda Formation.

The study area is located between Uberlândia and Araguari cities (Fig. 20A), in the state of Minas Gerais/Brazil (northeastern portion of the PEIP – Fig.19, area “A”), where volcanic units are overlying Precambrian metasedimentary and metaigneous rocks of the Brasília Belt. The Brasília Belt is a NW–SE trending structure evolved during the Neoproterozoic, and tectonically reactivated during the Upper Cretaceous and Cenozoic (Dardenne, 2000). According to Milani et al. (2007) this tectonic activity did not cause any deformation in the volcanic sequence of the study area. Few studies on the volcanological aspects of this region have recognized up to 250 meters thick volcanic sequences of subaerial and subaqueous lava flows, mostly composed by pahoehoe and subordinate pillow lavas, respectively (Ferreira, 1985; Moraes et al., 2018; Moraes and Seer, 2017; Pacheco et al., 2017). The stratigraphy proposed by those studies shows minor occurrences of pillow lavas and pyroclastic rocks locally

interbedded with pahoehoe lava flows from the upper stratigraphic levels (Moraes and Seer, 2017).

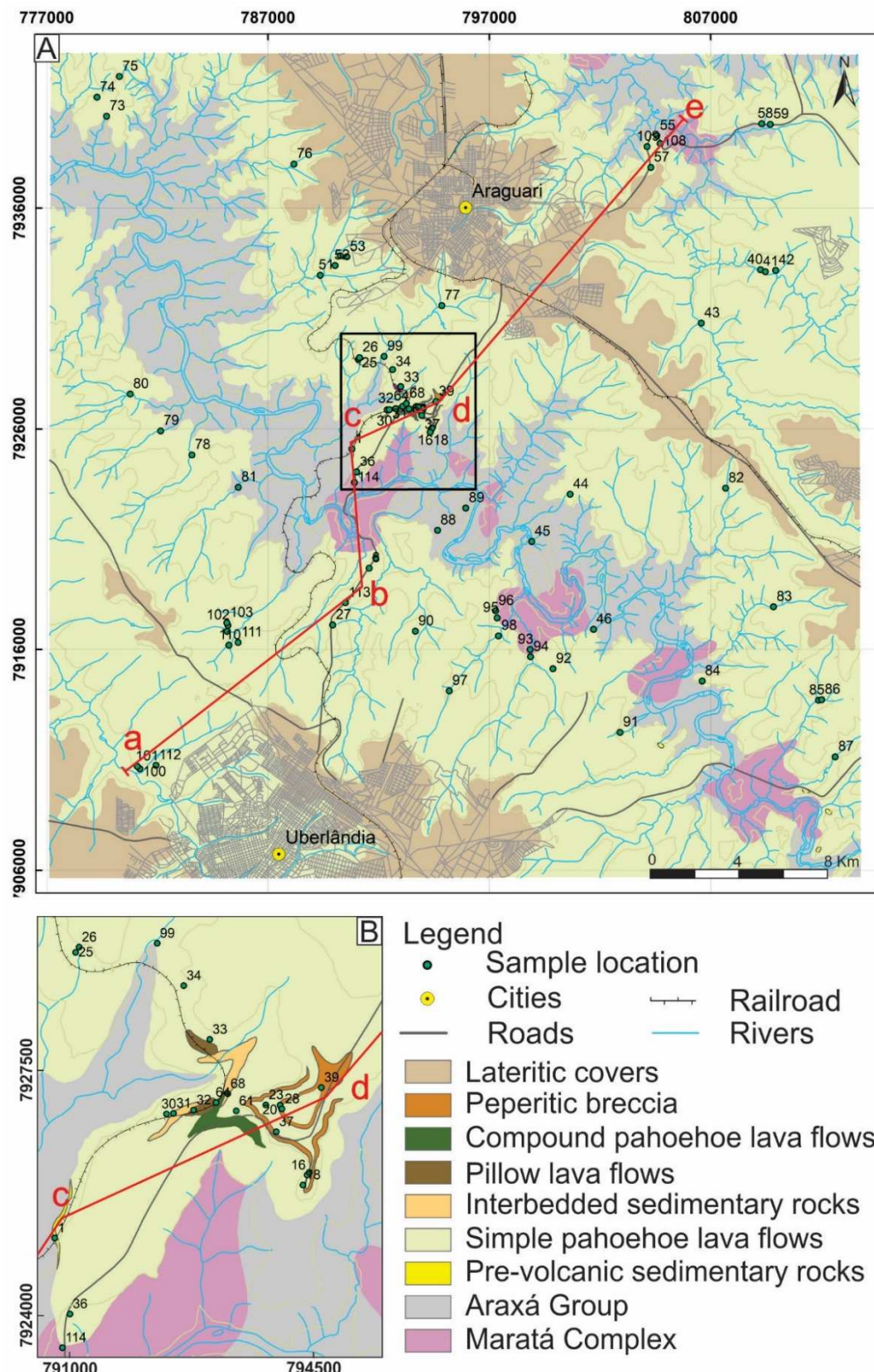


Fig. 20: A) Geological map of the Uberlândia-Araguari region with samples location (modified from Pacheco et al., 2017). B) Detail of the central portion of the study area. The red lines in figures A and B represent locations of the main stratigraphic logs across the study area.

An arid paleoenvironment is suggested since the onset of the PEIP volcanism, when the first lava flows interacted with the aeolian sand dunes of the Botucatu and Twyfelfontein formations, respectively in Brazil and Africa (Jerram et al., 1999a, 1999b; Scherer, 2000; Waichel et al., 2008), and persisted throughout the volcanic sequence, evidenced by the presence of interbedded continental aeolian sediments and lava flows, bypass surfaces at the top of the lava flows as well as fossils dunes isolated by lava (Jerram et al., 1999b; Scherer, 2000; Waichel et al., 2008). Nevertheless, some authors have described sparse deposits of peperite associated with wet sediments and pillow lavas, interpreted as an evidence of humid environments occurring mainly along the marginal parts of the Paraná province (Fig. 19) (Luchetti et al., 2014; Machado et al., 2015; Waichel et al., 2007). Besides occurring in the Uberlândia-Araguari area, pillow lavas also outcrop in the region of Usina de Foz de Areia (Rio Iguaçu, PR - Marques Filho et al., 1981) and Usina de Nova Avanandava (São Paulo State - Mano, 1987) (Fig. 19). Fluidal peperites containing mafic or felsic lava were also described in some portions of the PEIP (Luchetti et al., 2014; Machado et al., 2015; Waichel et al., 2007).

5.1.3 Material and methods

- Field procedures

For the stratigraphic characterization, five high-resolution composite sections were constructed. Lateral panels were created through photomosaic enabling the visualization of the lateral distribution and 2D geometry of lava flows.

Stratigraphic analysis in volcanic succession is based on lithofacies description, association, and interpretation. The term lithofacies is used in this work to describe rocks with a particular combination of lithology and physical structures, which can distinguish them from the adjacent rocks (Dalrymple, 2010). For igneous rocks, the composition and primary features (textures, structures, grain size, vesicles and amygdales patterns and the surficial lava flow features) are used to characterize different lithofacies. Lithofacies are represented by a code, following Miall (2000), in which capital letter represents lithology and lowercase the textures, structures and vesicles patterns (Barreto, 2016). The identified lithofacies were grouped in lithofacies associations, corresponding to genetically related facies with an environmental significance (Cas and Wright, 1987; Collinson, 1969; Dalrymple, 2010; Mcphie et al.,

1993), contributing for the reconstruction of paleotopography and the understanding of volcanic evolution.

- Petrography and mineralogy

A total of 111 samples from different lithofacies were petrographically characterized under an optical microscope, focused on their texture and mineralogy. In order to quantify the bulk mineralogy and to identify the major alteration products, 50 samples from different lithofacies were analyzed on an X-ray diffractometer (D/MAX - 2200/PC and Bruker D8). Both analyses were performed at Petrobras Research Center (CENPES) laboratories.

- Geochemical characterization

The geochemical characterization aimed to evaluate the chemical differences between lava flows throughout the stratigraphic sequence, within different portions (base, center, top) of the studied lava flows, and to compare with data from other parts of the Paraná Province. A total of 34 samples were analyzed for major, minor, and trace elements in Activation Laboratories Ltd. (Actlabs) under the packages Code S1, B3, RX6 and 4Litoresearch. The complete description of the analytical procedures, as well as the detection limit for each element, can be found at the Actlabs website (<https://actlabs.com/geochemistry/lithogeochemistry-and-whole-rock-analysis/lithogeochemistry/> and <https://actlabs.com/downloads/>).

5.1.4 Lithofacies description and associations

- Lithofacies

Sixteen lithofacies were recognized in the Araguari and Uberlândia lava flows. Lithofacies were defined emphasizing on the vesiculation patterns, textures, surface characteristics and geometry of lava flows (Tab. 2, Figs. 21, 22, and 23) Location of all outcrops presented in this work is displayed in Appendix B.

Tab. 2: Description and interpretation of the Uberlândia-Araguari volcanic lithofacies.

Lithofacies code	Description	Position within lava flow	Interpretation
Pillowed basalts (Bp)	Isolated circular, irregular, and elliptical lobes of dark gray to black coherent rock. Lobes vary from 25 cm to 5 m of diameter, surrounded by a glassy to low crystalline basaltic margin. Concentric fractures and vesicles are present. Vesicularity can reach up to 20% of the total rock volume and tends to concentrate in the upper part of the lobes.	-	Interconnected tubular lava lobes emplaced on a subaqueous environment.
Glassy basaltic breccia (Bgb)	Light green matrix-supported to locally clast-supported breccia. The glassy basaltic clasts are irregular, angular to curvilinear with dimensions of up to 15 cm. Jigsaw-fit texture and sparse vesicles are present in some clasts. Isolated pillows occur locally in some portions of the breccia. Matrix is composed of fine sandstone or mudstone.	-	Interaction of magma and lava with water led to quenching and fragmentation.
Aphanitic and vesicular basalt (Bv)	Dark gray to black coherent rock, aphanitic and vesicular. Vesicles are rounded and vary in size from 1 to 5 mm of diameter (average of 2 mm). Vesiculation can reach up to 15% of the total rock volume.	Base, upper crust	At the top of the flow, the upper crust confines gas bubbles rising from the underlying fluid. At the base, bubbles from the moving lava are trapped in the basal crust forming vesicles.
Aphanitic massive basalt with sparse vesicles (Bsv)	Dark gray to black coherent rock, aphanitic, with rounded vesicles varying from 1 mm to 1 cm of diameter.	Base, core	Fast cooling and low volatile supersaturation.
Basalt with proto-cylinder (Bproc)	Dark gray to black coherent rock, aphanitic, with an irregular to vertical trail of small vesicles (average of 2 mm) with indistinct limits. The vesicles trails can reach up to 25 cm length.	Base	Accumulation of vapor and differentiated melt.
Basalt with horizontal vesicle sheets (Bhvs)	Alternating sheets of vesicles. Vesicles are rounded to irregular and vary from 2 mm to 7 cm of diameter and sometimes are filled by secondary minerals. These sheets can reach up to 2 m thick.	Upper crust	Cooling front progressing downward into the lava accompanying inflation, fluctuations of pressure and/or flux during active inflation. Bubbles rising from the fluid core become trapped in the viscoelastic mush at the base of the upper crust.
Basalt with giant domed segregation vesicles (Bgv)	Dark gray to black coherent and aphanitic rock with domed to elongated vesicles. Vesicles can be filled by secondary minerals and reach up to 40 cm in diameter.	Upper crust	Coalescence of bubbles of different sizes by mass transfer over the lower solidification front.

Basaltic breccia (Bbr)	Clast-supported breccia with basaltic clasts (dark gray to dark-green) in a massive basaltic matrix. Clasts are sub-angular and rich in spherical, stretched/elongated vesicles (up to 10 mm of diameter).	Upper crust	Inflation and accumulation of volatiles due to tensile stress led to degassing and rupturing, while an increase in the effusion rates promotes brecciation.
Smooth billowy basaltic surface (Bbss)	Light brown to reddish surface of coherent basalt with some protuberances (about 10 cm high), rich in spherical and stretched vesicles filled by secondary minerals.	Upper crust	After the initial burst of liquid lava, the top of the flow becomes a smooth continuous flexible skin of cooled lava.
Ropy basaltic surface (Bros)	Corrugations of about 1 - 2 cm width on the surface of dark gray to black coherent basalt.	Upper crust	Flexible skin deformed by the motion of lava.
Basalt with pods filled by segregation vesicles (Bpod)	Dark gray to black coherent rock, aphanitic, with irregular zones of small vesicles (2 mm in diameter) with indistinct limits. Commonly, these pods have dimensions of around 6 cm and tend to be wider than proto-cylinders.	Base and core	Zone of segregation vesicles accumulation; frozen-in upward-rising gas bubbles.
Aphanitic and hypocrystalline columnar basalt (Bac)	Dark gray to black coherent rock with regularly spaced, well-developed columns with rectilinear or undulatory faces which usually have striations. Faces width vary from 15 cm to 2 m.	-	Slow cooling and crystallization led to contraction of solidified lava and formation of large and regular columns. Under a relative fast cooling regime and possibly water, the columns become narrow and with undulate limits.
Large coherent basaltic domain (Blcd)	Light to dark gray coherent rock of varied morphologies (lobe-like to tabular in 2D) and sizes (1 to 6 m long). These bodies are dispersed within breccia zones.	-	The large coherent basaltic domains represent the major feeder conduits that supplied magma to develop peperitic domains.
Close-packed sediment-matrix basalt breccia (Bcb)	Monolithic clast-supported breccia composed by basalt clasts within a sedimentary matrix. The basalt clasts are massive to scoriaceous and vary from 1 cm to 1,5 m in diameter. Fluidal and blocky clasts morphologies are present. Jigsaw-fit texture is a common feature.	-	Rock formed by interaction of lava and unconsolidated sediments. The progressive brittle failure of the quenched magma with little relative displacement of the basalt fragments results in close-packed peperites.

Disperse sediment-matrix basalt breccia (Bdb)	Monolithic matrix-supported breccia composed by basalt clasts within a sedimentary matrix. The basalt clasts are massive to scoriaceous and vary from 1 cm to 1,5 m of diameter. Fluidal and blocky clasts morphologies are present. Jigsaw-fit texture is a common feature.	-	Rock formed by the interaction of lava and unconsolidated sediments. Disperse peperites form when masses of quenched, fragmented magma become detached from larger feeder conduits and move short distances into the unconsolidated host sediment by fluidization or hydromagmatic explosions.
Laminated sediment-matrix basalt breccia (Blmb)	Monolithic breccia composed by basalt clasts within laminated sedimentary matrix. The lamination are few millimeter thick, and the dimension of blocky basaltic clasts vary from few centimeters to few decimeters.	-	Rock formed by the infiltration of sediment in the spaces between volcanic clasts in a pre-existing breccia.

- Lithofacies associations

The separate volcanic lithofacies can be grouped in lithofacies associations, which are a result of volcanic processes such as effusion rate, lava supply, paleotopographic and paleoenvironmental influences. Due to the limited lateral extent of the outcrops no direct observation could be made on the lateral variation of lithofacies association occurring with distances greater than 1-2 km. For this reason, we have used field morphological aspects to identify the lava types. We used the terms "simple" and "compound" lavas, introduced by Walker (1971), to describe the morphologies and their lithofacies associations.

Five lithofacies associations were identified in the Uberlândia-Araguari region: pillow lavas, compound lava flow, simple lava flow, and two lithofacies association involving sediment-matrix basalt breccia (peperite and sediment-infill basalt breccia) (Fig. 20 and Tab. 3), detailed in the following sections.



Fig. 21: Volcanic lithofacies of Uberlândia-Araguari region: A) Pillowed basalts (Bp, white dashed line) and glassy basaltic breccias (Bgp). The yellow arrows indicate flame structures of the underlying sedimentary rock; B) Detail of glassy basaltic breccia with glassy basaltic fragments (red arrows) and sedimentary matrix (black arrows); C) Aphanitic massive basalt with sparse vesicles (yellow arrows) and amygdales (white arrows) filled with zeolite; D) Basalt with pods filled by segregation vesicles at the base of the unit; E) Aphanitic vesicular basalt flow top; F) Basalt with proto-cylinder vesicles.

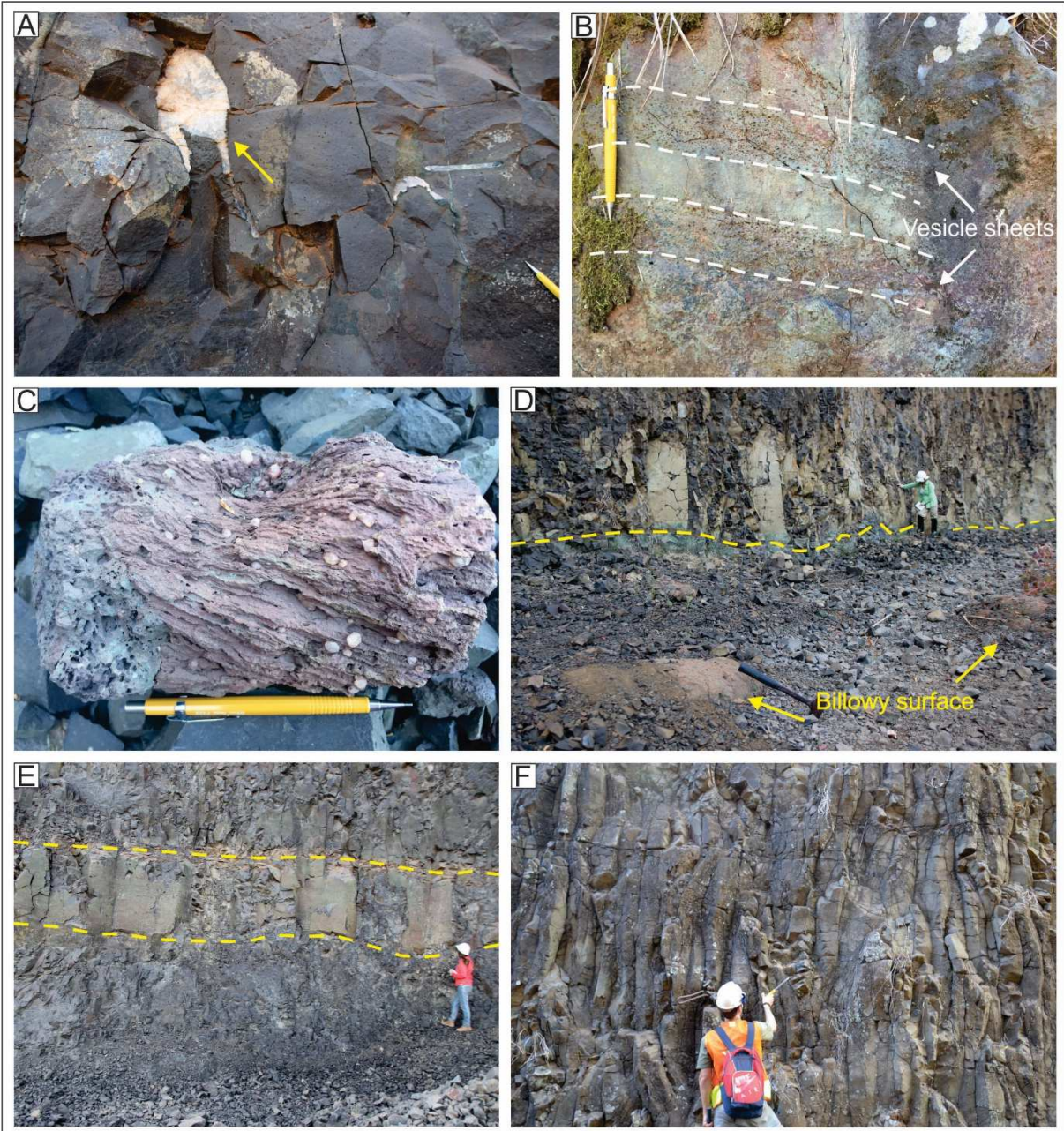


Fig. 22: Volcanic lithofacies of Uberlândia-Araguari region: A) Basalt with giant amygdales (< 40 cm, yellow arrow) filled with silica; B) Upper portion of basaltic lava with sheet vesicles (dashed lines); C) Basalt with ropy surface; D) Basalt with smooth billowy surface (yellow arrows). Dashed line shows the contact between two lavas; E) Columnar basalt with rectilinear faces; F) Columnar basalt with undulatory faces.

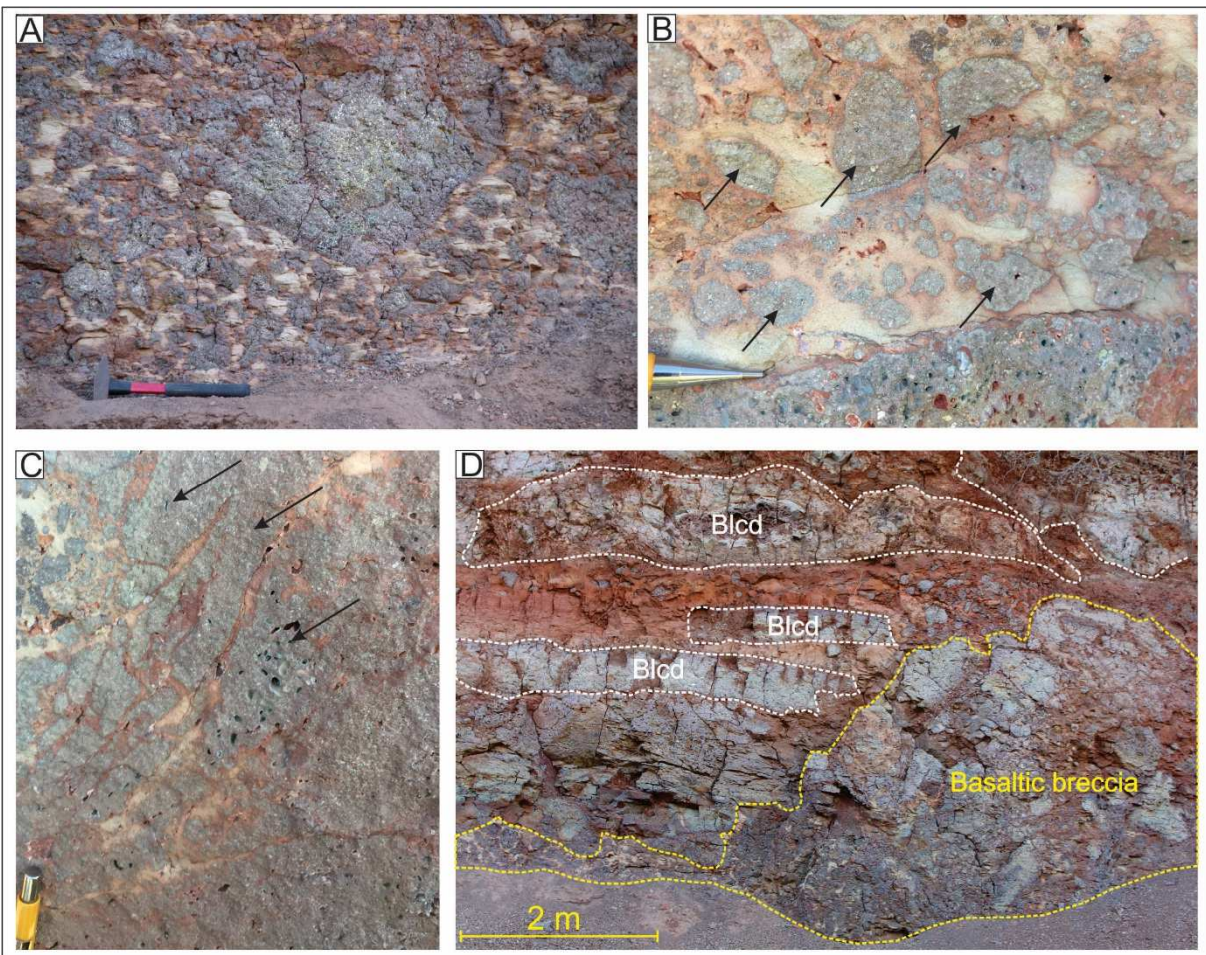
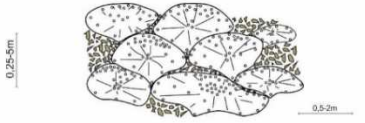
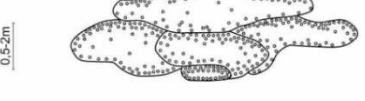
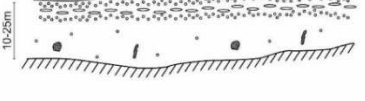
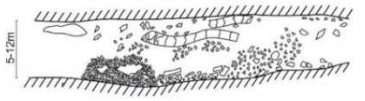


Fig. 23: Lithofacies of Uberlândia-Araguari region: A) Laminated sediment-matrix basalt breccia occurring on the top of a basalt unit from the central portion of the study area; B) Dispersed sediment-matrix basalt breccia occurring on the top of a basalt unit from the central portion of the study area. Basalt fragments (black arrows) are dispersed within a silty sandstone; C) Close-packed sediment-matrix basalt breccia occurring on the top of a basalt unit in the central portion of the study area. Basalt fragments are closely packed within a tight framework (black arrows); D) Peperitic domain with close-packed and dispersed sediment-matrix basalt breccia (yellow dashed lines) and large coherent basaltic domain (Blcd) lithofacies (white dashed lines).

Tab. 3: Lithofacies association of the Uberlândia-Araguari region (modified from Barreto et al., 2014; Duraiswami et al., 2013).

Lithofacies association	Description	Interpretation	Lithofacies	Lithofacies geometry
Pillow lava	Pillow lava deposits are formed by pillow lobes (Bp) and interpillow sediments rich in glassy basaltic breccias (Bgb). The pillow lobes exhibit individual thicknesses of 0,25 to 2,5 m.	Pillow lavas are formed under water and high cooling rates, low effusion rates and on gentle slopes. Lavas solidify under a semi-solid carapace. New pillows grow as old pillows stretch and crack extruding fresh lava.	Bp, Bgp	
Compound pahoehoe	P-type lobes exhibit individual thicknesses of 0,5 to 2 m including a vesicular base and top (Bv) and a core with sparse vesicles (Bsv). The thin glassy surfaces can be smoothy (Bbss) or ropy (Bros).	Compound pahoehoe lavas are emplaced under low effusion rates with intermittent lava supply and minimum inflation. Lavas fill the pre-existing topography controlled by the available accommodation space. Lavas solidify under a semi-solid carapace.	Bv, Bsv	
Simple pahoehoe	Simple pahoehoe flows exhibit individual thicknesses of up to 25 m of basalt with a vesicular crust (Bv), and sparse vesicles (Bsv) at the base and core. These flows include some features and segregation structures (Bhvs, Bgv, Bproc, Bpod, Bros, Bbss and Brt).	Simple pahoehoe flows are formed under low effusion rates with sustained lava supply, where the inflation process is dominant. The emplacement occurs on flat terrains. Lavas solidify under a semi-solid carapace, allowing the thickening of lobes.	Bsv, Bproc, Bpod, Bgv, Bhsv, Bv, Bbss, Brop, Bros, Brt	
Peperite	Peperite deposits are composed of large coherent basaltic domains (Bcd), close-packed and disperse volcanic breccia (Bcpb, Bdb). Basalt clasts can be blocky and fluidal. The host sediments can be vesicular, massive or have the pre-existing beds destroyed or deformed by fluid migration.	Peperites are formed by disintegration of lava mingling with unconsolidated or poorly consolidated, typically wet sediments. Developed in a wide variety of successions formed where magmatism and sedimentation are contemporaries.	Bcb, Bdb, Blcd	

Simplified stratigraphic logs are presented in figure 24. As previous studies have shown that the northern-northeastern portion of the PEIP was not affected by tectonism after lava emplacement (c.f. Milani et al., 2007), elevation has been used as basis for the construction of the stratigraphy of the study area.

Pillow lavas

The pillow lavas are restricted to the central study area and outcrop in road cuts of the Ferrovia Centro Atlântica railway, between the Stevenson and Pontilhão do Fundão stations. Two intervals of pillow lavas are identified at different altitudes along the railway, in the intermediate portion of the local stratigraphy (Fig. 24). The lower interval (709 m to 715 m of altitude) is well preserved, around 6 m thick and 300 m in length, whereas the upper interval (728 to 738 m of altitude) is highly altered and composed of close-packed and dispersed pillows, 10 m thick and 400 m in length (Fig. 21A and 7A). The dispersed pillows are immersed in a fine matrix of glassy fragments (Fig. 25A). The contact between the pillow lavas and adjacent rocks is abrupt, with a slightly inclined surface separating them from the superposed compound (lower interval) and simple pahoehoe lavas (upper interval) (Fig. 25C and 25D). Pillow lava

results from lava emplacement in subaqueous environment, usually associated with low effusion rates and topographic gradients (Gregg and Fink, 1995; Griffiths and Fink, 1992).

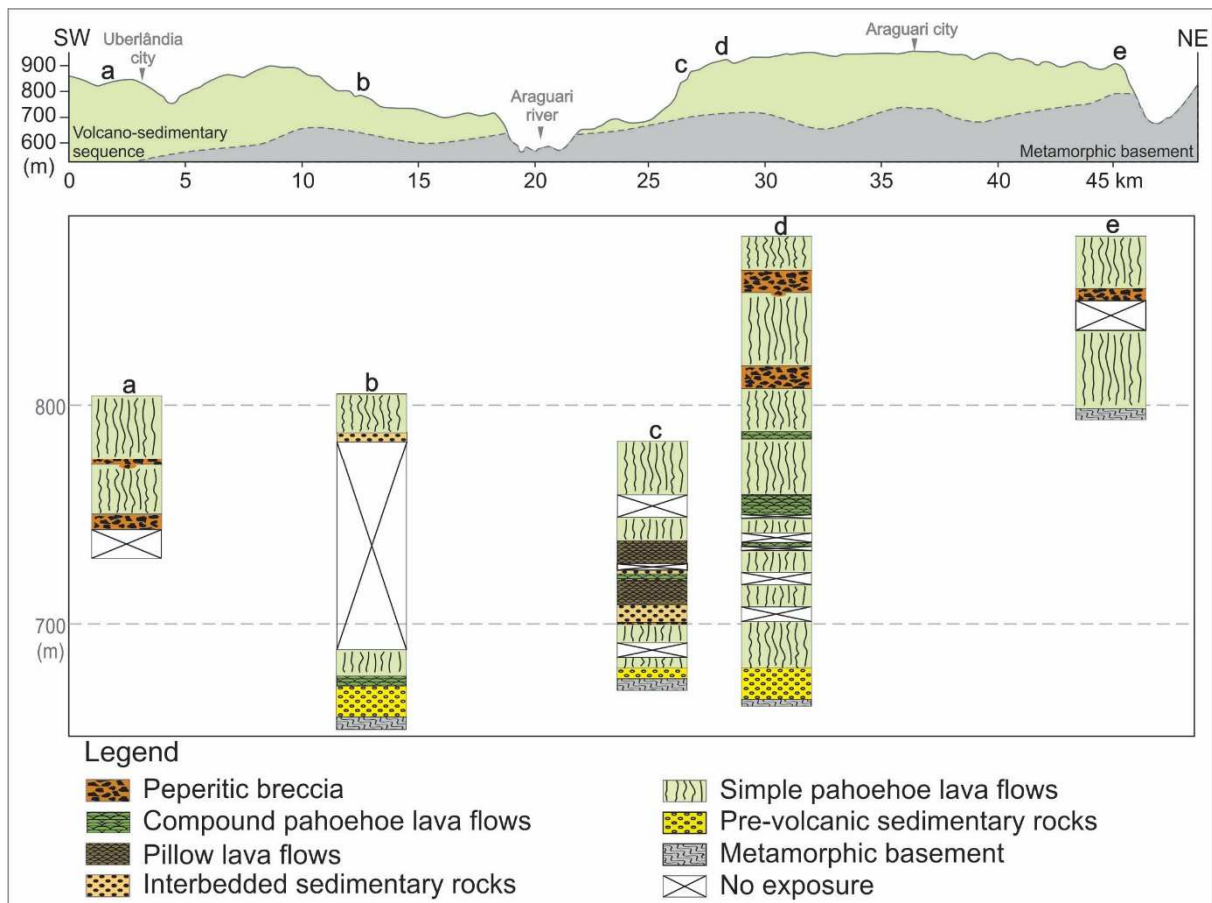


Fig. 24: Summary of stratigraphic cross-section with composite logs showing the lithofacies associations of each study site (see Fig 2A and 2B for the vertical profiles location). Elevation is used as the reference point for correlation (see discussion in the text).

Pillowed basalts and glassy basaltic breccia (Fig. 21A) compose this lithofacies association. The glassy basaltic breccias correspond to glassy clasts-rich deposits (hyaloclastites) formed in response to thermal stresses (Fig. 21B). Pillowed basalts vary in shapes and sizes (stretched to spherical - 25 cm to 5 m) (Fig. 25B) and are characterized by fine-grained hypohyaline and porphyritic basalts, with vesicles and glassy groundmass altered to smectite (Fig. 26A). Their external crust is more vitreous (60 – 90% of glass) than the core (20 – 50% of glass) (Fig. 26A, 26B). Vesicles and amygdales are abundant, partially or completely filled by smectite, celadonite, zeolite,

and calcite, and rare opaque minerals (Fig. 26A) occupying up to 20 % of the total rock volume and tend to concentrate in the upper and central portions of the structures.

The interpillow material is composed of altered vitreous fragments immersed in siliciclastic (mud and sand) and carbonate (calcrete lithoclasts) sedimentary rocks (Fig. 26C). The glassy clasts have curviplanar edges, and are altered to palagonite, smectite, and zeolite. Articulated and disjointed ostracod valves (< 1 mm) are common in the sedimentary matrix.

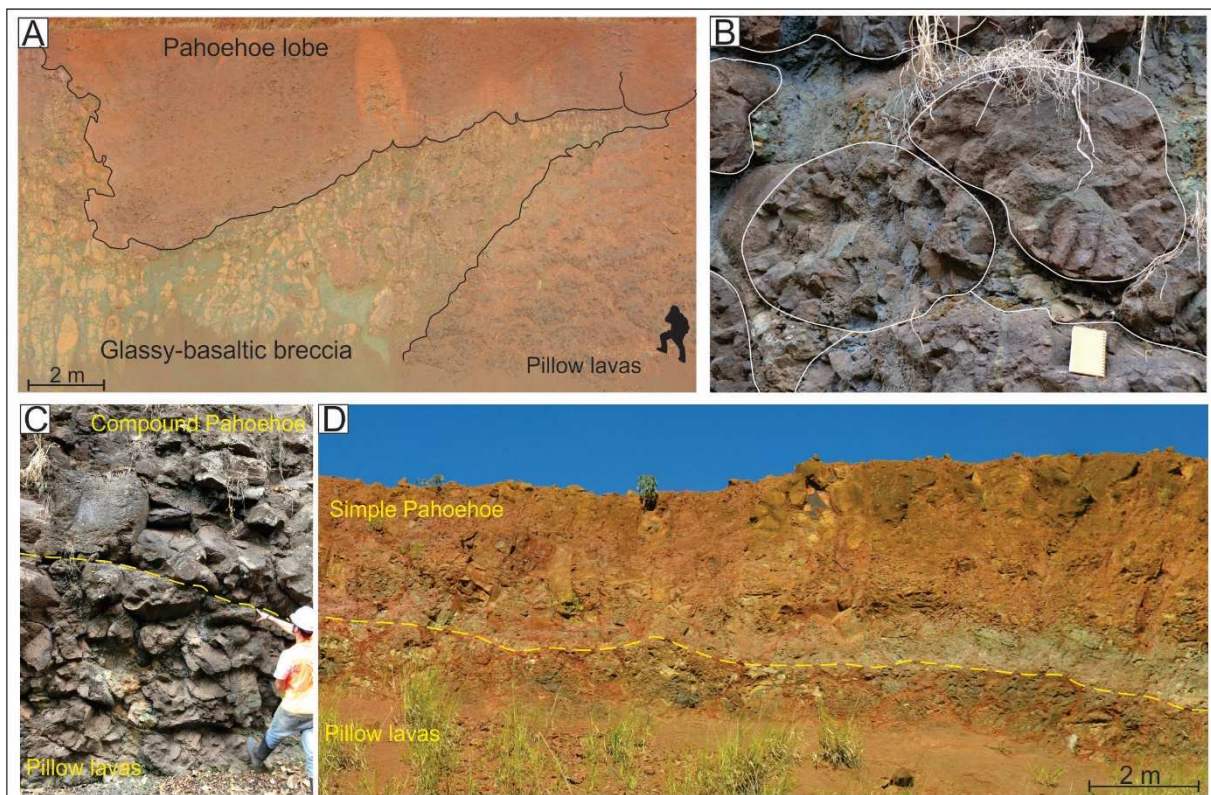


Fig. 25: Pillow lavas from the central portion of the study area. A) Highly-altered pillow lavas from the upper interval. Close-packed pillows superposed by glassy basaltic breccias and subaerial pahoehoe lobe; B) Pillow lavas with varied shapes and radial cracks; C) Contact between subaerial and pillow lavas from the lower interval; D) Contact between subaerial lava flows and pillow lavas from the upper interval.

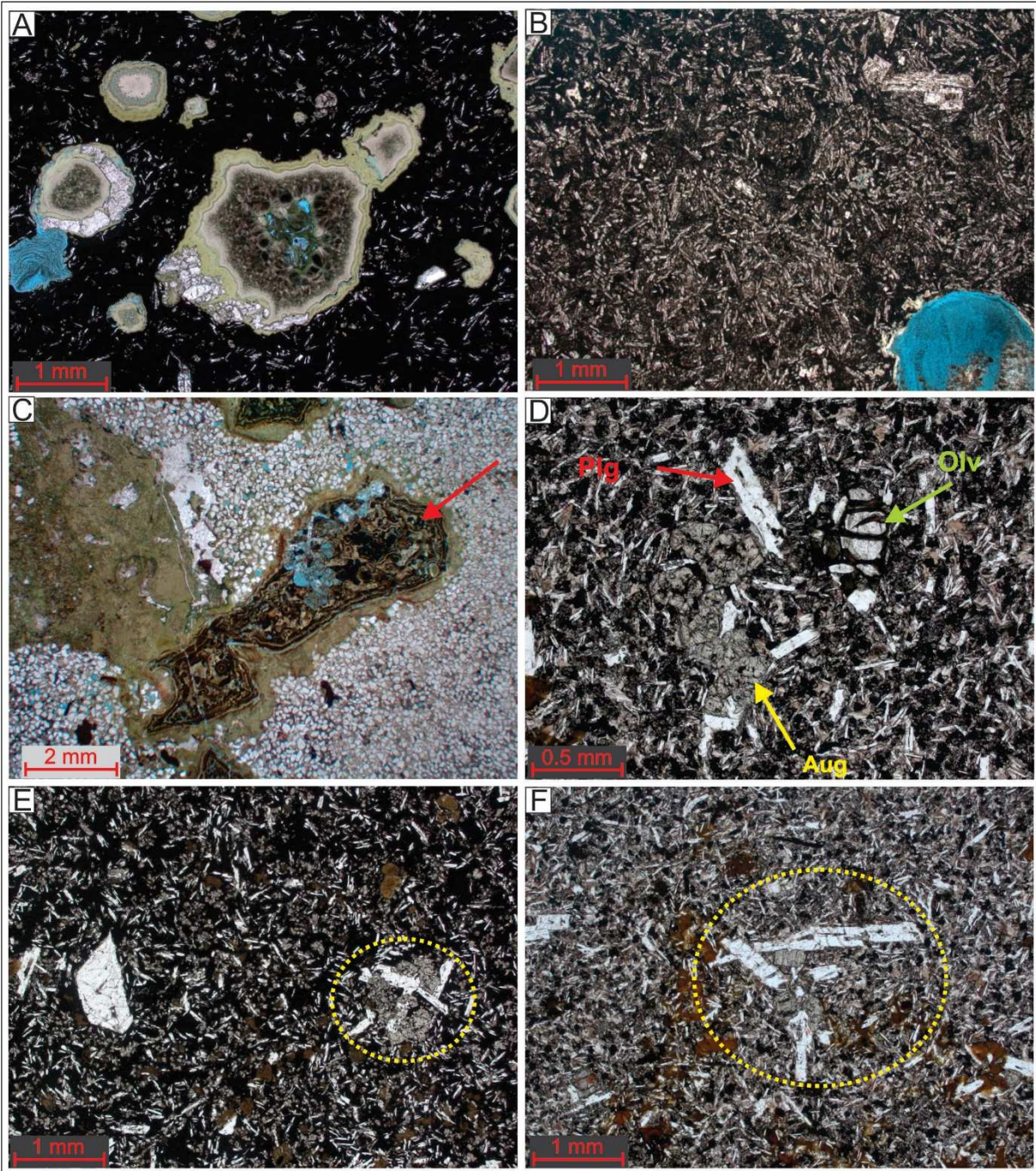


Fig. 26: Photomicrographs of the basaltic lavas: A) Amygdaloidal basalt from the margins of a pillow lava: vitrophyric basalt with plagioclase and augite microphenocrysts and large amygdales are filled with calcite and smectite, PP; B) Pillow lava central portion: basalt with plagioclase microphenocrysts and vesicles. Note a higher crystallinity when compared with the pillow margins in (A), PP. C) Vitreous clast with curviplanar edges (red arrow) and greenish mudstone clasts in a sandy matrix, PP; D) Detail of augite (Aug - yellow arrow), plagioclase (Plg - red arrow), and olivine (Olv - green arrow) phenocrysts. Olivine crystal is partially altered to iddingsite, PP; E) High glass content in basalt with undulatory columns. Dashed yellow circle highlights plagioclase and augite phenocrysts, PP; F) Lower glass content in basalt with rectilinear columns. Dashed yellow circle highlights plagioclase and augite phenocrysts, PP. PP= plane polarizer, blue color represents the resin color used in the slides preparation.

Compound and simple lava flows

The volcanic succession of the study area comprises compound and simple pahoehoe petrographically characterized by fine-grained hypohyaline and porphyritic basalts with groundmasses commonly altered to smectite (Fig. 26D).

The compound pahoehoe lava flows are restricted to the central portion in the study area and typically occur at the base of the simple pahoehoe lava that occupy low and intermediate stratigraphic levels (Fig. 24). Cross section through compound pahoehoe and pillow lavas can be very similar. These lobes were interpreted as subaerial compound pahoehoe because aqueous sediments, aquatic fossils and spalled-off glass fragments are absent between the lobes, and the aspect ratio of these lobes are bigger than the pillow lava of the studied area (c.f. Walker, 1971). The lava lobes vary from 0.5 to 2 m in diameter and are stacked in packages of up to 7 m thick. The lateral extent of the packages reaches up to 20 m. The contact with the adjacent rocks varies from gradual with sedimentary intervals to abrupt with pillow lavas of the central study area (Fig. 25C). Siliciclastic lenses are common at the base of the compound lava flows.

The lava lobes of the compound pahoehoe have a smooth surface and chilled margins, which are commonly oxidized. Spherical vesicles and amygdales (2 mm to 1 cm in diameter) are abundant at the top and base of the lobes and sparse in the central portion. Though pipe vesicles are absent, features such as a massive core and vesicular margins are typical of P-type lobes (Walker, 1971; Wilmoth and Walker, 1993).

Simple pahoehoe lava flows are the most abundant morphology occurring in the studied area, occupying upper stratigraphic levels and, subordinately, lower and intermediate levels (Fig. 20 and 24). The lowest simple pahoehoe lava flows are 7 m thick, whereas the upper ones reach up to 25 m thick and at least 2 km in length. Sedimentary and peperitic packages of up to 10 m thick occur interleaved with these lavas (Fig. 27A) further described in the following sections. The basal contacts of most of the simple pahoehoe lava flows are abrupt and concordant to the underlying sedimentary packages, which locally present preserved hyaloclasts or molds of lava lobes on their surfaces. In the central portion of the study area, an igneous body is bracketed by peperite and present a diffuse upper and lower contact with the peperites (Fig. 24 – Log d).



Fig. 27: Features of the subaerial flows in the study area. A) Panoramic view of simple pahoehoe lava flows separated by a thick peperite layer in the inactive Arpasa quarry (log D); B) Dome-like features filled by peperitic breccia at the top of the simple pahoehoe flow (yellow solid line) in the active Arpasa quarry (log D); the undulatory columns converge towards the dome-like features (yellow arrows) and the horizontal layer of columnar basalt with rectilinear faces (yellow dashed line) dips adjacent to this area; C) Basaltic breccia occurring locally on top of a simple pahoehoe in the inactive Arpasa quarry (log D).

The simple pahoehoe lavas are composed of basalt with poorly vesicular bases and cores, rare proto-cylinders and irregular vesicle pods. The upper lava crust is characterized by an increase in the vesicles content towards the top, in which giant vesicles (up to 40 cm in diameter) are filled by quartz, chalcedony and celadonite. Sheet vesicles are rare but can also occur at the top of the lava flow, characterized by levels rich in vesicles and amygdales. Ropy and smooth billowy surfaces were described in the central part of the study area. Rarely, the upper lava crust has been fragmented (Fig. 27C), interpreted as a product of increment of lava supply (Duraiswami et al., 2014). This lava morphology is interpreted as product of sustained lava supply and high effusion rates (Walker, 1971).

The formation of columnar joints in simple lava flows is related to cooling and subsequent advance of the isotherms towards the center of the lava flow (Forbes et al., 2014; Goehring, 2008; Lyle, 2000; Spry, 1962). The striations are structures formed at the columns surface due to the propagation of the cracks and their cyclic

terminations (Ryan and Sammis, 1978). The size of the columns and striations can possibly indicate the temperature gradient and cooling rates. Thermal models have shown that their sizes are inversely proportional to the cooling rates, thus thin columns and small striations suggest rapid cooling (Forbes et al., 2014; Grossenbacher and McDuffie, 1995).

Cooling joints are common features in the area, being represented by columnar basalts with rectilinear and wavy faces in long-sections. The undulatory columns are common, whereas the rectilinear columns are less common and occur as continuous zones (up to 2 m thick) in different portions of the lava flows (Fig. 22E, 22F, and 27B). The undulatory columns are narrow (15–50 cm across) with curvilinear borders, and are more vitreous (10 – 40% of glass – Fig. 26E) than the rectilinear columns (5 – 15% of glass – Fig. 26F), which are wider (1–2 m) with straight borders and longer striations (15 cm in length). In general, columns are perpendicular to lava flow boundaries. However, this pattern may vary nearby irregular dome-like features (4 m of diameter) filled by volcaniclastic breccia, as observed in some quarries, in which undulatory columns present a radial pattern around the dome-like features and the layer with rectilinear columns show a divergent pattern from the contact of the dome towards the center of the lava (Fig. 26B). Besides the radial columnar joints, the basalt close to the dome-like features can show local variation in its vesicle pattern.

The presence of both types of columns within a single unit suggests cooling rate variations during crystallization, with relatively higher cooling rates being associated with narrower columns (Forbes et al., 2014; Grossenbacher and McDuffie, 1995; Long and Wood, 1986). According to Goehring (2008), undulatory columns occur as a result of oscillatory instability of fracture tips caused by thermal stress, as they advance to form the columnar faces.

Sediment-matrix basalt breccia

In the southwest and central portions of the study area, intervals of sedimentary-matrix basalt breccia are present occurring as irregular to tabular layers of up to 12 m thick and at least 1.7 km long (Fig. 28A). These layers occur mainly along the lower contact of simple lava flows, but in the central portion of the study area, these breccias can occur in both upper and lower contacts of an igneous body.

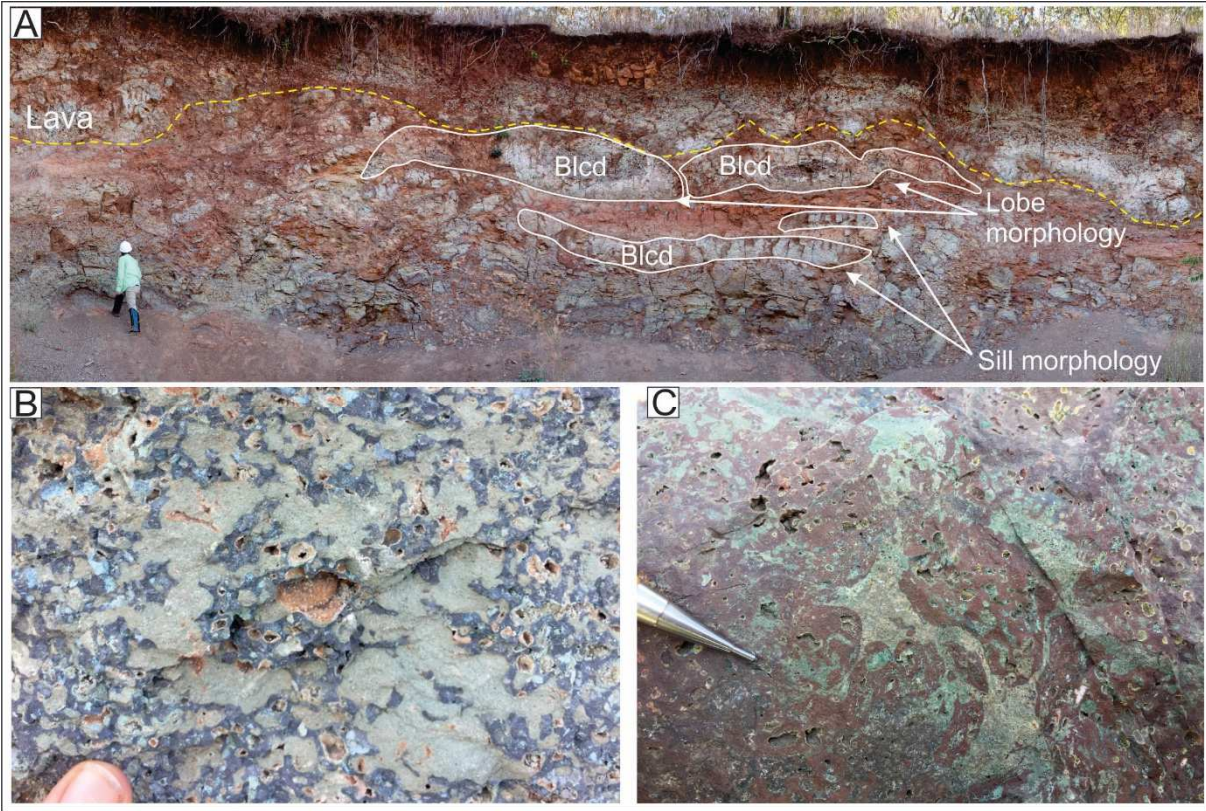


Fig. 28: General aspects of sedimentary-matrix igneous breccia intervals. A) Peperite layer on the base of a basaltic flow at Arpasa inactive quarry (yellow dashed line delimits the base of the lava flow and the top of the peperite, whereas the base of the peperite is covered by talus deposits); coherent igneous domains (Blcd) in the form of lobe and sill are represented by the white solid lines; B) Basaltic dark gray fragments with irregular blocky morphology; C) Basaltic reddish fragments with irregular fluidal morphology.

Two different facies association involving sediment-matrix volcanic breccia were identified in the study area. One facies association includes close-packed and dispersed sediment-matrix basalt breccias and coherent igneous domains in the form of lobes (up to 5 m) or sills (up to 1 m thick and 6 m in length) (Fig. 28A). The igneous clasts are texturally and mineralogically similar to the associated igneous body, with plagioclase and augite microphenocrysts, rare pseudomorphic olivine microphenocrysts immersed in a glassy groundmass with plagioclase microlites (Fig. 29A, 29B, and 29C). These clasts vary in size (<1 cm to 1.5 m) and shape (blocky or fluidal) (Fig. 28B and 28C). Their margins can be fluidal, cuspatc, curvilinear to sub-planar or with bulbous projections similar to toes (Fig. 29A and 29B). Jigsaw-fit texture is preserved evidencing the *in situ* fragmentation. The basalt fragments can contain spherical to irregular vesicles, partially or completely filled by celadonite, smectite, zeolite, sediments, and small sub-angular fragments of glassy basalt. The sedimentary

matrix is formed of generally massive silty sandstone, sandy mudstone, siltstone or mudstone, composed mainly of quartz with subordinate plagioclase, alkali feldspar and rare heavy minerals (tourmaline, zircon, and garnet), micas, and clay minerals (Fig. 29A, 29B and 29C). Vesicles and fractures in the basaltic clasts can be filled with sediment evidencing that sediments were unconsolidated. Additionally, vesicles of 2 mm in diameter, partially filled by microcrystalline silica, were also observed in the sedimentary matrix of peperitic breccias, near the contacts between the basaltic clasts and sedimentary matrix (Fig. 29C). These facies association are interpreted as peperite deposits which is formed by the disintegration of lava mingling with unconsolidated or poorly consolidated sediment (White et al., 2000).

The other facies identified in the study area occur locally on the top of a basalt and comprises laminated sediment-matrix basalt breccia (Fig. 23A). The basalt clasts are blocky, have irregular margins (varying from curvilinear to sub-planar) and can reach up to 80 cm. These clasts can be massive to vesicular, with vesicles partially or completely filled by celadonita, smectite and sediments. The sedimentary matrix of this domain is composed by slight horizontal laminations (up to ten millimeters) with different composition and granulometry. In general, these laminations are composed mainly of quartz (sand and silt granulometry) and clay minerals. The difference between distinct layers lies in their clay mineral content. These facies are interpreted as sediment infill basalt breccia, where the fine sediment are deposited in the void spaces between volcanic clasts in a pre-existing breccia (e.g. Rosa et al., 2016). Laminations are conformable with the regional bedding, suggesting they were developed during infiltration of sediments within the basaltic clasts.

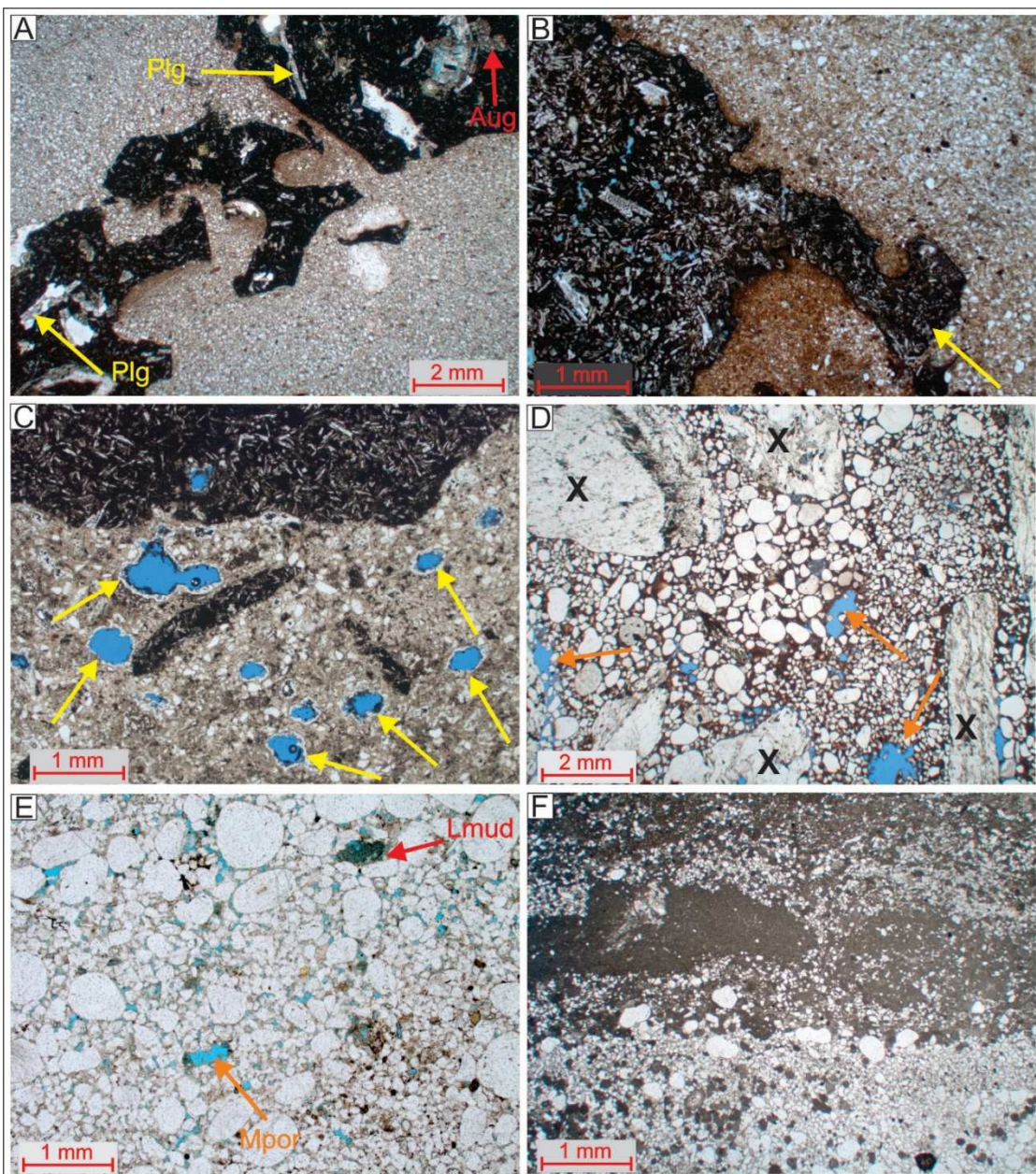


Fig. 29: Photomicrographs of sedimentary and peperitic levels. A) General aspects of peperite with irregular angular juvenile fragments with augite (Aug - red arrows) and plagioclase phenocrysts (Plg - yellow arrows). Dominant curvilinear to sub-planar margins, PP; B) Basalt fragments with dominant crenulate margins in contact with a silty sandstone matrix. Finger-like bulbous projection indicated by the yellow arrow, PP; C) Sedimentary portion of peperitic domain with vesicle rims partially filled by microcrystalline silica (yellow arrows), PP; D) Matrix-supported conglomerate with crystalline basement pebbles (indicated by letter X) occurring below the volcanic sequence (corresponding to pre-volcanic sedimentary rocks). Moldic porosity given by dissolution of lithic fragments is indicated by the orange arrows, PP; E) Bimodal sandstone composed of rounded quartz grains and subordinate alkali feldspars and mudstones lithoclasts (Lmud - red arrow). Moldic porosity given by the dissolution of the lithoclasts is indicated by the orange arrows (Mpor). Sample from sandstone layer occurring between the pillow lava and the compound pahoehoe lava flows, PP; F) Calcrete layer with sand levels and planar lamination occurring below the pillow lavas, PP. PP= parallel polarizer, blue color represents the resin color used in the slides preparation.

Sedimentary rocks

Sedimentary rocks occur at the base of the volcanic succession and as isolated packages (30 cm to 10 m thick) interleaved with lavas at different stratigraphic levels (Fig. 24). The maximum extension identified for these packages is of 600 m, though they can reach up to 1.2 km. The sedimentary layers are constituted of mudstones, calcrete, silty to conglomeratic sandstones, and conglomerate with basaltic and gneissic lithoclasts (up to 5 cm of diameter). In general, the conglomerates show slight normal grading beds of up to 1 m thick with imbricated lithoclasts and incipient cross stratification, whereas the sandstones may have slight granulometric laminations. Mudstones and calcrete are restricted to the central portion of the study area, associated with pillow lavas, whereas sandstones and conglomerates occur all over the area. Intense post-depositional alteration, such as calcrete formation, zeolitization, and silicification obliterated primary sedimentary structures and textures of the deposits in the central area. Load structures, molds of lava lobes and sediment lenses interleaved with compound pahoehoe suggest that unconsolidated or poorly consolidated sediments were deposited during volcanism breaks. These coarse sedimentary deposits are interpreted as alluvial fan deposits with contribution of aeolian sediments whereas the fine-grained rocks (mudstone) are interpreted as deposits of fluvio-lacustrine systems (c.f. Moraes and Seer, 2017; Moraes et al., 2018). The fluvio-lacustrine sedimentary rocks associated with pillow lavas occur at the intermediate stratigraphic level of the central area.

Petrographically, sandstones and conglomerates main constituents are sub-rounded to sub-angular quartz grains, with subordinate alkali feldspar, plagioclase and lithoclasts of gneisses, schists, basalt, mudstones, and calcrete (Fig. 29D and 29E). Heavy minerals (garnet, zircon, tourmaline, titanite, and opaque minerals) rarely occur. Lamination marked by granulometric and compositional variations can be present in some sandstones, which can have a film of oxide covering grains surface. The films of oxide and grains roundness, suggest contribution of aeolian sediments for these deposits. Porosity is dominantly intergranular, with subordinate moldic porosity caused by the dissolution of lithic fragments (Fig. 29D and 29E).

Mudstones intervals are mainly composed of quartz, plagioclase, alkali feldspar, and illite-smectite interstratified minerals based on optical petrography and XRD analysis (Appendix C). The calcrete layer is characterized by sand levels interleaved with beds of micritic calcrete, mudstones, and calcrete lithoclasts (Fig. 29F). Articulated

and disjointed ostracod valves (< 1 mm) are common in fluvio-lacustrine deposits. Post-depositional alteration, such as calcite, zeolite, and silica occur as cement, replacing primary minerals and obliterating primary sedimentary structures.

5.1.6 Geochemistry and relation to PEIP magma types

The thirty-four analyzed samples have major oxide contents recalculated to 100% on an anhydrous basis; SiO_2 contents vary from 51.05 to 46.33 wt.% (average 49.70 wt.%). MgO and TiO_2 vary, respectively, from 5.60 to 3.25 wt.% and 4.03 to 3.03 wt.%, and have averages of 4.90 and 3.44 wt.% (Appendix D). Based on the CIPW norm, all samples are classified as quartz tholeiites; normative quartz and hypersthene contents vary from 4.32 to 14.71% and 7.22 to 12.31%, respectively. In the TAS diagram (Le Bas et al., 1986), samples plot in the basalt and trachy-basalt fields (Fig. 30A), classified as subalkaline when plotted in the diagram based on the ratios of immobile elements (Winchester and Floyd, 1977) (Fig. 30C). Due to the elevated LOI values of the studied samples, the classification diagram based on immobile elements was considered in this study, because immobile elements are less affected by alteration processes.

Pahoehoe lava flows and pillow lavas present very similar values of major and trace elements (Tab. 4 and Appendix D). In general, pillow lavas have SiO_2 contents varying from 47.20 to 50.97 wt.%, MgO from 3.25 to 5.60 wt.%; and TiO_2 from 3.47 to 4.03 wt.%. The concentration of Ni ranges from 50 to 60 ppm, Zr from 275 to 329 ppm and Sr from 494 to 613 ppm. Similarly, pahoehoe lava flows have SiO_2 contents varying from 46.33 to 51.05 wt.%; MgO from 4.20 to 5.50 wt.% and TiO_2 from 3.03 to 4.02 wt.%. Trace elements concentrations are characterized by 50 to 110 ppm of Ni, 187 to 289 ppm of Zr, and 447 to 573 ppm of Sr (Appendix D). The strong enrichment in $\text{Fe}_2\text{O}_3^{(\text{t})}$, when compared to alkalis and MgO (Tab. 4), displays the tholeiitic affinity of all samples. The TiO_2 contents are higher than 3.0 wt.% and are compatible with the high- TiO_2 series of PEIP (Bellieni et al., 1984; Mantovani et al., 1985).

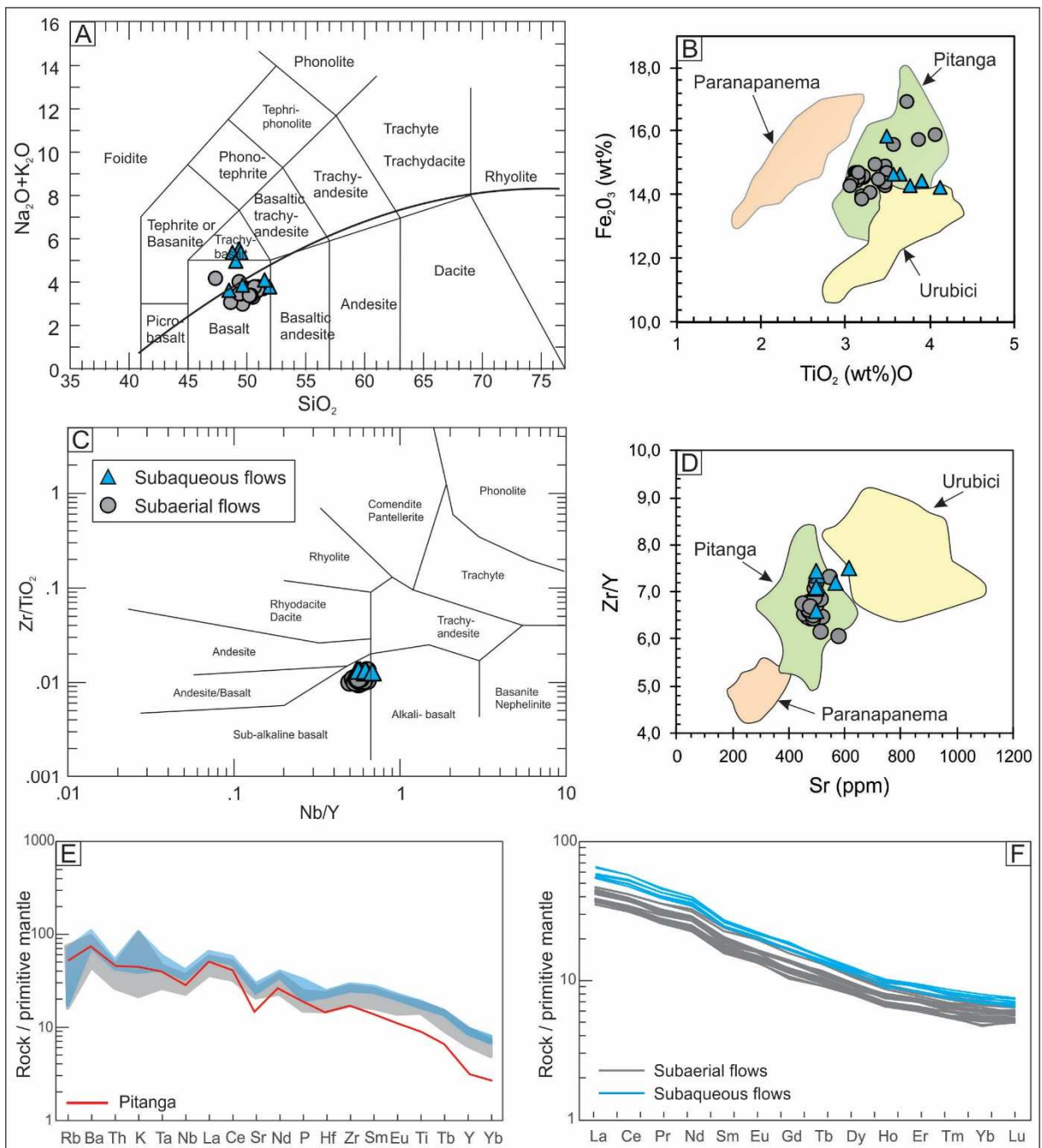


Fig. 30: Geochemical data of the Überlândia-Araguari lava flows. Major oxide contents are recalculated to 100% on an anhydrous basis. A) Total-Alkalies vs. Sílica diagram (modified from Le Bas et al., 1986); B) $\text{Fe}_2\text{O}_3^{(\text{t})}$ vs. TiO_2 diagram for discriminating the different PEIP magmas type (Peate et al., 1992); C) Winchester and Floyd (1977) classification diagram; D) Zr/Y vs Sr diagram for discriminating the different PEIP magmas type (Peate et al., 1992); E) Multi-element diagram normalized to primitive mantle (Sun and McDonough, 1989) for the distinct lavas recognized in the studied area in comparison with the general composition of the Pitanga Magma type from Peate et al. (1992); F) REE profiles normalized to primitive mantle (Sun and McDonough, 1989) for the distinct lavas recognized in the studied area.

Tab. 4: Representative geochemical data of subaerial lava flows and pillow lava samples of Uberlândia-Araguari region. The table includes samples with lower, intermediate and upper end of silica contents, all with low LOI values.

Lava types	Subaerial lava flows			Pillow lavas		
Sample	UB-NF- 16a	UB-NF- 27c	UB-NF- 32l	UB-NF- 32d	UB-NF- 32h	UB-NF- 33d
Major elements (wt. %)						
SiO ₂	48.77	51.05	46.33	48.80	48.55	50.97
TiO ₂	3.19	3.38	3.66	3.92	3.49	3.86
Al ₂ O ₃	13.03	12.51	13.36	13.77	12.69	13.31
Fe ₂ O ₃ (t)	14.30	14.35	16.52	14.02	14.61	14.54
MnO	0.23	0.19	0.26	0.25	0.26	0.19
MgO	5.26	4.65	5.09	4.34	5.60	3.41
CaO	9.69	9.09	8.11	7.95	8.34	8.17
Na ₂ O	2.33	2.57	2.51	2.67	2.26	2.52
K ₂ O	1.54	0.99	1.45	2.55	1.50	1.50
P ₂ O ₅	0.35	0.41	0.43	0.51	0.43	0.57
LOI	0.46	0.36	1.11	0.81	1.31	0.10
Total	99.14	99.55	98.83	99.60	99.05	99.14
Minor elements (ppm)						
Ba	371	406	650	490	507	556
Co	43	40	42	42	37	46
Nb	17	20	26	26	25	30
Ni	100	80	60	50	50	60
Rb	31	28	10	15	11	25
Sc	33	32	29	32	28	29
Sr	466	472	543	494	498	564
Y	29	34	41	45	39	43
Zr	187	227	298	315	275	304
La	25.1	29.8	37.5	39.8	38.4	44.0
Ce	57.9	68.5	87.7	93.4	87.3	101.0
Nd	32.90	38.30	47.70	51.30	47.70	54.30
Sm	7.49	8.90	10.80	11.80	10.70	12.20
Eu	2.40	2.70	3.43	3.73	3.38	3.76
Yb	2.55	3.03	3.53	3.95	3.44	3.81

Multi-element and REE diagrams (normalized by primitive mantle - Sun and McDonough, 1989) evidence the similarities in trace elements between pahoehoe lava flows and pillow lavas (Fig. 29E and 29F). In the multi-elements diagram, it is possible to observe enrichment of LILE in relation to HFSE, negative Sr anomalies and positive K anomalies (Fig. 30E). Pahoehoe lava flows and pillow lavas have similar REE contents; both show enrichment in light-REE compared to heavy-REE (Fig. 30F) and La/Yb^N varying from 8.77 to 6.47.

In comparison with the Paraná-Etendeka Province magma types from Peate et al. (1992), the Uberlândia-Araguari lava flows present features compatible to the high- TiO_2 Pitanga magma type (Fig. 30B, 30D and 30E).

5.1.7 Discussion

- Evidence of a wet environment

Pillow lavas are formed in subaqueous environments and observed in recent and active volcanoes (Garcia et al., 2012; Gregg and Fink, 1995; Kelly et al., 2014; Mcphie et al., 1993). The occurrence of pillow lavas in the PEIP evidences the presence of water during the emplacement of some lava flows (Ferreira, 1985; Mano, 1987; Marques Filho et al., 1981; Moraes and Seer, 2017; Moraes et al., 2018). Some authors have also showed the presence of peperites formed by the interaction between lava flows and wet lacustrine sediments in several parts of the province, mostly along the E-NE border of the PEIP (Costa, 2015; Luchetti et al., 2014; Machado et al., 2015; Waichel et al., 2007).

The morphology of pillow lavas can be useful to determine environmental conditions in which the pillows formed. The geometry of subaqueous pillow lobes reflects the degree of steepness of the substrate. They tend to be round and bulbous where emplaced over a near horizontal surface, and elongate over a moderate to high slope ($> 10^\circ$) (Umino et al., 2000). Besides form and size, terrain slope also influences in pillow packing, as lower slopes result in close-packed pillows, and higher slopes result in glassy basaltic breccias with isolated pillows (Walker, 1992). The dominance of round and close-packed pillows in the study area suggests near-horizontal emplacement surfaces ($<10^\circ$), but the local presence of associated pillow lavas and glassy basaltic breccias (hyaloclastites) occurring laterally to close-packed pillows reflects local higher slope. Substrate irregularities may be related to the lake edges or to the relief produced by stacking of pillow lavas. The dimensions of the pillow intervals (up to 10 meters thick and 400 meters long) suggest that the water body in the area had at least 6 m of depth and 400 m of extent, characterizing a small lake.

The studied pillow lavas occur in the central region between Uberlândia and Araguari, and one possible interpretation to their formation is the presence of subaerial basaltic lava flows from the surroundings, and at the same stratigraphic level (Fig. 24) that could have entered into a permanent body of water. Another evidence for this

interpretation is the predominance of hyaloclastite-rich packages occurring at the contact between pillow lava packages and lacustrine mudstones, at the lake edges.

In some portions of the study area, peperites occur associated with mudstones, suggesting the presence of wet environment in these areas. Also, peperites contain basalt fragments of varied morphologies, typical of blocky and fluidal peperites occurring in the same layer. The presence of fluidal juvenile clasts in the study area is an evidence of a ductile regime with the development of vapours film along the magma-sediment contacts preventing contact with the pore fluid. As the vapour film is more efficient in fine-grained, well-sorted wet sediments, within a loose framework (Busby-Spera and White, 1987), the presence of both fluidal and blocky peperites occurring in the same layer suggests that peperite formation in Uberlândia-Araguari area did not involve a single event or involve variations in the physical properties of the host sediment.

The presence of lacustrine and fluvial sedimentary rocks and pillow lavas at the base of lava flows with different types of joints observed in the central study area has been described in other igneous provinces (Lyle, 2000). These features indicate water presence also during the emplacement of those lavas. Even though pillow lavas are restricted only to the central study area, the undulatory columns with evidence of quenching are volumetrically important all over Uberlândia-Araguari region. Quenching in lava entablature has been associated with water influx to the lava flow interior along master joints, which modify the internal isotherms (DeGraff and Aydin, 1987; Lyle, 2000). The undulatory columns of the study area involved water, as great crystallinity differences occur between the rectilinear and undulatory columns.

In Uberlândia-Araguari area, the Precambrian basement occurs at different altitudes (621 to 803 m – Fig. 24), suggesting an irregular paleorelief during the emplacement of the lavas. The relief at the PEIP border could act as a humidity barrier and favor the development of ephemeral aqueous (flash) floods in a peridesert environment and the accumulation of water bodies as small lakes in the topographic lows (Machado et al., 2015; Moraes and Seer, 2017). The ephemeral character of these aqueous floods is also supported by the presence of calcrete horizons, a typical continental carbonate formed under arid to semiarid conditions, subjected to periods of subaerial exposure (Alonso-Zarza, 2003) and the presence of a fluvio-lacustrine conglomerate, sandstone, and mudstone interbedded with lava flows at different stratigraphic levels and portions of the study area.

Furthermore, the ostracod shells found in the mudstone levels corroborate the presence of water bodies in the area. Ostracods are still under investigation, in order to retrieve more information on the sedimentary environment.

Deposits formed in wet conditions are present in areas near the PEIP edges and in the upper stratigraphic levels of the central-north portion of PEIP reflecting different environmental conditions from those suggested for the onset of the magmatism, continuing the arid conditions of the Botucatu Formation (Luchetti et al., 2014; Waichel et al., 2007) and the equivalent stratigraphic levels on the Etendeka side of the PEIP (e.g. Jerram et al., 1999a, 1999b, 2000).

- Relation between lava flow morphology and petrographic/geochemical features

Pillow lavas, and compound and simple pahoehoe from Uberlândia-Araguari area are mineralogically very similar, composed mainly of plagioclase and pyroxene crystals, and altered volcanic glass. Substantial variations in glass content occur between the different types of lava flows, the glass content of pahoehoe lava flows being much lower than that of the pillow lavas (5 - 40% and 20 - 90% of glass, respectively). A difference in glass content is also observed in pahoehoe lava flows with distinct columns types (rectilinear and undulatory); rectilinear columns (5 - 15% of glass) have much less glass than the undulatory columns (10 - 40% of glass). The predominance of glass in portions with undulatory columns in pahoehoe lava flows reflects higher undercooling rates when compared with those portions with rectilinear columns of same composition, and within the same unit. As the content of glass in pillow lavas and in some subaerial lava flows is similar, crystallinity is not enough criteria to differentiate lava types, unless combined with lava structures and geometries.

In general, the different lava morphologies are geochemically classified as subalkaline basalts and have similar trace and rare earth element contents of the Pitanga magma type defined by Peate et al. (1992). When geochemical data/trends of the distinct lava flows are compared in detail, the pillow lavas are more evolved and have higher contents of trace and rare earth elements than most of the subaerial lava flows (Fig. 30E, 30F). Trace elements patterns for subaerial lava flows and pillow lavas are parallel, suggesting they are co-genetic; the negative Sr anomaly observed in the multi-element diagram suggests low pressure plagioclase fractionation.

The similar mineralogy and the SiO₂, MgO, and Fe₂O₃ contents of pillow lavas and pahoehoe lava flows (Tab. 4 and Appendix D) suggest that morphological variations depended more on eruption dynamics (e.g. effusion rate, lava supply) and depositional environment (e.g. subaerial versus subaqueous) than composition.

A pervasive K-rich alteration has affected specially the subaqueous lavas (Appendix C and D), and the fine sedimentary facies. A positive K anomaly present in most of the studied rocks reflects the presence of secondary minerals such as orthoclase and clay minerals (illite and illite-smectite) replacing the groundmass of pillow lavas and pahoehoe lava flows, and illite and illite-smectite as a cement of the sedimentary rocks. The other alteration products (silica, calcite, and zeolite) do not show any significant disturbance in the chemical compositions of the lavas.

- Stratigraphy and emplacement of Uberlândia-Araguari lava flows

Regionally, the volcanic sequence in the study area and surroundings was not affected by tectonism (Milani et al., 2007), therefore we used the elevation as the basis for lining up the stratigraphy between the logs, up to 45 km apart (Fig. 24). In the Uberlândia-Araguari area (northeastern of PEIP) the volcanic succession is composed of subaerial (simple and compound pahoehoe) and subaqueous lava flows (pillow lavas). The basal lava flows dominantly overlie the fluvio-lacustrine sedimentary rocks deposited over the crystalline basement. Those sedimentary rocks occur at different topographic levels, following the basement paleotopography, assumed to be the same observed today at the base of the logs. The onset of volcanic activity is characterized by thin simple pahoehoe (around 7 m thick) and compound pahoehoe (intervals of up to 7 m thick) located mainly at lower and intermediate stratigraphic levels (Fig. 24). The formation of compound pahoehoe lava flows are associated with a lobe-by-lobe emplacement (Baloga and Glaze, 2003), intermittent lava supply and low effusion rates (Walker, 1971). On the other side, simple pahoehoe are related with a higher effusion rate (Walker, 1971). Intermediate stratigraphic levels from the central part of the study area also comprise pillow lavas (intervals of up 10 m thick) (Fig. 24). The formation of pillow lavas is controlled by the presence of lakes in the area and likely the propagation of subaerial lavas into these lakes. Pillow lava is associated with low effusion rates and gentle slopes, and to higher cooling rates than the subaerial lavas (Gregg and Fink, 2000, 1995).

Upper stratigraphic levels are marked by thick simple pahoehoe lava flows (around 25 m thick) and peperitic intervals (up to 12 m thick) (Fig. 24). The predominance of simple lava flows in the upper stratigraphic levels indicates high effusion rates and relatively constant lava supply. In the study area, some features such as a vesicular upper crust, sheet vesicles and proto-cylinders suggest that the inflation process was important in the formation of the simple pahoehoe lava flows. The interpretation of dome-like features present at the top of some lava flows of the upper stratigraphic levels (Fig. 24 – log d and 27B) is challenging and, at first sight, the radial/convergence of the columnar joints is very similar to those features observed in collapsed lava tubes. However, the transitional contact to the superposed peperites, which is an *in situ* deposit and not deformed, makes it difficult to support the lava tube hypothesis. A second explanation would be invasive lava flows/shallow intrusions, where radial features and irregular lava flow top occur associated with irregular vesicle patterns at the top of the lava flows. These features have been observed in invasive lava flows/shallow intrusions in Karoo, South Africa (e.g. Rawlings et al., 1999). The irregularities of the upper crust (dome-like features) can also modify the isothermal pattern, resulting in radial columns. According to Millett et al. (2019), the process of lava invasion relies on the density difference between liquid lava and a typically wet sediment substrate and may be initiated by subtle topographic variations, dynamic mingling and substrate sediment properties such as density, water saturation, grain size, and porosity. This hypothesis seems to be plausible for this local occurrence, especially because of the presence of the transitional contact with the overlying peperites. The model for the development of the volcano-sedimentary sequence is summarized in Fig. 31.

- Comparisons with other areas of the Paraná-Etendeka Igneous Province

Similar to other portions of the PEIP (Jerram et al., 2000; Jerram and Stollhofen, 2002; Luchetti et al., 2014; Machado et al., 2015; Petry et al., 2007; Waichel et al., 2008), the intermittent character of volcanism in the study area is evidenced by the intercalation of sedimentary deposits with lava flows. These sedimentary packages of up to 12 m thick suggest hiatuses in the volcanic activity and the molds of lava lobes, load structures and sediment lenses amongst pahoehoe lobes suggest that sediments of the study area were unconsolidated during the emplacement of the lava flows.

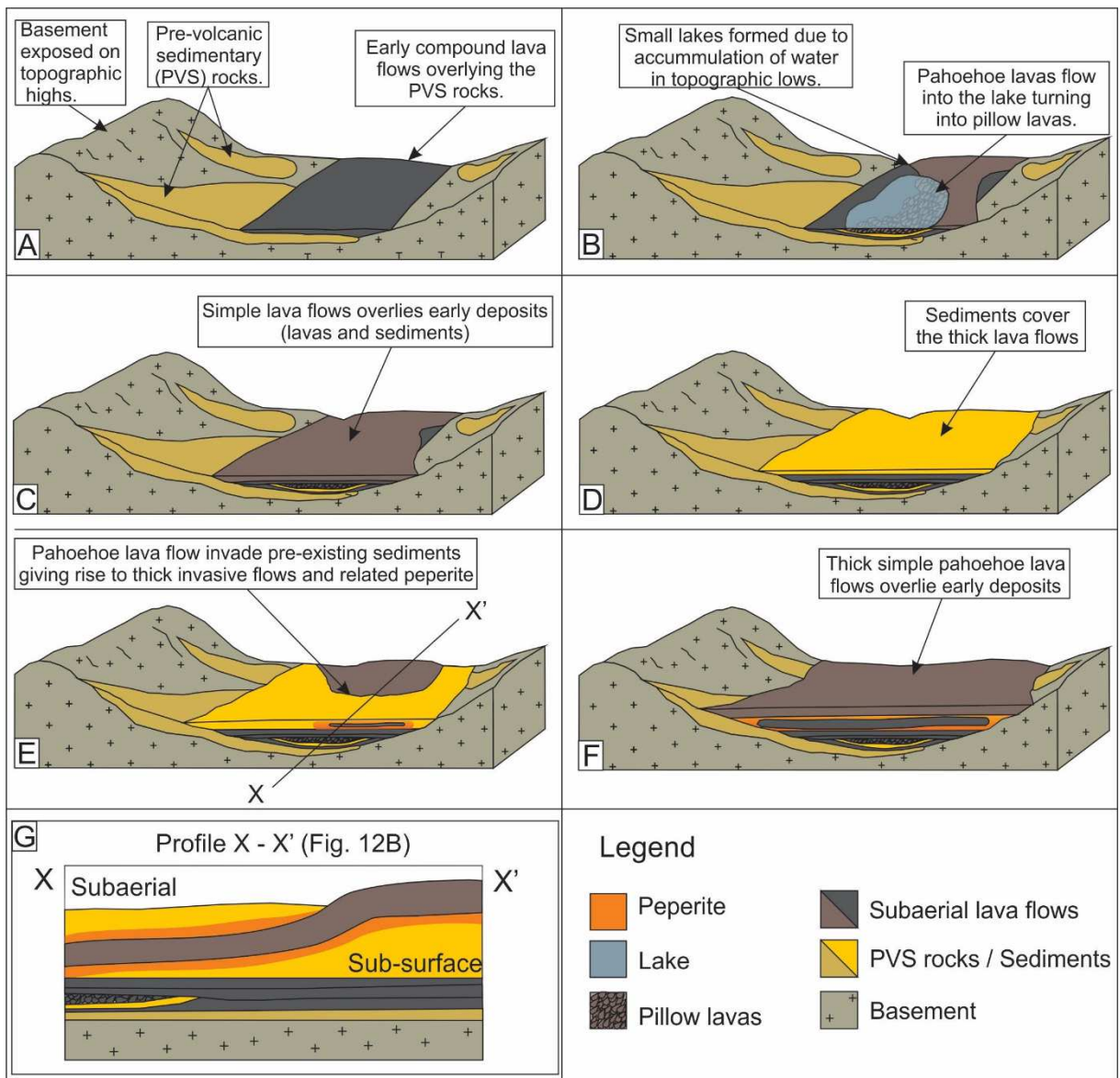


Fig. 31: f Diagram showing the lava flows emplacement in Uberlândia-Araguari area considering the invasive lava flow/shallow intrusion hypothesis. A) Beginning of volcanic activity characterized by thin simple and compound pahoehoe overlying pre-existing sediments of a peridesert environment; B) Topographic irregularities allowed the accumulation of small lakes where the subaerial lava flows became subaqueous resulting in pillow lavas; C) Thick simple pahoehoe lava flows covered the subaerial and subaqueous deposits; D) Sediments of peridesert environment covering the thick pahoehoe flows; E) Simple pahoehoe start to invade pre-existing sediments giving rise to thick invasive flows. The interaction between the invasive lava flow and pre-existing sediments resulted in thick (up to 7 m) of lower and upper peperite deposits; F) Thick pahoehoe lava flows covered the upper peperite related to the previous invasive flow. G) Profile X – X' of the figure 31E.

The stratigraphic style of the volcanic sequence recognized in the Uberlândia-Araguari area is very similar to the one recognized in the southern part of the province (Torres Syncline). Although the volcanic sequence in the southern part of PEIP is

thicker than the sequence in the northern area, with thickness of up to 1000 m and 300 m, respectively, both areas have similar stratigraphy. The two areas are characterized by dominance of compound pahoehoe lava flows at the base of the sequence. Effusion rate inferences based on lava morphologies has been done for lava sequences from the southern part of the PEIP (Barreto et al., 2014; Rossetti et al., 2018, 2014; Waichel et al., 2012). In the PEIP, the authors suggest that the climax of the magmatism is characterized by high effusion rates and sustained lava supply, resulting in simple pahoehoe (study area), and rubbly lava flows (southern portion of the PEIP) from the middle to the top of the sequence (Barreto et al., 2014; Rossetti et al., 2018, 2014; Waichel et al., 2012). However, the relationship between effusion rates and the characteristics of lava flows is complex. Besides the effusion rate, other parameters such as paleotopography and paleoenvironmental conditions have been used to explain lava morphologies (Beeson et al., 1989; Reidel and Tolan, 2013).

Geochemically different magma types are identified in the southern portion of the PEIP (low-TiO₂) and in the study area (northern portion of the PEIP – high-TiO₂), confirming the regional geochemical trend recognized for the PEIP (Peate et al., 1992). This regional geochemical trend has been related to different mantle sources and magma generation processes occurring over a wide area (Peate, 1997), hindering any stratigraphic correlation attempt between those portions. Some geochronological and paleomagnetic studies of intrusive and extrusive rocks of the PEIP suggest that volcanism in the northern portion is younger than in the south (Ernesto et al., 1999; Mincato et al., 2003; Renne et al., 1996, 1992) suggesting migration of volcanism from South to North.

- Interlava sedimentary facies of the Paraná-Etendeka and other Igneous Provinces

The characterization of interlava sedimentary rocks of the northeastern PEIP complements previous studies in the same area and shows dominance of fluvio-lacustrine sedimentary deposits (c.f. Moraes and Seer, 2017; Moraes et al., 2018). The thickness of the sedimentary deposits varies from a few meters to 10 m. The lava-sediment interaction in this area occurs as pillow lavas (with interpillow sediments) and peperites that can reach up to 10 and 12 m thick, respectively, typically associated with fluvio-lacustrine deposits. Peperite involving wet sediments and pillow lavas have been

described in the northwestern, central and eastern portions of the PEIP (Ferreira, 1985; Luchetti et al., 2014; Machado et al., 2015; Mano, 1987; Marques Filho et al., 1981; Waichel et al. 2007). These deposits are quite different from those described in the southern portion of the province, which are characterized by aeolian sand sheets, lenses of the Botucatu desert sand dunes field (Rossetti et al ., 2018; Scherer, 2000; Waichel et al., 2008) and peperite involving dry sediments (Petry et al., 2007) formed during the onset of the Paraná-Etendeka volcanism. The interlava aeolian deposits in the southern area can reach up to 10 m thick (Rossetti et al., 2018), similar thicknesses to those found in the northeastern portion. The occurrence of a humid environment in the PEIP has been attributed to paleoenvironmental changes, from a hyperarid climate at the beginning of volcanism (Scherer, 2002) to a more humid environment (fluvio-lacustrine) during its latest phases (Luchetti et al., 2014; Machado et al., 2015; Waichel et al., 2007). Alternative explanations for a wet environment in a desert context include the geographical position and topography (nearby mountains) of these occurrences (Machado et al., 2015; Moraes and Seer, 2007).

Pillow lavas and peperites are common in the Columbia River Flood Basalts and British Tertiary Igneous Province (Ebinghaus et al., 2014; Jolley et al., 2009; Moulin et al., 2011; Rawlings et al., 1999; Schmincke, 1967; Sethna, 1999; Tolan and Beeson, 1984; Williamson and Bell, 2012). Besides paleoenvironmental indicators, interlava sedimentary rocks and products of lava-sediment interactions in volcanic sequences became of interest because they may present relevant porosity, acting as hydrocarbon reservoirs in volcano-sedimentary basins (De Luca et al., 2015; Wu et al., 2019).

Among all Igneous Provinces described, Karoo Igneous Province (KIP) is the most similar to the PEIP in terms of paleoenvironment and interlava sedimentary deposits. Both provinces were initially emplaced in a desert paleoenvironment related to arid climate (Bordy and Catuneanu, 2002). At the beginning of volcanism, the Karoo lavas flowed over aeolian sediments (Bordy and Catuneanu, 2002), covering and, sometimes, preserving segments of aeolian sand dunes (Bristow, 1982), as has also been described in the PEIP by Jerram et al (2000) and Waichel et al. (2008). Interlava sedimentary rocks in the southern portion of KIP are dominantly aeolian sandstone and playa lake deposits (up to 4 m thick), whereas the western interlava deposits include fluvio-lacustrine sedimentary rocks (up to 15 m thick) (Moulin et al., 2011; Stollhofen et al., 1998; Sweeney et al., 1994). Previous works show that older lavas from the South of the KIP overlie sedimentary rocks formed under dry desert

conditions, whereas younger lavas in the North and Northwest cover sedimentary rocks related to wet desert regions (Jourdan et al., 2007; Smith et al., 1993; Visser, 1984). A similar pattern was observed in the PEIP, where studies suggest volcanism migration from South to North (Ernesto et al., 1999; Mincato et al., 2003; Renne et al., 1996; 1992), and a higher occurrence of wet environments in the northern area (Mano, 1987; Marque Filho, et al., 1981; Moraes and Seer, 2017).

5.1.8 Conclusion

Sixteen lithofacies were described and grouped into five lithofacies associations: pillow lavas, compound pahoehoe, simple pahoehoe, peperites and sediment-infill basalt breccia, forming the basic elements to construct the stratigraphic framework of the Uberlândia-Araguari area. The lowest stratigraphic volcanic sequence, overlapping fluvio-lacustrine sedimentary rocks deposited over the crystalline basement, is characterized by thin simple pahoehoe lava flows (~7 m – total thickness), compound pahoehoe (packages of up to 7 m) and pillow lavas (packages of up to 10 m). The formation of pillow lavas, which occurs in subaqueous environment, is associated with low effusion rates and gentle slopes. Simple pahoehoe lava flows and peperitic intervals dominate at the upper stratigraphic levels. The irregular and diffuse contact between the upper crust of these basalts and the superposed peperite, associated with the irregular vesicle pattern on the top of the basalt is suggestive of invasive lava flows/shallow intrusions. Sediment-infill basalt breccia occur locally at the upper stratigraphic level. The presence of interbedded, unconsolidated sedimentary deposits between lava flows reveals periods of quiescence of volcanic activity.

The subaerial lava flows and pillow lavas are chemically similar, classified as subalkaline basalts and comparable with the high-TiO₂ Pitanga magma type (Peate et al., 1992) from the southern part of the PEIP.

The occurrence of pillow lavas, fluvio-lacustrine deposits, and ostracods indicates the clear presence of significant water in the Uberlândia-Araguari area around the onset of early stratigraphic intervals. Such occurrence of water could be indicative of proximity to a major drainage system (river and associated lakes), and/or change from a predominantly arid setting further south to a wetter palaeoenvironment in the Uberlândia-Araguari area. Pillow lavas and peperites have been described in different parts of the PEIP (mostly along the E-NE border), suggesting that a wetter

palaeoenvironment is not exclusive to the investigated area. The geographic position and relief irregularities could explain ephemeral subaqueous lava flows in a peridesert environment, but the common presence of deposits formed in wet conditions in the central portion of PEIP makes a regional paleoenvironmental changes a possible alternative.

The construction of a stratigraphic framework for the northern portion of the PEIP in the Uberlândia-Araguari area provided evidence for a change from dry to wetter environmental conditions during the emplacement of the lavas in the Early Cretaceous.

Acknowledgements

This work was supported by Petrobras (CENPES R&D Projects PT-166.01.11923 and PT-166.01.13484) and CNPq (442812/2015-9). The Federal University of Rio Grande do Sul is acknowledged for additional support. Natália Famelli specially acknowledges to G. Marins, J. Millett, M. Hole, J. Weschenfelder, R. Ré, H. Seer, L. Moraes, F. Lourenço, J. Neto, B. Carvalho, I. Loutfi, Y. Parizek, L. De Ros, L. Bevilaqua for their support during fieldwork, discussions and/or software support. We thank the grinding plant of the 2º BFv, Arpasa, Ecobrix, Dois Irmãos, BT Construções, São Lucas quarries and the Ferrovia Centro-Atlântica (FCA – VLI Logística) for the permission to access the outcrop areas. We thank reviewers Jocelyne McPhie and Dougal Jerram for considerate and insightful reviews that considerably improved this manuscript.

References

- Abdelmalak, M.M., Planke, S., Faleide, J.I., Jerram, D.A., Zastrophnov, D., Eide, S., Myklebust, R., 2016. The development of volcanic sequences at rifted margins: New insights from the structure and morphology of the Vøring Escarpment, mid-Norwegian Margin. *J. Geophys. Res. Solid Earth* 121.
- Alonso-Zarza, A.M., 2003. Palaeoenvironmental significance of palustrine carbonates and calcretes in the geological record. *Earth-Science Rev.* 60, 261–298.
[https://doi.org/10.1016/S0012-8252\(02\)00106-X](https://doi.org/10.1016/S0012-8252(02)00106-X)

- Balog, S.M., Glaze, L.S., 2003. Pahoehoe transport as a correlated random walk. *J. Geophys. Res. Solid Earth* 108, 1–14. <https://doi.org/10.1029/2001jb001739>
- Barreto, C.J.S., 2016. Associação de fácies, padrões de vesiculação e petrologia dos derrames básicos da Formação Serra Geral na ombreira sul da Calha de Torres (RS). Ph.D. Thesis, Universidade Federal do Rio Grande do Sul, Porto Alegre.
- Barreto, C.J.S., Lima, E.F., Scherer, C.M., Rossetti, L.M.M., 2014. Lithofacies analysis of basic lava flows of the Paraná igneous province in the south hinge of Torres Syncline, Southern Brazil. *J. Volcanol. Geotherm. Res.* 285, 81–99. <https://doi.org/10.1016/j.jvolgeores.2014.08.008>
- Beeson, M.H., Tolan, T.L., Anderson, J.L., 1989. Geologic structures and other factors that controlled flow emplacement patterns, in: Reidel, S.P., Hooper, P.R. (Eds.), *Volcanism and Tectonism in the Columbia River Flood-Basalt Province*. Geological Society of America Special Paper, pp. 223–246. <https://doi.org/https://doi.org/10.1130/SPE239-p223>
- Bellieni, G., Comin-Chiaromonti, P., Marques, L.S., Melfi, A.J., Piccirillo, E.M., Nardy, A.J.R., Roisenberg, A., 1984. High- and Low-TiO₂ flood basalts from the Parana plateau (Brazil): petrology and geochemical aspects bearing on their mantle origin. *Neus Jahrb. Miner. Abh* 150, 273–306.
- Bordy, E.M., Catuneanu, O., 2002. Sedimentology of the lower Karoo Supergroup fluvial strata in the Tuli Basin, South Africa. *J. African Earth Sci.* 35, 503–521. [https://doi.org/10.1016/S0899-5362\(02\)00129-X](https://doi.org/10.1016/S0899-5362(02)00129-X)
- Bristow, J.W., 1982. Geology and structure of Karoo volcanic and sedimentary rocks of the northern and central Lebombo (South Africa). *Trans. - Geol. Soc. South Africa* 85, 167–178.
- Busby-Spera, C.J., White, J.D.L., 1987. Variation in peperito textures associated with differing host sediment properties. *Bull. Volcanol.* 49, 765–775.
- Cas, R.A.F., Wright, J. V, 1987. Volcanic successions, modern and ancient: a geological approach to processes, products and successions, 1st ed, *Volcanic Successions Modern and Ancient*. Chapman & Hall, London.

Collinson, J.D., 1969. The sedimentology of the Grindslow Shales and the Kinderscout Grit: a deltaic complex in the Namurian of northern England. *J. Sediment. Petrol.* 39, 194–221. <https://doi.org/10.1306/74D71C17-2B21-11D7-8648000102C1865D>

Costa, J., 2015. Estratigrafia e geoquímica da sequência de lavas da Província Magmática do Paraná na região da Usina De Itaipu (PR). Ph.D. Thesis. Universidade Federal do Paraná.

Dalrymple, R.W., 2010. Interpreting Sedimentary Successions: Facies, Facies Analysis and Facies Models., in: James, N.P., Dalrymple, R.W. (Eds.), *Facies Models 4*. Geological Association of Canada, pp. 3–17.

Dardenne, M.A., 2000. The Brazilian Fold Belt, in: Milani, E.J., Thomaz Filho, A., Campos, D.A. (Eds.), *Tectonic Evolution of South America*. Rio de Janeiro, pp. 231–263.

De Luca, P., Carballo, J., Filgueiras, A., Pimentel, G., Esteban, M., Tritlla, J., Villacorta, R., 2015. What is the role of volcanic rocks in the Brazilian pre-salt?, in: 77th EAGE Conference and Exhibition 2015: Earth Science for Energy and Environment. European Association of Geoscientists and Engineers, EAGE, pp. 1686–1690. <https://doi.org/10.3997/2214-4609.201412890>

Deckart, K., Féraud, G., Marques, L.S., Bertrand, H., 1998. New time constraints on dyke swarms related to the Paraná-Etendeka magmatic province, and subsequent South Atlantic opening, southeastern Brazil. *J. Volcanol. Geotherm. Res.* 80, 67–83. [https://doi.org/10.1016/S0377-0273\(97\)00038-3](https://doi.org/10.1016/S0377-0273(97)00038-3)

DeGraff, J.M., Aydin, A., 1987. Surface morphology of columnar joints and its significance to mechanics and direction of joint growth. *Geol. Soc. Am.* 99, 605–617. [https://doi.org/10.1130/0016-7606\(1987\)99<605:SMOCJA>2.0.CO;2](https://doi.org/10.1130/0016-7606(1987)99<605:SMOCJA>2.0.CO;2)

Duraiswami, R.A., Gadpallu, P., Shaikh, T.N., Cardin, N., 2014. Pahoehoe—a'a transitions in the lava flow fields of the western Deccan Traps, India—implications for emplacement dynamics, flood basalt architecture and volcanic stratigraphy. *J. Asian Earth Sci.* 84, 146–166. <https://doi.org/10.1016/J.JSEAES.2013.08.025>

Ebinghaus, A., Hartley, A.J., Jolley, D.W., Hole, M., Millett, J., 2014. Lava – Sediment Interaction and Drainage-System Development in a Large Igneous. *J. Sediment. Res.* 84, 1041–1063.

Ernesto, M., Raposo, M.I., Marques, L., Renne, P., Diogo, L., de Min, A., 1999. Paleomagnetism, geochemistry and $^{40}\text{Ar}/^{39}\text{Ar}$ dating of the North-eastern Paraná Magmatic Province: tectonic implications. *J. Geodyn.* 28, 321–340. [https://doi.org/10.1016/S0264-3707\(99\)00013-7](https://doi.org/10.1016/S0264-3707(99)00013-7)

Fantasia, A., Adatte, T., Spangenberg, J.E., Font, E., 2016. Palaeoenvironmental changes associated with Deccan volcanism, examples from terrestrial deposits from Central India. *Palaeogeogr. Palaeoclimatol. Palaeoecol.* 441, 165–180. <https://doi.org/10.1016/j.palaeo.2015.06.032>

Fernandes, A.J., Maldaner, C.H., Sobrinho, J.M.A., Pressinotti, M.M.N., Wahnfried, I., 2010. Estratigrafia dos derrames de basaltos da Formação Serra Geral (Ribeirão Preto - SP) baseada na geologia física, petrografia e geoquímica. *Geol. USP - Ser. Cient.* 10, 73–99. <https://doi.org/https://doi.org/10.5327/Z1519-874X2010000200006>

Ferreira, C.M., 1985. Ocorrência de “pillow lava” em vulcanitos da Fm Serra Geral em Araguari, MG, in: 3º Simpósio de Geologia de Minas Gerais. Anais do 3º simpósio de geologia de Minas Gerais, Belo Horizonte, pp. 235–237.

Forbes, a. E.S., Blake, S., Tuffen, H., 2014. Entablature: Fracture types and mechanisms. *Bull. Volcanol.* 76, 820. <https://doi.org/10.1007/s00445-014-0820-z>

Garcia, M.O., Hanano, D., Flinders, A., Weis, D., Ito, G., Kurz, M.D., 2012. Age , geology , geophysics , and geochemistry of Mahukona Volcano , Hawaii. *Bull. Volcanol.* 74, 1445–1463. <https://doi.org/10.1007/s00445-012-0602-4>

Goehring, L., 2008. On the scaling and ordering of columnar joints. Ph.D. Thesis, University of Toronto.

Gregg, T.K., Fink, J.H., 2000. A laboratory investigation into the effects of slope on lava flow morphology. *J. Volcanol. Geotherm. Res.* 96, 145–159. [https://doi.org/10.1016/S0377-0273\(99\)00148-1](https://doi.org/10.1016/S0377-0273(99)00148-1)

Gregg, T.K.P., Fink, J.H., 1995. Quantification of submarine lava-flow morphology through analog experiments. *Geology* 23, 73–76. [https://doi.org/10.1130/0091-7613\(1995\)023<0073:QOSLFM>2.3.CO;2](https://doi.org/10.1130/0091-7613(1995)023<0073:QOSLFM>2.3.CO;2)

Griffiths, R.W., Fink, J.H., 1992. Solidification and morphology of submarine lavas: a dependence on extrusion rate. *J. Geophys. Res.* 97, 729–737. <https://doi.org/DOI: 10.1029/92JB01594>

- Grossenbacher, K.A., McDuffie, S.M., 1995. Conductive cooling of lava: columnar joint diameter and stria width as functions of cooling rate and thermal gradient. *J. Volcanol. Geotherm. Res.* 69, 95–103. [https://doi.org/10.1016/0377-0273\(95\)00032-1](https://doi.org/10.1016/0377-0273(95)00032-1)
- Hawkesworth, C.J., Gallagher, K., Kirstein, L., Mantovani, M.S.M., 2000. Tectonic controls on magmatism associated with continental break-up: an example from the Paraná-Etendeka Province. *Science*. 289, 335–349. <https://doi.org/10.1126/science.289.5482.335>
- Jerram, D., Mountney, N., Holzförster, F., Stollhofen, H., 1999a. Internal stratigraphic relationships in the Etendeka Group in the Huab Basin, NW Namibia: Understanding the onset of flood volcanism. *J. Geodyn.* 28, 393–418. [https://doi.org/10.1016/S0264-3707\(99\)00018-6](https://doi.org/10.1016/S0264-3707(99)00018-6)
- Jerram, D., Mountney, N., Stollhofen, H., 1999b. Facies architecture of the Etjo Sandstone Formation and its interaction with the Basal Etendeka Flood Basalts of northwest Namibia: implications for offshore prospectivity. *Geol. Soc. Spec. Publ.* 153, 367–380. <https://doi.org/10.1144/GSL.SP.1999.153.01.22>
- Jerram, D.A., 2002. Volcanology and facies architecture of flood basalts, in: Menzies, M.A., Baker, J., Ebinger, C.J., Klempner, S.L. (Eds.), *Volcanic Rifted Margins*. Geological Society of America Special Paper, Colorado, pp. 121–135. <https://doi.org/https://doi.org/10.1130/0-8137-2362-0.119>
- Jerram, D.A., Mountney, N.P., Howell, J.A., Long, D., Stollhofen, H., 2000. Death of a sand sea: An active aeolian erg systematically buried by the Etendeka flood basalts of NW Namibia. *J. Geol. Soc. London*. 157, 513–516. <https://doi.org/10.1144/jgs.157.3.513>
- Jerram, D.A., Single, R.T., Hobbs, R.W., Nelson, C.E., 2009. Understanding the offshore flood basalt sequence using onshore volcanic facies analogues: An example from the Faroe-Shetland basin. *Geol. Mag.* 146, 353–367. <https://doi.org/10.1017/S0016756809005974>
- Jerram, D.A., Stollhofen, H., 2002. Lava-sediment interaction in desert settings; are all peperite-like textures the result of magma-water interaction? *J. Volcanol. Geotherm. Res.* 114, 231–249. [https://doi.org/10.1016/S0377-0273\(01\)00279-7](https://doi.org/10.1016/S0377-0273(01)00279-7)

- Jerram, D.A., Widdowson, M., 2005. The anatomy of Continental Flood Basalt Provinces: geological constraints on the processes and products of flood volcanism. *Lithos* 79, 385–405. <https://doi.org/10.1016/J.LITHOS.2004.09.009>
- Jourdan, F., Féraud, G., Bertrand, H., Watkeys, M.K., Renne, P.R., 2007. Distinct brief major events in the Karoo large igneous province clarified by new 40Ar/39Ar ages on the Lesotho basalts. *Lithos* 98, 195–209. <https://doi.org/10.1016/j.lithos.2007.03.002>
- Kelly, J.T., Carey, S., Pistolesi, M., Rosi, M., Croff-bell, K.L., Roman, C., 2014. Exploration of the 1891 Foerstner submarine vent site (Pantelleria , Italy): insights into the formation of basaltic balloons. *Bull. Volcanol.* 76, 1–18. <https://doi.org/10.1007/s00445-014-0844-4>
- Le Bas, M.J., Maitre, R.W.L., Streckeisen, A., Zanettin, B., 1986. A chemical classification of volcanic rocks based on the total alkali-silica diagram. *J. Petrol.* 27, 745–750. <https://doi.org/10.1093/petrology/27.3.745>
- Long, P.E., Wood, B.J., 1986. Structures, textures, and cooling histories of Columbia River basalt flows (USA). *Geol. Soc. Am. Bull.* 97, 1144–1155. [https://doi.org/10.1130/0016-7606\(1986\)97<1144:STACHO>2.0.CO;2](https://doi.org/10.1130/0016-7606(1986)97<1144:STACHO>2.0.CO;2)
- Luchetti, A.C.F., Nardy, A.J.R., Machado, F.B., Madeira, J.E.O., Arnoso, J.M., 2014. New insights on the occurrence of peperites and sedimentary deposits within the silicic volcanic sequences of the Paraná Magmatic Province, Brazil. *Solid Earth* 5, 121–130. <https://doi.org/10.5194/se-5-121-2014>
- Lyle, P., 2000. The eruption environment of multi-tiered columnar basalt lava flows. *J. Geol. Soc. London.* 157, 715–722. <https://doi.org/10.1144/jgs.157.4.715>
- Machado, F., Rocha-Júnior, E.R.V., Marques, L.S., Nardy, A.J.R., 2015. Volcanological aspects of the northwest region of Paraná continental flood basalts (Brazil). *Solid Earth* 6, 227–241. <https://doi.org/10.5194/se-6-227-2015>
- Mano, V.G.T., 1987. Estudos geológicos e geotécnicos das descontinuidades rochosas, “pillow lavas” e paleocanal nos basaltos de fundação da barragem de Nova Avanhandava, Rio Tiete (SP). Universidade de São Paulo.
- Mantovani, M.S.M., Marques, L.S., Souza, M.A., Civetta, L., Atalla, L., Innocenti, F., 1985. Trace element and strontium isotope constraints on the origin and evolution of

Paraná continental flood basalts of Santa Catarina state (Southern Brazil). *J. Petrol.* 26, 187–209.

Marques Filho, P.L., Correia, P.C., Levis, P., Andrade, C.A. V, 1981. Características usuais e aspectos peculiares do manto de alteração e transição solo-rocha em basaltos, in: Congresso Brasileiro de Engenharia. Congresso Brasileiro de Geologia de Engenharia, ABGE, Itapema, p. 53-72.

Mcphie, J., Doyle, M., Allen, R., 1993. Volcanic Textures: A guide to the interpretation of textures in volcanic rocks. University of Tasmania (191 pp.).

Miall, A.D., 2000. Principles of Sedimentary Basin Analysis, 3rd ed. Springer-Verlag Inc, New York, (616 pp.).

Milani, E.J., Melo, J.H.G. de, Souza, P.A. De, Fernandes, L.A., França, A.B., 2007. Bacia do Paraná. *Bol. Geociências da Petrobras* 15, 265–287.

Millett, J.M., Jerram, D.A., Planke, S., Hole, M.J., Famelli, N., Jolley, D.W., Peter, A., 2019. Top down or bottom up: identification and implications of invasive lavas versus shallow intrusions in sedimentary basins, in: LASI VI -The Physical Geology of Subvolcanic Systems - Laccoliths, Sills and Dykes. Malargue, Argentina, pp. 50-51.

Mincato, R.L., Enzweiler, J., Schrank, A., 2003. Novas idades ^{40}Ar - ^{39}Ar e implicações na metalogênese dos depósitos de sulfetos magmáticos de Ni-Cu-EGP na província ígnea Continental do Paraná, in: Congresso Brasileiro de Geoquímica. Anais do Congresso Brasileiro de Geoquímica, Belém, Pará, pp. 425–427.

Moraes, L.C. de, Seer, H.J., 2017. Pillow lavas and fluvio-lacustrine deposits in the northeast of Paraná Continental Magmatic Province, Brazil. *J. Volcanol. Geotherm. Res.* 355, 78–86. <https://doi.org/10.1016/J.JVOLGEORES.2017.03.024>

Moraes, L.C., Seer, H.J., Marques, L.S., 2018. Geology, geochemistry and petrology of basalts from Paraná Continental Magmatic Province in the Araguari, Uberlândia, Uberaba and Sacramento regions, Minas Gerais state, Brazil. *Brazilian J. Geol.* 48, 221–241. <https://doi.org/10.1590/2317-4889201820170091>

Moulin, M., Fluteau, F., Courtillot, V., Marsh, J., Delpech, G., Quidelleur, X., Gérard, M., Jay, A.E., 2011. An attempt to constrain the age, duration, and eruptive history of the Karoo flood basalt: Naude's Nek section (South Africa). *J. Geophys. Res. Solid Earth* 116, 1–27. <https://doi.org/10.1029/2011JB008210>

- Nelson, C.E., Jerram, D.A., Hobbs, R.W., 2009. Flood basalt facies from borehole data : implications for prospectivity and volcanology in volcanic rifted margins. *Pet. Geosci.* 15, 313–324. <https://doi.org/10.1144/1354-079309-842>
- Pacheco, F.E.R.C., Serrano, P.M., Caxito, F.A., Moura, C.D., Quintão, D.A., 2017. Projeto triângulo mineiro, Folha Uberlândia, Escala 1:100.000. Universidade Federal de Minas Gerais.
- Peate, D.P., Hawkesworth, C.J., Mantovani, M.S., 1992. Chemical stratigraphy of the Paraná lavas (South America): classification of magma types and their spatial distribution. *Bull. Volcanol.* 55, 119–139. <https://doi.org/DOI: 10.1007/BF00301125>
- Peate, D.W., 1997. The Parana-Etendeka Province, in: Mahoney, J.J., Coffin, M.F. (Eds.), *Large Igneous Provinces: Continental, Oceanic, and Planetary Flood Volcanism*. Geophysical Monographs: American Geophysical Union, pp. 217–245. <https://doi.org/10.1029/GM100p0217>
- Petry, K., Jerram, D.A., Almeida, P.M. De, Zerfass, H., 2007. Volcanic-sedimentary features in the Serra Geral Fm., Paraná Basin, southern Brazil: Examples of dynamic lava-sediment interactions in an arid setting 159, 313–325. <https://doi.org/10.1016/j.jvolgeores.2006.06.017>
- sethns, D.J., Watkeys, M.K., Sweeney, R.J., 1999. Peperitic upper margin of an invasive flow, Karoo flood basalt province, northern Lebombo. *South African J. Geol.* 102, 377–383.
- Reidel, S.P., Tolan, T.L., 2013. The late Cenozoic evolution of the Columbia River system in the Columbia River flood basalt province. *Spec. Pap. Geol. Soc. Am.* 497, 201–230. [https://doi.org/10.1130/2013.2497\(08\)](https://doi.org/10.1130/2013.2497(08))
- Renne, P.R., 2015. Age and Duration of the Paraná-Etendeka Flood Basalts and Related Plumbing System. *Am. Geophys. Union, Fall Meet. 2015, Abstr.* id. T32D-06.
- Renne, P.R., Deckart, K., Ernesto, M., Féraud, G., Piccirillo, E.M., 1996. Age of the Ponta Grossa dike swarm (Brazil), and implications to Paraná flood volcanism. *Earth Planet. Sci. Lett.* 144, 199–211. [https://doi.org/10.1016/0012-821X\(96\)00155-0](https://doi.org/10.1016/0012-821X(96)00155-0)
- Renne, P.R., Ernesto, M., Pacca, I.G., Coe, R.S., Glen, J.M., Prévot, M., Perrin, M., 1992. The Age of Parana Flood Volcanism , Rifting of Gondwanaland, and the

Jurassic-Cretaceous boundary. Science. 258, 975–979.
<https://doi.org/10.1126/science.258.5084.975>

Rosa, C.J.P., McPhie, J., Relvas, J.M.R.S., 2016. Distinguishing peperite from other sediment-matrix igneous breccias: Lessons from the Iberian Pyrite Belt. *J. Volcanol. Geotherm. Res.* 315, 28–39. <https://doi.org/10.1016/j.jvolgeores.2016.02.007>

Rossetti, L., Lima, E.F., Waichel, B.L., Hole, M.J., Simões, M.S., Scherer, C.M.S., 2018. Lithostratigraphy and volcanology of the Serra Geral Group, Paraná-Etendeka Igneous Province in Southern Brazil: Towards a formal stratigraphical framework. *J. Volcanol. Geotherm. Res.* 355, 98–114.
<https://doi.org/10.1016/j.jvolgeores.2017.05.008>

Rossetti, L., Lima, E.F., Waichel, B.L., Scherer, C.M., Barreto, C.J., 2014. Stratigraphical framework of basaltic lavas in Torres Syncline main valley, southern Parana-Etendeka Volcanic Province. *J. South Am. Earth Sci.* 56, 409–421.
<https://doi.org/10.1016/j.jsames.2014.09.025>

Ryan, M., Sammis, C., 1978. Cyclic fracture mechanisms in cooling basalt. *Geol. Soc. Am. Bull.* 89, 1295–1308. [https://doi.org/10.1130/0016-7606\(1978\)89<1295:CFMICB>2.0.CO;2](https://doi.org/10.1130/0016-7606(1978)89<1295:CFMICB>2.0.CO;2)

Scherer, C.M.S., 2000. Eolian dunes of the Botucatu Formation (Cretaceous) in southernmost Brazil: Morphology and origin. *Sediment. Geol.* 137, 63–84.
[https://doi.org/10.1016/S0037-0738\(00\)00135-4](https://doi.org/10.1016/S0037-0738(00)00135-4)

Self, L., Thordarson, T., Keszthelyi, L., 1997. Emplacement of Continental Flood Basalt Lava Flows, in: Mahoney, J. J., Coffin, M.L. (Ed.), *Large Igneous Provinces: Continental, Oceanic, and Planetary Flood Volcanism*. Geophysics Monography, AGU, pp. 381–410. <https://doi.org/10.1029/GM100p0381>

Shaw, H.R., Swanson, D.A., 1970. Eruption and flow rates of flood basalts, in: Gilmour, E.H., Stradling, D. (Eds.), *Proceedings of the Second Columbia River Basalt Symposium*. Washington, Eastern Washington State College Press, Cheney, Washington, pp. 271–299.

Single, R.T., Jerram, D.A., 2004. The 3D facies architecture of flood basalt provinces and their internal heterogeneity: examples from the Palaeogene Skye Lava Field. *J. Geol. Soc. London.* 161, 911–926. <https://doi.org/10.1144/0016-764903-136>

- Smith, R.M.H., Eriksson, P.G., Botha, W.J., 1993. A review of the stratigraphy and sedimentary environments of the Karoo-aged basins of Southern Africa. *J. African Earth Sci.* 16, 143–169. [https://doi.org/10.1016/0899-5362\(93\)90164-L](https://doi.org/10.1016/0899-5362(93)90164-L)
- Spry, A., 1962. The origin of columnar jointing, particularly in basalt flows. *J. Geol. Soc. Aust.* 8, 191–216. <https://doi.org/10.1080/14400956208527873>
- Stewart, K., Turner, S., Kelley, S., Hawkesworth, C., Kirstein, L., Mantovani, M., 1996. 3-D, 40Ar-39Ar geochronology in the Paraná continental flood basalt province. *Earth Planet. Sci. Lett.* 143, 95–109. [https://doi.org/10.1016/0012-821X\(96\)00132-X](https://doi.org/10.1016/0012-821X(96)00132-X)
- Stollhofen, H., Gerschütz, S., Stanistreet, I.G., Lorenz, V., 1998. Tectonic and volcanic controls on Early Jurassic rift-valley lake deposition during emplacement of Karoo flood basalts, southern Namibia. *Palaeogeogr. Palaeoclimatol. Palaeoecol.* 140, 185–215. [https://doi.org/10.1016/S0031-0182\(98\)00029-7](https://doi.org/10.1016/S0031-0182(98)00029-7)
- Sun, S.S., McDonough, W.F., 1989. Chemical and isotopic systematics of oceanic basalts: Implications for mantle composition and processes. *Geol. Soc. Spec. Publ.* 42, 313–345. <https://doi.org/10.1144/GSL.SP.1989.042.01.19>
- Svensen, H.H., Jerram, D.A., Polozov, A.G., Planke, S., Neal, C.R., Augland, L.E., Emeleus, H.C., 2019. Thinking about LIPs: A brief history of ideas in Large igneous province research. *Tectonophysics* 760, 229–251. <https://doi.org/10.1016/j.tecto.2018.12.008>
- Svensen, H.H., Torsvik, T.H., Callegaro, S., Augland, L., Heimdal, T.H., Jerram, D.A., Planke, S., Pereira, E., 2017. Gondwana Large Igneous Provinces: Plate reconstructions, volcanic basins and sill volumes, in: Sensarma, A., Storey, B.C. (Eds.), *Geological Society Special Publication*. Geological Society, London, pp. 17–40. <https://doi.org/10.1144/SP463.7>
- Sweeney, R.J., Duncan, A.R., Erlank, A.J., 1994. Geochemistry and petrogenesis of central lebombo basalts of the karoo igneous province. *J. Petrol.* 35, 95–125. <https://doi.org/10.1093/petrology/35.1.95>
- Thiede, D.S., Vasconcelos, P.M., 2010. Paraná flood basalts: Rapid extrusion hypothesis confirmed by new 40Ar/39Ar results. *Geology* 38, 747–750. <https://doi.org/10.1130/G30919.1>

- Umino, S., 2000. Subaqueous lava flow lobes , observed on ROV KAIKO dives off Hawaii 7613. [https://doi.org/10.1130/0091-7613\(2000\)28<503](https://doi.org/10.1130/0091-7613(2000)28<503)
- Visser, J., 1984. A review of the Stromberg group and Drakensberg volcanics in Southern Africa. *Palaeontol. Africana* 25, 5–27.
- Waichel, B.L., Lima, E.F., Sommer, C.A., 2006. Tipos de Derrame e Reconhecimento de Estruturas nos Basaltos da Formação Serra Geral : Terminologia e Aspectos de Campo. *Pesqui. em Geociencias* 33, 123–133.
- Waichel, B.L., Lima, E.F., Sommer, C.A., Lubachesky, R., 2007. Peperite formed by lava flows over sediments: An example from the central Paraná Continental Flood Basalts, Brazil. *J. Volcanol. Geotherm. Res.* 159, 343–354. <https://doi.org/10.1016/j.jvolgeores.2006.07.009>
- Waichel, B.L., Lima, E.F., Viana, A.R., Scherer, C.M., Bueno, G. V, Dutra, G., 2012. Stratigraphy and volcanic facies architecture of the Torres Syncline, Southern Brazil, and its role in understanding the Paraná-Etendeka Continental Flood Basalt Province. *J. Volcanol. Geotherm. Res.* 215–216, 74–82. <https://doi.org/10.1016/j.jvolgeores.2011.12.004>
- Waichel, B.L., Scherer, C.M.S., Frank, H.T., 2008. Basaltic lava flows covering active aeolian dunes in the Paraná Basin in southern Brazil: Features and emplacement aspects. *J. Volcanol. Geotherm. Res.* 171, 59–72. <https://doi.org/10.1016/j.jvolgeores.2007.11.004>
- Walker, G.P.L., 1992. Morphometric study of pillow-size spectrum among pillow lavas. *Bull. Volcanol.* 54, 459–474. <https://doi.org/10.1007/BF00301392>
- Walker, G.P.L., 1971. Compound and Simple Lava Flows and Flood Basalts. *Bull. Volcanol.* 35, 579–590. <https://doi.org/10.1007/BF02596829>
- White, J.D.L., Mcphie, J., Skilling, I., 2000. Peperite: A useful genetic term. *Bull. Volcanol.* 62, 65–66. <https://doi.org/10.1007/s004450050293>
- Wilmoth, R.A., Walker, G.P.L., 1993. P-type and Stype pahoehoe: a study of vesicle distribution patterns in Hawaiian lava flows. *J. Volcanol. Geotherm. Res.* 55, 42. [https://doi.org/10.1016/0377-0273\(93\)90094-8](https://doi.org/10.1016/0377-0273(93)90094-8)

Winchester, J.A., Floyd, P.A., 1977. Geochemical discrimination of different magma series and their differentiation products using immobile elements. *Chem. Geol.* 20, 325–343. [https://doi.org/10.1016/0009-2541\(77\)90057-2](https://doi.org/10.1016/0009-2541(77)90057-2)

Wu, S., Zhu, R., Yang, Z., Mao, Z., Cui, J., Zhang, X., 2019. Distribution and characteristics of lacustrine tight oil reservoirs in China. *J. Asian Earth Sci.* 178, 20–36. [https://doi.org/https://doi.org/10.1016/j.jseas.2018.05.013](https://doi.org/10.1016/j.jseas.2018.05.013)

5.2 ARTIGO B

Characterizing the nature and importance of lava-sediment interactions in sedimentary basins with the aid of field outcrop analogues.

Authors: Natália Famelli^{a,b,*}, John Millett^{c,d}, Malcolm Hole^c, Evandro F. Lima^a, Isabela de O. Carmo^b, Dougal A. Jerram^{e,f}, David W. Jolley^c, Jessica H. Pugsley^c, John A. Howell^c

Filiation Adress:

^a Instituto de Geociências, Universidade Federal do Rio Grande do Sul, Av. Bento Gonçalves, 9500, Prédio 43136, Caixa Postal 15001, Agronomia, Porto Alegre, 91501-970, Rio Grande do Sul, RS, Brazil

^b Centro de Pesquisas e Desenvolvimento Leopoldo Américo Miguez de Mello – CENPES/PETROBRAS, Av. Horácio de Macedo, 950, Cidade Universitária, 21941-915, Rio de Janeiro, RJ, Brazil

^c Department of Geology & Petroleum Geology, University of Aberdeen, UK

^d VBPR AS, Oslo Science Park, Gaustadalléen 21, N-0349 Oslo, Norway

^e Centre for Earth Evolution and Dynamics (CEED), University of Oslo, Norway

^f DougalEARTH Ltd., Solihull, UK

* Corresponding author: E-mail: natfamelli@gmail.com

Abstract

The emplacement of lava flows into poorly consolidated sediments during the onset of volcanism can lead to a wide range of lava-sediment interaction processes. Understanding these processes and their products is critical for appraising reservoir quality and connectivity in both intra- and sub-volcanic prospectivity settings. This study investigates the nature of lava-sediment interactions during the onset of magmatism in sedimentary basins with the aid of field outcrops in the Paraná-Etendeka Igneous Province (Brazil), Mull Lava Field (UK), and Midland Valley Basin (UK). Both subaerial and invasive lava flows were identified with associated features ranging from peperites, loading structures, pillow-like peperites, rootless cones, and lavas with sharp contacts. Density contrasts between liquid magma and unconsolidated sediments make lava invasion a predictable phenomena in such environments, however, variations in sediment properties such as water saturation, porosity and cohesion may effectively restrict the process of invasion, the degree of loading and more dynamic processes leading to peperite and pillow-like peperite. Surface outcrop analogues form a key component to understand the potential impact of volcanism and magma-sediment interactions on non-volcanic reservoir rocks located proximal to the basalt-sediment transition. The intimate mixing of magma with sediment is generally restricted to a few meters from the lava-sediment contact, with an associated minor impact on reservoir quality. However, the process of lava invasion may extend this impact further and may lead to partial or complete compartmentalization of associated reservoir units and may additionally impact correlation at the detailed reservoir level.

Keywords: Volcanic-sedimentary interaction; Peperite; Invasive flow.

5.2.1 Introduction

Volcanic activity, both effusive and intrusive, has influenced vast areas of sedimentary basins globally (e.g. Bischoff et al., 2017; Caineng et al., 2013; Coffin and Eldholm, 1994; De Luca et al., 2015; Senger et al., 2017). The sedimentary system that is active at the onset of volcanism can have a marked influence on the volcanic and sedimentary facies types that occur and get preserved (e.g. Ebinghaus et al., 2014; Hole et al., 2013; Jerram et al., 2016a, 2016b; Ross et al., 2005; Waichel et al., 2007), and can lead to the development of interbedded volcanic and sedimentary stratigraphy (e.g. Jerram et al., 2000; Rossetti et al., 2018). Stratigraphic successions that are intruded result in a significantly modified basin architecture effecting rock properties and fluid flow (e.g. Senger et al., 2017; Spacapan et al., 2019), and the transition horizons from intrusive to eruptive settings can be complex and sometimes difficult to interpret where intrusions end and subaerial eruptions start (Angkasa et al., 2017; Greenfield et al. 2019). Additionally, significant deposits of volcanic material and/or intrusions related to recent hydrocarbon discoveries has increased interest in understanding of the role of igneous products, both positive and negative, on volcano-sedimentary systems (e.g. Bischoff et al., 2017; De Luca et al., 2015; Jerram, 2015; Nelson et al., 2009; Schutter, 2003; Senger et al., 2017; Watton et al., 2014).

During the onset of volcanism in a sedimentary basin, magma is often emplaced into and/or onto poorly consolidated sediments, which can lead to a wide range of processes including loading, slope failure, lava invasion, dynamic volcano-sedimentary interaction, and the formation of peperites (Chen et al., 2016; Jerram and Stollhofen, 2002; Kwon and Gihm, 2017; Németh et al., 2008; Petry et al., 2007; Rawcliffe, 2016; Rosa et al., 2016; Skilling et al., 2002). In the context of basin evolution, understanding the nature and distribution of these different processes in prospective sedimentary basins can be critical for correlation, reservoir quality and distribution. The volcanic successions and their transition into the sediments beneath can have strong influences on seismic imaging of the base-basalt transition, often making it difficult to image any deeper structures and stratigraphy (Angkasa et al., 2017; Davison et al., 2010; Gallagher and Dromgoole, 2007; Planke et al., 2000). Surface outcrop analogues form a key component for studying variability in both the occurrence and characteristics of volcano-sedimentary interactions and their resulting facies. Better understanding of the onset of volcanism in sedimentary basins is an important step for appraising both intra- and sub-volcanic prospectivity.

This contribution presents new field observations from a number of localities in order to summarize the range of different facies that can be present at the onset of volcanism in sedimentary basins. Field areas include the NE portion of the Paraná-Etendeka Igneous Province (Paraná Basin, Brazil), St. Cyrus (Midland Valley Basin, UK), and the Isle of Mull (Mull Lava Field, UK), presented as separate case studies. Based on these field observations we discuss the range of factors responsible for the studied interaction types, and their likely implications for prospective petroleum systems.

5.2.2 Dataset and methods

This study includes fieldwork and examples from three different areas including the Uberlândia and Araguari cities (Paraná Basin – Brazil), St. Cyrus (Midland Valley Basin - Scotland) and Carraig Mhór (Mull Lava Field - Scotland), emplaced at different times. These areas present excellent exposures that allowed the detailed study of a variety of lava-sediment interactions. Detailed field observations, high-resolution photograph transects, and two photogrammetry based virtual outcrops models (St. Cyrus and Carraig Mhór) were used for this study.

Field observations focused on the lava flows, invasive flows/shallow intrusion, and their interactions with adjacent sediments. This approach allowed the characterization, illustration, and understanding of distinct types of lava-sediment interactions by defining the morphology of contacts and juvenile clasts, and host sediment characteristics.

The virtual outcrops models were constructed using high-resolution photographs acquired by a DJI Phantom 4 Pro drone with a mounted camera FC6310. The sensor user was 1" CMOS with 20 Megapixels, stabilization of the DJI fixed by GPS/Glonass accuracy. The high-resolution photographs were processed using Agisoft Photoscan 1.4.5. at the University of Aberdeen. All the post-fieldwork interpretation and measurement of the virtual outcrop models were done with LIME 3D viewer software (Buckley et al., 2019; Greenfield et al., 2019). The virtual outcrop was used to interrogate inaccessible parts of the study areas and to understand the distribution patterns of the different products of lava-sediment interactions.

5.2.3 Paraná basin case study

- Geological setting

The Paraná Basin developed as an intracontinental basin with sedimentary successions formed essentially from siliciclastic rocks related to successive Paleozoic transgressive-regressive cycles (Milani and Thomaz Filho, 2000; Milani and Zalán, 1999), along with magmatism from the Paraná-Etendeka Igneous Province (PEIP). The most significant part of this basin is in southern Brazil, extending into Paraguay, Argentina, and Uruguay, covering a total area of around 1.5 million km² (Fig. 32). The stratigraphic record of the Paraná Basin includes six supersequences: Rio Ivaí (Caradocian-Llandoverian), Paraná (Lochkovian-Frasnian), Gondwana I (Westphalian-Scythian), Gondwana II (Anisian-Norian), Gondwana III (Late Jurassic-Berriasian) and Bauru (Aptian-Maastrichtian) (Milani et al., 2007, 1994). The Gondwana III comprises the sedimentary rocks of Botucatu Formation and the volcanics of Serra Geral Group, which are the focus of this study.

The Serra Geral Group, together with the stratigraphic equivalents in the Etendeka (Africa), associated dike swarms, and other intrusive igneous rocks compose the Paraná-Etendeka Igneous Province (PEIP) (Fig. 32), which is associated with the Gondwana supercontinent break-up and formation of the South Atlantic Ocean starting at around 135 Ma (Renne, 2015; Thiede and Vasconcelos, 2010). These volcanic rock successions are composed mainly of tholeiitic basalts, and subordinate rhyolites and rhyodacites in the upper portion of the stratigraphy (Jerram et al., 1999; Marsh et al., 2001; Peate, 1997; Rossetti et al., 2018). This lava succession overlies sandstones of Botucatu Formation which was defined as a predominantly dry eolian system by sedimentological studies in the southern portion of the Paraná Basin (Scherer, 2000) and its conjugated counterpart in Etendeka (Jerram et al., 1999b, 2000; Mountney et al., 1998). Dynamic interaction of lavas and sediments within this arid setting have locally resulted in peperites as described in the Torres Syncline and the neighboring (pre-rift) Huab Basin in Namibia (Jerram and Stollhofen, 2002; Petry et al., 2007). Nevertheless, humid environments are sparsely recorded by the presence of pillow lavas and fluidal peperites, formed in the presence of water mainly along the marginal parts of the Paraná province (Famelli et al., submitted; Ferreira, 1985; Luchetti et al., 2014; Machado et al., 2015; Mano, 1987; Marques Filho et al., 1981; Moraes and Seer, 2017; Waichel et al., 2007). Within the context of this study we will focus on the interaction of volcanics and sediments within these wetter settings using outcrop

examples from the Uberlândia-Araguari area (Minas Gerais state, Brazil), before contrasting these observations with other similar examples from the NAIP.

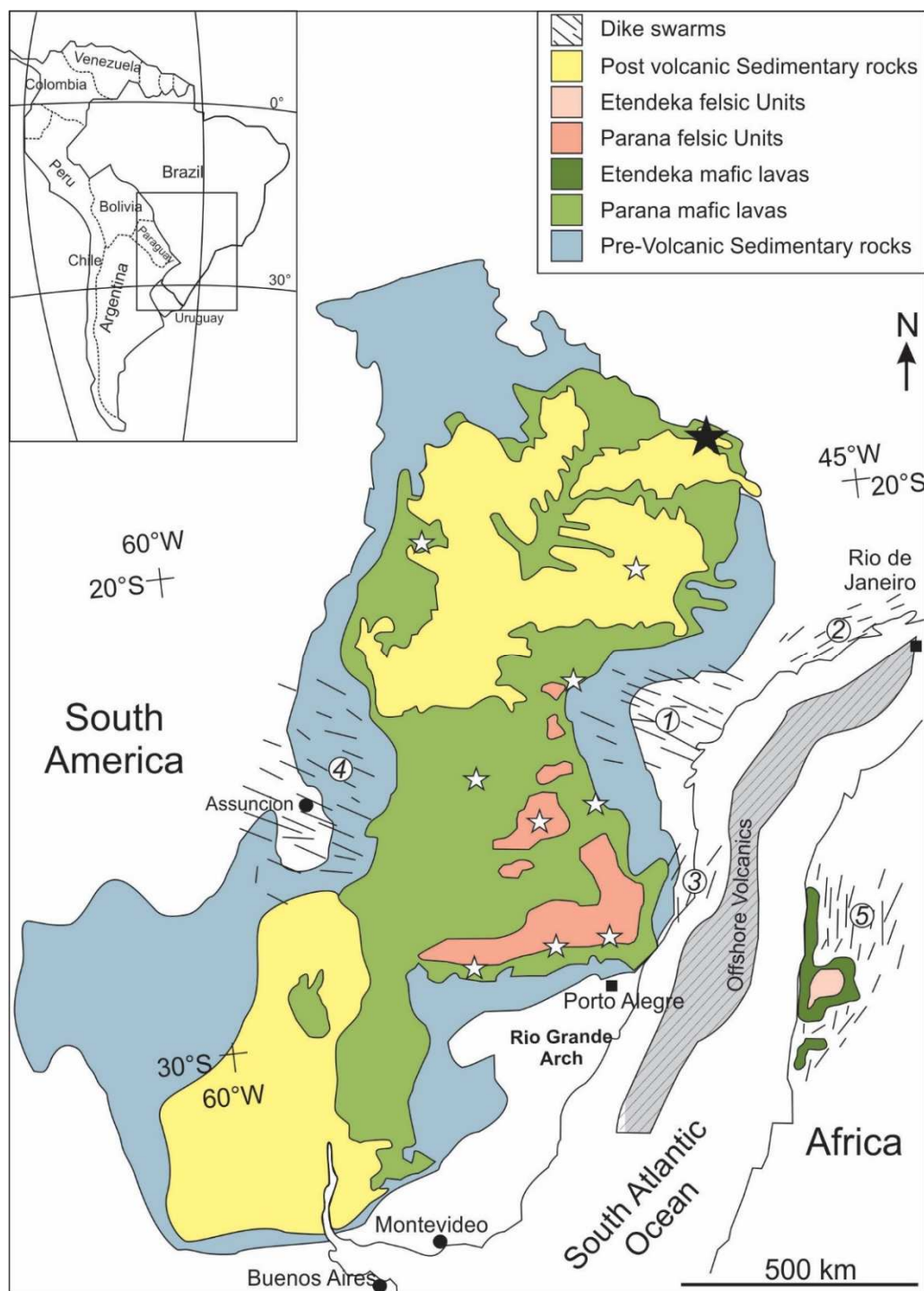


Fig. 32: Geological map of the Paraná Basin (modified after Hawkesworth et al., 2000; Peate et al., 1992; Rossetti et al., 2018; Stewart et al., 1996). Dike swarms: 1 – Ponta Grossa; 2 – Santos-Rio de Janeiro; 3 – Florianópolis; 4 – Paraguay; 5 – Skeleton Coast. Stars represent pillow lava and peperite occurrences. The black star highlights the location of the study area.

- Field outcrops: Uberlândia-Araguari area

The studied lava-sediment interactions crop out along rock quarry, highways, railways and waterfalls located between Uberlândia and Araguari cities (Minas Gerais state, Brazil). In the study area, two main types of lava-sediment interactions are identified including igneous bodies displaying peperite at both the upper and lower contacts along with other examples with sharp lower contacts (Fig. 33). In the latter type, interaction and or deformation of the overlying sediments gives evidence supporting an invasive lava flow or shallow intrusion origin. The term invasive flow refers to surface lava flows that locally transgress into the subsurface, while a shallow intrusion has evolved totally in the subsurface (Byerly and Swanson, 1978; Hooper, 1997; Rawlings et al., 1999). The distinction between these phenomena can be challenging, especially when the nature of their upper contacts over their entire extent is unknown. Some authors have proposed key criteria for distinguishing these processes which are - the lack of dikes and the abundance of lava flows in a specific region would suggest that igneous bodies showing peperites at their irregular upper crust correspond to invasive flows instead of shallow intrusions (Beresford and Cas, 2001) or stratigraphic approach (Swanson and Wright, 1981) that argues that if the basalt is at its proper stratigraphic position relative to overlying flows, it is almost certainly that a flow invaded sediments at the ground surface.

The examples presented here are interpreted as invasive flows due to the lack of any undisturbed sediment identified above the upper peperite, as outlined in Famelli et al. (submitted). Additionally, the lack of dikes and the abundance of lava flows, together with geochemical data (e.g. Famelli et al. submitted), show that this igneous body occurs at its expected stratigraphic position relative to overlying flows suggest the invasive nature of this igneous body (c.f. Swanson and Wright, 1981).

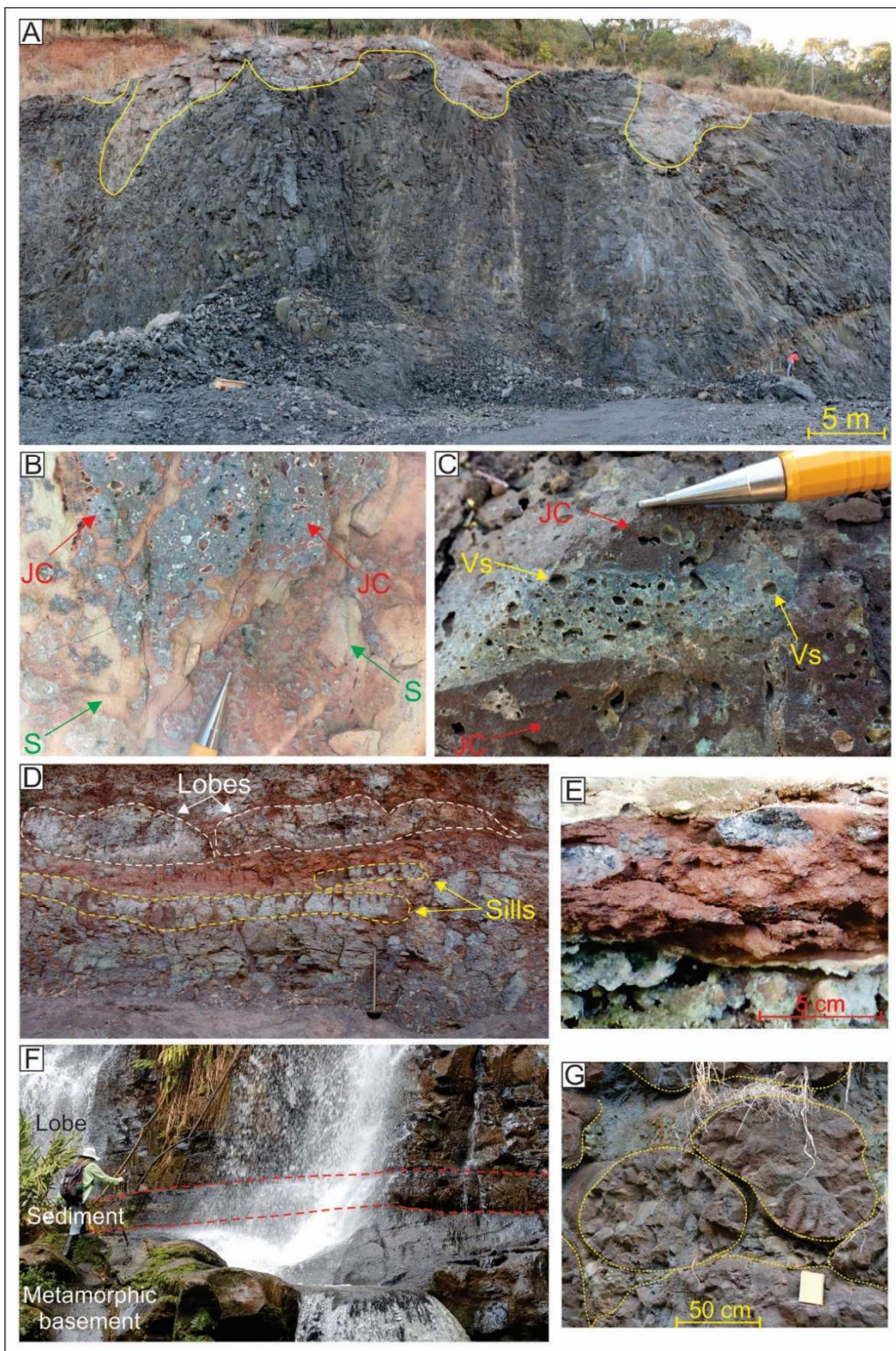


Fig. 33: Lava and sediment features from Uberlândia-Araguari; A) Irregular upper contact (yellow line) of an invasive lava flow overlain by peperites; B) Disperse peperite with irregular juvenile clasts (JC - red arrows) and host sediment (S - green arrows); C) Juvenile clasts (JC - red arrows) and vesiculated host sediment (Vs - yellow arrows); D) Coherent igneous domains from peperitic interval; lobes morphologies delimited by white dashed line, and sill morphologies highlighted by yellow dashed line; E) Detail of the conglomeratic sandstone with metamorphic basement lithoclasts; F) Sharp contact between subaerial lava flow and underlying sediment; G) Pillow lavas (dashed lines) with different sizes and shapes.

The studied peperitic layer can reach up to 12 m thick, 1.7 km in length, and occurs associated with both lower and upper contact of a thick invasive flow (up to 25 m total thickness) at the top of the volcanic succession of about 200 m thick (Famelli et al., submitted). The invasive flow has an upper crust marked by irregular vesicle patterns, and irregular upper and lower contacts that grade into peperites (Fig. 33A). The peperite domain usually occurs as tabular layers of mainly dispersed and locally close-packed peperites (Fig. 33B). Close-packed peperite consists of tightly fitting clasts separated by sediment-filled fractures, and dispersed peperite comprises a sedimentary matrix surrounding widely separated juvenile clasts (Hanson and Wilson, 1993).

Juvenile clasts vary in size from <1 cm to 1.5 m and may be blocky or fluidal (Fig. 33B). Coherent igneous domains up to 6 m in extent have morphologies resembling lobe and sill (tabular) forms (Fig. 33D). Juvenile clasts margins can be curviplanar to planar, but amoeboid surfaces are also observed. Besides the variable morphologies, most of these juvenile clasts are vesiculated with irregular to rounded vesicles (up to 5 mm), that may be filled with host sediment. Vesicles are also present in the adjacent host sediment, which mainly comprises massive silty sandstone (quartz and subordinate feldspar grains) with minor amounts of clay (Fig. 33C).

Sharp lower contacts also occur in the northern portion of the PEIP (Uberlândia-Araguari area), between lava flows and underlying conglomeratic sandstone (Fig. 33F). The conglomeratic sandstone is composed mainly by quartz and feldspar grains (sand size), and metamorphic lithoclasts (cobble size) derived from the underlying crystalline basement (Fig. 33E). These siliciclastic rocks have been attributed to occasional aqueous flows, which resulted in alluvial fans and/or localized and ephemeral fluvio-lacustrine deposits (Moraes and Seer, 2017). The existence of localized bodies of water in the study area is suggested by the presence of pillow lavas (Fig. 33G), and lacustrine sediments containing ostracod fossils at c. 1 km from the invasive flow exposure (Famelli et al., submitted; Moraes and Seer, 2017).

5.2.4. Midland Valley basin of Scotland case study

- Geological setting

The Midland Valley Basin (MVB) of Scotland is a Late Palaeozoic sedimentary basin filled by a variety of sedimentary, volcanic, and plutonic rocks, and bounded by the Highland Boundary Fault and the Southern Uplands Fault (Fig. 34). The closure and suturing of Iapetus Ocean in southern Scotland at around 420 Ma gave rise to Caledonian Mountains, which were eroded and deformed, synchronously with the Midland Valley Basin development (Oliver et al., 2008).

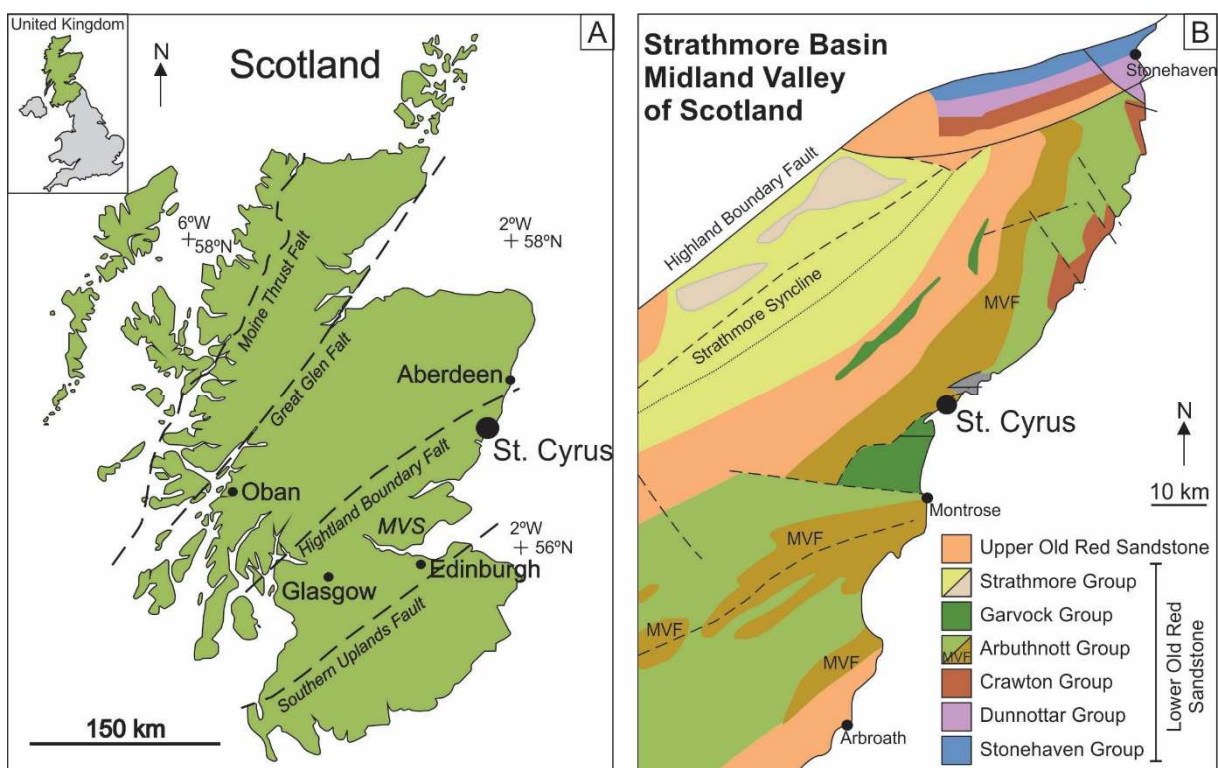


Fig. 34: A) Map of Scotland showing the location of the study area in St. Cyrus; B) Geological map of Old Red Sandstone age strata of the area between Stonehaven and Arbroath (modified after Hole et al., 2013; Rawcliffe, 2016). MVF = Montrose Volcanic Formation (in brown on map B) which is part of the Arbuthnott Group.

The study area is located at St Cyrus in the northern part of the MVB and, dominated by the Lower Old Red Sandstone (ORS). This succession is characterized by six groups (Stonehaven, Dunnottar, Crawton, Arbuthnott, Garvoeck and Strathmore) with Mid-Silurian to Devonian ages, composed mainly by terrestrial conglomerates, sandstones and mudstones, with intercalated volcanic rocks (Hole et al., 2013). The Montrose Volcanic Formation (MVF), which forms part of the Arbuthnott Group, is dominated by basalts and basaltic andesite (Thirlwall, 1981), and is exposed from

north of Crawton to Arbroath (Fig 34). There are no absolute age determinations available for MVF but these basalts must be younger than 415.5 ± 5.8 Ma, which is the age of the underlying volcanic rocks from Crawton Volcanic Formation (Thirlwall, 1988).

The study area at St. Cyrus coast is composed of intercalated lava-sediment succession of the MVF, where it is faulted against sedimentary rocks of the Upper ORS (Hole et al., 2013). In these areas, lava tube fed pahoehoe flow fields, generally less than c. 5 m thick. Hole et al. (2013) described localized occurrences of agglutinated spatter with thin interlayers of sediment, indicating explosive activity for localized surface, potentially enhanced by near surface interaction with water saturated sediment. Similar deposits were also described from rootless cone volcanism in Iceland (Hamilton et al., 2017), suggesting sections of spatter ramparts described at St. Cyrus could also form as rootless cones. A wide diversity of magma sediment interactions are recorded at St. Cyrus, including examples of sediment loading and spectacular peperites (Hole et al., 2013).

- Field outcrops: St. Cyrus

Lava-sediment interaction crops out along 2.3 km cliff at St. Cyrus (Montrose – Scotland), and this study focuses on a 500 m section close to the Woodston Fishery (NO 7585 6486 - Fig. 35A). In this area, three main types of lava-sediment interaction were identified: blocky to fluidal peperite associated with subaerial and invasive lava flows, pillow-like peperite, and invasive flow with sharp contacts. The term pillow-like peperite is used here as a purely descriptive denomination based mainly on the juvenile clasts morphologies resembling pillow lavas.

The blocky to fluidal peperite is associated with lava units and crops out as irregular packages (up to 4 m thick) in sections of the cliff and in some stacks located at the beach (NO 7593 6488 - about 200 m to northeastern of the Woodston Fishery, location 2 in Fig. 35A). The discontinuous nature of the exposures causes difficulties in understanding the lateral extent of the deposits. However, isolated packages of peperite of up to 8 m in length (Fig. 35B) can be seen. The juvenile clasts are generally centimeter to decimeter scale (up to 40 cm) and have very complex outlines, some of which have curviplanar to planar surfaces (Fig. 35C). Rounded to elongated vesicles are common features of juvenile clasts and may be filled with sediment. The host

sediment is mainly composed of green to red color fine-grained siltstone and sandstones (Fig. 35C), but mudstones can be present. These fine sediments were interpreted as wave and current reworked air-fall tuff deposits (Hole et al., 2013) with different colors reflecting weathering and differential oxidation around juvenile volcanic clasts.

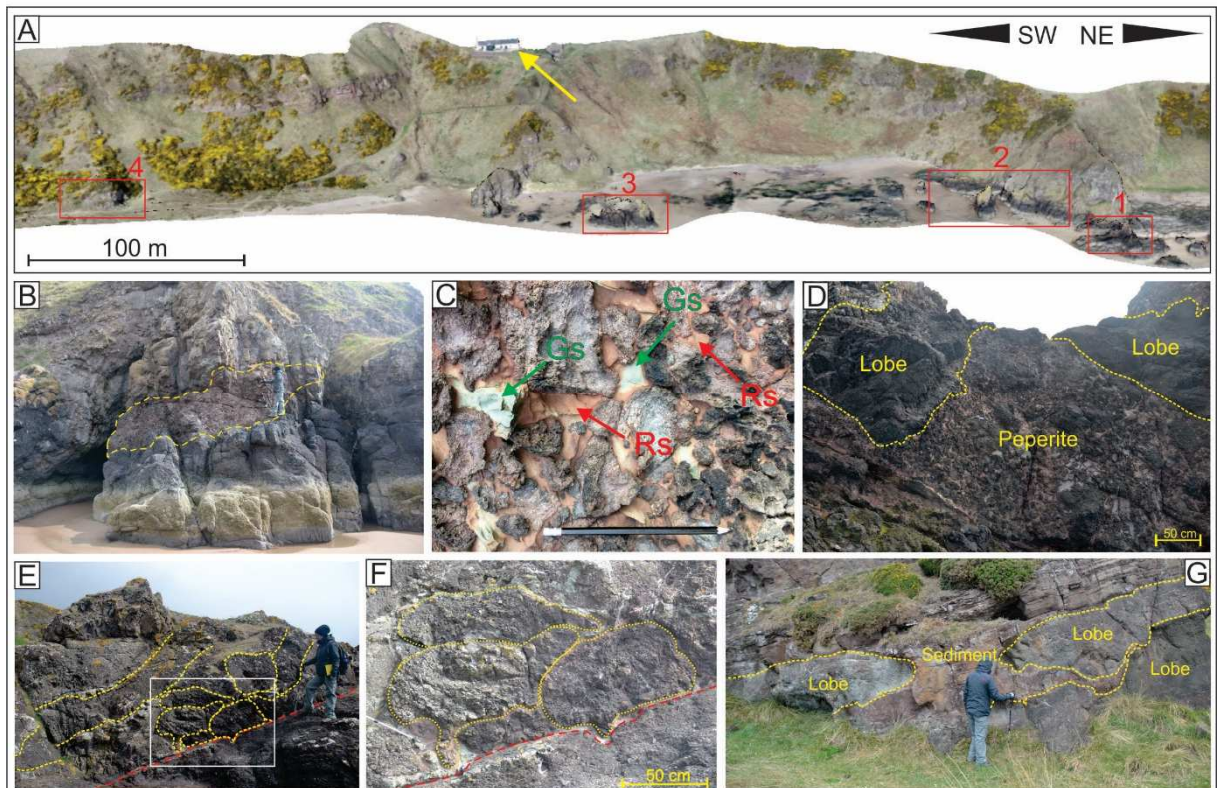


Fig. 35: Lava and sediment features from St. Cyrus area. A) Virtual outcrop of the study area in St. Cyrus. Red squares represent the location of studied outcrops and the yellow arrow indicates the Woodston Fishery location; B) Irregular morphology of peperite; C) Irregular juvenile clasts and host sediment with distinct colors - green (Gs - green arrow) and red (Rs - red arrows); D) Invasive lobes with irregular contacts and related peperites; E) Pillow-like peperites. Depending on the cross-section direction it is possible to observe elongated lobe or pillow morphologies; F) Detail of the figure 35E (white square) where it is possible to observe pillow-like peperites of decimeter size; G) Invasive lobes with sharp contacts.

Although peperite may modify original sedimentary structures, the host sediment may display relict original stratification, developed during infiltration of sediment in the previous formed peperite, or formed during the sediment fluidization (Skilling et al., 2002). In the St. Cyrus area, the peperite contains consolidated inclusions of coherent sedimentary rocks (fine grained siltstone and sandstone). The

host sediment lamination seems to represent the remnant stratigraphy due to its similar dip to the regional rocks (Hole et al., 2013). Furthermore, the lack of lamination disturbance in these sedimentary inclusions suggests that the sequence was partially consolidated prior to peperite formation at St. Cyrus.

Lava lobes of about 50 cm thick with peperites in the upper and lower contacts are also present at St. Cyrus (NO 7556 6474 location 1 in the Fig. 35A). The juvenile clast morphologies and the host sediment characteristics are similar to the peperites described above, which are related with subaerial lava flows. The occurrence of peperites in both contacts suggests that these lobes were not emplaced subaerially (Fig. 35D), and can represent shallow intrusions or invasive lava flows. As these lobes occur in an isolated stack, it is not possible to trace them laterally to prove their intrusive or invasive nature. Nevertheless, the surrounding cliff and stacks composed of subaerial lobes show no evidences of intrusions, and these lobes may represent an invasive portion of subaerial lavas. Additionally, the occurrence of proven invasive flows in other areas of St. Cyrus (e.g. invasive flows that can be traced laterally, where they show clear subaerial characteristics - Hole et al., 2013), suggests that this process was common during lava flows emplacement in the study area.

Pillow-like peperites of St. Cyrus can be observed in the stack located in front of the Woodston Fishery (NO 7578 6481 - location 3 in the Fig. 35A) where rounded juvenile igneous bodies of variable sizes resemble pillow lavas in a c. 3 m thick succession (Fig. 35E and 35F). The host sediment of the pillow-like peperite is similar to the block to fluidal peperite formation (described above). Despite the similarity with pillow lavas, these rounded juvenile clasts do not have chilled rinds, radial joints, or vesicle distribution patterns that characterize pillow lavas outcrops (McPhie et al., 1993; Walker, 1992). These pillow-like fragments have complex margins marked by many small re-entrances filled with host sediment at their base and top that suggests invasive/intrusive nature of these pillowed features into pre-existing soft sediment.

To the south of the study area (also south of the Woodston Fishery – location 4 in the figure 35A) lava lobes of around 80 cm thick with relatively sharp contacts crop out (Fig. 35G). In general, the lobes edges are relatively smooth and rounded, but they may have small benches resembling small steps. Minor mingling occurs along the upper and lower crusts of these lobes, which is good evidence for their invasive rather than extrusive nature. The host sediment is mainly composed by laminated fine to medium sandstone, which grades up into cross-bedded gravel bearing sand units. The

fine-grained sediments are dominantly undisturbed away from the igneous contacts; however, a stringer of sediment is strongly distorted and squeezed between two separate magma lobes (Fig. 35G).

5.2.5 Mull Lava Field case study

- Geological setting

The Mull Lava Field (MLF) is preserved in western Scotland on the Isle of Mull, and represents a remnant of the North Atlantic Igneous Province along the European margin of the NE Atlantic, dated at ca. 60.5 ± 0.5 Ma (Bailey et al., 1924; Emeleus and Bell, 2005; Williamson and Bell, 2012). The entire lava field ranges between 1800 and 2200 m thick (e.g. Walker, 1970), emplaced over a period of 2.52 ± 0.36 Ma (Chambers and Pringle, 2001). The Mull Lava Group covers an area of about 840 km² (Emeleus, 1991) and its stratigraphy includes the Staffa Lava (oldest), Mull Plateau Lava, and Mull Central Lava (youngest) Formations (Emeleus and Bell, 2005). Many studies focusing on the geochemistry and petrology of Mull show that the Paleogene MLF are mainly of transitional to alkaline basalts and its derivatives, and subordinates tholeiitic basalt and its derivatives (Bailey et al., 1924; Beckinsale et al., 1978; Kerr, 1995a, 1995b; Kerr et al., 1999; Morrison et al., 1985; Thompson et al., 1986).

This volcanic succession is predominantly formed of subaerial lava flows from fissure eruptions. Hyaloclastites and pillow lavas occur within the basal Staffa Lava Formation, indicating either subaqueous eruptions or the transport of lava into a body of water. Locally significant vent activity produced spatter and tephra, and evolved magmas generated ignimbrites, which also characterize the MLF (Williamson and Bell, 2012).

The study area at Carraig Mhór (NW 556 211) is located east of Carsaig Bay in the Ross of Mull peninsula (Isle of Mull - Scotland) and exposes lavas and intra-lava-sediments from Staffa and Mull Plateau Lava Formations (Mull lava field) (Fig. 36) (Brown and Bell, 2007; Williamson and Bell, 2012). According to Williamson and Bell (2012; Figs 38, 40a), this area includes thin silicic ignimbrites interbedded with mudstones and siltstones, blocky basaltic lava, stratiform peperite, compound basaltic lava and breccia facies (Staffa Lava Formation), overlaid by relatively thin, compound sheet flows of basalt separated by palaeosols (Mull Plateau Lava Formation).

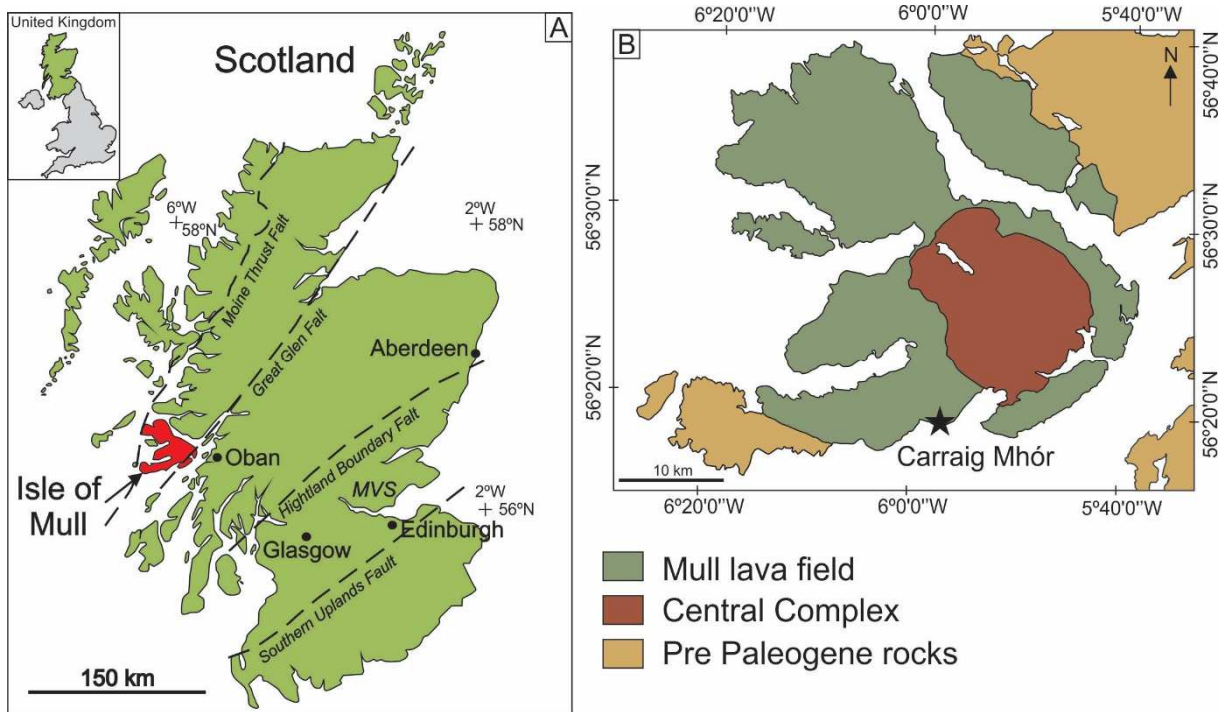


Fig. 36: A) Location map of Scotland, indicating the position of the Isle of Mull (in red); B) Simplified geological map of the Isle of Mull with the location of the study area in Carraig Mhór (black star) (Modified after Brown and Bell, 2007).

- Field outcrops: Carraig Mhór

Within the foreshore section at Carraig Mhór (Fig. 37A), a pahoehoe lava flow of 2-4 m thick (Staffa Lava Formation) overlies a sequence of mixed volcaniclastic and siliciclastic estuarine sediments intruded by several irregular and sheet like dolerite intrusions. Three main types of lava-sediment interaction occurred due to lava flowing over water saturated sediments: loading structures, fluidal and blocky peperite, and rootless cone formations.

Previous studies (e.g. Brown and Bell, 2007) interpreted this pahoehoe lava as an intrusion. However, typical features of lava flow emplacement include pipe vesicles at the lower contact, vesicle cylinders and vesicle sheets at the upper portion of the lava flow, together with preserved ropy pahoehoe features on lobes cropping out along the foreshore area (Fig. 37B, 37C, 37D and 37E), suggesting an extrusive origin. It is important to state that intrusions are abundant, but volumetrically subordinate and cross cut the lava flows of the area.

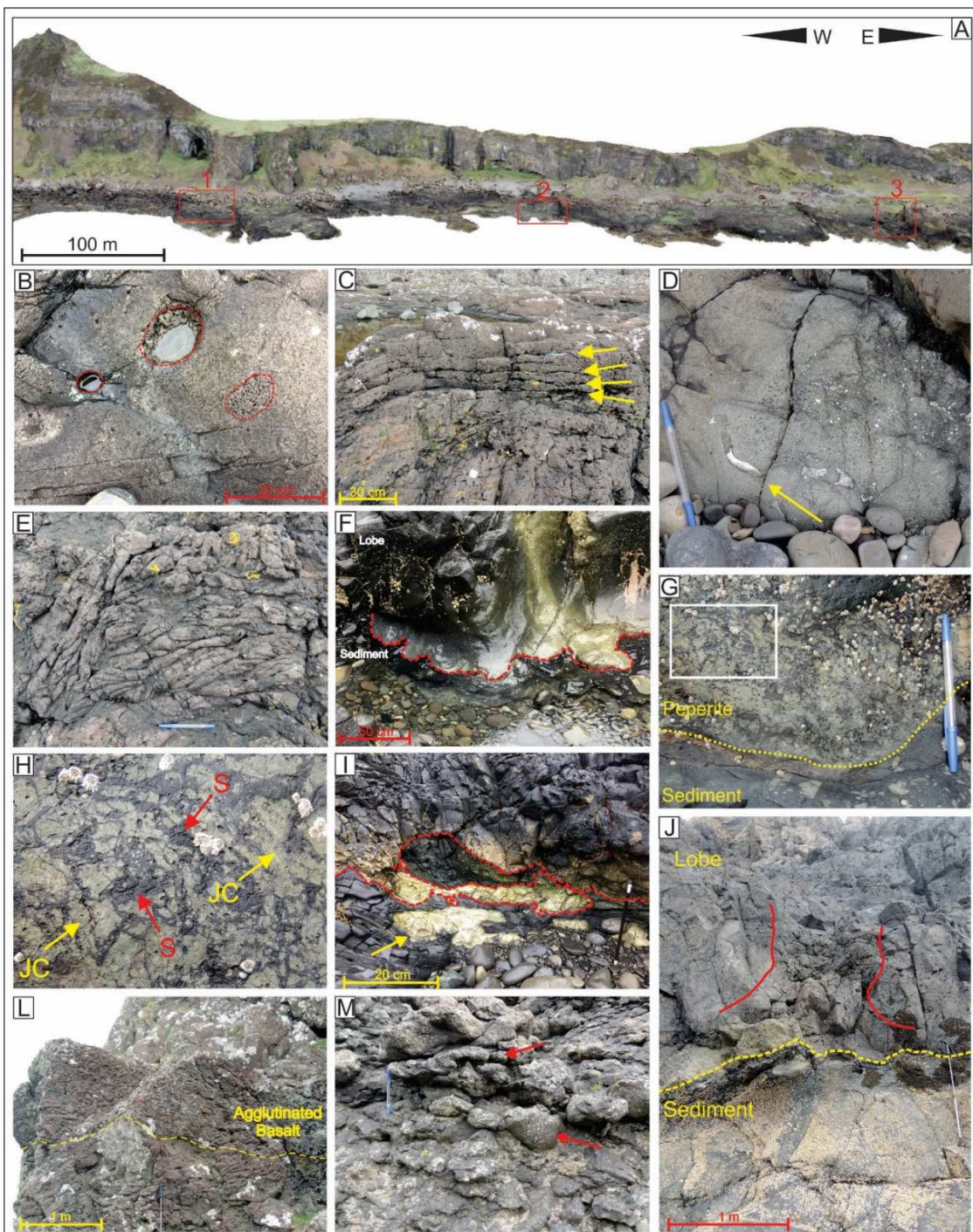


Fig. 37: Lava and sediment features from Carraig Mhor (Isle of Mull); A) Virtual outcrop of the study area in Carraig Mhor. Red squares represent the location of the studied outcrops; B) Vesicle cylinders in the lava core; C) Vesicle sheets (yellow arrows) on the upper crust of a pahoehoe lava flow; D) Pipe vesicle (yellow arrow) at the basal portion of the flow; E) Ropy structure at the surface of the lava flow; F) Loading structure at the basal contact of a subaerial lava flow; G) Blocky peperite with juvenile clasts of a few centimeters size; H) Close-up of the white square in figure 6F showing juvenile clasts (JC – red arrows) with curviplanar to planar surfaces and jigsaw-fit texture embedded in mudstone (S – red arrow); I) Fluidal juvenile clast (yellow arrow) and bulbous lava lobe invading the underlying sediment (dashed red line); J) Preferential zone of fluid scape of volatile with a major concentration of vesicles and cylinders occurring between the two red lines; K) Agglutinate deposit; L) Detail of the agglutinate deposit with rounded to flatten fragments of lava (red arrows).

The contact between the pahoehoe lower crust and the sediments is clearly marked by decimeter scale loading structures (Fig 37F). Features resembling flame and dome structures (load structures), such as sediments injected into the overlying lava flow, are present at this interface but do not exceed a few centimeters high. Locally, this contact results in fluidal or blocky peperite, which may develop into a sharp contact for a few meters along the lower crust of the lava flow. The sharp contact is marked by regular and rectilinear limits, which can have small benches resembling small steps reaching up to 10 cm high. The blocky peperite occurs usually smaller than 20 cm long, and juvenile clasts have dimensions of around 2 cm in diameter, curviplanar to planar surfaces, and jigsaw-fit texture (Fig. 37G and 37H). The juvenile clasts present in the fluidal peperite are massive, and vary from irregular to amoeboid. In the same area where the fluidal clasts occur, there is a bulbous lava lobe of about 60 cm projecting into the underlying sediment (Fig. 37I).

Besides the classic subaerial lava flow, agglutinate deposits also occur at Carraig Mhór. Agglutinate comprises airfall spatter (vesicular, fluidal, juvenile pyroclasts) and bombs related to explosive eruptions of low viscosity magmas (McPhie et al., 1993). Alternatively, agglutinate can result from the interaction of lava with surface or near-surface water or water saturated sediments (Rader et al., 2018). In the study area, the lava spatter and bombs (up to decimeter size) are rounded to flattened with occasion ‘bread-crust’ morphologies and are welded together (Fig. 37L and 37M). This agglutinated deposit has a clustered geometry, and flows emanating from it are absent, which is consistent with a rootless cone origin (Bruno et al., 2004). The lava flow interior, which forms the wave-cut platform close to the agglutinate deposits, includes numerous examples of vesicle cylinders, and in some areas, vesicles are preferentially concentrated into zones, reflecting fluid escape (Fig. 37J). Also, the fact that the lava flowed over water saturated sediments at this location provides strong support for the presence of a rootless cone associated with the studied pahoehoe lava.

5.2.6 Discussion

- Invasive and subaerial lava flows

The case studies evidence two main types of lava-sediment interaction: lava flowing on the surface (subaerial flows) and invading unconsolidated or poorly consolidated sediments (invasive flows). Previous studies show that some lobes of St.

Cyrus were emplaced beneath the partly consolidated sedimentary rocks, but the same lobes can be traced laterally over few meters, where they present subaerial features suggesting an invasive nature (Hole et al., 2013; Rawcliffe, 2016). Similarly, previous work from Famelli et al. (submitted) interpreted the Uberlândia-Araguari lobe (Paraná basin) as an invasive flow due to its textural and structural similarities to invasive flows from other Igneous Province (e.g. Beresford and Cas, 2001; Rawlings et al., 1999; Swanson and Wright, 1981).

As discussed before, the term invasive flow is used to describe lava flows that invade sediment and migrate laterally essentially as very shallow sills (Byerly and Swanson, 1978; Hooper, 1997). This process has been associated with variations in gravitational potential energy that commonly result in gravitationally unstable vertical profile of bulk density, where denser material overlies relatively less dense material leading to a Raleigh-Taylor instability (Owen, 2003; Rawlings et al., 1999).

Density contrast and gravity instability

In general, basaltic magma is erupted at temperatures between 1000-1300 °C and its density at low pressure is around c. 2700 kg·m⁻³ (Lesher and Spera, 2015). For Paraná lavas, using a representative tholeiitic basalt composition (sample UB-20c, Famelli et al., submitted) gives a calculated dry density of c. 2750 kg·m⁻³ at surface pressure conditions, 1000 °C (method of Iacovino and Till, 2019). At low pressures, dissolved gasses segregate into vesicles that effectively decrease lava density (Hole et al., 2013). Rossetti et al. (2019) evaluated the petrophysical properties of volcanic-sedimentary sequences from Paraná-Etendeka Large Igneous Province and showed that upper crust and core of pahoehoe flows of Torres Formation have present day porosity averages of 12.3 and <3 %, respectively. However, initial porosity at the time of emplacement was likely higher with vesicular porosities greater than 50 %, common for vent proximal magmas, reducing via degassing to ca. 20 % at ca. 12 km from the vent as measured in lava tube samples from Hawai'i (Cashman et al., 1994).

Considering an average vesicularity (porosity of ca. 20% – Cashman et al., 1994), the basaltic magma density would be ca. 2200 kg·m⁻³. Even in more vesiculated magmas (porosity of 30%) the density would be c. 1920 kg·m⁻³, still higher than the density of some lithified sandstones of Paraná-Etendeka Igneous Province (1700 kg·m⁻³, Rossetti et al., 2019). For St. Cyrus case, the estimated density for vesiculated

basalt (ca. 20% of vesicles) at 1000 °C and wet sediment composed of kaolinite and sand-grade quartz are c. 2000 and 1800·kg m⁻³, respectively (Hole et al., 2013). Unconsolidated and uncompacted sediments vary in density depending on grain size, composition, saturation, compaction, and sorting. However an average value of 1600 kg·m⁻³ appears to be a reasonable guide value for surficial sediments (e.g. Tenzer and Gladkikh, 2014). Therefore, a gravitationally unstable vertical profile can be easily, if not inevitably, achieved in volcano-sedimentary basins during the emplacement of lava flows on the surface of unconsolidated sedimentary sequences.

Mechanisms for sinking of a lava flow into unconsolidated sediments

Besides the gravitational instability, the sinking of a lava flow into unconsolidated sediments requires that the applied stress exceeds the sediment strength. This condition may be achieved through an increase in applied stress (e.g. emplacement of a lava flowing above a sedimentary layer) or through a temporary reduction in sediment strength (liquidization). Similarly to Allen (1977) and Owen (2003), the term liquidization will be used here in reference to the change of sediment state from solid-like to liquid-like. There are several possible liquidization mechanisms (e.g. fluidization, liquefaction, and thixotropic) which are initiated by a triggering agent such as rapid rock deposition or seismic effects (Owen, 2003).

Active magmatic systems associated with volcanoes are known to produce a wide range of seismic signals (volcanic earthquakes) due to input of gas and heat and the migration of fluids through cracks and connected pore space (Park et al., 2019). Volcanic earthquakes are often observed prior and during the eruptive activity (e.g. Ateba et al., 2009; Domínguez et al., 2001; Franco et al., 2019; Hurst et al., 2014; Machacca-Puma et al., 2019). For pahoehoe flow fields, individual flow lobes will only remain fluid for relatively short time periods before cooling and solidification, providing a very short time period for lava-sediment interaction to occur. Indeed, Self et al. (1996) argue that such flow fields may take years to accumulate. Consequently, fluidization of sediment by seismic activity during eruption is an attractive mechanism for triggering lava-sediment interaction in the study areas because it does not rely entirely on density-driven mingling.

However, the emplacement of hot lava over water saturated sediments has an additional and highly important potential mechanism for fluidizing sediments. The rapid

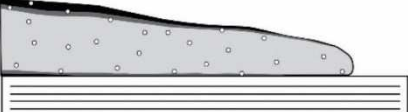
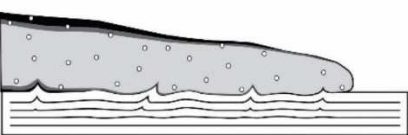
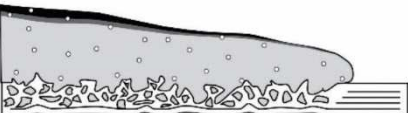
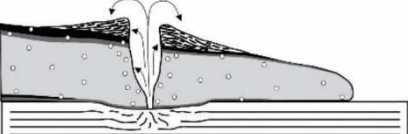
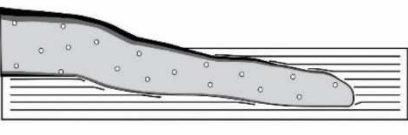
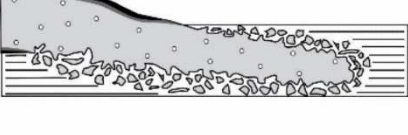
heating and expansion of pore fluids can cause both gradual, explosive or intermediate expansion leading to fluidization of sediments (Kokelaar, 1982). Linked to this is the process of peperite formation, which can lead to dynamic mingling of magma and fluidized sediment (Skilling et al., 2002), providing further clear evidence for sediment fluidization and potentially acting as a viable triggering mechanism for lava flow invasion.

- Interaction type and related processes

A summary of the different modes of interaction of lava and sediment observed in the study areas is presented in Tab. 5. During volcanism, lava flows with different emplacement styles (invasive or subaerial flows) may mingle with adjacent sediment leading to a range of interactions products (cf. Ebinghaus et al., 2014; Skilling et al., 2002; Wohletz, 2002). In the studied areas, lava flows (invasive and subaerial) can be associated with peperites or have sharp contacts. However, loading structures, pillow-like peperites, and rootless cones occur associated only with free-surface flows in the studied examples.

Gravitational instability and sediment strength are important not only in determining if a lava flow will sink or flow at the surface, but also in dictating the products of the lava-sediment interaction. The deformation of the underlying sediment can result in a variety of loading morphologies, similar but more extreme than seen in sedimentary sequences (Owen, 2003) and, in some cases, it can lead to disruption of the lava flow resulting in fluidal or blocky peperites.

Tab. 5: Lava-sediment interactions observed in the study areas. Emp.Type = Emplacement types; Loc. = Location; P = Paraná Basin, M = Isle of Mull; S = St. Cyrus.

Emp. Type	Interaction types	Description	Loc.	Illustrative scheme
Subaerial	Sharp contacts	The lava flow is emplaced on the surface and its lower crust do not interact with the underlying sediments.	P - M	
	Loading	The lava load and flowing at the surface deforms the underlying sediments leading to flames and domes structures (cm scale).	M	
	Peperite (blocky/fluidal)	Fluidal and blocky peperites occur associated with the lower crust of the lava flow that was emplaced on the surface.	S - M	
	Peperite (pillow-like)	Juvenile clasts resembling pillows occur at the base of the lava flow emplaced on the surface.	S	
	Rootless cone	Agglutinated deposits occur close to the top of subaerial lava flows, occasionally with abundant pipe vesicles and vesicle cylinders (preferential zones for vesicles ascension).	M	
	Sharp contacts	The upper and lower contacts of the invasive flows are relatively sharp, but can be smooth and rounded.	S	
Invasive flow	Peperite	The upper and lower contacts of the invasive lava flows are irregular and grade to peperite domains.	P - S	

Loading and pillow-like peperites

The loading structures described at Carraig Mhór (Mull) correspond to simple load casts, an end-member of Owen's (2003) classification. According to Owen (2003),

deformation could result in the development of other morphologies (e.g. pendulous load casts, attached pseudonodules, detached pseudonodules, ball-and-pillow structures) depending on the duration of the liquidized state of the underlying sediment. For simple load casts, such as those that only require liquidization, it seems that this process may have limited duration. However, if the underlying sediment remains liquidized for a relatively long time, detached pseudonodules or ball-and-pillow structures, could develop (Owen, 2003). Besides the similarities in nomenclature, in the ball-and-pillow structures described by Owen (2003) the dominant process is gravity-driven, whereas the pillow-like peperites of St. Cyrus involve both gravity and a directional component subparallel to the surface. The formation of the pillow-like peperites at St. Cyrus may require outward-directed magma pressure causing accentuated surface instability, which in turn leads to propagation of pillows into adjacent wet-sediment (Befus et al., 2009). It is important to reiterate that density contrasts between wet sediment and magma may be fundamental in the formation of the pillow-like peperites present at St. Cyrus.

The effects of vapor film on lava-sediment interaction

The ductile deformation and fragmentation without significant quenching or explosive disruption of magma, might explain the sharp contacts in invasive flows, loading structures and the pillow-like peperites found in this study. According to Skilling et al. (2002), the only plausible explanation for this ductile deformation is the formation of a film of vaporized pore water in the sediment adjacent to contacts during the initial stages of magma wet-sediment interaction. Besides preventing immediate explosive interaction, the poor thermal conductivity of the vapor film allows the magma to stay fluid leading to fluid-fluid mingling behavior during the interaction with sediment (Hole et al., 2013; Wohletz, 2002). The insulating effects of the vapor film would explain the different fluidal clasts morphologies and its complex fluidal contacts described in the literature and in the studied areas (e.g. Befus et al., 2009; Branney and Kokelaar, 2002; Brown and Bell, 2007; Busby-Spera and White, 1987; Hole et al., 2013; Khalaf et al., 2015; Waichel et al., 2007).

Factors influencing the vapor film behavior

It is not clear how vapor films remain stable during the deformation of clasts, but its development is appointed to be more efficient in fine-grained, well-sorted and loosely packed sediments (Busby-Spera and White, 1987; Skilling et al., 2002). At Carraig Mhór and at St. Cyrus, the interaction of magma and wet, fine-grained sediments (clay rich volcaniclastic sediments in Mull, and fine-grained siltstone and sandstone, with subordinate mudstone in St. Cyrus) resulted in not only fluidal and pillow-like peperites, formed by non-explosive interaction, but also in the formation of blocky and rootless cone deposits caused by explosive interaction. This suggests that peperite formation can be complex and involve many factors besides the sediment granulometry.

Experimental studies have shown the importance of the absolute temperature and heat content of the wet sediments and magma, and mingling magma and the rate of heat transfer between them (Wohletz, 2002). Depending on how the vapor film behaves, which influences the heat transfer mechanism, passive quenching or explosive fragmentation may occur. When the vapor film acts as an insulating barrier, passive quenching will occur. However, if the vapor film become unstable, it can act as a potential energy reservoir that causes magma fragmentation, mingling of magma with sediments, and explosive quenching (Wohletz, 2002). An important parameter in determining the behavior of the vapor film is the value of R_s , which can be expressed as a function of the sediment mass (including pore water), m_s , and magma mass, m_m , $R_s = m_s/m_m$. If $R_s > 3.0$ there is enough water in the sediment leading to convective heat transfer that promotes passive cooling, not likely explosive. For $R_s < 1.3$ most of the water remains in the vapor state after expansion, leading to the likelihood of explosive behavior (Wohletz, 2002).

In terms of thermal equilibrium, the R_s in St. Cyrus attained values >3 , which allowed the formation of fluidal clasts (Hole et al., 2013). However, the formation of blocky peperites, described in this work and previously by Rawcliffe (2016), requires quenching, mechanical stress or hydromagmatic explosions (Skilling et al., 2002). In the latter case, local variation in R_s along the St. Cyrus transect is required to allow a variety of lava-sediment interactions, which includes the formation of blocky and fluidal peperites, pillow-like peperites, and invasive lavas with sharp contacts.

At Carraig Mhór, Rs is variable. $Rs < 1.3$ was probably required for the formation of the rootless cones (Hamilton et al., 2017), whilst $Rs > 3$ would promote the formation of loading and fluidal peperites. Explosive and non-explosive products in both St. Cyrus and Carraig Mhór, located less than 300 m distant from each other, suggest local changes in physical properties of magma and/or sediment, and consequently in Rs values. This range of products indicates that these are probably heterogeneous systems at any scale. Alternatively, the formation of the rootless cone relieves the pressure of the underlying sediments in the region, what may explain the presence of non-explosive interactions (e.g. loading and peperite) in the immediate vicinity.

For the Paraná Basin, blocky and fluidal fragments occurring at the same layer in Uberlândia-Araguari area also suggest complex processes for peperite formation, again involving localized variations in Rs . Due to the predicted relative arid climate at the time, with sparse and torrential rains (Moraes and Seer, 2017), changes in water saturation of surficial sediments could have been heterogeneous over fairly short time periods, potentially during the emplacement of individual flows, which could also have contributed to variable Rs in this setting. Additionally, the sharp contacts of lava flows described in the Northern area of the Paraná Basin suggest that fluidization and/or gravitational instability were probably not important processes during the beginning of the volcanism, potentially due to the physical properties of the underlying sediments (conglomeratic sandstones) or absence of an effective trigger agent.

- Importance for petroleum systems

The presence of igneous rocks in prospective volcano-sedimentary basin sequences and their role in petroleum systems have been widely discussed recently (Bischoff et al., 2017; DeLuca et al., 2015; Mizusaki, 1986; Schutter, 2003; Zhu et al., 2007). Similarly, it is well known that igneous rock can act as reservoirs, lead to maturation, create fluid migration pathways through dikes and sills, act as seals and promote structures where hydrocarbons may be trapped, (Galland et al., 2018; Jerram, 2015; Miranda et al., 2018; Plazibat et al., 2019; Rateau et al., 2013; Schofield et al., 2017). However, the identification and interpretation of the basalt-sediment transition still remains challenging, because it involves variations in the physical properties of the volcanic and sedimentary facies and their distribution (Angkasa et al., 2017; Davison et al., 2010; Millett et al., 2020). The studied cases showed that the lava-sediment

interplay can result of at least seven interaction types, causing variable degrees of host sediment disruption. In those interactions involving sharp contacts between lava and sediment, such as in Uberlândia-Araguari in Brazil, and St. Cyrus in Scotland, the properties of volcanic and sedimentary facies should not have changed considerably. However, disruption and mingling of lava and sediment during the formation of blocky peperites related to both subaerial and invasive flows in Uberlândia-Araguari (Brazil) and St. Cyrus (Scotland) may modify the original sediment characteristics (Skilling et al., 2002). Even though invasive flows with sharp contacts found in St. Cyrus were not associated with explosive events, such as the rootless cones seen at Carraig Mhór, they may compartmentalize the host sediment, modifying fluid movement pathways (Rateau et al., 2013; Schofield et al., 2017).

Peperites have been described as a particular kind of hydrocarbon reservoir with satisfactory exploration potential in China. In this case, the reservoir is called tight, due to its particular physical characteristics (matrix permeability at overburden pressure is equal to or less than $0.1 \cdot 10^{-3} \mu\text{m}^2$ - air permeability is less than $1 \cdot 10^{-3} \mu\text{m}^2$) (Wu et al., 2019). Besides the relatively low permeability, commercial oil production becomes possible under certain economic conditions and technical measures (Wu et al., 2019, 2016). Although potential reservoirs involving peperites were not reported in the Brazilian Atlantic Passive Margins Basins, the common presence of volcanic rocks found in several Pre-salt exploration wells suggests that the product of interaction between lava and sediment may exist and are yet to be described from offshore. Indeed the outcrops of peperites and associated sediment-lava features found along the Paraná-Etendeka outcrops in Brazil/Namibia, and the younger pre-salt outcrops in Angola, suggest this facies may be more widely distributed (e.g. Jerram et al., 2019; Jerram and Stollhofen, 2002; Petry et al., 2007). Thus, understanding the lava-sediment interaction in terms of processes (mingling of magma and sediment, passive or explosive quenching) and products (geometry, porosity, and facies distribution) is essential for a more accurate delineation of the subsurface and hydrocarbon exploration. Finally, with a potentially wide diversity of magma-sediment distributions and geometries in different interaction styles, the resulting seismic properties of the base-basalt transition may vary substantially, causing significant differences in seismic scattering, attenuation and associated imaging in volcano-sedimentary sequences (Millett et al., 2020). Understanding the seismic characteristics of these sequences will form the subject of a future study.

5.2.7 Conclusion

The study of lava-sediment interaction of the NE portion of Paraná-Etendeka Igneous Province (Paraná Basin, Brazil), St. Cyrus (Midland Valley Basin, UK), and Isle of Mull (Mull Lava Field, UK) demonstrates how diverse these interactions can be in terms of processes and products. The results presented allowed the following conclusions:

1. There are two main types of lava flows present in the study area: subaerial and invasive lava flows; both can have sharp or irregular contacts associated with peperites. Loading structures, pillow-like peperites and rootless cones were observed as common features associated.
2. Gravitational instability and the overcoming of the sediment strength is required for the development of invasive flows, loading structures and pillow-like peperites. Gravitational instability was easily achieved in the study areas by the flow of basaltic lavas (denser) over unconsolidated siliciclastic sediments (less dense). The outward-directed magma pressure or a temporary reduction in sediment strength (e.g. liquidization), given by a trigger (e.g. seismic events, sediment pore water expansion, or peperite interactions), were seen as viable mechanism for initiation of invasion.
3. Different types of lava-sediment interactions, analogous to those found in volcano-sedimentary basin successions and explored by oil and gas companies, were recognized and described in this work. Most of them do not change considerably the underlying sedimentary rocks. Therefore, the impact on reservoir quality is negligible, restricted to a few meters from the lava-sediment contact.
4. The presence of invasive flows may compartmentalize the reservoir units leading to modifications in fluid movement pathways, and may add a degree of complexity to detailed reservoir correlation. This can be particular problematic where limited information is available (e.g. only core or wireline) in offshore settings, where the identification of invasive flows may be problematic.

Acknowledgements

This work was supported by Petrobras (CENPES R&D Projects PT-166.01.11923 and PT-166.01.13484) and CNPq (442812/2015-9). The Federal University of Rio Grande do Sul and University of Aberdeen are acknowledged for

additional support. Natália Famelli specially acknowledges to M. Chmielewska, G. Bertolini; J. Machado, G. Marins, L. Bevilaqua, R. Rizzo for their support during fieldwork, discussions and/or software support. We thank the grinding plant of the 2º BFv, Arpasa, Ecobrix, Dois Irmãos, BT Construções, São Lucas quarries and the Ferrovia Centro-Atlântica (FCA – VLI Logística) for the permission to access the outcrop areas.

References

- Allen, J.R.L., 1977. The possible mechanics of convolute lamination in graded sand beds. *J. Geol. Soc. London*. 134, 19–31. <https://doi.org/10.1144/gsjgs.134.1.0019>
- Angkasa, S.S., Jerram, D.A., Millett, J.M., Svensen, H.H., Planke, S., Taylor, R.A., Schofield, N., Howell, J., 2017. Mafic intrusions, hydrothermal venting and the basalt-sediment transition: Linking onshore and offshore examples from the north atlantic igneous province. *Interpretation* 5, 83–101. <https://doi.org/10.1190/int-2016-0162.1>
- Ateba, B., Dorbath, C., Dorbath, L., Ntepe, N., Frogneux, M., Aka, F.T., Hell, J. V., Delmond, J.C., Manguelle, D., 2009. Eruptive and earthquake activities related to the 2000 eruption of Mount Cameroon volcano (West Africa). *J. Volcanol. Geotherm. Res.* 179, 206–216. <https://doi.org/10.1016/j.jvolgeores.2008.11.021>
- Bailey, E.B., Clough, C.T., Wright, W.B., Richey, J.E., Wilson, G.V., 1924. Tertiary and Post-Tertiary Geology of Mull, Loch Aline and Oban, in: Memoir of the Geological Survey of Great Britain. HMSO, Edinburgh.
- Beckinsale, R.D., Pankhurst, R.J., Skelhorn, R.R., Walsh, J.N., 1978. Geochemistry and Petrogenesis of the Early Tertiary Lava Pile of the Isle of Mull, Scotland. *Contrib. to Mineral. Petrol.* 67, 439. <https://doi.org/10.1007/BF00383303>
- Befus, K.S., Hanson, R.E., Miggins, D.P., Breyer, J.A., Busbey, A.B., 2009. Nonexplosive and explosive magma/wet-sediment interaction during emplacement of Eocene intrusions into Cretaceous to Eocene strata, Trans-Pecos igneous province, West Texas. *J. Volcanol. Geotherm. Res.* 181, 155–172. <https://doi.org/10.1016/j.jvolgeores.2008.12.017>
- Beresford, S.W., Cas, R.A.F., 2001. Komatiitic invasive lava flows, Kambalda, Western Australia. *Can. Mineral.* 39, 525–535. <https://doi.org/10.2113/gscanmin.39.2.525>

- Bischoff, A.P., Nicol, A., Beggs, M., 2017. Stratigraphy of architectural elements in a buried volcanic system and implications for hydrocarbon exploration. *Soc. Explor. Geophys. Am. Assoc. Pet. Geol.* 5, 1–19.
- Branney, M.J., Kokelaar, 2002. Pyroclastic Density Currents and the Sedimentation of Ignimbrites, Memoirs. ed. Geological Society of London.
- Brown, D.J., Bell, B.R., 2007. How do you grade peperites? *J. Volcanol. Geotherm. Res.* 159, 409–420. <https://doi.org/10.1016/j.jvolgeores.2006.08.008>
- Bruno, B.C., Fagents, S.A., Thordarson, T., Baloga, S.M., Pilger, E., 2004. Clustering within rootless cone groups on Iceland and Mars: Effect of nonrandom processes. *J. Geophys. Res. E Planets* 109. <https://doi.org/10.1029/2004JE002273>
- Buckley, S.J., Ringdal, K., Naumann, N., Dolva, B., Kurz, T.H., Howell, J.A., Dewez, T.J.B., 2019. LIME: Software for 3-D visualization, interpretation, and communication of virtual geoscience models. *Geosphere* 15, 222–235. <https://doi.org/10.1130/GES02002.1>
- Busby-Spera, C.J., White, J.D.L., 1987. Variation in peperito textures associated with differing host sediment properties. *Bull. Volcanol.* 49, 765–775.
- Byerly, G., Swanson, D., 1978. Invasive Columbia River Basalt flows along the northwestern margin of the Columbia Plateau, north-central Washington. *Abstr. Prgrms. Geol. Soc. Am.* 10, 98.
- Caineng, Z., Guangya, Z., Rukai, Z., Xuanjun, Y., Xia, Z., Lianhua, H., Baihong, W., Xiaozhi, W., 2013. Volcanic Reservoirs in Petroleum Exploration Volcanic Reservoirs in Petroleum Exploration. Elsevier, Beijing. <https://doi.org/10.1016/B978-0-12-397163-0.09993-0>
- Cashman, K. V., Mangan, M.T., Newman, S., 1994. Surface degassing and modifications to vesicle size distributions in active basalt flows. *J. Volcanol. Geotherm. Res.* 61, 45–68. [https://doi.org/10.1016/0377-0273\(94\)00015-8](https://doi.org/10.1016/0377-0273(94)00015-8)
- Chambers, L.M., Pringle, M.S., 2001. Age and duration of activity at the Isle of Mull Tertiary igneous centre, Scotland, and confirmation of the existence of subchrons during Anomaly 26r. *Earth Planet. Sci. Lett.* 193, 333–345. [https://doi.org/10.1016/S0012-821X\(01\)00499-X](https://doi.org/10.1016/S0012-821X(01)00499-X)

- Chen, S., Guo, Z., Qi, J., Zhang, Y., Pe-Piper, G., Piper, D.J.W., 2016. Early Permian volcano-sedimentary successions, Beishan, NW China: Peperites demonstrate an evolving rift basin. *J. Volcanol. Geotherm. Res.* 309, 31–44. <https://doi.org/10.1016/j.jvolgeores.2015.11.004>
- Coffin, M.F., Eldholm, O., 1994. Large Igneous Provinces: Crustal Structure , Dimensions ,. *Rev. Geophys.* 32, 1–36.
- Davison, I., Stasiuk, S., Nuttall, P., Keane, P., 2010. Sub-basalt hydrocarbon prospectivity in the Rockall, Faroe-Shetland and Møre basins, NE Atlantic. *Pet. Geol. Conf. Proc.* 7, 1025–1032. <https://doi.org/10.1144/0071025>
- De Luca, P., Carballo, J., Filgueiras, A., Pimentel, G., Esteban, M., Tritlla, J., Villacorta, R., 2015. What is the role of volcanic rocks in the Brazilian pre-salt?, in: 77th EAGE Conference and Exhibition 2015: Earth Science for Energy and Environment. European Association of Geoscientists and Engineers, EAGE, pp. 1686–1690. <https://doi.org/10.3997/2214-4609.201412890>
- Domínguez, T., Zobin, V.M., Reyes-Davila, G.A., 2001. The fracturing in volcanic edifice before an eruption: The June-July 1998 high-frequency earthquake swarm at Volcán de Colima, México. *J. Volcanol. Geotherm. Res.* 105, 65–75. [https://doi.org/10.1016/S0377-0273\(00\)00243-2](https://doi.org/10.1016/S0377-0273(00)00243-2)
- Ebinghaus, A., Hartley, A.J., Jolley, D.W., Hole, M., Millett, J., 2014. Lava – Sediment Interaction and Drainage-System Development in a Large Igneous. *J. Sediment. Res.* 84, 1041–1063.
- Emeleus, C., 1991. Tertiary igneous activity.pdf, in: Craig, G.Y. (Ed.), *Geology of Scotland*. Geological Society, London, pp. 455–502.
- Emeleus, C., Bell, B., 2005. Igneous geology : regional setting, Palaeogene volcanic districts of Scotland, in: *British Regional Geology*. British Geological Survey, Nottingham.
- Famelli, N., Lima, E.F., Carmo, I. de O., n.d. Lithostratigraphy of the Serra Geral Formation in the Northern portion of the Paraná-Etendeka Igneous Province: A tool for tracking Early-Cretaceous paleoenvironmental changes. Submitted.

Ferreira, C.M., 1985. Ocorrência de “pillow lava” em vulcanitos da Fm Serra Geral em Araguari, MG, in: 3o Simpósio de Geologia de Minas Gerais. Anais do 3o simpósio de geologia de Minas Gerais, Belo Horizonte, pp. 235–237.

Franco, L., Palma, J.L., Lara, L.E., Gil-Cruz, F., Cardona, C., Basualto, D., San Martín, J., 2019. Eruptive sequence and seismic activity of Llaima volcano (Chile) during the 2007–2009 eruptive period: Inferences of the magmatic feeding system. *J. Volcanol. Geotherm. Res.* 379, 90–105. <https://doi.org/10.1016/j.jvolgeores.2019.04.014>

Gallagher, J.W., Dromgoole, P.W., 2007. Exploring below the basalt, offshore Faroes: A case history of sub-basalt imaging. *Pet. Geosci.* 13, 213–225. <https://doi.org/10.1144/1354-079306-711>

Galland, O., Holohan, E., van Wyk de Vries, B., Burchardt, S., 2018. Laboratory Modelling of Volcano Plumbing Systems: A Review, in: *Advances in Volcanology*. Springer, pp. 147–214. https://doi.org/10.1007/11157_2015_9

Greenfield, L., Millett, J.M., Howell, J., Jerram, D.A., Watton, T., Healy, D., Hole, M.J., Planke, S., 2019. The 3D facies architecture and petrophysical properties of hyaloclastite delta deposits: An integrated photogrammetry and petrophysical study from southern Iceland. *Basin Res.* 1–24. <https://doi.org/10.1111/bre.12415>

Hamilton, C.W., Fitch, E.P., Fagents, S.A., Thordarson, T., 2017. Rootless tephra stratigraphy and emplacement processes. *Bull. Volcanol.* 79, 1–19. <https://doi.org/10.1007/s00445-016-1086-4>

Hanson, R.E., Wilson, T.J., 1993. Large-scale rhyolite peperites (Jurassic, southern Chile). *J. Volcanol. Geotherm. Res.* 54, 247–264. [https://doi.org/10.1016/0377-0273\(93\)90066-Z](https://doi.org/10.1016/0377-0273(93)90066-Z)

Hawkesworth, C.J., Gallagher, K., Kirstein, L., Mantovani, M.S.M., 2000. Tectonic controls on magmatism associated with continental break-up: an example from the Paraná-Etendeka Province. *Science* (80-.). 179, 335–349. [https://doi.org/10.1016/S0012-821X\(00\)00114-X](https://doi.org/10.1016/S0012-821X(00)00114-X)

Hole, M., Jolley, D., Hartley, A., Leleu, S., John, N., Ball, M., 2013. Lava – sediment interactions in an Old Red Sandstone basin, NE Scotland. *Journal Geol. Soc.* 170, 641–655. <https://doi.org/10.1144/jgs2012-107>

- Hooper, P.R., 1997. The Columbia River flood basalt provinces; current status. Large igneous Prov. Cont. Ocean. Planet. flood volcanism.
- Hurst, T., Jolly, A.D., Sherburn, S., 2014. Precursory characteristics of the seismicity before the 6 August 2012 eruption of Tongariro volcano, North Island, New Zealand. *J. Volcanol. Geotherm. Res.* 286, 294–302. <https://doi.org/10.1016/j.jvolgeores.2014.03.004>
- Iacovino, K., Till, C.B., 2019. DensityX: A program for calculating the densities of magmatic liquids up to 1,627 oC and 30 kbar. *Volcanica* 2, 1–10.
- Jerram, D., 2015. Hot Rocks and Oil: Are Volcanic Margins the New Frontier? Elsevier R&D Solut. Oil Gas.
- Jerram, D., Mountney, N., Holzförster, F., Stollhofen, H., 1999a. Internal stratigraphic relationships in the Etendeka Group in the Huab Basin, NW Namibia: Understanding the onset of flood volcanism. *J. Geodyn.* 28, 393–418. [https://doi.org/10.1016/S0264-3707\(99\)00018-6](https://doi.org/10.1016/S0264-3707(99)00018-6)
- Jerram, D., Mountney, N., Stollhofen, H., 1999b. Facies architecture of the Etjo Sandstone Formation and its interaction with the Basal Etendeka Flood Basalts of northwest Namibia: implications for offshore prospectivity. *Geol. Soc. Spec. Publ.* 153, 367–380. <https://doi.org/10.1144/GSL.SP.1999.153.01.22>
- Jerram, D.A., Mountney, N.P., Howell, J.A., Long, D., Stollhofen, H., 2000. Death of a sand sea: An active aeolian erg systematically buried by the Etendeka flood basalts of NW Namibia. *J. Geol. Soc. London.* 157, 513–516. <https://doi.org/10.1144/jgs.157.3.513>
- Jerram, D.A., Sharp, I.R., Torsvik, T.H., Poulsen, R., Watton, T., Freitag, U., Halton, A., Sherlock, S.C., Malley, J.A.S., Finley, A., Roberge, J., Swart, R., Puigdefabregas, C., Ferreira, C.H., Machado, V., 2019. Volcanic constraints on the unzipping of Africa from South America: Insights from new geochronological controls along the Angola margin. *Tectonophysics* 760, 252–266. <https://doi.org/10.1016/j.tecto.2018.07.027>
- Jerram, D.A., Stollhofen, H., 2002. Lava-sediment interaction in desert settings; are all peperite-like textures the result of magma-water interaction? *J. Volcanol. Geotherm. Res.* 114, 231–249. [https://doi.org/10.1016/S0377-0273\(01\)00279-7](https://doi.org/10.1016/S0377-0273(01)00279-7)

- Jerram, D.A., Svensen, H.H., Planke, S., Polozov, A.G., Torsvik, T.H., 2016a. The onset of flood volcanism in the north-western part of the Siberian Traps: Explosive volcanism versus effusive lava flows. *Palaeogeogr. Palaeoclimatol. Palaeoecol.* 441, 38–50. <https://doi.org/10.1016/j.palaeo.2015.04.022>
- Jerram, D.A., Widdowson, M., Wignall, P.B., Sun, Y., Lai, X., Bond, D.P.G., Torsvik, T.H., 2016b. Submarine palaeoenvironments during Emeishan flood basalt volcanism, SW China: Implications for plume-lithosphere interaction during the Capitanian, Middle Permian ('end Guadalupian') extinction event. *Palaeogeogr. Palaeoclimatol. Palaeoecol.* 441, 65–73. <https://doi.org/10.1016/j.palaeo.2015.06.009>
- Kerr, A.C., 1995a. The geochemical stratigraphy, field relations and temporal variation of the Mull-Morvern Tertiary lava succession, NW Scotland. *Trans. R. Soc. Edinb. Earth Sci.* 86, 35–47. <https://doi.org/10.1017/S0263593300002145>
- Kerr, A.C., 1995b. The geochemistry of the Mull-Morvern Tertiary lava succession, NW Scotland: an assessment of mantle sources during plume-related volcanism. *Chem. Geol.* 122, 43–58. [https://doi.org/10.1016/0009-2541\(95\)00009-B](https://doi.org/10.1016/0009-2541(95)00009-B)
- Khalaf, E.A., Abdel Motelib, A., Hammed, M.S., El Manawi, A.H., 2015. Volcano-sedimentary characteristics in the Abu Treifiya Basin, Cairo-Suez District, Egypt: Example of dynamics and fluidization over sedimentary and volcaniclastic beds by emplacement of syn-volcanic basaltic rocks. *J. Volcanol. Geotherm. Res.* 308, 158–178. <https://doi.org/10.1016/j.jvolgeores.2015.10.023>
- Kokelaar, B.P., 1982. Fluidization of wet sediments during the emplacement and cooling of various igneous bodies. *J. Geol. Soc. London.* 139, 21–33. <https://doi.org/10.1144/gsjgs.139.1.0021>
- Kwon, C.W., Gihm, Y.S., 2017. Fluidization of host sediments and its impacts on peperites-forming processes, the Cretaceous Buan Volcanics, Korea. *J. Volcanol. Geotherm. Res.* 341, 84–93. <https://doi.org/10.1016/j.jvolgeores.2017.05.019>
- Lesher, C.E., Spera, F.J., 2015. Thermodynamic and Transport Properties of Silicate Melts and Magma. *Encycl. Volcanoes* 113–141. <https://doi.org/10.1016/b978-0-12-385938-9.00005-5>
- Luchetti, A.C.F., Nardy, A.J.R., Machado, F.B., Madeira, J.E.O., Arnosio, J.M., 2014. New insights on the occurrence of peperites and sedimentary deposits within the silicic

volcanic sequences of the Paraná Magmatic Province, Brazil. Solid Earth 5, 121–130. <https://doi.org/10.5194/se-5-121-2014>

Machacca-Puma, R., Lesage, P., Larose, E., Lacroix, P., Anccasi-Figueroa, R.M., 2019. Detection of pre-eruptive seismic velocity variations at an andesitic volcano using ambient noise correlation on 3-component stations: Ubinas volcano, Peru, 2014. J. Volcanol. Geotherm. Res. 381, 83–100. <https://doi.org/10.1016/j.jvolgeores.2019.05.014>

Machado, F., Rocha-Júnior, E.R.V., Marques, L.S., Nardy, A.J.R., 2015. Volcanological aspects of the northwest region of Paraná continental flood basalts (Brazil). Solid Earth 6, 227–241. <https://doi.org/10.5194/se-6-227-2015>

Mano, V.G.T., 1987. Estudos geológicos e geotécnicos das descontinuidades rochosas, “pillow lavas” e paleocanal nos basaltos de fundação da barragem de Nova Avanhandava, Rio Tiete (SP). Universidade de São Paulo.

Marques Filho, P.L., Correia, P.C., Levis, P., Andrade, C.A. V, 1981. Características usuais e aspectos peculiares do manto de alteração e transição solo-rocha em basaltos, in: Congresso Brasileiro de Engenharia. Congresso Brasileiro de Geologia de Engenharia, ABGE, Itapema, pp. 53–72.

Marsh, J.S., Ewart, A., Milner, S.C., Duncan, A.R., Miller, R.M.G., 2001. The Etendeka Igneous Province: Magma types and their stratigraphic distribution with implications for the evolution of the Paraná-Etendeka flood basalt province. Bull. Volcanol. 62, 464–486. <https://doi.org/10.1007/s004450000115>

Mcphie, J., Doyle, M., Allen, R., 1993. Volcanic Textures: A guide to the interpretation of textures in volcanic rocks. University of Tasmania.

Milani, E.J., França, A.B., Schneider, R., 1994. Bacia do Paraná. Bol. Geociências da Petrobras 8, 69–82.

Milani, E.J., Melo, J.H.G. de, Souza, P.A. De, Fernandes, L.A., França, A.B., 2007. Bacia do Paraná. Bol. Geociências da Petrobras 15, 265–287.

Milani, E.J., Zalán, P. V, 1999. An outline of the geology and petroleum systems of the Paleozoic interior basins of South America. Petrobras 22, 199–205.

Milani, Edison José, Thomaz Filho, Antonio, 2000. Sedimentary Basins of South America, in: Cordani, U.G., Milani, E.J., Thomaz Filho, A., Campos, D.A. (Eds.),

Tectonic Evolution of South America. 31 International Geological Congress, Rio de Janeiro, pp. 389–449.

Millett, J.M., Manton, B.M., Zastrozhnov, D., Planke, S., Maharjan, D., Bellwald, B., Gernigon, L., Faleide, J.I., Jolley, D.W., Walker, F., Abdelmalak, M.M., Jerram, D.A., Myklebust, R., Kjølhamar, B.E., Halliday, J., Birch-Hawkins, A., 2020. Basin structure and prospectivity of the NE Atlantic volcanic rifted margin: cross-border examples from the Faroe–Shetland, Møre and Southern Vørings basins. *Geol. Soc. London, Spec. Publ.* SP495-2019–12. <https://doi.org/10.1144/sp495-2019-12>

Miranda, F.S. de, Vettorazzi, A.L., Cunha, P.R.D.C., Aragão, F.B., Michelon, D., Caldeira, J.L., Porsche, E., Martins, C., Ribeiro, R.B., Vilela, A.F., Corrêa, J.R., Silveira, L.S., Andreola, K., 2018. Atypical igneous-sedimentary petroleum systems of the Parnaíba Basin, Brazil: Seismic, well logs and cores. *Geol. Soc. Spec. Publ.* 472, 341–360. <https://doi.org/10.1144/SP472.15>

Mizuzaki, A.M.P., 1986. Rochas ígneo-básicas do Neocomiano da Bacia do Campos - Caracterização e comportamento como reservatório de hidrocarbonetos. Universidade Federal do Rio de Janeiro.

Moraes, L.C. de, Seer, H.J., 2017. Pillow lavas and fluvio-lacustrine deposits in the northeast of Paraná Continental Magmatic Province, Brazil. *J. Volcanol. Geotherm. Res.* 355, 78–86. <https://doi.org/10.1016/J.JVOLGEORES.2017.03.024>

Morrison, M.A., Thompson, R.N., Dickin, A.P., 1985. Geochemical evidence for complex magmatic plumbing during development of a continental volcanic center. *Geology* 13, 581–584. [https://doi.org/10.1130/0091-7613\(1985\)13<581:GEFCMP>2.0.CO;2](https://doi.org/10.1130/0091-7613(1985)13<581:GEFCMP>2.0.CO;2)

Mountney, N., Howell, J., Flint, S., Jerram, D., 1998. Aeolian and alluvial deposition within the Mesozoic Etjo Sandstone Formation, northwest Namibia. *J. African Earth Sci.* 27, 175–192. [https://doi.org/10.1016/S0899-5362\(98\)00056-6](https://doi.org/10.1016/S0899-5362(98)00056-6)

Nelson, C.E., Jerram, D.A., Hobbs, R.W., 2009. Flood basalt facies from borehole data : implications for prospectivity and volcanology in volcanic rifted margins. *Pet. Geosci.* 15, 313–324. <https://doi.org/10.1144/1354-079309-842>

Németh, K., Pécskay, Z., Martin, U., Gmélinc, K., Molnár, F., Cronin, S.J., 2008. Hyaloclastites, peperites and soft-sediment deformation textures of a shallow

subaqueous Miocene rhyolitic dome-cryptodome complex, Pálháza, Hungary. *Geol. Soc. Spec. Publ.* 302, 63–86. <https://doi.org/10.1144/SP302.5>

Oliver, G.J.H., Wilde, S.A., Wan, Y., 2008. Geochronology and geodynamics of Scottish granitoids from the late neoproterozoic break-up of Rodinia to Palaeozoic collision. *J. Geol. Soc. London.* 165, 661–674. <https://doi.org/10.1144/0016-76492007-105>

Owen, G., 2003. Load structures: Gravity-driven sediment mobilization in the shallow subsurface. *Geol. Soc. Spec. Publ.* 216, 21–34. <https://doi.org/10.1144/GSL.SP.2003.216.01.03>

Park, I., Jolly, A., Kim, K.Y., Kennedy, B., 2019. Temporal variations of repeating low frequency volcanic earthquakes at Ngauruhoe Volcano, New Zealand. *J. Volcanol. Geotherm. Res.* 373, 108–119. <https://doi.org/10.1016/j.jvolgeores.2019.01.024>

Peate, D.P., Hawkesworth, C.J., Mantovani, M.S., 1992. Chemical stratigraphy of the Paraná lavas (South America): classification of magma types and their spatial distribution. *Bull. Volcanol.* 55, 119–139. <https://doi.org/DOI: 10.1007/BF00301125>

Peate, D.W., 1997. The Parana-Etendeka Province, in: Mahoney, J.J., Coffin, M.F. (Eds.), *Large Igneous Provinces: Continental, Oceanic, and Planetary Flood Volcanism*. Geophysical Monographs: American Geophysical Union, pp. 217–245. <https://doi.org/10.1029/GM100p0217>

Petry, K., Jerram, D.A., Almeida, P.M. De, Zerfass, H., 2007. Volcanic-sedimentary features in the Serra Geral Fm., Paraná Basin, southern Brazil: Examples of dynamic lava-sediment interactions in an arid setting 159, 313–325. <https://doi.org/10.1016/j.jvolgeores.2006.06.017>

Planke, S., Symonds, P.A., Alvestad, E., Skogseid, J., 2000. Seismic volcanostratigraphy of large-volume basaltic extrusive complexes on rifted margins. *J. Geophys. Res. Solid Earth* 105, 19335–19351. <https://doi.org/10.1029/1999jb900005>

Plazibat, S., Rasgado, A., Paredes, J.M., 2019. Subsurface characterization of Cenozoic igneous activity at Cerro Dragón area (Golfo San Jorge Basin, central Patagonia): Implications for basin evolution and hydrocarbon prospectivity. *J. South Am. Earth Sci.* 96, 102389. <https://doi.org/10.1016/j.jsames.2019.102389>

Rateau, R., Schofield, N., Smith, M., 2013. The potential role of igneous intrusions on hydrocarbon migration, West of Shetland. *Pet. Geosci.* 19, 259–272. <https://doi.org/10.1144/petgeo2012-035>

Rawcliffe, H.J., 2016. Lava - Water - Sediment Interaction: Processes, Products and Petroleum Systems. University of Glasgow.

Rawlings, D.J., Watkeys, M.K., Sweeney, R.J., 1999. Peperitic upper margin of an invasive flow, Karoo flood basalt province, northern Lebombo. *South African J. Geol.* 102, 377–383.

Renne, P.R., 2015. Age and Duration of the Paraná-Etendeka Flood Basalts and Related Plumbing System. *Am. Geophys. Union, Fall Meet. 2015, Abstr.* id. T32D-06.

Rosa, C.J.P., McPhie, J., Relvas, J.M.R.S., 2016. Distinguishing peperite from other sediment-matrix igneous breccias: Lessons from the Iberian Pyrite Belt. *J. Volcanol. Geotherm. Res.* 315, 28–39. <https://doi.org/10.1016/j.jvolgeores.2016.02.007>

Ross, P.S., Ukstins Peate, I., McClintock, M.K., Xu, Y.G., Skilling, I.P., White, J.D.L., Houghton, B.F., 2005. Mafic volcaniclastic deposits in flood basalt provinces: A review. *J. Volcanol. Geotherm. Res.* 145, 281–314. <https://doi.org/10.1016/j.jvolgeores.2005.02.003>

Rossetti, L., Lima, E.F., Waichel, B.L., Hole, M.J., Simões, M.S., Scherer, C.M.S., 2018. Lithostratigraphy and volcanology of the Serra Geral Group, Paraná-Etendeka Igneous Province in Southern Brazil: Towards a formal stratigraphical framework. *J. Volcanol. Geotherm. Res.* 355, 98–114. <https://doi.org/10.1016/j.jvolgeores.2017.05.008>

Rossetti, L.M., Healy, D., Hole, M.J., Millett, J.M., de Lima, E.F., Jerram, D.A., Rossetti, M.M.M., 2019. Evaluating petrophysical properties of volcano-sedimentary sequences: A case study in the Paraná-Etendeka Large Igneous Province. *Mar. Pet. Geol.* 102, 638–656. <https://doi.org/10.1016/j.marpetgeo.2019.01.028>

Scherer, C.M.S., 2000. Eolian dunes of the Botucatu Formation (Cretaceous) in southernmost Brazil: Morphology and origin. *Sediment. Geol.* 137, 63–84. [https://doi.org/10.1016/S0037-0738\(00\)00135-4](https://doi.org/10.1016/S0037-0738(00)00135-4)

Schofield, N., Holford, S., Millett, J., Brown, D., Jolley, D., Passey, S.R., Muirhead, D., Grove, C., Magee, C., Murray, J., Hole, M., Jackson, C.A.L., Stevenson, C., 2017.

Regional magma plumbing and emplacement mechanisms of the Faroe-Shetland Sill Complex: implications for magma transport and petroleum systems within sedimentary basins. *Basin Res.* 29, 41–63. <https://doi.org/10.1111/bre.12164>

Schutter, S.R., 2003. Hydrocarbon occurrence and exploration in and around igneous rocks. *Geol. Soc. Spec. Publ.* 214, 7–33. <https://doi.org/10.1144/GSL.SP.2003.214.01.02>

Self, S., Thordarson, T., Keszthelyi, L., Walker, G.P.L., Hon, K., Murphy, M.T., Long, P., Finnemore, S., 1996. A new model for emplacement of Columbia River basalts as large, inflated pahoehoe lava flow fields. *Geophys. Res. Lett.* 23, 2689–2692. <https://doi.org/10.1029/96GL02450>

Senger, K., Millett, J., Planke, S., Ogata, K., Eide, C.H., Festøy, M., Galland, O., Jerram, D., 2017. Effects of igneous intrusions on the petroleum system: a review. *First Break* 35, 47–56.

Skilling, I.P., White, J.D.L., McPhie, J., 2002. Peperite: a review of magma–sediment mingling. *J. Volcanol. Geotherm. Res.* 114, 1–17. [https://doi.org/10.1016/S0377-0273\(01\)00278-5](https://doi.org/10.1016/S0377-0273(01)00278-5)

Spacapan, J.B., D’Odorico, A., Palma, O., Galland, O., Senger, K., Ruiz, R., Manceda, R., Leanza, H.A., 2019. Low resistivity zones at contacts of igneous intrusions emplaced in organic-rich formations and their implications on fluid flow and petroleum systems: A case study in the northern Neuquén Basin, Argentina. *Basin Res.* 32, 3–24. <https://doi.org/10.1111/bre.12363>

Stewart, K., Turner, S., Kelley, S., Hawkesworth, C., Kirstein, L., Mantovani, M., 1996. 3-D, 40Ar-39Ar geochronology in the Paraná continental flood basalt province. *Earth Planet. Sci. Lett.* 143, 95–109. [https://doi.org/10.1016/0012-821X\(96\)00132-X](https://doi.org/10.1016/0012-821X(96)00132-X)

Swanson, D.A., Wright, T.L., 1981. Guides to some volcanic terranes in Washington, Idaho, Oregon and northern California., US Geological Survey, Circular. U.S. Geological Survey Circular. <https://doi.org/10.3133/cir838>

Tenzer, R., Gladkikh, V., 2014. Assessment of density variations of marine sediments with ocean and sediment depths. *Sci. World J.* 2014, 1–9. <https://doi.org/10.1155/2014/823296>

- Thiede, D.S., Vasconcelos, P.M., 2010. Paraná flood basalts: Rapid extrusion hypothesis confirmed by new $40\text{Ar}/39\text{Ar}$ results. *Geology* 38, 747–750. <https://doi.org/10.1130/G30919.1>
- Thirlwall, M.F., 1988. Geochronology of Late Caledonian magmatism in northern Britain. *J. - Geol. Soc.* 145, 951–967. <https://doi.org/10.1144/gsjgs.145.6.0951>
- Thirlwall, M.F., 1981. Implications for Caledonian plate tectonic models of chemical data from volcanic rocks of the British Old Red Sandstone. *J. Geol. Soc. London.* 138, 123–138. <https://doi.org/10.1144/gsjgs.138.2.0123>
- Thompson, R.N., Morrison, M.A., Dickin, A.P., Gibson, I.L., Harmon, R.S., 1986. Two contrasting styles of interaction between basic magmas and continental crust in the British Tertiary Volcanic Province. *J. Geophys. Res.* 91, 5985. <https://doi.org/10.1029/jb091ib06p05985>
- Waichel, B.L., Lima, E.F., Sommer, C.A., Lubachesky, R., 2007. Peperite formed by lava flows over sediments: An example from the central Paraná Continental Flood Basalts, Brazil. *J. Volcanol. Geotherm. Res.* 159, 343–354. <https://doi.org/10.1016/j.jvolgeores.2006.07.009>
- Walker, G.P.L., 1992. Morphometric study of pillow-size spectrum among pillow lavas. *Bull. Volcanol.* 54, 459–474. <https://doi.org/10.1007/BF00301392>
- Walker, G.P.L., 1970. The distribution of amygdale minerals in Mull and Morvern (West Scotland), in: Murty, T.V.V.G.R., Rao, S.S. (Eds.), *Studies in Earth Sciences, West Commemoration Volume*. University of Saugar, India, pp. 181–194.
- Watton, T.J., Cannon, S., Brown, R.J., Dougal, A., Waichel, B.L., 2014. First onshore analogues to distinguish volcanic lithofacies in boreholes : examples from Palaeogene successions in the Faroe – Shetland Basin , NE Atlantic Using formation micro-imaging , wireline. <https://doi.org/10.1144/SP397.7>
- Williamson, I.T., Bell, B.R., 2012. The Staffa Lava formation: Graben-related volcanism, associated sedimentation and landscape character during the early development of the palaeogene Mull Lava field, NW Scotland. *Scottish J. Geol.* 48, 1–46. <https://doi.org/10.1144/0036-9276/01-439>

Wohletz, K., 2002. Water/magma interaction: Some theory and experiments on peperite formation. *J. Volcanol. Geotherm. Res.* 114, 19–35. [https://doi.org/10.1016/S0377-0273\(01\)00280-3](https://doi.org/10.1016/S0377-0273(01)00280-3)

Wu, S., Zhu, R., Yang, Z., Mao, Z., Cui, J., Zhang, X., 2019. Distribution and characteristics of lacustrine tight oil reservoirs in China. *J. Asian Earth Sci.* 178, 20–36. <https://doi.org/10.1016/j.jseaes.2018.05.013>

Wu, S., Zou, C., Zhu, R., Yao, J., Tao, S., Yang, Z., Zhai, X., Cui, J., Lin, S., 2016. Characteristics and origin of tight oil accumulation in the Upper Triassic Yanchang Formation of the Ordos Basin, North-Central China. *Acta Geol. Sin. (English Ed.* 5, 1821–1837. <https://doi.org/10.1111/1755-6724.12819>

Zhu, D., Jin, Z., Hu, W., Song, Y., Gao, X., 2007. Effect of igneous activity on hydrocarbon source rocks in Jiyang sub-basin, eastern China. *J. Pet. Sci. Eng.* 59, 309–320. <https://doi.org/10.1016/j.petrol.2007.05.002>

5.3 ARTIGO C

Understanding the petrophysical properties, seismic responses and impacts of the basalt-sediment transition in prospective sedimentary basins.

Authors: Natália Famelli^{a,b,*}, John M. Millett^{c,d}, Malcolm Hole^c, Dougal A. Jerram^{e,f}, Leonardo C. de Oliveira^g, Evandro F. Lima^a, Isabela de O. Carmo^b, Sverre Planke^{d,e}, Jessica Pugsley^c, Magda Chmielewska^c, John A. Howell^c, David W. Jolley^c

Filiations, Adress:

^a Instituto de Geociências, Universidade Federal do Rio Grande do Sul, Av. Bento Gonçalves, 9500, Prédio 43136, Caixa Postal 15001, Agronomia, Porto Alegre, 91501-970, Rio Grande do Sul, RS, Brazil

^b Centro de Pesquisas e Desenvolvimento Leopoldo Américo Migues de Mello – CENPES/PETROBRAS, Av. Horácio de Macedo, 950, Cidade Universitária, 21941-915, Rio de Janeiro, RJ, Brazil

^c Department of Geology and Geophysics, University of Aberdeen, UK

^d VBPR AS, Høienhald, Blindernveien 5, Oslo, Norway

^e Centre for Earth Evolution and Dynamics (CEED), University of Oslo, Norway

^f DougalEARTH Ltd., Solihull, UK

^g Petrobras, Av. República do Chile, 330, Centro, Rio de Janeiro, Brazil

* Corresponding author: E-mail: natfamelli@gmail.com

Abstract

Volcanic rocks form major components in many prospective sedimentary basins around the world and are increasingly being found in association with significant hydrocarbon reserves. Application of seismic forward modelling to volcano-sedimentary sequences has been crucial to cover the gaps between outcrop observations and seismic data. Within this study we combine 3D virtual outcrop model from the North Atlantic Igneous Province with laboratory petrophysical measurements from Paraná-Etendeka Igneous Province field outcrop analogues to develop synthetic seismic forward models for four different base-basalt transition scenarios. A base-model comprising a mixed lava flow package overlying homogenous sandstone is presented with subsequent models developed to incorporate known field based variations including layered sediments, intrusions and invasive lava flows with associated peperite. The models were run using source wavelets with different frequency spectrums in order to assess variations in seismic reflection character and detectability of the volcanic features along with the basalt-sediment transition. The results of this study clearly demonstrate how geological variability associated with the basalt-sediment transition can influence seismic imaging and complicate interpretation. In particular, features such as invasive lava flows may be challenging to differentiate from sill intrusions in seismic data, and therefore their potentially very different impacts on reservoir properties and connectivity must be appraised carefully. This study demonstrates the power of integrating outcrop analogue studies with seismic forward modelling to improve seismic interpretation in prospective mixed volcano-sedimentary systems.

Keywords: Lava sediment interaction, virtual outcrop models, synthetic seismic, volcanic petrophysics

5.3.1 Introduction

In recent years, occurrences of hydrocarbons with commercial significance have been discovered within sedimentary basins in association with volcanic rocks (e.g., Schutter, 2003; Helland-Hansen, 2009; De Luca et al., 2015). Igneous rocks have a potential to directly influence the petroleum system (e.g., Senger et al. 2017), and in some cases, the rocks may also have reservoir properties and significant hydrocarbon columns (e.g., Schutter, 2003; Schofield et al., 2016; Millett et al., 2020). However, the study and characterization of volcanic facies in offshore settings, with a focus on petroleum systems is a relatively new area of focus (e.g., Jerram et al., 2009; Senger et al., 2017).

Seismic reflection data, are often the primary basis for the mapping and characterization of geological/volcanological features in prospective areas (e.g., Magee et al., 2013). However, seismic imaging of volcanic rocks can often be challenging due to high impedance contrasts and heterogeneity which cause scattering and rapid attenuation of higher frequencies (Planke et al., 2015). In particular, accurately imaging the basalt-sediment transition during exploration for sub-basalt prospects has met with significant historical challenges (Davison et al., 2010; Millett et al., 2020). Seismic forward modelling of field analogues is an important tool for improving seismic interpretation as it creates a vital link between geological field observations and their expression in seismic data (e.g., Lecomte et al., 2016; Rabbel et al., 2018). Outcrop models can be populated with physical properties in a number of ways including using sections of relevant well data, or by measuring petrophysical properties such as velocity, density and porosity from outcrop analogue samples (Single and Jerram, 2004; Lenhardt and Götz, 2011; Greenfield et al., 2019).

Studies involving outcrop based seismic forward modelling of igneous rocks commonly focus on igneous intrusions and associated vent features (e.g., Magee et al., 2015; Planke et al., 2018; Rabbel et al., 2018). For extrusive volcanic sequences, more focus has been given to borehole synthetic studies and seismic data analyses (e.g., Japsen et al., 2005; Planke et al., 2017) whereas field outcrop studies and modelling have largely stopped at assessments of velocity variations (Single and Jerram, 2004; Greenfield et al., 2019). Thus, as volcanic and inter-volcanic reservoirs have become increasingly investigated exploration targets, it is essential to have a good understanding of how real geometries of volcanic sequences are imaged in the subsurface (Eide et al., 2018).

In this study, we present the seismic forward modelling of 4 different geological scenarios (using different frequency bands), which were constructed combining 3D virtual outcrop model and laboratory measurements of petrophysical data (density and P- and S- wave velocities) from outcrop analogues. Petrophysical data, including porosity and permeability, are also presented and discussed in order to understand the physical properties of northern Paraná-Etendeka Igneous Province (PEIP) volcano-sedimentary sequence. The aim of this study is to investigate the seismic characteristics of the basalt-sediment transition in volcano-sedimentary basins. These results help to better inform interpretation approaches for real data and pave the way for future studies into the seismic characterization of other elements of volcanic sequences.

5.3.2 Background and regional settings of data used to develop seismic models

The rationale for addressing the base-basalt transition using a combination of separate outcrop analogues, stems from the need to constrain and understand the possible effects of key volcanic facies within sequences which lack seismic-scale exposures. In such instances, seismic-scale outcrops from other regions that contain the same essential volcanic facies types and associations of interest can be used. By combining analogue field sections with petrophysical data collected from small-scale exposures within a target region, the likely seismic responses in the offshore parts of a region can be investigated. In this contribution we use this approach to better constrain volcanic facies and the base-basalt transition in the Uberlândia region (NE of PEIP, Brazil) in combination with seismic scale outcrop analogue data collected from the Isle of Mull (west coast of Scotland), part of the North Atlantic Igneous Province. Below we briefly introduce and summarize the background and regional settings of the study areas, before introducing the methods and data in more detail.

- Paraná-Etendeka Igneous Province

The Early Cretaceous flood volcanism and associated intrusions in the South Atlantic region resulted in the Paraná-Etendeka Igneous Province (PEIP), which is a Continental Flood Basalt Province (CFBP) related to the Gondwana supercontinent break-up and to the formation of the South Atlantic Ocean around 135 Ma (e.g., Thiede and Vasconcelos, 2010; Renne, 2015). The PEIP occupies an area of $1.2 \times 10^6 \text{ km}^2$,

volumes of c. 0.8×106 km³ (Bellieni et al., 1984), and its remains may be found in South America (Brazil, Argentina and Uruguay) and in the southwestern Africa (Namibia and Angola) (Peate et al., 1992) (Fig. 38).

This magmatism is strongly bimodal, with more than 90% of the lavas classified as basalts and basaltic andesites, and subordinate amount of acidic rocks (Peate, 1997). Years of geochemical studies allowed defining a regional stratigraphy based on regional distribution of magma types, with high-TiO₂ and Ti/Y > 310 lavas occurring dominantly in the north, and low-TiO₂ and Ti/Y < 310 lavas prevailing in the south of the PEIP (Bellieni et al., 1984; Piccirillo et al., 1989; Peate, 1997). Recently, studies focusing on volcanic architecture, lava morphologies, and its stratigraphic position allowed the construction of a formal lithostratigraphy for the southern portion of the PEIP where the PEIP lavas fall within the Serra Geral Group (Rossetti et al., 2018). Compound pahoehoe and rubbly pahoehoe are the main morphologies described in this portion of the PEIP (e.g., Waichel et al., 2012; Barreto et al., 2014; Rossetti et al., 2014). However, subordinate deposits of peperites associated with wet sediments and pillow lavas have been described occurring mainly along the marginal parts of the Paraná province (Waichel et al., 2007; Machado et al., 2015; Moraes and Seer, 2017). In the study area (northern portion of the PEIP), where there are evidences for presence of significant water, subaerial lava flows (compound and simple lava flows), peperites, pillow lavas and a possibly invasive lava flow have been described (Famelli et al., submitted).

The PEIP lavas seem to have extended underneath the adjacent prolific offshore basins in the Brazilian southern/southeastern margin (Stica et al., 2014). In the Pelotas Basin this lava sequence remains as homonymous unit (Serra Geral), whereas in Campos and Santos Basins, the PEIP lavas are stratigraphically correlated with the Cabiúnas and Camboriú volcanic sequence, respectively (e.g., Moreira et al., 2007; Winter et al., 2007). Different lava morphologies, such as compound pahoehoe, rubbly pahoehoe, sheet pahoehoe, and slabby pahoehoe have been described in the Campos and/or Santos Basins (Zucchetti et al., 2015; Marins et al., 2018; Fornero et al., 2019) showing that, even in terms of lava morphologies, onshore exposures can be used as analogous to volcanic sequences occurring offshore.

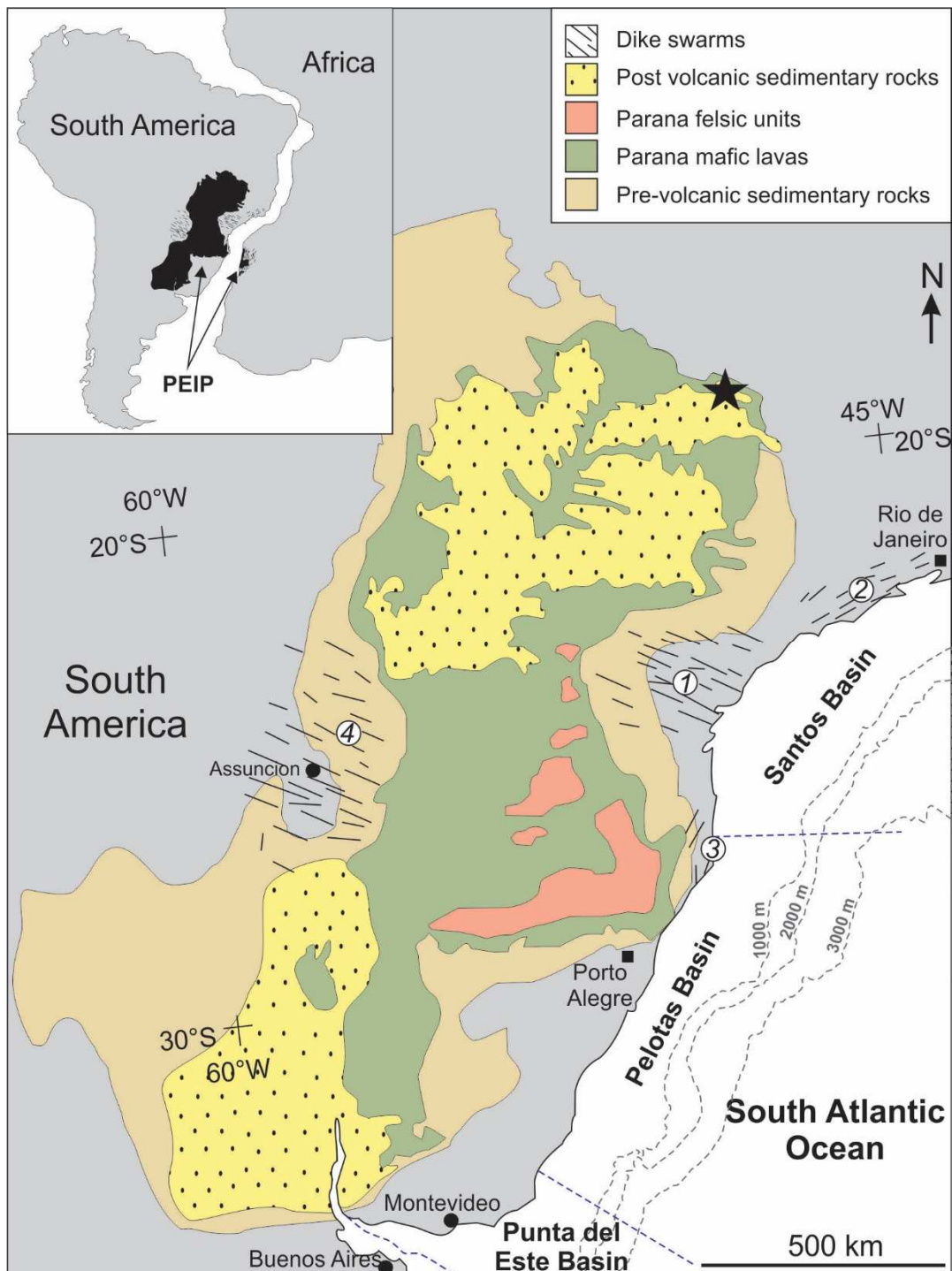


Fig. 38: Geological map of the major volcanic units of the Paraná-Etendeka Igneous Province (modified after Peate et al., 1992; Stewart et al., 1996; Hawkesworth et al., 2000). Dyke swarms: 1 – Ponta Grossa; 2 – Santos-Rio de Janeiro; 3 – Florianópolis; 4 – Paraguay; 5 – Skeleton Coast. The study area location is highlighted by the black star.

- North Atlantic Igneous Province

The North Atlantic Igneous Province (NAIP) was formed during rifting and breakup of the Northeast and Northwest Atlantic regions starting from around 62-61

Ma (e.g., Saunders et al., 1997; Hansen et al., 2009; Abelmanak et al., 2019). The NAIP lava flows cover an area of 1.3×106 km², volumes of 1.8×106 km³ (Eldholm and Grue, 1994), and its remains are now exposed in outcrops on east and west Greenland, the British Paleogene Igneous Province (BPIP; e.g., inner Hebrides Isles of Scotland, and Antrim in Northern Ireland), and Faeroe Islands (Fig. 39) (Jerram and Widdowson, 2005). Significant amount of the lava sequences is found offshore, occurring as various seismic facies within the Eurasian and Greenland volcanic margins (Planke et al., 2000; Abelmanak et al., 2019).

Tholeiitic basalts are the main product of the NAIP volcanism, although alkali basalts are common. Subordinately, differentiated rocks may be found on continental areas and along the rifted margins (Saunders et al., 1997). A large variety of subaerial lava flow morphologies have been described on the NAIP, such as, sheet flows, braided and compound pahoehoe, with subordinate a'a lava flows (e.g., Kent et al., 1998; Jerram 2002; Single and Jerram, 2004). Besides the dominance of subaerial products, pillow lavas and hyaloclastites can often be found, commonly towards the base of the stratigraphy (e.g., Jerram and Widdowson, 2005; Williamson and Bell, 2012), highlighting that the early lava flows interacted with water bodies in some portions of the NAIP, in some cases resulting in significant lava delta facies (Jerram et al., 2009; Wright et al., 2012; Abelmanak et al., 2016).

The NAIP lava flows found offshore are as variable in terms of morphology as the onshore occurrences. Works integrating composite well logs, formation micro-imaging, ditch cuttings, and seismic images have identified tabular simple flows, compound lava flows, pillow lavas and hyaloclastite deltas such as in the Faroe-Shetland Basin and Vøring Margin (e.g., Jerram, 2009; Wright et al., 2012; Watton et al., 2014; Millett et al., 2016).

In the study area, the NAIP remains are represented by volcanic rocks of Mull Lava Field, which forms part of the BPIP (Emeleus and Bell, 2005). The Mull Lava Field is preserved in western Scotland on the Isle of Mull covering an area of about 840 km² (Fig. 39) (Emeleus, 1991). This volcanic succession can reach 2200 m thick (Walker, 1970), but in the study area, it reaches up to 300 m and occur overlying Jurassic shallow marine sandstone (Williamson and Bell, 2012).

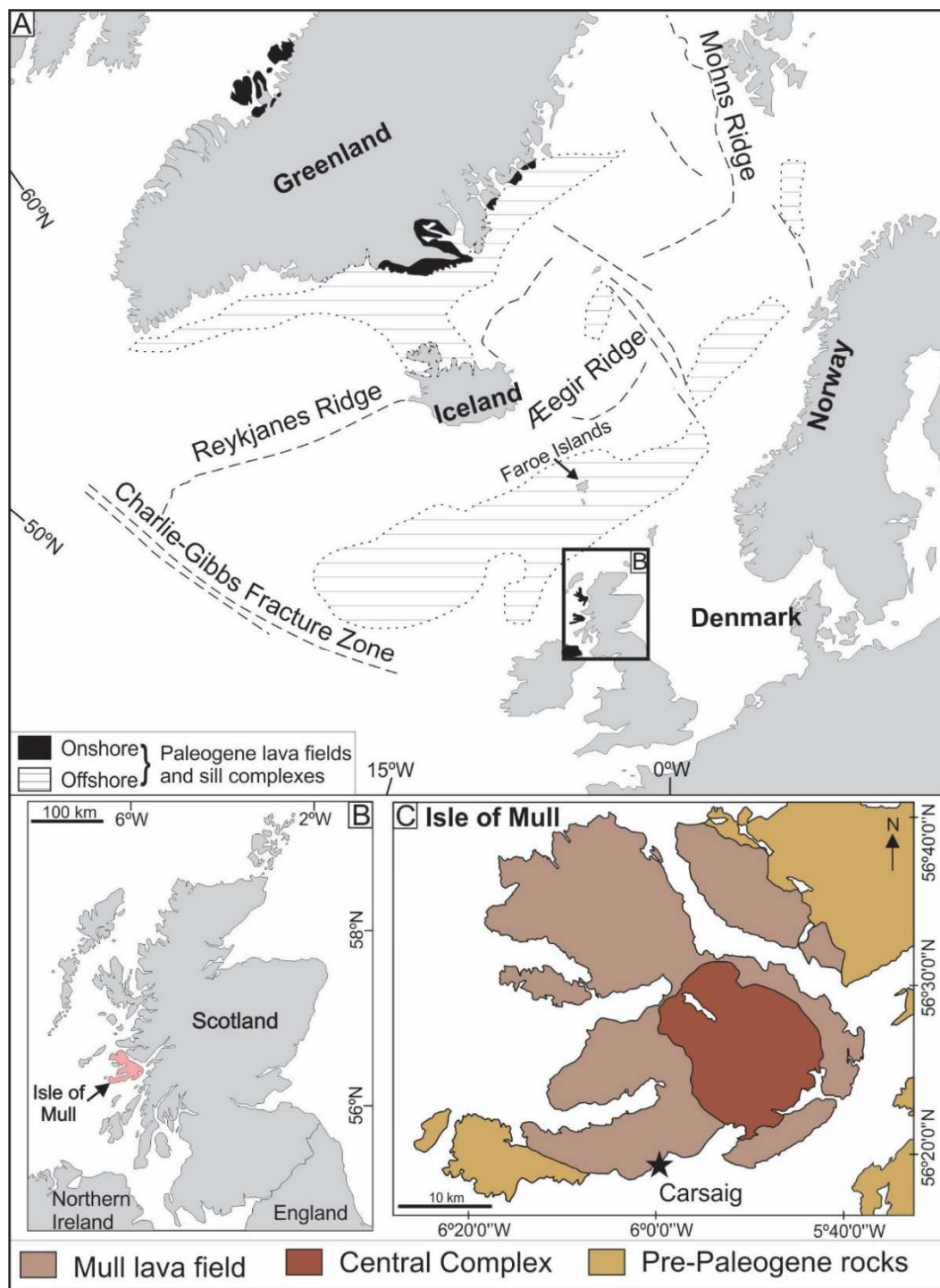


Fig. 39: A) Outline of the North Atlantic Igneous Province (modified after Ganerød et al., 2008). B) Location map of Scotland, indicating the position of the Isle of Mull (in pink). C) Simplified geological map of the Isle of Mull with the location of the study area (black star) between Carsaig Bay and Carsaig Arches (modified after Brown and Bell, 2007).

5.2.3 Material and methods

- Study areas

Outcrop exposures from the Isle of Mull were used as the basis for the geological model to provide a seismic scale example of the basalt-sediment transition, since the Paraná exposures are not vertically and laterally continuous, and both areas comprise similar lava flow morphologies and volcanic facies types. The 3D virtual outcrop model includes approximately 5 km of cliff with variably excellent to partial exposure. This section exposes a Paleocene-aged lava dominated succession comprising mixed simple, compound, and ponded lava flow morphologies with subsidiary volcaniclastic interlayers and sheet intrusions overlying Jurassic shallow marine sedimentary deposits.

The fieldwork in Uberlândia (Brazil) focused on collecting samples of representative facies for petrophysical analysis (density, porosity, permeability and P- and S- wave velocities) to be used as input to the seismic forward modelling. In addition, a photomosaic of peperite exposures associated with an invasive lava flow were used to define the morphologies of these units for additional model configurations, in order to test their impact on seismic responses and to assess their likely resolvability in real data. Stratigraphic control, and facies characterization of lava flows and peperite were based on detailed logs, and outcrop descriptions (c.f. Famelli et al., submitted).

- Virtual outcrop models

The virtual outcrop model was constructed using high-resolution photographs acquired by a DJI Phantom 4 Pro drone with a mounted camera FC6310. The sensor user was 1" CMOS with 20 Megapixels, stabilization of the DJI fixed by GPS/Glonass accuracy. Agisoft Photoscan 1.4.5 was used to process the high-resolution photographs, reconstruct the geometry of the outcrop and create a 3D texture mesh. The post-fieldwork interpretation and measurement of the virtual outcrop model was undertaken with LIME 3D viewer software (Buckley et al., 2019) at the University of Aberdeen.

- Geological scenarios

For the present study, simplified geological cross-sections were created based on 2D projections of the virtual outcrop model from Carsaig Bay. In total, four models with different geological configurations were constructed combining features from both Carsaig Arches and Überlândia outcrops. Lobe geometries of the volcanic succession were based on Carsaig Arches exposures while the peperite geometry was based on Überlândia outcrops.

A layer of sandstone (150 – 200 m thick) and water (100 m thick) were added above the volcanic succession in order to simulate a shallow water offshore setting, while the thickness of the sedimentary succession below the volcanic rocks were duplicated aiming to leave enough space to simulate different igneous intrusions and invasive lava flow geometries. Additionally, in order to avoid unwanted edge-effects during modelling, a mirror image of 200 m at both ends of the model were added prior to modelling.

- Physical properties of rock

A total of 45 representative samples were selected for conventional petrophysical analyses (density, porosity, and permeability) along with measurements of P- and S- wave velocities (V_p and V_s). These samples were drilled using a diamond impregnated core bit resulting in 81 core plugs of igneous (subaerial basaltic lava flows), peperite, and sedimentary (sandstone and mudstone) rocks preferentially oriented (vertical and/horizontal). The plugs have diameter of c. 1.5 inches (c. 3.81 cm) and lengths of up to 2 inches (c. 5.08 cm). After drilling, the samples were washed and dried at 60°C and 45% relative humidity (Humidity Oven Drying methodology) aiming to eliminate water from the pores and to prevent the clays from collapsing (McPhee et al., 2015). The core plugs weight, lengths and diameters were measured with high precision balance and calipers. The 81 plugs were analyzed for density, helium porosity and permeability (Appendix E), whereas 22 plugs of representative facies (preferentially vertically oriented) were analyzed for P- and S- wave velocities (V_p and V_s) (Appendix F).

- Porosity and density

Determination of the effective porosity (connected pores) was measured using a helium porosimeter (or pycnometer) manufactured by Weatherford Companies, following the methodology described by American Petroleum Institute (1998) and McPhee et al. (2015).

- Permeability

Permeability was measured in a steady state permeameter with a coreholder (Hassler sleeve) under a confining stress of ~ 4.8 MPa. These analyses involves a flux of gas being continuously applied to the axial axis of the plug while the pressure, temperature and flow rate are electronically monitored by the equipment. When these parameters stabilized, the modified Darcy equation - which normalizes changes in pressure by mean pressure - is used to obtain the permeability values (American Petroleum Institute 1998; McPhee et al., 2015). Only 20 among 81 tested samples revealed permeability higher than the detection limit of the permeameter (>0.001 mD) and therefore, were considered in this study (Appendix E).

- Wave velocities acquisition

Compressional and shear wave velocities (V_p and V_s) were determined at Petrobras Researcher Center (CENPES) using an ultrasonic pulser/receiver with the pulser operating at 700 kHz. The 22 samples were measured under variable confining pressure (Appendix F). The V_p and V_s velocities were acquired at every ~ 3.4 MPa increment during the increasing and decreasing of confining pressure ~ 6.9 – 34.5 – 6.9 MPa. Data discussed in the following section 4.3.3 correspond to those acquired under a confining pressure of ~ 6.9 MPa (ascendant stress).

- Seismic forward modeling

Seismic forward models were developed in seismic modeling software (in-house software) at CENPES, which uses as input a reflectivity model outcome of velocity and density models. These models consist in the geological model converted into a color

drawing, then into a color image, which was converted into gray-scale image where each color corresponds to a specific density and velocity value.

We adopted a fixed spread acquisition geometry consisting of 100 receivers spaced 10 m apart and the same number of shots also spaced 10 m apart, both at a depth of 6 m. The computer-generated seismic data were used as input in a seismic imaging algorithm to form the depth and migrated seismic image (Bording and Lines, 1997). For this, we employed the widely used reverse time migration algorithms due to its efficacy in imaging complex geological structures with large lateral velocity variations, and Inverse Scattering Image Condition (in-house algorithm) in order to attenuate the backscattering noise. Three Ricker wavelets were used for constructing the 30, 50 and 70 Hz dominant frequency models, with cutoff frequencies of 90, 150 and 210 Hz, respectively. Increasing acoustic impedance is characterized by black reflections.

5.3.4 Results

- Virtual outcrop model

At Carsaig Bay on Mull, the volcanic sequences can reach thicknesses up to c. 300 m at the southwestern part of the transect, whereas the thickest exposure of sedimentary deposits (c. 60 m thick) occur at the northeastern portion of the cliff (Fig. 40). Due to the good exposure continuity and the best exposures of sub-basalt sediments, the northeastern section of the virtual model was selected to be the base for the geological models (Fig. 40A).

In the area selected for the forward seismic modeling, it was possible to recognize four different main facies: sedimentary rocks, intrusions, simple and compound lava flows. The description of these four facies is presented in this section and it considers occurrence in areas beyond that selected for the modeling. The terms “simple” and “compound” lavas, introduced by Walker (1971), were used to characterize the lava flow morphologies.

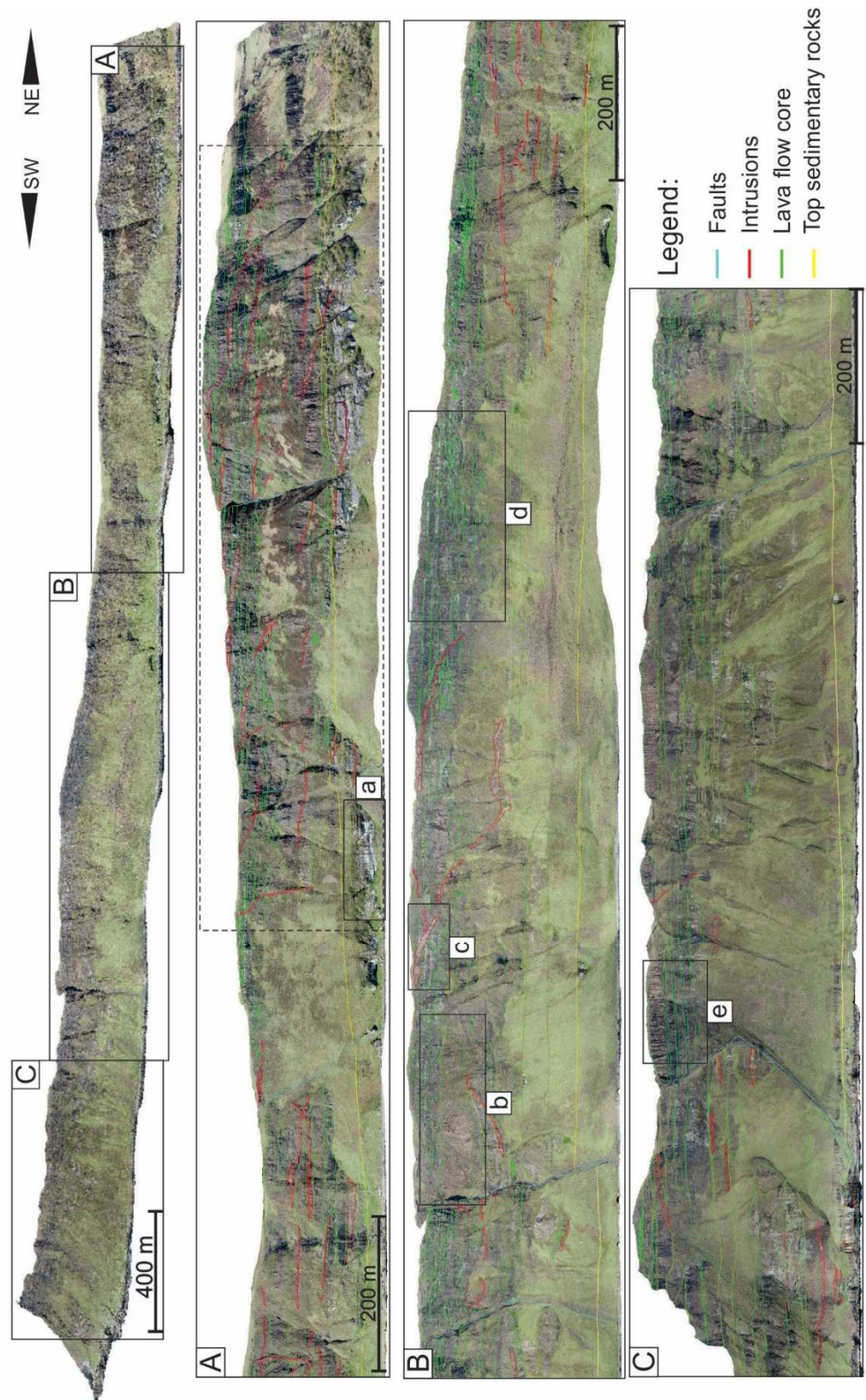


Fig. 40: Virtual outcrop model of Carsaig Arches area subdivided in three main sections. A) Northeastern section of the studied area. The sedimentary outcrop is evidenced in the black square a. The area selected for the seismic forward modelling is delimited by the dashed black square. B) Central section of the studied area. Black squares b and c show the occurrence of an intrusion and compounded flows, respectively. C) Southwestern section of the studied area. The location with the best exposure simple lava flows is highlighted in the square d.

Sedimentary rocks

The sedimentary rocks exposed within the outcrop model include sub-volcanic Mesozoic sediments, and some minor inter-volcanic sediments which have been the focus of many studies (e.g., Jolley et al., 2009; Williamson and Bell, 2012). The sub-basalt sediments within the model extent are dominated by tidally influenced shallow marine sandstone with large carbonate ‘doggers’ and clear evidence for herring bone cross stratification. In the selected area, the tabular sandstone layer cropping out at the base of the volcanic succession is c. 65 m thick and has few intrusions (Fig. 41A).

Intrusions

Intrusions described in this work include both dykes and sills with variable geometries, dimensions and orientation (Fig. 41B). In general, they are tabular, and their thickness varies between c. 3 to 10 meters. These intrusions often present a brighter color when compared with the lava flows and usually have well-formed sharp prismatic joints perpendicular to their contacts. In the selected area, these sills tend to intrude geological discontinuities such as contacts between lobes or sedimentary layers whereas the dykes are dominantly inclined to sub-vertical

Compound lava flows

The compound lava flows consist of relatively small lobes with complex and heterogeneous stacking pattern and lateral distributions. The lobe width and thicknesses may vary from 7 to 96 m and 4 to 12 m, respectively (Fig. 41C). Besides the dominant occurrence of compound lava flows in the northeastern section, the best exposures are seen in the central section of the virtual outcrop.

Simple lava flows

The simple lava flows can be seen along the entire cliff section; however, they are more common at the southwestern region of the virtual outcrop extent. The thicker flows can reach up to c. 50 m while the thinner flows are c. 10 m thick. In general, the simple lava flows crop out as continuous layers for c. 150 m (extent of individual exposures) long occurring stacked on top of each other (Fig. 41D). However, few

isolated lava flows can be identified in areas dominated by compound flows at the northeastern portion of the cliff (e.g., in the modelled section). Colonnade and entablature jointing are often present in these flows, suggesting that they were ponded in palaeo-depressions, a feature that is typical of the Staffa Formation (Williamson and Bell, 2012).

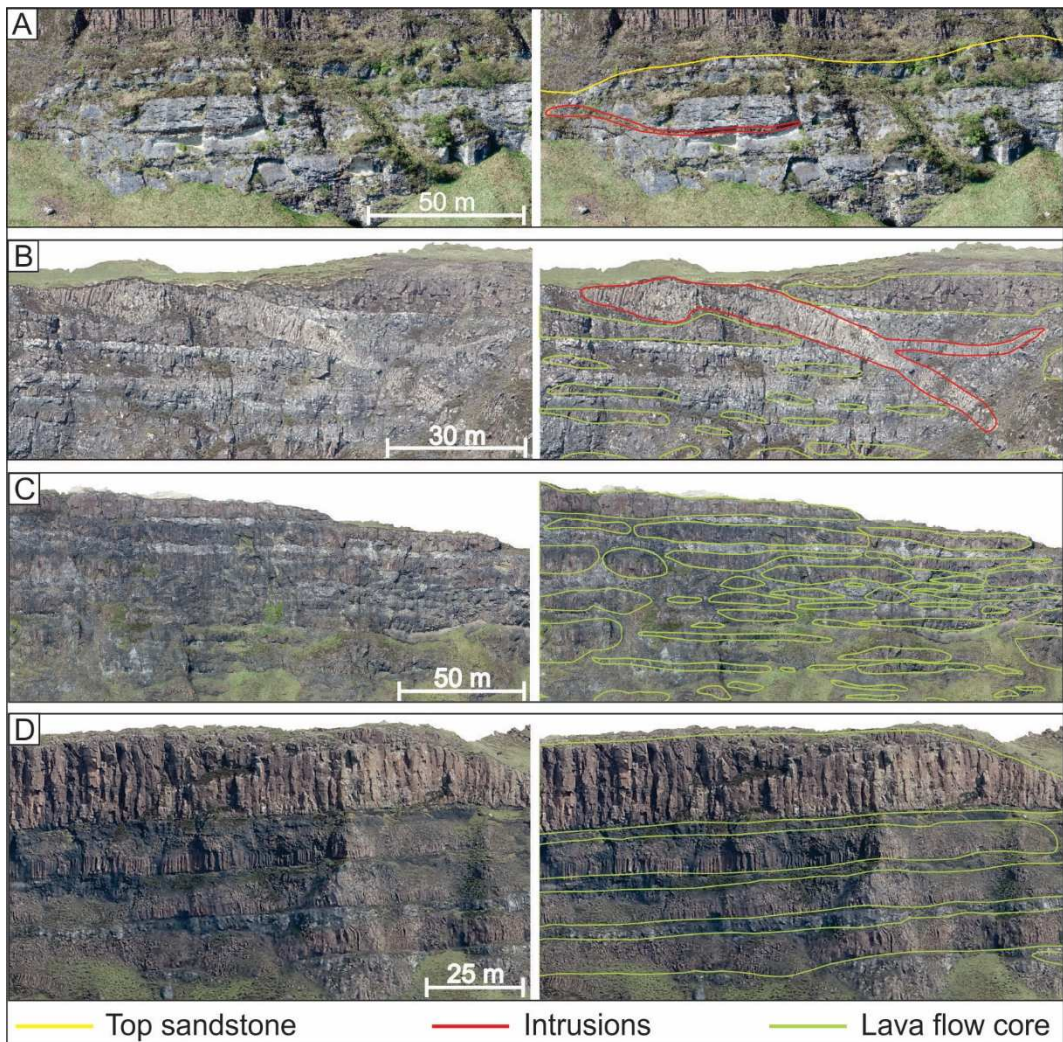


Fig. 41: Detailed view of the virtual outcrop model of Carsaig Arches. Non-interpreted (on left) and interpreted (on right) images showing the facies recognized in the virtual outcrop model (black squares in Fig. 40). A) Sandstone exposure with intrusion. B) Intrusive rock. C) Image of compound lava flows. D) Image of simple lava flows.

Peperite and heterogenic sedimentary sequence

In the chosen Carsaig Bay model section, the sub-volcanic Jurassic sediments were consolidated and dry at the time of lava eruption leading to no interactions between the initial lava flows and the sediment. In the case of the NE PEIP, evidence

for magma-sediment interaction accompanying invasive lava/intrusion emplacement into unconsolidated sediments of the Botucatu Fm. has been documented (Famelli et al., submitted). To address this different setting, alternative scenarios considering more complex base-basalt settings where the volcanic succession overlies a heterogeneous sedimentary sequence with or without sub-basalt sheet intrusions and an invasive lava flow were also compiled. In the sheet intrusion and invasive lava flow scenarios, a carapace of peperite was included to simulate the interaction with unconsolidated sub-basalt sediments. The morphology and physical properties of the peperite (juvenile clast and host sediments) were based on Uberlândia outcrops (Fig. 42), whereas the heterogeneous sedimentary succession where compiled from Rabbel et al. (2018). These sedimentary rocks were described in Los Cavaos oilfield (Argentina) and the interval used in our models includes organic-rich shales, carbonate and evaporites occurring between 2.17 and 2.35 km depth.

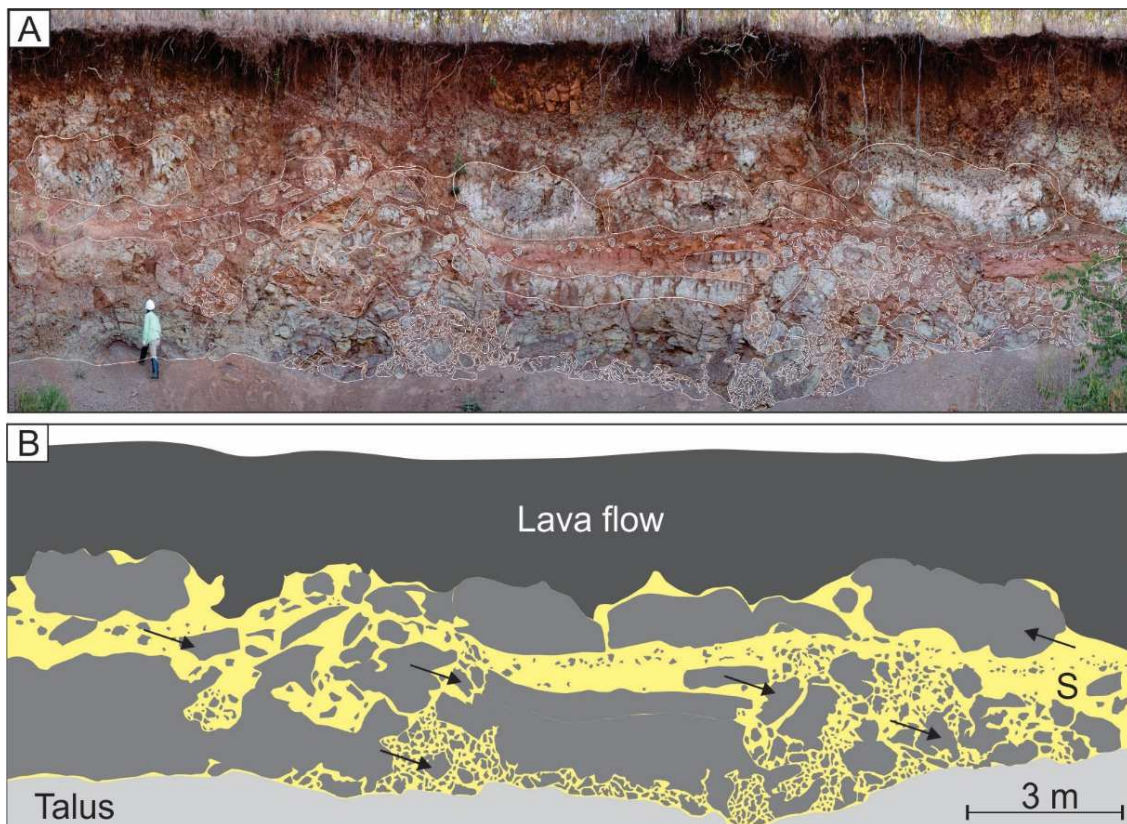


Fig. 42: Juvenile clasts geometries of a peperitic deposit from PEIP (Uberlândia, Brazil). A) Picture of a peperite outcrop with juvenile clasts delimited by the white line. B) Geological model for a peperitic interval based on the PEIP outcrop. Black arrows highlight juvenile clasts. S = sedimentary matrix.

- Geological models

The area selected for this study at Isle of Mull consists of a volcanic sequence (up to 166 m thick) composed of subaerial lava flows (compound and simple lavas) overlying sedimentary layer composed by sandstone (c. 30 m thick). Intrusive rocks occur cross cutting both the volcanic and the sedimentary rocks along the cliff (Fig. 43).

The un-exposed portions in the model area were populated with lobe geometries described in other portions of this cliff. As there is a tendency for the lava flows getting thinner toward the northeast of the studied area (Jolley et al., 2009), the covered portions were populated mainly with compound flows geometries (Fig. 43).

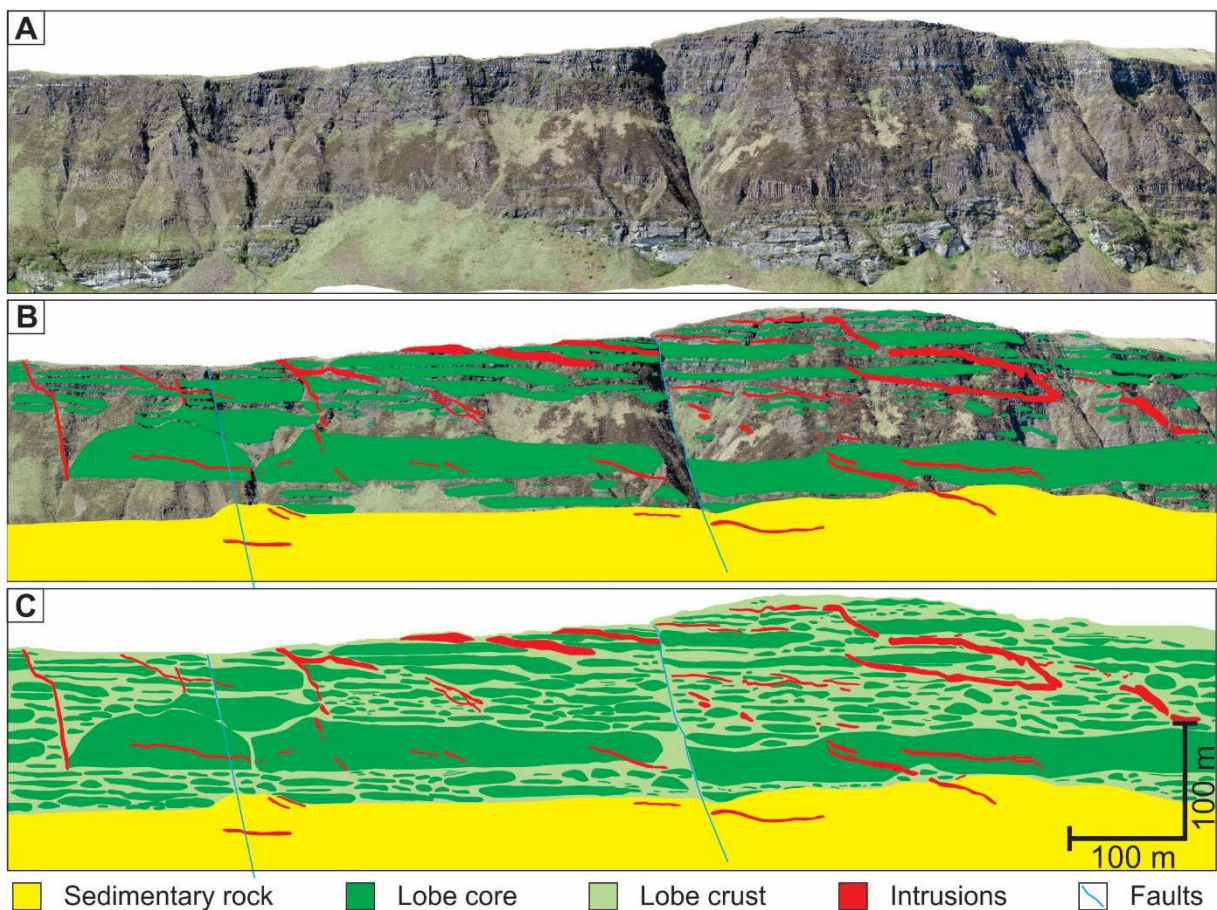


Fig. 43: Interpretation of the virtual outcrop model and construction of the geological model, along Carsaig Arches cliff: A) 2D projection of the area selected for the seismic forward modeling. B) Interpretation of the geological features in areas with good exposures. C) Geological model interpreted for the selected area. The covered areas were populated with compounded lobe morphologies.

Four geological models simulating four different base-basalt settings are presented in Fig. 44. All models comprise the same volcanic succession (135 to 166 m thick) overlain by a sandstone layer (150 to 200 m thick) at a water depth of 100 m. The differences between these four models consist of features added to the sedimentary layer below the volcanic sequence, which had its original thickness doubled compared to the outcrop.

In model 1, the sedimentary rock below the volcanic succession is composed of homogeneous sandstone (Fig. 44A). In model 2, the sub-basalt sandstone is replaced by a layered sedimentary package compiled from Rabbel et al. (2018) (Fig. 44B). In models 3 and 4, a hypothetical sill (c. 25 m thick) and invasive lava flow (c. 25 m thick), each with an envelope of peperite were added to the heterogeneous sedimentary package respectively (Figs. 44C, 44D). The peperite model and properties compiled from the PEIP outcrops was repeated at true scale along the model in order to avoid scale distortion. All hypothetical models are 560 m thick and 1030 m long.

- Petrophysical properties

Basalt samples were collected from lava flow crust and core with the flow crust being more altered with a greater abundance of vesicles and amygdales than the flow core, which is dominantly massive with sparse vesicles. These vesicles and amygdales have variable size and may be totally to partially filled by secondary minerals such as clay minerals and chalcedony. The studied lava flows are porphyritic, with plagioclase and augite as the main phenocryst phases, and these lava flows may reach up to 25 m thick (Famelli et al., submitted).

The studied sedimentary layers vary from a few centimeters to a few meters in thickness (up to 12 m thick) and occur interleaved with lava flows in the studied area. Sandstone is, in general, moderately sorted, and composed mainly of sub-rounded to sub-angular quartz grains, with grain size varying from very fine to coarse. Laminations marked by granulometric variations are present in places. Porosity is dominantly intergranular, with subordinate moldic porosity caused by the dissolution of lithic fragments (Famelli et al., submitted). The mudstone is massive and mainly composed of quartz and interstratified clay minerals such as illite-smectite. These rocks have been interpreted as deposits of fluvio-lacustrine systems (c.f. Moraes and Seer, 2017).

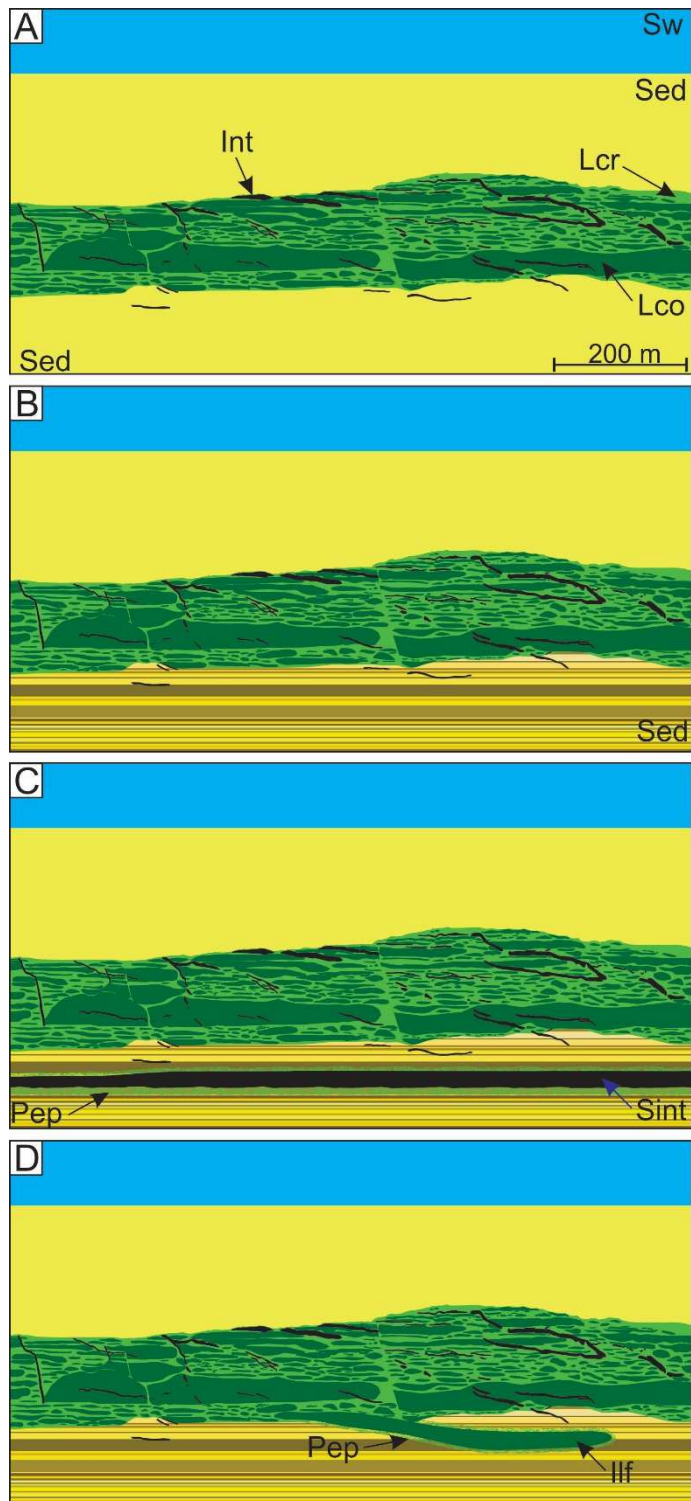


Fig. 44: Geological models used for the seismic forward modeling. All models were simulated at water depth of 100 m. A) Model 1: Volcanic succession occurring between sandstone layers. B) Model 2: Volcanic succession superposed by sandstone and overlying heterogeneous sedimentary sequence. C) Model 3: Similar to model 2, but an intrusive rock with peperite at its contacts occur cross cutting the heterogeneous sedimentary sequence. D) Similar to model 2, but an invasive flow with peperite occurring on its contacts occur invading the heterogeneous sedimentary sequence. Sw = Sea water; Sed = Sediments; Int = Intrusions; Lco = Lobe core; Lcr = Lobe crust; Sint = Sheet intrusion; Pep = Peperite; Ilf = Invasive lava flow.

The studied peperites are composed by basalt fragments within a sedimentary matrix composed mainly of very fine-grained sandstone. The basalt fragments are highly vesiculated, but vesicles may be partially filled by secondary minerals (clay minerals and zeolite) (Famelli et al. submitted). Plugs of representative facies are presented in Fig. 45, whereas the petrophysical data of the Paraná-Etendeka Igneous Province samples is summarized in Tab. 6.

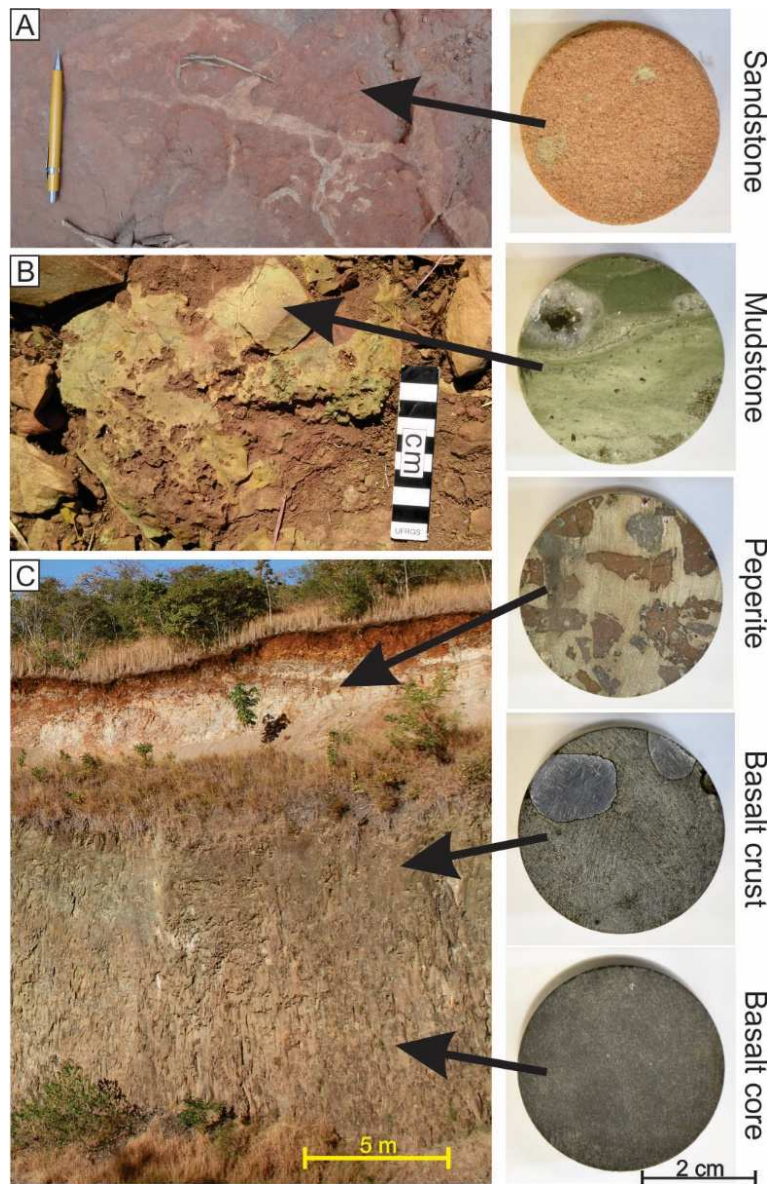


Fig. 45: Outcrops exemplifying the type of material where plugs were taken. A) Exposure of sandstone. B) Mudstone outcrop. C) Core and upper crust of a lava flow superposed by a layer of peperite related to the base of the superposed lava flow.

Tab. 6: Statistics of petrophysical data collected from the study area in Uberlândia area (Brazil). The wave velocities present in this table were acquired under a confining stress of 6.9 MPa.

Rock type/facies		Sandstone	Mudstone	Peperite	Basalt/crust	Basalt/core
No. of samples		5	3	6	19	48
Density (g/cm ³)	Range	2.17 - 2.47	2.18 - 2.27	2.15 - 2.45	2.05 - 2.91	2.79 - 2.95
	Mean	2.39	2.20	2.26	2.75	2.88
	Standard deviation	0.13	0.04	0.12	0.24	0.03
Porosity (%)	Range	3.51 - 16.6	7.40 - 14.59	3.87 - 19.26	0.28 - 24.67	0.08 - 3.08
	Mean	8.53	11.74	13.32	4.12	0.53
	Standard deviation	4.95	3.82	5.85	7.23	0.5
No. of samples		4	2	5	3	6
Permeability (mD)	Range	0.004 -	0.001 -	0,017 -	0,014 -	0,001 -
	Mean	72.2	0.011	0,201	0,103	0,087
	Standard deviation	18.1	0.006	0.125	0.046	0.029
No. of samples		1	1	3	6	11
P wave velocity (km/s)	Range	3.08	4.62	2.65 - 4.56	4.13 - 5.86	5.32 - 6.22
	Mean	-	-	3.55	5.2	5.85
	Standard deviation	-	-	0.96	0.6	0.34
S wave velocity (Km/s)	Range	2.06	3.00	1.74 - 3.00	2.53 - 3.33	3.15 - 3.53
	Mean	-	-	2.3	3.03	3.37
	Standard deviation	-	-	0.64	0.28	0.13

Porosity and density

Variations in physical properties of igneous and sedimentary interbed rocks from the Paraná-Etendeka Igneous Province are illustrated in Fig. 46 and Tab. 6. The porosity data presented here (Appendix E) represent the total effective porosity for the samples. For the sedimentary rocks, porosity is dominantly inter-granular with minor secondary mouldic porosity. For the lava flow samples, porosity is inferred to be largely primary and associated with vesicles; however, some inter-crystalline micro-porosity likely contributes to the samples (not fractures are present in the analyses samples). The peperite samples incorporate both inter-granular sedimentary and primary intra-volcanic clast vesicular porosity.

Sedimentary samples of Uberlândia area have relatively high porosity when compared with the igneous rocks from the same area, except for a few lava lobe crust samples. Sandstone and mudstone have porosity varying from 3.5 to 16.6% (mean 8.5%), and 7.4 to 14.6% (mean 11.7%), whereas their density varies from 2.2 to 2.5

g/cm^3 (mean 2.4 g/cm^3), and 2.2 to 2.3 g/cm^3 (mean 2.2 g/cm^3), respectively. Similarly, the porosity of peperite varies widely from 3.9 to 19.3% (mean 13.3%), whereas its density varies from 2.2 to 2.4 g/cm^3 (mean 2.2 g/cm^3) (Tab. 6). Famelli et al. (submitted) have shown occurrence of quartz, calcite, zeolite and chlorite/smectite as cement in some sedimentary rocks, and filling amygdalites in juvenile clasts of peperite, which can explain the wide variation in the porosity of the studied rocks.

In general, the porosity in the studied igneous rocks oscillates from 0.08 to 24.7% (mean 1.5%), whereas the density varies from 2.0 to 3.0 g/cm^3 . As would be expected, the analysis of the physical properties of different intra-facies shows that the lobe cores are denser and less porous than the lobe crust (Fig 46B and Tab. 6). The 48 representative lobe core samples have porosity varying from 0.08 to 3.08% and density varying from 2.8 – 2.9 g/cm^3 , whereas porosity and density of the 19 lobe crust samples vary from 0.28 to 24.67 , and from 2.0 to 2.9 g/cm^3 , respectively (Tab. 6). The negative correlation between density and porosity for all samples shows that the porosity variations can effectively explain the density of those rocks, supported by an average grain density of 2.9 g/cm^3 (Figs. 46A, 46B). Negative correlation between porosity and density were also observed in igneous samples from the southern portion of the Paraná-Etendeka Igneous Province (Rossetti et al., 2019). However, the porosity of lobe crust found by these authors (mean 12.3%) is higher than those found in this work (mean 4.1%). This relatively lower porosity of the Uberlândia lava flows reflects the presence of pervasive secondary minerals in the vesicles (amygdalites).

Permeability

In general, the permeability of the studied samples varies widely, and it tends to increase with increasing porosity (Fig. 46C). The highest permeability was found in the massive sandstone (72.2 mD), whereas the lowest permeability (0.001 mD) was found in a massive mudstone and basalt core samples (also including examples not shown in Fig. 46 due to being below detection). Due to the small amount of permeability data it was not possible to define a confident behavior for the studied samples but it is possible to see a slight positive correlation between permeability and porosity for sandstone and volcanic rocks (Figs. 46C, 46D), also observed in the southern portion of the PEIP (Rossetti et al., 2019).

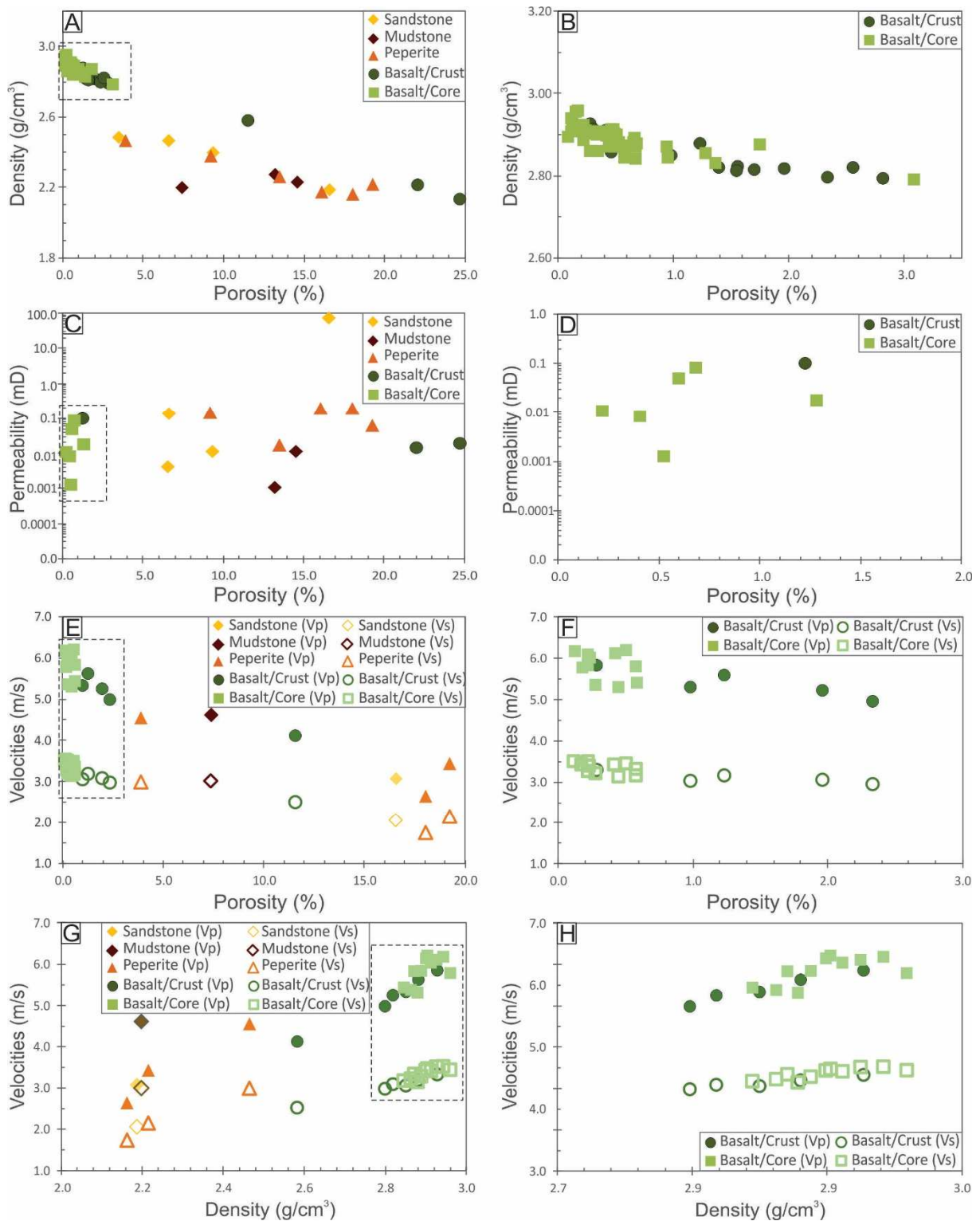


Fig. 46: Petrophysical variations of the PEIP samples (Uberlândia area, Brazil). A) Density plotted against porosity for all studied samples. B) Detail of the dashed square in diagram A showing only volcanic samples. C) Permeability plotted against porosity for all studied samples. D) Relationship between permeability and porosity of volcanic samples (detail of the dashed square in the diagram C). E) V_p and V_s plotted against porosity for all the studied samples. F) Variation of V_p and V_s against porosity for volcanic rocks (detail of the dashed square in the diagram E). G) V_p and V_s against density for all samples. H) V_p and V_s against density showing only volcanic samples.

Wave velocities

In general, the wave velocities (V_p and V_s) are negatively correlated with porosity and positively correlated with density (Figs. 46E, 46F, 46G, 46H). The lower velocities occur in sedimentary rocks, including peperites, while the higher velocities were found in igneous rock from the lobe core (Tab. 6).

The sedimentary group includes one sandstone and one mudstone with 3.1 and 4.6 km/s for V_p , respectively. For peperites, the velocities are variable ranging from V_p 2.6 to 4.6 km/s. Similarly, the igneous rock velocities vary widely with V_p c.4.1–6.2 km/s and V_s c. 2.5–3.5 km/s (Tab. 6). In general, the lobe crusts have the lowest velocities among the igneous rocks (e.g., sample UB-32I with V_p = 4.1 km/s), which are related to higher porosity given by the vesicles found in this facies.

- Seismic model parameters

Density and velocity models used as input to the seismic forward modeling were constructed based on a combination of the laboratory and well data shown in Tab. 7. The petrophysical properties used for lobes (crust and core), invasive flow, peperite and sandstone correspond to representative samples from the PEIP presented in this work, whereas for intrusive rocks we used laboratory data of a dolerite from an offshore basin located in southeast Brazil. The V_p laboratory data used in these models correspond to those acquired under a confining pressure of 6.9 MPa (ascendant stress). The density and velocity data used for the layered sedimentary deposits on models 3 and 4 correspond to well log data compiled from Rabbel et al. (2018, Fig. 4) with ranges presented in Tab. 7.

Tab. 7: Velocity and density data for the representative facies used for the seismic forward modeling. Velocities and densities used for the heterogeneous sedimentary sequence were compiled from Rabbel et al. (2018).

Facies	Sample I.D.	V_p (km/s)	Density (g/cm ³)
Homogeneous sandstone	UB-01	3.08	2.17
Heterogeneous sedimentary sequence	-	3.25-5.75	2.4-2.8
Lobe crust	UB-26bV	4.99	2.79
Lobe core	UB-16eV	6.22	2.90
Intrusions	-	6.61	3.03

- Seismic forward modeling

In all models, the volcanic sequence presents a tabular external form (top marked by a high-amplitude reflection) with a dominantly chaotic pattern making up the internal reflection configurations. The chaotic pattern is characterized by discordant and discontinuous reflections attributed to the disordered arrangement of reflection surfaces (Mitchum et al., 1977). Subparallel, discontinuous reflections occur locally in the volcanic succession. These reflection pattern is similar to those identified in seismic facies of subaerially erupted and emplaced flood basalts described by Planke et al. (2000). The sedimentary package composed by homogeneous sandstone (model 1 – Fig. 47) are reflection free, whereas the layered sedimentary rocks in models 2, 3 and 4 (Fig. 47 and 11) present parallel and, generally, continuous reflection configuration (c.f. Mitchum et al., 1977) which can be seen in all models regardless of the frequency content.

The parallelism between the sheet intrusion with peperite at its contacts, and the layered sedimentary rocks of model 3 (Fig. 48) make it hard to distinguish them in all models due to a lack of transgression (Planke et al., 2005). However, the high amplitude of the top reflection, which is disrupted in low frequency model (30 Hz dominant frequency) and become continuous with the frequency increment, suggests the occurrence of a high impedance layer (sheet intrusion) within the sedimentary rock.

Minor intrusive rocks (up to 10 m thick) cross cutting sedimentary rocks lead to a strong acoustic impedance contrast and abrupt terminations which make them detectable mainly in higher frequency models at 50 and 70 Hz dominant frequency. The identification of these intrusive rocks can be more difficult if they are parallel to layered sedimentary rocks such as models 2, 3 and 4 (Figs. 47 and 48). The invasive flow in model 4 also leads to a strong acoustic impedance contrast and laterally confined amplitude variation, and it is detectable in all models (30, 50 and 70 Hz – Fig. 48).

The base-basalt transition is detectable in all models, especially in those with higher dominant frequencies (50 and 70 Hz). However, the transition is most clearly visible in model 1 (regardless of the dominant frequency; Fig. 47), where the underlying sedimentary sequence is homogeneous, and becomes less clear as more complexity is added to the models (models 2, 3 and 4; Figs. 47 and 48). In models 2, 3 and 4 (30 Hz dominant frequency), the base-basalt transition is hardly distinguishable, only being

identified due to different internal reflection configurations that produce variable seismic facies for the different geological packages. Therefore, the volcanic succession is recognized by the dominant chaotic pattern, whereas the underlying sedimentary rock is recognized by its continuous parallel reflection configuration (Fig. 49).

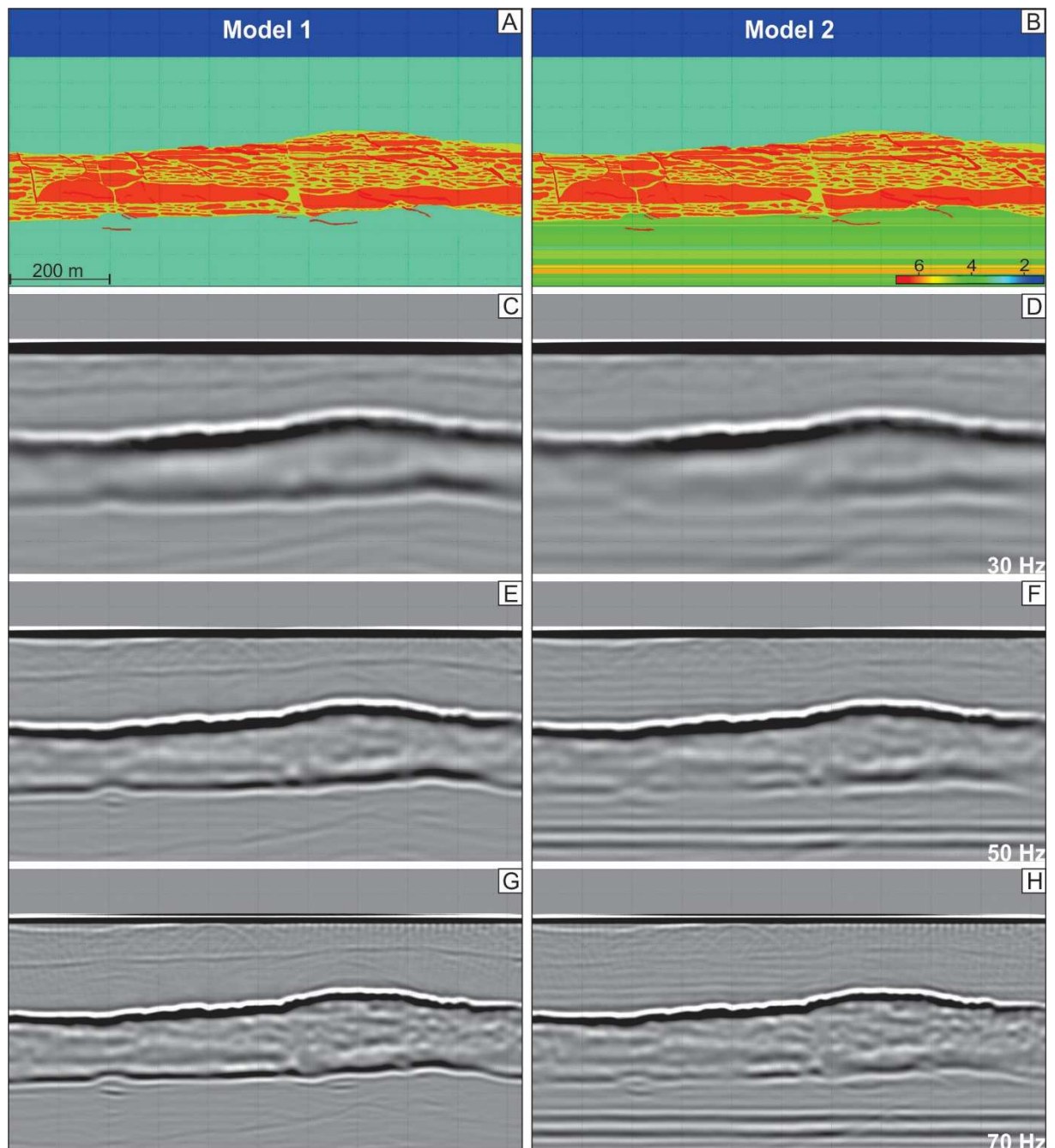


Fig. 47: Models 1 and 2. A, B) Velocity model. C, D) Seismic forward modelling, dominant frequency of 30 Hz. E, F) Seismic forward modelling, dominant frequency of 50 Hz. G, H) Seismic forward modelling, dominant frequency of 70 Hz.

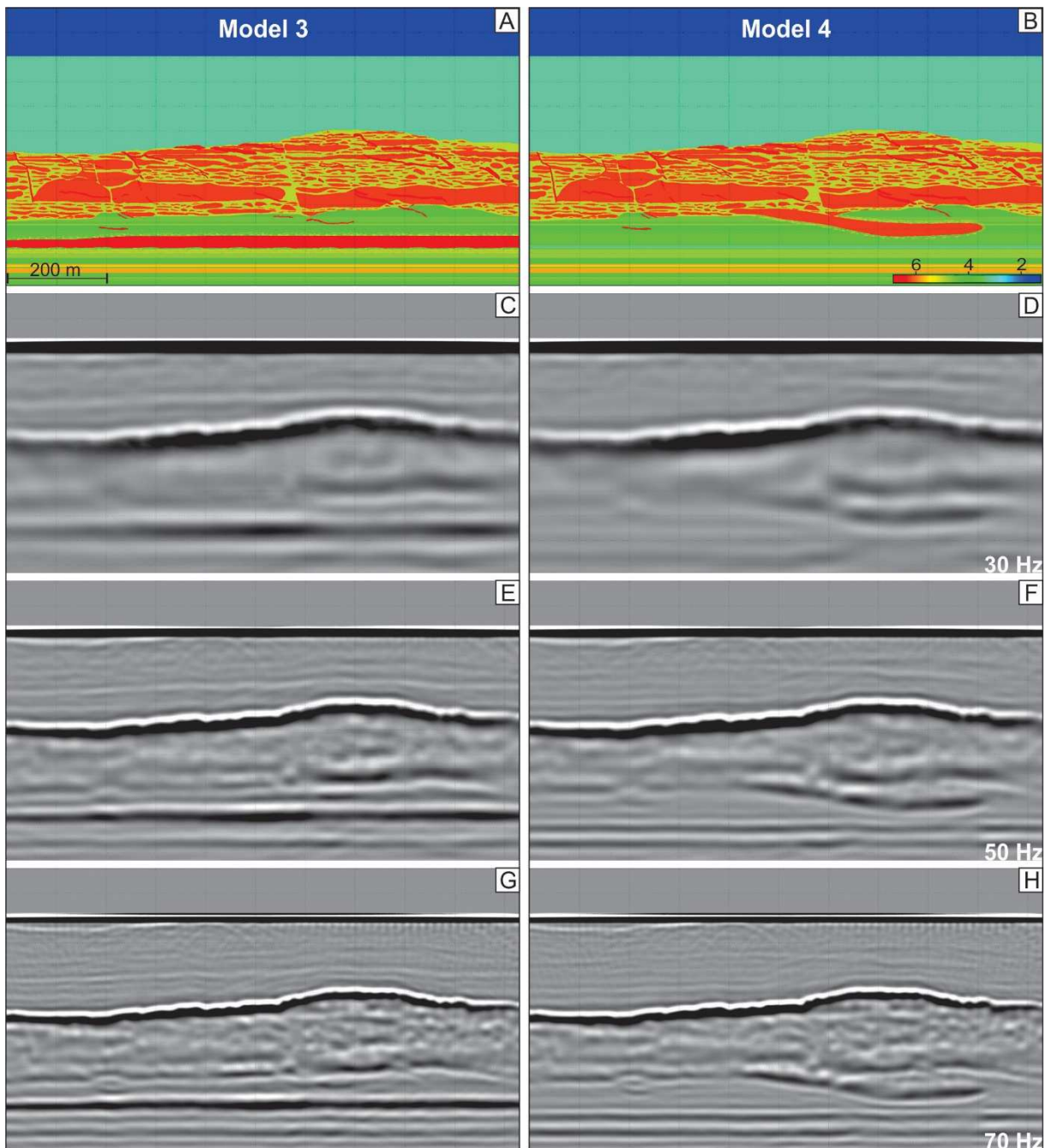


Fig. 48: Models 3 and 4. A, B) Velocity model. C, D) Seismic forward modelling, dominant frequency of 30 Hz. E, F) Seismic forward modelling, dominant frequency of 50 Hz. G, H) Seismic forward modelling, dominant frequency of 70 Hz.

The low resolution at 30 Hz dominant frequency only allows distinguishing the broad lithological packages (e.g., volcanic succession, sedimentary packages, sheet intrusion and invasive flow) (Figs. 47C, 47D, 48C and 48D). Features inside these packages, such as lava flows, dykes and faults are hardly distinguishable (Fig. 49). Near vertical faults and dykes within the volcanic succession are hardly detectable, being characterized by abrupt interruption of horizontal reflections (Fig. 49). However,

it is important to state that not all interrupted reflections represent geological faults in the seismic forward modeling. Some may represent seismic artifacts that may be related to the low frequency content, interference phenomena and tuning effects. For instance, a slightly convex-upward reflection in model 2 (Fig. 49) corresponds to an artifact that could easily be misinterpreted as a channel.

As expected, the resolution increasing leads to a larger number of reflections in the 50 Hz images (Figs. 47E, 47F, 48E and 48F). However, the identification of some features (e.g., intrusions, individual lobes) inside the volcanic sequence may still be challenging. For instance, reflections from compound pahoehoe tend to be more discontinuous (i.e. chaotic seismic facies) than areas dominated by thick simple lava flows, which have internal parallel to subparallel reflection configurations (Fig. 50). Additionally, near-vertical faults and intrusions within the volcanic sequence are hardly detectable (Fig. 50).

In the 70 Hz images, the greater number of reflections leads to a higher resolution comparing to the other images (30 and 50 Hz dominant frequency images) (Figs. 47G, 47H, 48G and 48H). Thus, areas dominated by compound lava flows can be clearly distinguished from areas of simple lava flows due to differences in their internal reflection pattern as has been inferred from real seismic examples (Jerram et al., 2009). Similarly to the 50 Hz images, compound lava flows are characterized by chaotic seismic facies, whereas simple flows with internal reflections are parallel to subparallel, and generally discontinuous as with the model setup (Fig. 51). Faults are well characterized by abrupt terminations of amplitudes whereas dykes are hardly detectable within the volcanic sequence (Fig. 51). Some dykes may be represented by strongly vertical reflections with negative amplitude that occur crossing the geological framework (Fig. 51). It is important to note that the negative amplitude of dykes is relative because when it occurs crossing low impedance geological packages, the impedance contrast may vary.

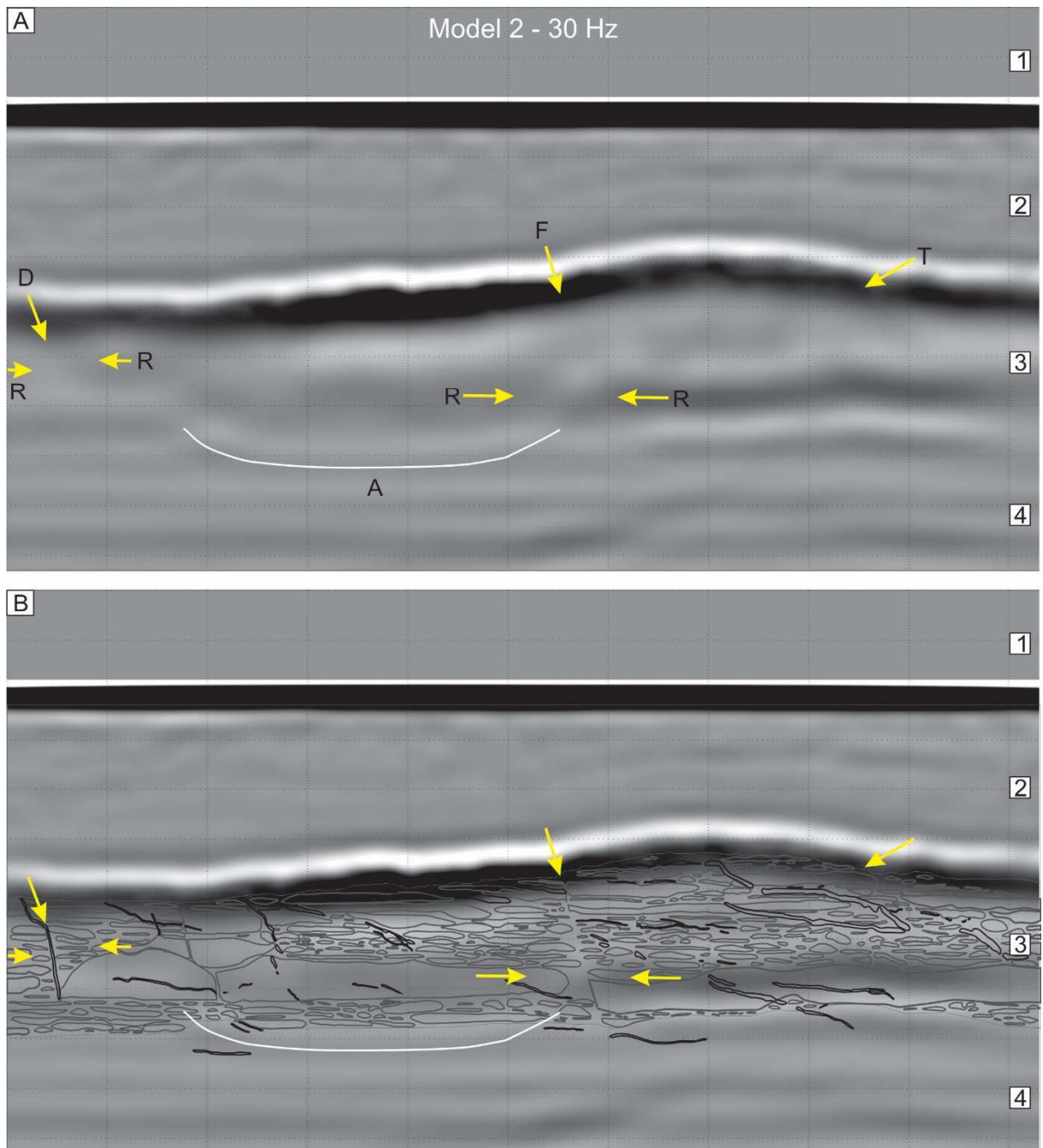


Fig. 49: Model 2 (30 Hz dominant frequency). A) Non-interpreted seismic model. B) Igneous features interpreted in the seismic model. D = dyke; F = Fault; T = Top of the volcanic sequence; R = Discontinuous reflectors; A = Artefact. 1 = Water layer; 2 = Homogeneous sedimentary rock; 3 = Volcanic succession; 4 = Layered sedimentary rock.

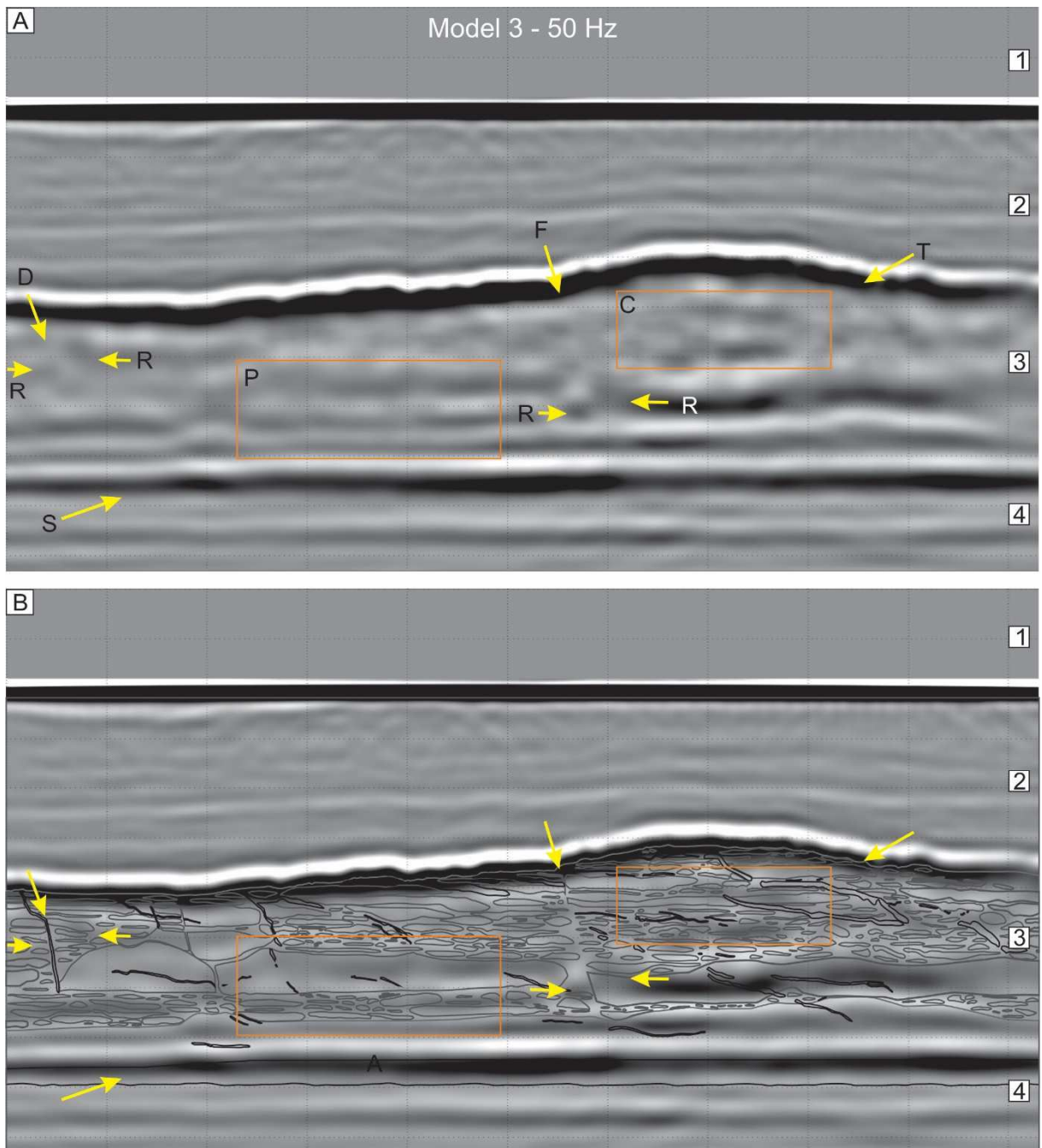


Fig. 50: Model 3 (50 Hz dominant frequency). A) Non-interpreted seismic model. B) Igneous features interpreted in the seismic model. D = dyke; F = Fault; T = Top of the volcanic sequence; R = Discontinuous reflectors; S = Sheet intrusion; Orange square with letter C = Area dominated by compound lava flows; Orange square with letter P = Area dominated by simple lava flows. 1 = Water layer; 2 = Homogeneous sedimentary rock; 3 = Volcanic succession; 4 = Layered sedimentary rock intruded by a sheet intrusion.

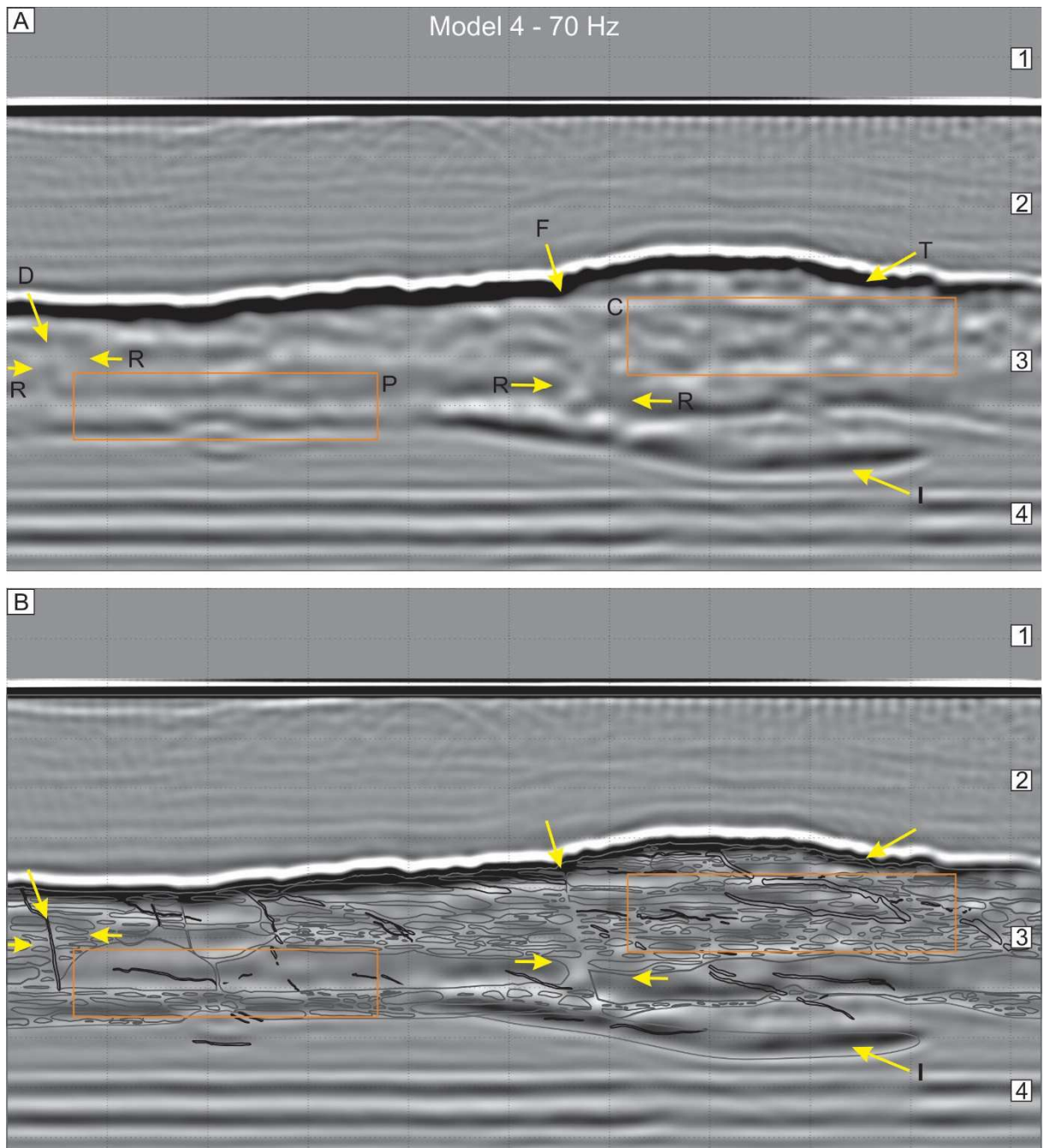


Fig. 51: Model 4 (70 Hz dominant frequency). A) Non-interpreted seismic model. B) Igneous features interpreted in the seismic model. D = dyke; F = Fault; T = Top of the volcanic sequence; R = Discontinuous reflectors; I = Invasive lava flow; Orange square with letter C = Area dominated by compound lava flows; Orange square with letter P = Area dominated by simple lava flows. 1 = Water layer; 2 = Homogeneous sedimentary rock; 3 = Volcanic succession; 4 = Layered sedimentary rock invaded by an invasive flow.

5.3.5 Discussion

- Physical properties of lava flows

Physical properties such as porosity, bulk density and wave velocities vary widely within lava flows (e.g., Watton et al., 2014; Mordensky et al., 2018). In the studied area, within-lobe variations reflect vertical contrasts in vesicularity of core and crust portions.

These relations between lava crust and lava core porosity are well documented in the southern portion of the PEIP and in other provinces (e.g., Zakharova et al., 2012; Vedanti et al., 2015). In the northern PEIP, the lava flows studied are slightly less porous than those occurring in the southern region. The pahoehoe lava flows from the south (Torres Formation) have porosity means of 10.08 and 2.70% for crust and core samples, respectively, whereas the northern lava flows have mean crust and core porosities of 4.12 and 0.53%, respectively (Rossetti et al., 2019). The pahoehoe lava flows of both areas have similar internal architecture suggesting that the difference between the present day effective porosity of the two areas reflects post-depositional variations in secondary mineralization (Barreto et al., 2014; Famelli et al., submitted).

The relatively high porosity of lava crusts makes them the best candidates for reservoir rocks in a volcanic succession (Rossetti et al., 2019). However, besides their relatively good porosity, the permeability for the studied rocks (mean 0.04 mD) is extremely low even to be considered tight reservoir (air permeability lower than 1 mD) (c.f. Wu et al., 2019). Such low permeability is expected for vesicular rocks with low effective porosity due to the pore network falling beneath the percolation threshold for randomly distributed spheres such as vesicles (Bai et al., 2010). Since laboratory analysis using core plugs cannot consider larger scale porosities (e.g., fractures and inter-rubble porosity), volcanic sequences should not be eliminated as a candidate for potential hydrocarbon reservoirs, especially because occurrences of good hydrocarbon reservoirs involving volcanic rocks have been reported in many areas (Mizusaki et al., 1988; Schutter, 2003; Kawada and Yamada, 2014).

- Petrophysical behavior of inter-lava sedimentary rocks and peperite

The clastic rocks analyzed in this work include sandstone, mudstone and peperite. Diagenesis and sorting play a major role in controlling porosity and

permeability of sedimentary rocks. Within this study, the most porous and permeable sample (UB-01) has the best sorting and lowest cement content among the sandstone samples, whereas the poorly sorted and strongly quartz cemented UB-31a sample revealed lower porosity and permeability.

During peperite genesis, the host sediment characteristics may be modified leading to a number of processes that may increase or decrease its porosity (e.g., cementation, contact metamorphism, compaction, sediment vesiculation). Similarly, the lava fragmentation during peperite genesis may result in juvenile clasts with different vesicularity, varying from poorly vesiculated to pumiceous clasts (Skilling et al., 2002). In the studied area, the majority of the peperite samples have porosity values higher than the sandstone and mudstone, suggesting, based on the available analyses that the interaction between lava and sediment did not necessarily result in porosity reduction. The relatively small number of analyzed samples precludes any generalizations associated with peperite formation and reservoir properties and this aspect of lava-sediment interactions merits further study.

- Intrusive rocks and volcanic successions in seismic forward modelling

Intrusive rocks cross cutting sedimentary rocks and their impact on seismic imaging has been the subject of many studies (e.g., Planke et al., 2015; Schofield et al., 2017; Eide et al., 2018). In the study area, minor intrusions (3 to 10 m thick) occur crossing both the sedimentary and volcanic successions. The ability to identify these intrusions and determine their thickness in seismic imaging is given by the vertical detectability and resolution, respectively. The limit of vertical resolution is the Rayleigh's peak-to-trough separation, which corresponds to one-quarter wavelength ($\lambda/4$) of the dominant frequency of a given seismic volume (Kallweit and Wood, 1982). This leads to a vertical resolution of c. 24 m for the studied intrusions in 70 Hz dominant frequency images, what is not enough to resolve the minor intrusions of the study area. Conversely, the seismic detection is more difficult to quantify than the seismic resolution, but some studies have shown values as low as one-thirtieth of the dominant wavelength ($\lambda/30$) (Planke et al., 2015). This would lead to a potential vertical detection limit of c. 4 m at the extreme minimum for the studied intrusions at 70 Hz. However, in the studied volcanic sequence, most of these intrusions could not be detected in any model regardless of the frequency content, except for a few near-vertical intrusions in

the 70 Hz dominant frequency image. Schofield et al. (2017) presented a review of sill intrusions penetrated by boreholes in the Faroe Shetland Basin and found that over 80% of penetrated intrusions were below the vertical resolution of the seismic data.

Besides thickness, a number of factors may influence the detectability of intrusions such as acoustic impedance contrasts, the wavelet spectrum, the signal-to-noise ratio of the seismic, and intrusions orientation and spacing (Zhang and Castagna, 2011; Phillips et al., 2018). In the studied case, the intrusive rocks and the volcanic succession have similar physical properties, and therefore, small acoustic impedance contrasts, which can explain the lack of detectability within the volcanic sequence. In addition, the sub-vertical nature of some intrusions means that they can act as high velocity wave-guides with no impedance contrasts for near-vertical seismic waves (Planke and Flovenz, 1996; Millett et al., 2018). In this case, all the energy carries on downwards and may lead to local seismic disruption or incoherence that may be visible in 3D seismic data (Planke and Flovenz, 1996).

The volcanic sequence studied in this work is composed dominantly of compound lava flows with subordinate simple lava flows. Similarly, to the intrusions described above, the acoustic impedance contrast between lobes is small, however, the internal acoustic impedance contrasts between flow core and crust is larger and therefore leads to reflectivity within the sequence. The flow thicknesses of individual lava flow lobes are dominantly below seismic resolution for all but the thickest lavas in the highest frequency models. However, differences in facies architecture of these lava flows lead to specific character and geometry of internal seismic reflections, which result from interference phenomena (Planke and Cambay, 1998). Complex and heterogeneous stacking patterns and lateral distributions of lobes in compound lava sequences cause significant scattering and attenuation of seismic energy (e.g., Jerram et al., 2009), resulting in discontinuous reflections. In contrast, simple lava flows sequences are characterized by strong amplitude, horizontal to sub-horizontal, parallel to subparallel, laterally persistent internal reflections (e.g., Planke et al., 2000; Jerram et al., 2009; Wright et al., 2012). These two different internal reflection patterns are distinguishable in the 50 and 70 Hz dominant frequency models, confirming the facies variability identified from real seismic examples (e.g., Japsen et al., 2006; Jerram et al., 2009; Wright et al., 2012).

- Seismic response of base-basalt transition

The base-basalt transition in volcano-sedimentary basins has been the focus of much study (e.g., Jerram et al., 2009) and may differ widely in terms of deposits depending on the paleoenvironment and eruption characteristics (Millett et al., 2020). In particular, the presence (subaqueous) or lack (subaerial) of standing water provides a key environmental control on different volcanic products (e.g., McPhie et al., 1993). The best documented subaqueous features are pillow lavas and hyaloclastite deposits, whereas subaerial lava flows may result in different morphologies, varying from compound pahoehoe through transitional to a'a lava flows (e.g., McPhie et al., 1993; Cashman and Mangan, 2014). Besides being subaerial or subaqueous, lava flows may interact with underlying sediments leading to peperite formation, loading structures, and invasive flows (Skilling et al., 2002; Dostal and MacRae, 2018), which inevitably increases the complexity of the base-basalt transition on seismic data.

The base-basalt transition in the area selected for seismic forward modelling at Isle of Mull is characterized by a sharp transition from a sequence dominated by Jurassic sandstone, into a c. 166 m thick subaerial flood basalt sequence. Other scenarios considering underlying heterogeneous sedimentary rocks, sheet intrusions and an invasive flow with peperites were also tested. In model 1 (volcanic succession overlying a homogeneous sandstone), this transition is well marked by a strong amplitude and continuous reflection. However, the base-basalt transition becomes less clear with increasing geological complexity, especially in the 30 Hz dominant frequency models where tuning effects become more important (Eide et al., 2018).

Another feature that has an important influence in imaging the base-basalt transition is the overburden effect (e.g., Gallagher and Dromgoole, 2007; Eide et al., 2018). The frequency content decreases rapidly once the seismic waves hit the overlying high velocity layers such as the lava flows and shallow intrusions. Therefore, imaging of the base-basalt transition is inherently more challenging beneath thicker volcanic sequences (Planke et al., 2000). However, understanding the internal reflection configuration of volcanic sequences and the characteristic base-basalt transition signatures is important for appraising the nature and the location of the transition alongside associated sub-basalt prospectivity (Angkasa et al., 2017; Millett et al., 2020).

- Differentiating shallow intrusions and invasive flows in seismic data

Intrusions are an integral component of all volcanic successions in sedimentary basins and may vary in scale, preserved thickness, geometry and distribution, but cannot be absent (e.g., Cartwright and Hansen, 2006; Muirhead et al., 2014). Intrusions may play an important role in a sedimentary basin by creating barriers and baffles to fluid flow along with potentially leading to compartmentalization of source and reservoir units (Rateau et al., 2013; Schofield et al., 2017). In the Skye lava field, sill intrusions occurring within the underlying sedimentary rocks can comprise more than 50% of the rock volume within the upper few tens of meters of the sub-basalt stratigraphy (Angkasa et al., 2017). Intrusions nearby to the base-basalt transition may therefore be common in volcano-sedimentary settings and must be included in base-basalt interpretation scenarios (Millett et al., 2020; Walker et al., 2020). In real seismic data, shallow intrusions often display saucer-shaped geometries and transgressive segments, which aid in their identification (e.g., Planke et al., 2005), however, extensive layer parallel examples with no obvious transgression also occur.

In the seismic forward modeling (model 4 – Figs. 48 and 51), the simple invasive lava flow geometry comprises a flat-lying and slightly convex-upward high amplitude reflection that terminates abruptly, similar to intrusion-related reflections described in real data (Schofield et al., 2017; Planke et al., 2017). Therefore, distinguishing invasive lava flows from shallow intrusions by their seismic signal may potentially be highly challenging. Despite these similarities, some considerations may be discussed to help address uncertainty in real seismic examples. As invasive flows consist of surface lava flows that locally transgress into the subsurface (Byerly and Swanson, 1978; Hooper, 1997), cases where clear features such as conformable lava flows that clearly flowed over a paleo-surface (e.g., Planke et al., 2017), are related to an igneous body transgressing down into the underlying sedimentary rocks only at the lava flow edges, may suggest invasion processes. In contrast, if a transgressive feeder system (e.g., Planke et al., 2005) occurs linked to a surface volcanic body (e.g., Magee et al., 2013), it is more likely to represent an intrusion. Regarding hydrocarbon prospectivity, the occurrence of invasive flows is inferred to cause less severe impacts on a hydrocarbon system than intrusions due to lesser thermal impacts and the discontinuous nature of possible barriers to flow. This minor impact in terms of barriers is suggested due to the likelihood that invasion only occurs within the very shallow sedimentary succession beneath the base of originally extrusive lava flows whereas intrusions must cross the

entire stratigraphy up to shallowest emplacement depth. It is also important to remember that intrusions and lava flow invasion are 3D processes, whilst our study considers only a simple 2D scenario. Therefore, interpreting features such as invasive flows or shallow intrusions in 2D sections should be done carefully as their geometry may vary widely depending on the orientation of the studied section.

5.3.6 Conclusion

This work presents seismic forward modelling of a volcano-sedimentary sequence, which integrates outcrop and laboratory petrophysical data of the PEIP rocks as well as geomorphological data from the NAIP. Four different models were tested in order to investigate variations in seismic response of the base-basalt transition with variable geological settings, and frequency contents (30, 50 and 70 Hz dominant frequency). From the results presented, we can draw the following conclusions:

- The seismic response of the base-basalt transition may vary widely depending on frequency contents of the seismic data, geological complexity and impedance contrast between the volcanic and sedimentary rocks.
- Different facies architecture of compound and simple lava flows leads to specific character and geometry of internal seismic reflections, which are visible in those images with higher frequency content (50 Hz and 70 Hz dominant frequency).
- Distinguishing invasive lava flows and shallow intrusions from seismic images is a challenging task as these features may have similar petrophysical and geometrical characteristics. Key features such as the depth extent of transgressive reflectors and evidence for 3D lava flow features in concordant reflector segments can help aid interpretation of base-basalt scenarios.
- Recognition of seismic responses of volcanic sequences and related rocks in the forward modelling scenarios can help to improve confidence in seismic interpretation of real subsurface data.
- Finally, porosity and permeability measurements from mingled lava-sediment peperite facies within this study provisionally suggest that reservoir potential can remain good and even potentially be improved compared to unaffected sediments. Complexity of these rock types and the limited number of analyses presented here,

highlight the need for further detailed study on these rock types to better understand these complex relationships.

Acknowledgements

This work was supported by Petrobras (CENPES R&D Projects PT-166.01.11923 and PT-166.01.13484) and CNPq (442812/2015-9). The Federal University of Rio Grande do Sul and University of Aberdeen are acknowledged for additional support. Natália Famelli specially acknowledges to A. Bulcão for the support with the seismic forward modelling. M. Chmielewska, G. Bertolini; J. Machado, G. Marins, L. Bevilaqua, R. Rizzo are thanked for their support during fieldwork, discussions and/or software support. We thank the grinding plant of the 2º BFv, Arpasa, Ecobrix, Dois Irmãos, BT Construções, São Lucas quarries and the Ferrovia Centro-Atlântica (FCA – VLI Logística) for the permission to access the outcrop areas.

References

- Abdelmalak, M. M., S. Planke, J. I. Faleide, D. A. Jerram, D. Zastrophnov, S. Eide, and R. Myklebust, 2016, The development of volcanic sequences at rifted margins: New insights from the structure and morphology of the Vøring Escarpment, mid-Norwegian Margin: *Journal of Geophysical Research: Solid Earth*, v. 121, no. 7, pp. 5212-5236. <https://doi.org/10.1002/2015JB012788>
- Abdelmalak, M.M., Planke, S., Polteau, S., Hartz, E.H., Faleide, J.I., Tegner, C., Jerram, D.A., Millett, J.M. and Myklebust, R., 2019. Breakup volcanism and plate tectonics in the NW Atlantic. *Tectonophysics*, 760, pp.267-296. doi:10.1016/j.tecto.2018.08.002.
- American Petroleum Institute, 1998, Recommended practices for core analysis: New York, American Petroleum Institute, 220 p.
- Angkasa, S. S., D. A. Jerram, J. M. Millett, H. H. Svensen, S. Planke, R. A. Taylor, N. Schofield, and J. Howell, 2017, Mafic intrusions, hydrothermal venting and the basalt-sediment transition: Linking onshore and offshore examples from the north atlantic igneous province: *Interpretation*, v. 5, no. 3, p. 83–101, doi:10.1190/int-2016-0162.1.

Bai, L., D. R. Baker, and R. J. Hill, 2010, Permeability of vesicular Stromboli basaltic glass: Lattice Boltzmann simulations and laboratory measurements: *Journal of Geophysical Research*, v. 115, no. B7, p. 1–16, doi:10.1029/2009jb007047.

Barreto, C. J. S., E. F. Lima, C. M. Scherer, and L. M. M. Rossetti, 2014, Lithofacies analysis of basic lava flows of the Paraná igneous province in the south hinge of Torres Syncline, Southern Brazil: *Journal of Volcanology and Geothermal Research*, v. 285, p. 81–99, doi:10.1016/j.jvolgeores.2014.08.008.

Bellieni, G., P. Comin-Chiaromonti, L. S. Marques, A. J. Melfi, E. M. Piccirillo, A. J. R. Nardy, and A. Roisenberg, 1984, High- and Low-TiO₂ flood basalts from the Parana plateau (Brazil): petrology and geochemical aspects bearing on their mantle origin: *Neus Jahrbuch Miner. Abh*, v. 150, no. 3, p. 273–306.

Bischoff, A. P., A. Nicol, and M. Beggs, 2017, Stratigraphy of architectural elements in a buried volcanic system and implications for hydrocarbon exploration: Society of Exploration Geophysicists and American Association of Petroleum Geologists, v. 5, no. 3, p. 1–19,

Bording, R. P., and L. R. Lines, 1997, Seismic Modeling and Imaging with the Complete Wave Equation: *Seismic Modeling and Imaging with the Complete Wave Equation*, doi:10.1190/1.9781560801870.

Brown, D. J., and B. R. Bell, 2007, How do you grade peperites? *Journal of Volcanology and Geothermal Research*, v. 159, no. 4, p. 409–420, doi:10.1016/j.jvolgeores.2006.08.008.

Buckley, S. J., K. Ringdal, N. Naumann, B. Dolva, T. H. Kurz, J. A. Howell, and T. J. B. Dewez, 2019, LIME: Software for 3-D visualization, interpretation, and communication of virtual geoscience models: *Geosphere*, v. 15, no. 1, p. 222–235, doi:10.1130/GES02002.1.

Byerly, G., and D. Swanson, 1978, Invasive Columbia River Basalt flows along the northwestern margin of the Columbia Plateau, north-central Washington: *Abstr. Prgrms. Geological Society of America*, v. 10, p. 98.

Cartwright, J., and D. M. Hansen, 2006, Magma transport through the crust via interconnected sill complexes: *Geology*, v. 34, no. 11, p. 929–932, doi:10.1130/G22758A.1.

Cashman, B. K. V., and M. T. Mangan, 2014, A Century of Studying Effusive Eruptions in Hawaii: Characteristics of Hawaiian Volcanoes-U.S. Geological Survey Professional Paper 1801, p. 357–394, doi:10.3133/pp1801.

Davison, I., S. Stasiuk, P. Nuttall, and P. Keane, 2010, Sub-basalt hydrocarbon prospectivity in the Rockall, Faroe-Shetland and Møre basins, NE Atlantic: Petroleum Geology Conference Proceedings, v. 7, no. 0, p. 1025–1032, doi:10.1144/0071025.

Dostal, J., and A. MacRae, 2018, Cretaceous basalts of the High Arctic large igneous province at Axel Heiberg Island (Canada): Volcanic stratigraphy, geodynamic setting, and origin: *Geological Journal*, v. 53, no. 6, p. 2918–2934, doi:10.1002/gj.3132.

Eide, C. H., N. Schofield, I. Lecomte, S. J. Buckley, and J. A. Howell, 2018, Seismic interpretation of sill complexes in sedimentary basins: Implications for the sub-sill imaging problem: *Journal of the Geological Society*, v. 175, no. 2, p. 193–209, doi:10.1144/jgs2017-096.

Eldholm, O., and K. Grue, 1994, North Atlantic volcanic margins: Dimensions and production rates: *Journal of Geophysical Research*, v. 99, no. B2, p. 2955–2968, doi:10.1029/93JB02879.

Emeleus, C., 1991, Tertiary igneous activity.pdf, in G. Y. Craig, ed., *Geology of Scotland*: London, Geological Society, p. 455–502.

Emeleus, C., and B. Bell, 2005, Igneous geology: regional setting, Palaeogene volcanic districts of Scotland, in *British Regional Geology*: Nottingham, British Geological Survey.

Famelli, N., E. F. Lima, and I. de O. Carmo, n.d., Lithostratigraphy of the Serra Geral Formation in the Northern portion of the Paraná-Etendeka Igneous Province: A tool for tracking Early-Cretaceous paleoenvironmental changes.: Submitted.

Fornero, S. A., G. M. Marins, J. T. Lobo, A. F. M. Freire, and E. F. de Lima, 2019, Characterization of subaerial volcanic facies using acoustic image logs: Lithofacies and log-facies of a lava-flow deposit in the Brazilian pre-salt , deepwater of Santos Basin: *Marine and Petroleum Geology*, v. 99, p. 156–174, doi:10.1016/j.marpetgeo.2018.09.029.

Gallagher, J. W., and P. W. Dromgoole, 2007, Exploring below the basalt, offshore Faroes: A case history of sub-basalt imaging: *Petroleum Geoscience*, v. 13, no. 3, p. 213–225, doi:10.1144/1354-079306-711.

Ganerød, M., M. A. Smethurst, S. Rousse, T. H. Torsvik, and T. Prestvik, 2008, Reassembling the Paleogene-Eocene North Atlantic igneous province: New paleomagnetic constraints from the Isle of Mull, Scotland: *Earth and Planetary Science Letters*, v. 272, no. 1–2, p. 464–475, doi:10.1016/j.epsl.2008.05.016.

Hansen, J., D. A. Jerram, K. McCaffrey, and S. R. Passey, 2009, The onset of the North Atlantic Igneous Province in a rifting perspective: *Geological Magazine*, v. 146, no. 3, p. 309–325, doi:10.1017/S0016756809006347.

Hawkesworth, C. J., K. Gallagher, L. Kirstein, and M. S. M. Mantovani, 2000, Tectonic controls on magmatism associated with continental break-up: an example from the Paraná-Etendeka Province: *Science*, v. 179, p. 335–349, doi:10.1016/S0012-821X(00)00114-X.

Helland-Hansen, D., 2009, Rosebank: challenges to development from a subsurface perspective, in 2nd Faroe Islands Exploration Conference. Proceedings: Ann. Soc. Sci. Faroensis: p. 241–245.

Hooper, P. R., 1997, The Columbia River flood basalt provinces: Current status, in J. J. Mahoney, and M. F. Coffin, eds., *Geophysical Monograph Series*: Washington, American Geophysical Union, p. 1–27, doi:10.1029/GM100p0001.

Japsen, P. et al., 2005, Preliminary results from investigations of seismic and petrophysical properties of Faroes basalts in the SeiFaBa project, in *Petroleum Geology Conference Proceedings*: p. 1461–1470, doi:10.1144/0061461.

Japsen, P., M. S. Andersen, L. O. Boldreel, R. Waagstein, R. S. White, M. Worthington, P. Japsen, M. S. Andersen, and L. O. Boldreel, 2006, Seismic and petrophysical properties of Faroes basalts (the SeiFaBa project) Final Report Funded by the Sindri group Seismic and petrophysical properties of Faroes basalts (the SeiFaBa project) Final Report Funded by the Sindri group.

Jerram, D. A., 2002, Volcanology and facies architecture of flood basalts, in M. A. Menzies, J. Baker, C. J. Ebinger, and S. L. Klemperer, eds., *Volcanic Rifted Margins*: Colorado, Geological Society of America Special Paper, p. 121–135, doi:<https://doi.org/10.1130/0-8137-2362-0.119>.

Jerram, D. A., R. T. Single, R. W. Hobbs, and C. E. Nelson, 2009, Understanding the offshore flood basalt sequence using onshore volcanic facies analogues: An example from the Faroe-Shetland basin: *Geological Magazine*, v. 146, no. 3, p. 353–367, doi:10.1017/S0016756809005974.

Jerram, D. A., and M. Widdowson, 2005, The anatomy of Continental Flood Basalt Provinces: geological constraints on the processes and products of flood volcanism: *Lithos*, v. 79, no. 3–4, p. 385–405, doi:10.1016/J.LITHOS.2004.09.009.

Jolley, D. W., B. R. Bell, I. T. Williamson, and I. Prince, 2009, Syn-eruption vegetation dynamics, paleosurfaces and structural controls on lava field vegetation: An example from the Palaeogene Staffa Formation, Mull Lava Field, Scotland: *Review of Palaeobotany and Palynology*, v. 153, no. 1–2, p. 19–33, doi:10.1016/j.revpalbo.2008.06.003.

Kallweit, R. S., and L. C. Wood, 1982, The limits of resolution of zero-phase wavelets.: *Geophysics*, v. 47, no. 7, p. 1035–1046, doi:10.1190/1.1441367.

Kawada, K., and Y. Yamada, 2014, Basaltic Reservoirs of the Yurihara oil and gas field : a path to geological modeling, in 21st World Petroleum Congress.

Kent, R. W., B. A. Thomson, R. R. Skelhorn, A. C. Kerr, M. J. Norry, and J. N. Walsh, 1998, Emplacement of Hebridean Tertiary flood basalts: evidence from an inflated pahoehoe lava flow on Mull, Scotland: *Journal of the Geological Society*, v. 155, no. 4, p. 599–607, doi:10.1144/gsjgs.155.4.0599.

Lecomte, I., P. L. Lavadera, C. Botter, I. Anell, S. J. Buckley, C. H. Eide, A. Grippa, V. Mascolo, and S. Kjoberg, 2016, 2(3)D convolution modelling of complex geological targets beyond – 1D convolution: *First Break*, v. 34, no. 5, p. 99–107.

Lenhardt, N., and A. E. Götz, 2011, Volcanic settings and their reservoir potential: An outcrop analog study on the Miocene Tepoztlán Formation, Central Mexico: *Journal of Volcanology and Geothermal Research*, v. 204, no. 1–4, p. 66–75, doi:10.1016/j.jvolgeores.2011.03.007.

De Luca, P., J. Carballo, A. Filgueiras, G. Pimentel, M. Esteban, J. Tritlla, and R. Villacorta, 2015, What is the role of volcanic rocks in the Brazilian pre-salt?, in 77th EAGE Conference and Exhibition 2015: Earth Science for Energy and Environment: European Association of Geoscientists and Engineers, EAGE, p. 1686–1690, doi:10.3997/2214-4609.201412890.

Machado, F., E. R. V. Rocha-Júnior, L. S. Marques, and A. J. R. Nardy, 2015, Volcanological aspects of the northwest region of Paraná continental flood basalts (Brazil): *Solid Earth*, v. 6, no. 1, p. 227–241, doi:10.5194/se-6-227-2015.

Magee, C., E. Hunt-Stewart, and C. A. L. Jackson, 2013, Volcano growth mechanisms and the role of sub-volcanic intrusions: Insights from 2D seismic reflection data: *Earth and Planetary Science Letters*, v. 373, p. 41–53, doi:10.1016/j.epsl.2013.04.041.

Magee, C., S. M. Maharaj, T. Wrona, and C. A. L. Jackson, 2015, Controls on the expression of igneous intrusions in seismic reflection data: *Geosphere*, v. 11, no. 4, p. 1024–1041, doi:10.1130/GES01150.1.

Marins, G. M., Y. M. Parizek-Silva, I. de O. Carmo, and L. A. Bevilaqua, 2018, Revisão da sucessão vulcânica basáltica testemunhada de um poço do campo de Badejo, da bacia de Campos/RJ. Uma análise vulcão-estratigráfica, in N. Palermo, H. I. e Araújo Jr., F. B. Machado, A. Corval, S. de C. Valente, and P. F. Dal'bó, eds., 49º Congresso Brasileiro de Geologia: Sociedade Brasileira de Geologia, p. 2001.

McPhee, C., J. Reed, and I. Zubizarreta, 2015, Core Analysis. A Best Practice Guide.: 852 p., doi:10.1016/B978-0-444-63533-4.00005-6.

Mcphie, J., M. Doyle, and R. Allen, 1993, Volcanic Textures: A guide to the interpretation of textures in volcanic rocks: University of Tasmania, 191 p.

Millett, J. M. et al., 2020, Basin structure and prospectivity of the NE Atlantic volcanic rifted margin: cross-border examples from the Faroe–Shetland, Møre and Southern Vøring basins: Geological Society, London, Special Publications, p. SP495-2019-12, doi:10.1144/sp495-2019-12.

Millett, J. M. et al., 2018, Sub-surface geology and velocity structure of the Krafla high temperature geothermal field, Iceland: Integrated ditch cuttings, wireline and zero offset vertical seismic profile analysis: *Journal of Volcanology and Geothermal Research*, v. 391, p. 18, doi:10.1016/j.jvolgeores.2018.03.024.

Millett, J. M., M. J. Hole, D. W. Jolley, N. Schofield, and E. Campbell, 2016, Frontier exploration and the North Atlantic Igneous Province: new insights from a 2.6km offshore volcanic sequence in the NE Faroe-Shetland Basin: *Journal of the Geological Society*, v. 173, no. 2, p. 320–336, doi:10.1144/jgs2015-069.

- Mitchum, R. M., P. R. Vail, and J. B. Sangree, 1977, Seismic Stratigraphy and Global Changes of Sea Level , Part 6 : Stratigraphic Interpretation of Seismic Reflection PaHerns in: AAPG Memoir, v. 22, p. 117–133, doi:<https://doi.org/10.1306/M26490C6>.
- Mizusaki, A. M. P., A. Thomaz Filho, and J. Valen a, 1988, Volcano-sedimentary sequence of Neocomian age in Campos Basin (Brazil): Revista Brasileira de Geoci ncias, v. 18, no. 3, p. 247–251, doi:[10.25249/0375-7536.1988247251](https://doi.org/10.25249/0375-7536.1988247251).
- Moraes, L. C. de, and H. J. Seer, 2017, Pillow lavas and fluvio-lacustrine deposits in the northeast of Paran  Continental Magmatic Province, Brazil: Journal of Volcanology and Geothermal Research, v. 355, p. 78–86, doi:[10.1016/J.JVOLGEORES.2017.03.024](https://doi.org/10.1016/J.JVOLGEORES.2017.03.024).
- Mordensky, S. P., M. C. Villeneuve, B. M. Kennedy, M. J. Heap, D. M. Gravley, J. I. Farquharson, and T. Reuschl , 2018, Physical and mechanical property relationships of a shallow intrusion and volcanic host rock, Pinnacle Ridge, Mt. Ruapehu, New Zealand: Journal of Volcanology and Geothermal Research, v. 359, p. 1–20, doi:[10.1016/j.jvolgeores.2018.05.020](https://doi.org/10.1016/j.jvolgeores.2018.05.020).
- Moreira, J. L. P., C. Valdetaro, J. A. Gil, and M. A. P. Machado, 2007, Bacia de Santos: Boletim de Geociencias da Petrobras, v. 15, no. 2, p. 531–549.
- Muirhead, J. D., G. Airoldi, J. D. L. White, and J. V. Rowland, 2014, Cracking the lid: Sill-fed dikes are the likely feeders of flood basalt eruptions: Earth and Planetary Science Letters, v. 406, p. 187–197, doi:[10.1016/j.epsl.2014.08.036](https://doi.org/10.1016/j.epsl.2014.08.036).
- Oliveira, L. C. De, C. C. Rancan, and M. J. R. Oliveira, 2019, Sill emplacement mechanisms and their relationship with the Pre- Salt stratigraphic framework of the Libra Area (Santos Basin , Brazil), in LASI 6 Conference - The physical geology of subvolcanic systems - Laccoliths, sills and dykes.
- Peate, D. W., 1997, The Parana-Etendeka Province, in J. J. Mahoney, and M. F. Coffin, eds., Large Igneous Provinces: Continental, Oceanic, and Planetary Flood Volcanism: Geophysical Monographs: American Geophysical Union, p. 217–245, doi:[10.1029/GM100p0217](https://doi.org/10.1029/GM100p0217).
- Peate, D. P., C. J. Hawkesworth, and M. S. Mantovani, 1992, Chemical stratigraphy of the Paran  lavas (South America): cassification of magma types and their spatial distribution: Bulletin of Volcanology, v. 55, p. 119–139, doi:[10.1007/BF00301125](https://doi.org/10.1007/BF00301125).

Phillips, T. B., C. Magee, C. A. L. Jackson, and R. E. Bell, 2018, Determining the three-dimensional geometry of a dike swarm and its impact on later rift geometry using seismic reflection data: *Geology*, v. 46, no. 2, p. 119–122, doi:10.1130/G39672.1.

Piccirillo, E. M., L. Civetta, R. Petrini, A. Longinelli, G. Bellieni, P. Comin-Chiaromonti, L. S. Marques, and A. J. Melfi, 1989, Regional variations within the Parana flood basalts (southern Brazil): evidence for subcontinental mantle heterogeneity and crustal contamination: *Chem. Geol.*, v. 75, p. 103–122.

Planke, S., and H. Cambray, 1998, Seismic properties of flood basalts from Hole 917A downhole data, southeast Greenland volcanic margin: *Proceedings of the Ocean Drilling Program: Scientific Results*, v. 152, no. 2, p. 453–462, doi:10.2973/odp.proc.sr.152.247.1998.

Planke, S., and Ó. G. Flóvenz, 1996, Seismic properties of flood basalts, in Norwegian Petroleum Society Conference on Seismic Lithology: p. 11–13.

Planke, S. S., J. M. Millett, D. Maharjan, D. A. Jerram, M. M. Abdelmalak, A. Groth, J. Hoffmann, C. Berndt, and R. Myklebust, 2017, Igneous seismic geomorphology of buried lava fields and coastal escarpments on the Vøring volcanic rifted margin: *Interpretation*, v. 5, no. 3, p. SK161–SK177, doi:10.1190/INT-2016-0164.1.

Planke, S., O. Rabbel, O. Galland, J. M. Millet, B. Manton, D. A. Jerram, O. J. Palma, and J. B. Spacapan, 2018, Seismic imaging and petroleum implications of igneous intrusions in sedimentary basins constrained by outcrop analogues and seismic data from the Neuquén Basin and the NE Atlantic: *10o Congreso de Exploración y Desarrollo de Hidrocarburos*, no. February, p. 343–365.

Planke, S. S., T. Rasmussen, S. S. Rey, and R. Myklebust, 2005, Seismic characteristics and distribution of volcanic intrusions and hydrothermal vent complexes in the Vøring and Møre basins: *Petroleum Geology Conference Proceedings*, v. 6, no. 0, p. 833–844, doi:10.1144/0060833.

Planke, S., H. Svensen, R. Myklebust, S. Bannister, B. Manton, and L. Lorenz, 2015, *Geophysics and Remote Sensing*: Springer, Berlin, p. 1–16, doi:10.1007/11157.

Planke, S. S., P. A. Symonds, E. Alvestad, and J. Skogseid, 2000, Seismic volcanostratigraphy of large-volume basaltic extrusive complexes on rifted margins: *Journal of Geophysical Research: Solid Earth*, v. 105, no. B8, p. 19335–19351, doi:10.1029/1999jb900005.

Plazibat, S., A. Rasgado, and J. M. Paredes, 2019, Subsurface characterization of Cenozoic igneous activity at Cerro Dragón area (Golfo San Jorge Basin, central Patagonia): Implications for basin evolution and hydrocarbon prospectivity: *Journal of South American Earth Sciences*, v. 96, no. October, p. 102389, doi:10.1016/j.jsames.2019.102389.

Rabbel, O., O. Galland, K. Mair, I. Lecomte, K. Senger, J. B. Spacapan, and R. Manceda, 2018, From field analogues to realistic seismic modelling: A case study of an oil-producing andesitic sill complex in the Neuquén Basin, Argentina: *Journal of the Geological Society*, v. 175, no. 4, p. 580–593, doi:10.1144/jgs2017-116.

Rateau, R., N. Schofield, and M. Smith, 2013, The potential role of igneous intrusions on hydrocarbon migration, West of Shetland: *Petroleum Geoscience*, v. 19, no. 3, p. 259–272, doi:10.1144/petgeo2012-035.

Renne, P. R., 2015, Age and Duration of the Paraná-Etendeka Flood Basalts and Related Plumbing System: *American Geophysical Union, Fall Meeting 2015*, abstract id. T32D-06.

Rossetti, L. M., D. Healy, M. J. Hole, J. M. Millett, E. F. de Lima, D. A. Jerram, and M. M. M. Rossetti, 2019, Evaluating petrophysical properties of volcano-sedimentary sequences: A case study in the Paraná-Etendeka Large Igneous Province: *Marine and Petroleum Geology*, v. 102, no. January, p. 638–656, doi:10.1016/j.marpetgeo.2019.01.028.

Rossetti, L., E. F. Lima, B. L. Waichel, M. J. Hole, M. S. Simões, and C. M. S. Scherer, 2018, Lithostratigraphy and volcanology of the Serra Geral Group, Paraná-Etendeka Igneous Province in Southern Brazil: Towards a formal stratigraphical framework: *Journal of Volcanology and Geothermal Research*, v. 355, p. 98–114, doi:10.1016/j.jvolgeores.2017.05.008.

Rossetti, L., E. F. Lima, B. L. Waichel, C. M. Scherer, and C. J. Barreto, 2014, Stratigraphical framework of basaltic lavas in Torres Syncline main valley, southern Parana-Etendeka Volcanic Province: *Journal of South American Earth Sciences*, v. 56, p. 409–421, doi:10.1016/j.jsames.2014.09.025.

Saunders, A. D., J. G. Fitton, A. C. Kerr, M. J. Norry, and R. W. Kent, 1997, The North Atlantic igneous province: *Geophysical Monograph Series*, v. 100, no. January, p. 45–93, doi:10.1029/GM100p0045.

Schofield, N. et al., 2017, Regional magma plumbing and emplacement mechanisms of the Faroe-Shetland Sill Complex: implications for magma transport and petroleum systems within sedimentary basins: *Basin Research*, v. 1, p. 23, doi:10.1111/bre.12164.

Schofield, N. et al., 2016, Sills in Sedimentary Basins and Petroleum Systems, in C. Breitkreuz, and S. Rocchi, eds., *Physical Geology of Shallow Magmatic Systems: Dykes, Sills and Laccoliths*: Cham, Switzerland, Springer, p. 273–294, doi:10.1007/11157_2015_17.

Schutter, S. R., 2003, Hydrocarbon occurrence and exploration in and around igneous rocks: *Geological Society Special Publication*, v. 214, p. 7–33, doi:10.1144/GSL.SP.2003.214.01.02.

Senger, K., J. Millett, S. Planke, K. Ogata, C. H. Eide, M. Festøy, O. Galland, and D. Jerram, 2017, Effects of igneous intrusions on the petroleum system: a review: *First Break*, v. 35, no. 6, p. 47–56, doi:10.3997/1365-2397.2017011

Single, R. T., and D. A. Jerram, 2004, The 3D facies architecture of flood basalt provinces and their internal heterogeneity: examples from the Palaeogene Skye Lava Field: *Journal of the Geological Society*, v. 161, p. 911–926, doi:<https://doi.org/10.1144/0016-764903-136>.

Skilling, I. P., J. D. L. White, and J. McPhie, 2002, Peperite: A review of magma-sediment mingling: *Journal of Volcanology and Geothermal Research*, v. 114, p. 1–17, doi:10.1016/S0377-0273(01)00278-5.

Stewart, K., S. Turner, S. Kelley, C. Hawkesworth, L. Kirstein, and M. Mantovani, 1996, 3-D, 40Ar-39Ar geochronology in the Paraná continental flood basalt province: *Earth and Planetary Science Letters*, v. 143, no. 1–4, p. 95–109, doi:10.1016/0012-821X(96)00132-X.

Stica, J. M., P. V. Zalán, and A. L. Ferrari, 2014, The evolution of rifting on the volcanic margin of the Pelotas Basin and the contextualization of the Paraná-Etendeka LIP in the separation of Gondwana in the South Atlantic: *Marine and Petroleum Geology*, v. 50, p. 1–21, doi:10.1016/j.marpetgeo.2013.10.015.

Thiede, D. S., and P. M. Vasconcelos, 2010, Paraná flood basalts: Rapid extrusion hypothesis confirmed by new 40Ar/39Ar results: *Geology*, v. 38, no. 8, p. 747–750, doi:10.1130/G30919.1.

Vedanti, N., K. J. P. Lakshmi, S. Dutta, A. Malkoti, and O. P. Pandey, 2015, Investigation of petrophysical properties and ultrasonic P-and S- wave attenuation in Deccan flood Basalts, India: SEG Technical Program Expanded Abstracts, v. 34, no. v, p. 3274–3278, doi:10.1190/segam2015-5858683.1.

Waichel, B. L., E. F. de Lima, A. R. Viana, C. M. Scherer, G. V. Bueno, and G. Dutra, 2012, Stratigraphy and volcanic facies architecture of the Torres Syncline, Southern Brazil, and its role in understanding the Paraná-Etendeka Continental Flood Basalt Province: *Journal of Volcanology and Geothermal Research*, v. 215–216, p. 74–82, doi:10.1016/j.jvolgeores.2011.12.004.

Waichel, B. L., E. F. Lima, C. A. Sommer, and R. Lubachesky, 2007, Peperite formed by lava flows over sediments: An example from the central Paraná Continental Flood Basalts, Brazil: *Journal of Volcanology and Geothermal Research*, v. 159, no. 4, p. 343–354, doi:10.1016/j.jvolgeores.2006.07.009.

Walker, G. P. L., 1971, Compound and Simple Lava Flows and Flood Basalts: *Bulletin Volcanologique*, v. 35, no. 3, p. 579–590.

Walker, G. P. L., 1970, The distribution of amygdale minerals in Mull and Morvern (West Scotland), in T. V. V. G. R. . Murty, and S. S. Rao, eds., *Studies in Earth Sciences, West Commemoration Volume*: India, University of Saugar, p. 181–194.

Walker, F., N. Schofield, J. Millett, D. Jolley, M. Hole, and M. Stewart, 2020, Paleogene volcanic rocks in the northern Faroe–Shetland Basin and Møre Marginal High: understanding lava field stratigraphy, in D. Chiarella, S. G. Archer, J. A. Howell, C. A.-L. Jackson, H. Kombrink, and S. Patruno, eds., *Cross-Border Themes in Petroleum Geology II: Atlantic Margin and Barents Sea.*: Geological Society, London, Special Publications, doi:10.1144/sp495-2019-13.

Watton, T. J., S. Cannon, R. J. Brown, D. A. Jerram, and B. L. Waichel, 2014, Using formation micro-imaging, wireline logs and onshore analogues to distinguish volcanic lithofacies in boreholes: Examples from Palaeogene successions in the Faroe-Shetland Basin, NE Atlantic: *Geological Society Special Publication*, v. 397, no. 1, p. 173–192, doi:10.1144/SP397.7.

Williamson, I. T., and B. R. Bell, 2012, The Staffa Lava formation: Graben-related volcanism, associated sedimentation and landscape character during the early

development of the palaeogene Mull Lava field, NW Scotland: Scottish Journal of Geology, v. 48, no. 1, p. 1–46, doi:10.1144/0036-9276/01-439.

Winter, W. R., R. J. Jahnert, and A. B. França, 2007, Bacia de Campos: Boletim de Geociencias da Petrobras, v. 15, no. 2, p. 511–529.

Wright, K. A., R. J. Davies, D. A. Jerram, J. Morris, and R. Fletcher, 2012, Application of seismic and sequence stratigraphic concepts to a lava-fed delta system in the Faroe-Shetland Basin, UK and Faroes: Basin Research, v. 24, no. 1, p. 91–106, doi:10.1111/j.1365-2117.2011.00513.x.

Wu, S., R. Zhu, Z. Yang, Z. Mao, J. Cui, and X. Zhang, 2019, Distribution and characteristics of lacustrine tight oil reservoirs in China: Journal of Asian Earth Sciences, v. 178, no. May 2018, p. 20–36, doi:10.1016/j.jseaes.2018.05.013.

Zakharova, N. V., D. S. Goldberg, E. C. Sullivan, M. M. Herron, and J. A. Grau, 2012, Petrophysical and geochemical properties of Columbia River flood basalt: Implications for carbon sequestration: Geochemistry, Geophysics, Geosystems, v. 13, no. 11, p. 1–22, doi:10.1029/2012GC004305.

Zhang, R., and J. Castagna, 2011, Seismic sparse-layer reflectivity inversion using basis pursuit decomposition: Geophysics, v. 76, no. 6, doi:10.1190/geo2011-0103.1.

Zucchetti, M., J. Costa, and I. de O. Carmo, 2015, Vulcanismo subaquoso nas bacias marginais brasileiras, in VI Simpósio de Vulcanismo e Ambientes Associados.

CAPÍTULO VI

Neste capítulo consiste em uma síntese integradora com as principais conclusões obtidas durante o desenvolvimento desta tese.

6. SÍNTESE E CONCLUSÕES

Os estudos desenvolvidos na porção norte da PIPE, região entre Uberlândia e Araguari, e seus resultados foram apresentados em três artigos científicos submetidos as revistas *Journal of Volcanology and Geothermal Research*, *Jounal of South American Earth Sciences* e *AAPG Bulletin*.

O primeiro artigo (capítulo V – seção 5.1) possibilitou um estudo detalhado das sucessões vulcânicas e sedimentares da porção nordeste da PIPE apoiado no uso de litofácies e associação de litofácies, e geoquímica. Foram identificadas dezesseis litofácies que foram agrupadas em cinco associação de litofácies: *pillow* lavas, lavas *pahoehoe* compostas, lavas *pahoehoe* simples, peperito e brecha basáltica de matriz infiltrada. As manifestações vulcânicas identificadas cobriram sedimentos fluvio-lacustres depositados sobre o embasamento cristalino e correspondem a derrames *pahoehoe* simples (~7 m de espessura total), derrames *pahoehoe* compostos (pacotes de até 7 m de espessura) e *pillow* lavas (pacotes de até 10 m de espessura). A formação destas últimas está associada à colocação das lavas sob baixas taxas de efusão em substrato subaquoso de baixa declividade.

Os derrames *pahoehoe* simples e intervalos peperíticos ocorrem predominantemente nas porções superiores da estratigrafia. O contato irregular e difuso entre a crosta superior desses basaltos e os peperitos superpostos, associado ao padrão irregular de distribuição das vesículas no topo desses basaltos, sugerem que esses corpos ígneos correspondam a intrusões rasas ou lavas invasivas. Brechas basálticas com matriz infiltrada por sedimentos ocorrem localmente nos níveis estratigráficos superiores. A presença de sedimentos originalmente inconsolidados ocorrendo entre essas lavas revelam períodos de quiescência da atividade vulcânica.

Lavas subaéreas e as *pillow* lavas são quimicamente similares, e são classificadas como basaltos subalcalinos e compatíveis com magmas do tipo Pitanga descritos na porção sul da PIPE por Peate et al. (1992).

Adicionalmente, a ocorrência de *pillow* lavas, depósitos sedimentares flúvio-lacustres e ostracodes indicam a presença de água nas áreas próximas a Uberlândia e Araguari durante o início do magmatismo. Essas ocorrências sugerem proximidade a um sistema de drenagem maior (rios e lagos associados), e/ou mudanças de um cenário predominantemente árido na porção sul para um paleoambiente mais úmido na porção norte da PIPE. Como *pillow* lavas e peperitos também foram descritos em outras partes da PIPE (em geral, ao longo das bordas E-NE), é provável que a ocorrência de um paleoambiente úmido não seja exclusiva da área investigada. A posição geográfica e as irregularidades do relevo podem explicar a ocorrência localizada de derrames subaquosos em corpos aquosos efêmeros de ambiente peridesértico. Entretanto, a presença comum de depósitos formados em condições úmidas na porção central da PIPE torna mudança paleoambiental decorrente do magmatismo uma alternativa possível.

A colocação desse imenso volume de lava da PIPE sobre os sedimentos inconsolidados da Bacia do Paraná resultou em uma série de produtos de interação entre lava e sedimento. Observações de campo desse tipo de interação feitas na região entre Uberlândia e Araguari (porção nordeste da PIPE), em conjunto com observações de campo feitas em Saint Cyrus (Bacia de Midland Valley, Escócia) e na Ilha de Mull (Campo de Lavas de Mull, Escócia), permitiram summarizar alguns diferentes tipos processos e produtos que podem se formar durante o início do vulcanismo em bacias sedimentares. Esses resultados foram apresentados no segundo artigo, apresentada no capítulo V (seção 5.2). Neste foram considerados dois tipos principais de lavas: lavas subaéreas e lavas invasivas. O contato desses dois tipos de lavas com as rochas sedimentares adjacentes pode variar de retilíneo a irregular com peperito associado. Além desses dois tipos de interação, estruturas de carga, peperito do tipo *pillow* e pseudocrateras (*rootless cones*) são feições frequentes nas áreas investigadas.

A formação de lavas invasivas, estruturas de carga e peperitos do tipo *pillow* está relacionada possivelmente a instabilidades gravitacionais e à baixa resistência à deformação dos sedimentos sotopostos. A instabilidade gravitacional é facilmente atingida durante a colocação de lavas basálticas (mais densas) sobre sedimentos inconsolidados (menos densos). A pressão direcional dada pelo fluxo da lava durante a colocação, e a redução temporária da resistência dos sedimentos (p. ex. por liquefação) são mecanismos viáveis para o desenvolvimento de lavas invasivas. A

redução da resistência dos sedimentos à deformação pode ser iniciada por diferentes processos tais como, eventos sísmicos, expansão dos fluidos de poro dos sedimentos, ou ainda a formação de peperito.

Alguns dos produtos de interação entre lava e sedimento descritos neste artigo foram identificados e descritos em sucessões vulcâno-sedimentares de bacias exploradas por companhias de óleo e gás. Estes processos aparentemente não modificam as rochas sedimentares abaixo, sendo, portanto, o impacto na qualidade do reservatório negligenciável e restrito a poucos metros a partir do contato lava-sedimento. Entretanto, lavas invasivas podem compartmentalizar o reservatório sedimentar levando a modificações no padrão de movimentação de fluidos e adicionar um grau de complexidade durante a correlação detalhada de reservatórios, principalmente em locais com informações limitadas (p.ex. testemunhos ou perfis de poços).

A investigação tanto das propriedades petrofísicas (porosidade e permeabilidade) quanto a caracterização em sísmica da sucessão vulcânica foram apresentadas e discutidas no terceiro artigo (capítulo 5 – seção 5.3).

Dados sobre propriedades físicas em rochas vulcânicas e sedimentares associadas são fundamentais para a caracterização de potenciais reservatórios relacionados à sequências vulcânicas. Adicionalmente, a investigação das características sísmicas de sucessões envolvendo modelos de sísmica sintética de afloramentos análogos permitem estabelecer correlações entre dados de campo e sua expressão em imagens sísmicas.

A caracterização da sucessão vulcânica em sísmica foi realizada a partir da integração de dados de campo e petrofísicos de laboratório da PIPE com dados geomorfológicos de afloramentos da NAIP. A combinação de resultados obtidos em afloramentos análogos de diferentes províncias ígneas permite construir e compreender o arranjo e a distribuição de fácies vulcânicas importantes dentro de sequências que carecem de exposição em escala sísmica (p.ex. afloramentos da porção norte da PIPE). Nessas circunstâncias, afloramentos de escamas sísmicas de regiões com litofácies e associação de litofácies similares (p.ex. afloramentos da Ilha de Mull) podem ser utilizadas. Desta forma, quatro modelos diferentes foram testados para investigação das variações nas respostas sísmicas da transição da base do

basalto em diferentes cenários geológicos e diferentes conteúdos de frequência (frequências dominantes de 30, 50 e 70 Hz).

Esses modelos sintéticos indicam que a resposta sísmica da transição sedimento-basalto pode variar bastante dependendo do conteúdo de frequência do dado sísmico, da complexidade geológica e do contraste de impedância entre as rochas vulcânicas e sedimentares sotopostas. Adicionalmente, os diferentes tipos de derrames (compostos e simples) resultam em refletores com geometrias e disposições específicas ocorrendo dentro da sucessão vulcânica, os quais são visíveis apenas nos modelos com maior conteúdo de frequência (frequências dominantes de 50 e 70 Hz).

A distinção entre lavas invasivas e intrusões tabulares rasas é dificultada pelo fato das características petrofísicas e geométricas de ambas serem semelhantes. Entretanto, algumas observações podem auxiliar na interpretação de possíveis cenários na base desses derrames. Por exemplo, a extensão de refletores transgressivos em direção à base da bacia sugere a ocorrência de intrusão, enquanto que a existência de lavas invasivas é sugerida pela presença de refletores que ocorrem invadindo as rochas sedimentares subjacentes, e que são conectados à base da sucessão vulcânica.

Finalmente, os dados de porosidade e permeabilidade de fácies peperíticas, quando comparados os dados de rochas sedimentares dentro da área de estudo, sugerem que o potencial reservatório pode ser melhorado durante a interação lava-sedimento. Entretanto, a complexidade desse tipo de rocha e o número limitado de análises obtidos reforçam a necessidade de estudos detalhados neste tipo de rocha que permitam entender melhor essa complexa relação entre lavas e sedimentos.

REFERÊNCIAS

Abdelmalak, M. M. et al. (2019) 'Breakup volcanism and plate tectonics in the NW Atlantic', *Tectonophysics*. Elsevier, 760(July 2017), pp. 267–296. doi: 10.1016/j.tecto.2018.08.002.

American Petroleum Institute (1998) Recommended practices for core analysis. Second edi, Recommended Practice 40. Second edi. New York: American Petroleum Institute.

Anderson, S. W. et al. (1998) ‘Block size distributions on silicic lava flow surfaces: implications for emplacement conditions’, Geological Society of America Bulletin, 110, pp. 1258–1267.

Aubele, J. C., Crumpler, L. S. and Elston, W. (1988) ‘Vesicle zonation and vertical structure of basalt flows’, Journal of Volcanology and Geothermal Research, 35, pp. 349–374.

Bailey, E. B. et al. (1924) ‘Tertiary and Post-Tertiary Geology of Mull, Loch Aline and Oban’, in Memoir of the Geological Survey of Great Britain. Edinburgh: HMSO.

Baksi, A. K. (2017) ‘Paraná flood basalt volcanism primarily limited to ~ 1 Myr beginning at 135 Ma: New 40 Ar/ 39 Ar ages for rocks from Rio Grande do Sul, and critical evaluation of published radiometric data’, Journal of Volcanology and Geothermal Research. Elsevier B.V., pp. 1–12. doi: 10.1016/j.jvolgeores.2017.02.016.

Barreto, C. J. S. et al. (2014) ‘Lithofacies analysis of basic lava flows of the Paraná igneous province in the south hinge of Torres Syncline, Southern Brazil’, Journal of Volcanology and Geothermal Research. Elsevier B.V., 285, pp. 81–99. doi: 10.1016/j.jvolgeores.2014.08.008.

Beckinsale, R. D. et al. (1978) ‘Geochemistry and Petrogenesis of the Early Tertiary Lava Pile of the Isle of Mull, Scotland’, Contributions to Mineralogy and Petrology, 67(4), p. 439. doi: 10.1007/BF00383303.

Bellieni, G. et al. (1984) ‘High- and Low-TiO₂ flood basalts from the Parana plateau (Brazil): petrology and geochemical aspects bearing on their mantle origin’, Neus Jahrbuch Miner. Abh, 150(3), pp. 273–306.

Brown, D. J. and Bell, B. R. (2007) ‘How do you grade peperites?’, Journal of Volcanology and Geothermal Research, 159(4), pp. 409–420. doi: 10.1016/j.jvolgeores.2006.08.008.

Brown, R. J. et al. (2011) ‘Aā lava flows in the Deccan Volcanic Province, India, and their significance for the nature of continental flood basalt eruptions’, Bulletin of Volcanology, 73(6), pp. 737–752. doi: 10.1007/s00445-011-0450-7.

Bryan, S. E. et al. (2010) ‘The largest volcanic eruptions on Earth’, Earth-Science Reviews. Elsevier B.V., 102(3–4), pp. 207–229. doi: 10.1016/j.earscirev.2010.07.001.

- Bryan, S. E. and Ernst, R. E. (2008) 'Revised definition of Large Igneous Provinces (LIPs)', *Earth-Science Reviews*, 86(1–4), pp. 175–202. doi: 10.1016/j.earscirev.2007.08.008.
- Bryan, S. E. and Ferrari, L. (2013) 'Large igneous provinces and silicic large igneous provinces: Progress in our understanding over the last 25 years', *Bulletin of the Geological Society of America*, 125(7–8), pp. 1053–1078. doi: 10.1130/B30820.1.
- Buckley, S. J. et al. (2019) 'LIME: Software for 3-D visualization, interpretation, and communication of virtual geoscience models', *Geosphere*, 15(1), pp. 222–235. doi: 10.1130/GES02002.1.
- Busby-Spera, C. J. and White, J. D. L. (1987) 'Variation in peperito textures associated with differing host sediment properties', *Bulletin of Volcanology*, 49, pp. 765–775.
- Caineng, Z. et al. (2013) *Volcanic Reservoirs in Petroleum Exploration*. Beijing: Elsevier. doi: 10.1016/B978-0-12-397163-0.09993-0.
- Chambers, L. M. and Pringle, M. S. (2001) 'Age and duration of activity at the Isle of Mull Tertiary igneous centre, Scotland, and confirmation of the existence of subchrons during Anomaly 26r', *Earth and Planetary Science Letters*, 193(3–4), pp. 333–345. doi: 10.1016/S0012-821X(01)00499-X.
- Coffin, M. F. and Eldholm, O. (1992) 'Volcanism and continental break-up: a global compilation of large igneous provinces', *Geological Society, London, Special Publications*, 68(1), pp. 17–30. doi: 10.1144/GSL.SP.1992.068.01.02.
- Coffin, M. F. and Eldholm, O. (1994) 'Large Igneous Provinces : Crustal Structure , Dimensions ', *Reviews of Geophysics*, 32, pp. 1–36.
- Costa, J. (2015) Estratigrafia e geoquímica da sequência de lavas da Província Magmática do Paraná na região da Usina De Itaipu (PR). Universidade Federal do Paraná.
- Degraff, J. M., Philip, E. L. and Aydin, A. (1989) 'Use of joint-growth directions and rock textures to infer thermal regimes during solidification of basaltic lava flows', *Journal of Volcanology and Geothermal Research*, 38, pp. 309–324. doi: [https://doi.org/10.1016/0377-0273\(89\)90045-0](https://doi.org/10.1016/0377-0273(89)90045-0).

- Dimroth, E. et al. (1978) ‘Structure and organization of Archean subaqueous basalt flows, Rouyn- Noranda area, Quebec, Canada: Canadian’, Journal of Earth Science, 15, pp. 902–918.
- Duraiswami, R. A. et al. (2014) ‘Pahoehoe-a’ा transitions in the lava flow fields of the western Deccan Traps, India-implications for emplacement dynamics, flood basalt architecture and volcanic stratigraphy’, Journal of Asian Earth Sciences. Pergamon, 84, pp. 146–166. doi: 10.1016/j.jseaes.2013.08.025.
- Ebinghaus, A. et al. (2014) ‘Lava – Sediment Interaction and Drainage-System Development in a Large Igneous’, Journal of Sedimentary Research, 84, pp. 1041–1063.
- Eldholm, O. and Grue, K. (1994) ‘North Atlantic volcanic margins: Dimensions and production rates’, Journal of Geophysical Research, 99(B2), pp. 2955–2968. doi: 10.1029/93JB02879.
- Emeleus, C. . (1991) ‘Tertiary igneous activity.pdf’, in Craig, G. Y. (ed.) Geology of Scotland. London: Geological Society, pp. 455–502.
- Emeleus, C. . and Bell, B. . (2005) ‘Igneous geology : regional setting, Palaeogene volcanic districts of Scotland’, in British Regional Geology. Nottingham: British Geological Survey.
- Ferreira, C. M. (1985) ‘Ocorrência de “pillow lava” em vulcanitos da Fm Serra Geral em Araguari, MG’, in 3o simpósio de geologia de Minas Gerais. Belo Horizonte: Anais do 3o simpósio de geologia de Minas Gerais, pp. 235–237.
- Forbes, a. E. S., Blake, S. and Tuffen, H. (2014) ‘Entablature: Fracture types and mechanisms’, Bulletin of Volcanology, 76, p. 820. doi: 10.1007/s00445-014-0820-z.
- Ganerød, M. et al. (2008) ‘Reassembling the Paleogene-Eocene North Atlantic igneous province: New paleomagnetic constraints from the Isle of Mull, Scotland’, Earth and Planetary Science Letters, 272(1–2), pp. 464–475. doi: 10.1016/j.epsl.2008.05.016.
- Gifkins, C. C., McPhie, J. and Allen, R. L. (2002) ‘Pumiceous rhyolitic peperite in ancient submarine volcanic successions’, Journal of Volcanology and Geothermal Research, 114(1–2), pp. 181–203. doi: 10.1016/S0377-0273(01)00284-0.

- Gillis, K. M. and Sapp, K. (1997) 'Distribution of porosity in a section of upper oceanic crust exposed in the Troodos Ophiolite', *Journal of Geophysical Research*, 102(B5), pp. 133–149.
- Goehring, L. (2008) On the scaling and ordering of columnar joints. University of Toronto.
- Gonçalves, L., Compan, A. L. M. and Wanderley, L. dos R. (2019) 'Principais técnicas laboratoriais utilizadas na avaliação petrofísica de reservatórios carbonáticos do pré-sal', in 10o Congresso Brasileiro de Pesquisa e Desenvolvimento em Petróleo e Gás.
- Gregg, T. K. . and Fink, J. H. (2000) 'A laboratory investigation into the effects of slope on lava flow morphology', *Journal of Volcanology and Geothermal Research*. Elsevier, 96(3–4), pp. 145–159. doi: 10.1016/S0377-0273(99)00148-1.
- Gregg, T. K. P. (2017) 'Patterns and processes: Subaerial lava flow morphologies: A review', *Journal of Volcanology and Geothermal Research*. Elsevier, 342, pp. 3–12. doi: 10.1016/J.JVOLGEORES.2017.04.022.
- Gregg, T. K. P. and Fink, J. H. (1995) 'Quantification of submarine lava-flow morphology through analog experiments', *Geology*, 23(1), pp. 73–76. doi: 10.1130/0091-7613(1995)023<0073:QOSLFM>2.3.CO;2.
- Gregg, T. K. P. and Fornari, D. J. (1998) 'Long submarine lava flows: Observations and results from numerical modeling', *Journal of Geophysical Research: Solid Earth*, 103(B11), pp. 27517–27531. doi: 10.1029/98jb02465.
- Grossenbacher, K. A. and McDuffie, S. M. (1995) 'Conductive cooling of lava: columnar joint diameter and stria width as functions of cooling rate and thermal gradient', *Journal of Volcanology and Geothermal Research*. Elsevier, 69(1–2), pp. 95–103. doi: 10.1016/0377-0273(95)00032-1.
- Guilbaud, M. et al. (2005) 'Morphology, surface structures, and emplacement of lavas produced by Laki, A.D.', *Geological Society of America Special Papers*, pp. 1783–1784. doi: 10.1130/0-8137-2396-5.81.
- Hamilton, C. W. et al. (2017) 'Rootless tephra stratigraphy and emplacement processes', *Bulletin of Volcanology*. *Bulletin of Volcanology*, 79(1), pp. 1–19. doi: 10.1007/s00445-016-1086-4.

Hansen, J. et al. (2009) 'The onset of the North Atlantic Igneous Province in a rifting perspective', *Geological Magazine*, 146(3), pp. 309–325. doi: 10.1017/S0016756809006347.

Hanson, R. E. and Wilson, T. J. (1993) 'Large-scale rhyolite peperites (Jurassic, southern Chile)', *Journal of Volcanology and Geothermal Research*. Elsevier, 54(3–4), pp. 247–264. doi: 10.1016/0377-0273(93)90066-Z.

Harris, A. J. L. et al. (2017) 'Pahoehoe, 'a'a, and block lava: an illustrated history of the nomenclature', *Bulletin of Volcanology*. *Bulletin of Volcanology*, 79(1). doi: 10.1007/s00445-016-1075-7.

Hawkesworth, C. J. et al. (2000) 'Tectonic controls on magmatism associated with continental break-up: an example from the Paraná-Etendeka Province', *Science*, 179, pp. 335–349. doi: 10.1016/S0012-821X(00)00114-X.

Hole, M. et al. (2013) 'Lava – sediment interactions in an Old Red Sandstone basin, NE Scotland', *Jounal of the Geological Society*, 170, pp. 641–655. doi: 10.1144/jgs2012-107.

Hon, K., Gansecki, C. and Kauahikaua, J. (2003) 'The transition from 'a'a to pāhoehoe crust on flows emplaced during the Pu'u 'Ō'ō - Kūpaianaha eruption', US Geological Survey Professional Paper.

Hunns, S. R. and McPhie, J. (1999) 'Pumiceous peperite in a submarine volcanic succession at Mount Chalmers, Queensland, Australia', *Journal of Volcanology and Geothermal Research*, 88(4), pp. 239–254. doi: 10.1016/S0377-0273(99)00015-3.

Jackson, C. A. L., Schofield, N. and Golenkov, B. (2013) 'Geometry and controls on the development of igneous sill-related forced folds: A 2-D seismic reflection case study from offshore southern Australia', *Bulletin of the Geological Society of America*, 125(11–12), pp. 1874–1890. doi: 10.1130/B30833.1.

Jerram, D. A. (2002) 'Volcanology and facies architecture of flood basalts', in Menzies, M. A. et al. (eds) *Volcanic Rifted Margins*. Colorado: Geological Society of America Special Paper, pp. 121–135. doi: <https://doi.org/10.1130/0-8137-2362-0.119>.

Jerram, D. A. et al. (2009) 'Understanding the offshore flood basalt sequence using onshore volcanic facies analogues: An example from the Faroe-Shetland basin', *Geological Magazine*, 146(3), pp. 353–367. doi: 10.1017/S0016756809005974.

- Jerram, D. A. and Petford, N. (2014) Descrição de Rochas Ígneas: guia geológico de campo. 2nd edn. Porto Alegre: Bookman.
- Jerram, D. A. and Stollhofen, H. (2002) ‘Lava-sediment interaction in desert settings; are all peperite-like textures the result of magma-water interaction?’, *Journal of Volcanology and Geothermal Research*, 114(1–2), pp. 231–249. doi: 10.1016/S0377-0273(01)00279-7.
- Jerram, D. A. and Widdowson, M. (2005) ‘The anatomy of Continental Flood Basalt Provinces: geological constraints on the processes and products of flood volcanism’, *Lithos*. Elsevier, 79(3–4), pp. 385–405. doi: 10.1016/J.LITHOS.2004.09.009.
- Jones, J. G. (1969) ‘Pillow Lavas as Depth Indicators’, *American Journal of Science*, 267, pp. 181–195.
- Kent, R. W. et al. (1998) ‘Emplacement of Hebridean Tertiary flood basalts: evidence from an inflated pahoehoe lava flow on Mull, Scotland’, *Journal of the Geological Society*, 155(4), pp. 599–607. doi: 10.1144/gsjgs.155.4.0599.
- Kerr, A. C. (1995a) ‘The geochemical stratigraphy, field relations and temporal variation of the Mull-Morvern Tertiary lava succession, NW Scotland’, *Transactions of the Royal Society of Edinburgh: Earth Sciences*, 86(1), pp. 35–47. doi: 10.1017/S0263593300002145.
- Kerr, A. C. (1995b) ‘The geochemistry of the Mull-Morvern Tertiary lava succession, NW Scotland: an assessment of mantle sources during plume-related volcanism’, *Chemical Geology*, 122(1–4), pp. 43–58. doi: 10.1016/0009-2541(95)00009-B.
- Kerr, A. C. et al. (1999) ‘Geochemical evolution of the Tertiary Mull volcano, western Scotland’, *Journal of Petrology*, 40(6), pp. 873–908. doi: 10.1093/petroj/40.6.873.
- Keszthelyi, L. (2002) ‘Classification of the Mafica Lava Flows from ODP leg 183’, 183, pp. 1–28. doi: 10.4996/fireecology.0701013.
- Keszthelyi, L. et al. (2004) ‘Icelandic analogs to Martian flood lavas’, *Geochemistry, Geophysics, Geosystems*, 5, p. 14. doi: 10.1029/2004GC000758.
- Kokelaar, B. P. (1982) ‘Fluidization of wet sediments during the emplacement and cooling of various igneous bodies.’, *Journal of the Geological Society*, 139(1), pp. 21–33. doi: 10.1144/gsjgs.139.1.0021.

- Larsen, L. M., Pedersen, A. K. and Pedersen, G. K. (2006) 'A subaqueous rootless cone field at Niuluut, Disko, Paleocene of West Greenland', *Lithos*, 92, pp. 20–32.
- Long, P. E. and Wood, B. J. (1986) 'Structures, textures, and cooling histories of Columbia River basalt flows (USA).', *Geological Society of America Bulletin*, 97(9), pp. 1144–1155. doi: [https://doi.org/10.1130/0016-7606\(1986\)97<1144:STACHO>2.0.CO;2](https://doi.org/10.1130/0016-7606(1986)97<1144:STACHO>2.0.CO;2).
- Loock, S., Benjamin, van W. de V. and Hénot, J. M. (2010) 'Clinker formation in basaltic and trachybasaltic lava flows', *Bulletin of Volcanology*, 72(7), pp. 859–870. doi: 10.1007/s00445-010-0362-y.
- Lore, J., Gao, H. J. and Aydin, A. (2000) 'Viscoelastic thermal stress in cooling basalt flows', *Journal of Geophysical Research Solid Earth*, 105, pp. 23695–23709.
- Luchetti, A. C. F. et al. (2014) 'New insights on the occurrence of peperites and sedimentary deposits within the silicic volcanic sequences of the Paraná Magmatic Province, Brazil', *Solid Earth*, 5(1), pp. 121–130. doi: 10.5194/se-5-121-2014.
- Lyle, P. (2000) 'The eruption environment of multi-tiered columnar basalt lava flows', *Journal of the Geological Society*, 157, pp. 715–722. doi: 10.1144/jgs.157.4.715.
- Macdonald, G. A. (1953) 'Pahoehoe, aa, and block lava', *American Journal of Science*, 251, pp. 169–191.
- Magee, C., Hunt-Stewart, E. and Jackson, C. A. L. (2013) 'Volcano growth mechanisms and the role of sub-volcanic intrusions: Insights from 2D seismic reflection data', *Earth and Planetary Science Letters*. Elsevier, 373, pp. 41–53. doi: 10.1016/j.epsl.2013.04.041.
- Mano, V. G. T. (1987) Estudos geológicos e geotécnicos das descontinuidades rochosas, 'pillow lavas' e paleocanal nos basaltos de fundação da barragem de Nova Avanhandava, Rio Tiete (SP). Universidade de São Paulo.
- Mantovani, M. S. M. et al. (1985) 'Trace element and strontium isotope constraints on the origin and evolution of Paraná continental flood basalts of Santa Catarina state (Southern Brazil)', *Journal of Petrology*, 26, pp. 187–209.
- Marques Filho, P. L. et al. (1981) 'Características usuais e aspectos peculiares do manto de alteração e transição solo-rocha em basaltos', in *Congresso Brasileiro de*

Engenharia. Itapema: Congresso Brasileiro de Geologia de Engenharia, ABGE, pp. 53–72.

McPhee, C., Reed, J. and Zubizarreta, I. (2015) Routine Core Analysis, Developments in Petroleum Science. doi: 10.1016/B978-0-444-63533-4.00005-6.

Mcphie, J., Doyle, M. and Allen, R. (1993) Volcanic Textures: A guide to the interpretation of textures in volcanic rocks. University of Tasmania.

Melfi, A. J., Piccirillo, E. M. and Nardy, A. J. R. (1988) 'Geological and magmatic aspects of the Paraná Basin an introduction', in Piccirillo, E. M. and Melfi, A. J. (eds) The Mezosoic Flood Volcanism of the Paraná Basin: Petrogenetic and Geophysical Aspects. IAG-USP, pp. 1–13.

Merle, R. et al. (2005) 'Segregation vesicles, cylinders, and sheets in vapor-differentiated pillow lavas: Examples from Tore-Madeira Rise and Chile Triple Junction', Journal of Volcanology and Geothermal Research, 141(1–2), pp. 109–122. doi: 10.1016/j.jvolgeores.2004.09.007.

Milani, E. J. et al. (2007) 'Bacia do Paraná', Boletim de Geociências da Petrobras, 15(2), pp. 265–287.

Milani, E. J. and Zalán, P. V (1999) 'An outline of the geology and petroleum systems of the Paleozoic interior basins of South America', Petrobras, 22(3), pp. 199–205.

Milani, Edison José and Thomaz Filho, Antonio (2000) 'Sedimentary Basins of South America', in Cordani, U. G. et al. (eds) Tectonic Evolution of South America. Rio de Janeiro: 31 International Geological Congress, pp. 389–449.

Mizusaki, A. M. P., Thomaz Filho, A. and Valença, J. (1988) 'Volcano-sedimentary sequence of Neocomian age in Campos Basin (Brazil)', Revista Brasileira de Geociências, 18(3), pp. 247–251. doi: 10.25249/0375-7536.1988247251.

Mizuzaki, A. M. P. (1986) Rochas ígneo-básicas do Neocomiano da Bacia do Campos - Caracterização e comportamento como reservatório de hidrocarbonetos. Universidade Federal do Rio de Janeiro.

Moore, J. G. (1965) 'Petrology of Deep-Sea Basalt Near Hawaii', American Journal of Science, 263, pp. 40–52.

Moraes, L. C. de and Seer, H. J. (2017) 'Pillow lavas and fluvio-lacustrine deposits in the northeast of Paraná Continental Magmatic Province, Brazil', Journal of

Volcanology and Geothermal Research. Elsevier, 355, pp. 78–86. doi: 10.1016/J.JVOLGEORES.2017.03.024.

Morrison, M. A., Thompson, R. N. and Dickin, A. P. (1985) ‘Geochemical evidence for complex magmatic plumbing during development of a continental volcanic center.’, *Geology*, 13(8), pp. 581–584. doi: 10.1130/0091-7613(1985)13<581:GEFCMP>2.0.CO;2.

Nardy, A. J. R., Machado, F. B. and F, O. M. A. (2008) ‘As rochas vulcânicas mesozóicas ácidas da Bacia do Paraná: litoestratigrafia e considerações geoquímico-estratigráficas’, *Brazilian Journal of ...*, 38(1), pp. 178–195. Available at: <http://rbg.sbg.org.br/index.php/rbg/article/view/1353>.

Németh, K. and Martin, U. (2007) ‘Practical Volcanology. Lecture Notes for understanding Volcanic Rocks from Field Based Studies.’, Occasional Papers of the Geological Institute of Hungary. Budapest, 207.

Oliver, G. J. H., Wilde, S. A. and Wan, Y. (2008) ‘Geochronology and geodynamics of Scottish granitoids from the late neoproterozoic break-up of Rodinia to Palaeozoic collision’, *Journal of the Geological Society*, 165(3), pp. 661–674. doi: 10.1144/0016-76492007-105.

Peate, D. P., Hawkesworth, C. J. and Mantovani, M. S. (1992) ‘Chemical stratigraphy of the Paraná lavas (South America): classification of magma types and their spatial distribution’, *Bulletin of Volcanology*, 55, pp. 119–139. doi: DOI: 10.1007/BF00301125.

Peate, D. W. (1997) ‘The Parana-Etendeka Province’, in Mahoney, J. J. and Coffin, M. F. (eds) Large Igneous Provinces: Continental, Oceanic, and Planetary Flood Volcanism. Geophysical Monographs: American Geophysical Union, pp. 217–245. doi: 10.1029/GM100p0217.

Peterson, D. W. and Tilling, R. I. (1980) ‘Transition of basaltic lava from pahoehoe to aa, Kilauea Volcano, Hawaii: Field observations and key factors’, *Journal of Volcanology and Geothermal Research*, 7, pp. 271–293. doi: 10.1016/0377-0273(80)90033-5.

Petry, K. et al. (2007) ‘Volcanic-sedimentary features in the Serra Geral Fm., Paraná Basin, southern Brazil: Examples of dynamic lava-sediment interactions in an arid setting’, 159, pp. 313–325. doi: 10.1016/j.jvolgeores.2006.06.017.

Phillips, J. C. et al. (2013) Columnar Joints Produced by Cooling in Basalt, *Journal of business ethics*. doi: 10.1063/1.2756072.

Philpotts, A. R. and Lewis, C. L. (1987) 'Pipe vesicles – an alternative model for their origin', *Geology*, 15, pp. 971–974.

Pinkerton, H. and Sparks, R. S. J. (1976) 'The 1975 sub-terminal lavas, Mount Etna: a case history of the formation of a compound lava field', *Journal of Volcanology and Geothermal Research*, 1, pp. 167–182.

Planke, S. et al. (2000) 'Seismic volcanostratigraphy of large-volume basaltic extrusive complexes on rifted margins', *Journal of Geophysical Research: Solid Earth*, 105(B8), pp. 19335–19351. doi: 10.1029/1999jb900005.

Planke, S. et al. (2005) 'Seismic characteristics and distribution of volcanic intrusions and hydrothermal vent complexes in the Vøringsfjord and Møre basins', *Petroleum Geology Conference Proceedings*, 6(0), pp. 833–844. doi: 10.1144/0060833.

Rawcliffe, H. J. (2016) *Lava - Water - Sediment Interaction: Processes, Products and Petroleum Systems*. University of Glasgow.

Renne, P. R. et al. (1992) 'The Age of Parana Flood Volcanism , Rifting of Gondwanaland, and the Jurassic-Cretaceous boundary', *Science*, 258, pp. 975–979. doi: 10.1126/science.258.5084.975.

Renne, P. R. et al. (1996) 'Age of the Ponta Grossa dike swarm (Brazil), and implications to Paraná flood volcanism', *Earth and Planetary Science Letters*. Elsevier, 144(1–2), pp. 199–211. doi: 10.1016/0012-821x(96)00155-0.

Renne, P. R. (2015) 'Age and Duration of the Paraná-Etendeka Flood Basalts and Related Plumbing System', American Geophysical Union, Fall Meeting 2015, abstract id. T32D-06.

Rossetti, L. et al. (2018) 'Lithostratigraphy and volcanology of the Serra Geral Group, Paraná-Etendeka Igneous Province in Southern Brazil: Towards a formal stratigraphical framework', *Journal of Volcanology and Geothermal Research*. Elsevier B.V., 355, pp. 98–114. doi: 10.1016/j.jvolgeores.2017.05.008.

Rossetti, L. M. et al. (2014) 'Stratigraphical framework of basaltic lavas in Torres Syncline main valley, southern Parana-Etendeka Volcanic Province', *Journal of South*

American Earth Sciences. Pergamon, 56, pp. 409–421. doi: 10.1016/J.JSAMES.2014.09.025.

Rowland, S. K. and Walker, G. P. L. (1987) ‘Toothpaste lava: characteristics and origin of a lava structural type transition between pahoehoe and aa’, *Bulletin of Volcanology*, 49, pp. 631–641.

Rowland, S. K. and Walker, G. P. L. (1990) ‘Pahoehoe and aa in Hawaii: volumetric flow rate controls the lava structure’, *Bulletin of Volcanology*, 52, pp. 615–628. doi: 10.1007/BF00301212.

Ryan, M. and Sammis, C. (1978) ‘Cyclic fracture mechanisms in cooling basalt’, *Geological Society of America Bulletin*, 89(9), pp. 1295–1308. doi: [https://doi.org/10.1130/0016-7606\(1978\)89<1295:CFMICB>2.0.CO;2](https://doi.org/10.1130/0016-7606(1978)89<1295:CFMICB>2.0.CO;2).

Saemundsson, K. (1970) ‘Interglacial lava flows in the lowlands of southern Iceland and the problem of two-tiered columnar jointing’, *Jokull*, 20, pp. 62–77.

Saunders, A. D. et al. (1997) ‘The North Atlantic igneous province’, *Geophysical Monograph Series*, 100(January), pp. 45–93. doi: 10.1029/GM100p0045.

Schaefer, C. J. and Kattenhorn, S. a. (2004) ‘Characterization and evolution of fractures in low-volume pahoehoe lava flows, eastern Snake River Plain, Idaho’, *Bulletin of the Geological Society of America*, 116(3–4). doi: 10.1130/B25335.1.

Schmiedel, T. et al. (2017) ‘Mechanisms of overburden deformation associated with the emplacement of the Tulipan sill, mid-Norwegian margin’, *Interpretation*, 5(3), pp. SK23–SK38. doi: 10.1190/INT-2016-0155.1.

Schofield, N. et al. (2016) ‘Sills in Sedimentary Basins and Petroleum Systems’, in Breitkreuz, C. and Rocchi, S. (eds) *Physical Geology of Shallow Magmatic Systems: Dykes, Sills and Laccoliths*. Cham, Switzerland: Springer, pp. 273–294. doi: 10.1007/11157_2015_17.

Self, S. et al. (1996) ‘A new model for emplacement of Columbia River basalts as large, inflated pahoehoe lava flow fields’, *Geophysical Research Letters*, 23(19), pp. 2689–2692. doi: 10.1029/96GL02450.

Self, S., Keszthelyi, L. and Thordarson, T. (1998) ‘The importance of pahoehoe’, *Annu. Rev. Earth Planet. Sci.*, 26, pp. 81–110. doi: 10.1146/annurev.earth.26.1.81.

- Single, R. T. and Jerram, D. A. (2004) 'The 3D facies architecture of flood basalt provinces and their internal heterogeneity: examples from the Palaeogene Skye Lava Field', *Journal of the Geological Society*, 161, pp. 911–926. doi: <https://doi.org/10.1144/0016-764903-136>.
- Skilling, I. P., White, J. D. L. and McPhie, J. (2002) 'Peperite: A review of magma-sediment mingling', *Journal of Volcanology and Geothermal Research*, 114, pp. 1–17. doi: 10.1016/S0377-0273(01)00278-5.
- Soule, S. A. et al. (2005) 'Channelized lava flows at the East Pacific Rise crest 9°–10°N: The importance of off-axis lava transport in developing the architecture of young oceanic crust', *Geochemistry, Geophysics, Geosystems*, 6(8). doi: 10.1029/2005GC000912.
- Stevenson, J. A. et al. (2012) 'Widespread inflation and drainage of a pāhoehoe flow field: The Nesjahraun, Pingvellir, Iceland', *Bulletin of Volcanology*, 74, pp. 15–31. doi: 10.1007/s00445-011-0482-z.
- Stewart, K. et al. (1996) '3-D, 40Ar-39Ar geochronology in the Paraná continental flood basalt province', *Earth and Planetary Science Letters*. Elsevier, 143(1–4), pp. 95–109. doi: 10.1016/0012-821X(96)00132-X.
- Stica, J. M., Zalán, P. V. and Ferrari, A. L. (2014) 'The evolution of rifting on the volcanic margin of the Pelotas Basin and the contextualization of the Paraná-Etendeka LIP in the separation of Gondwana in the South Atlantic', *Marine and Petroleum Geology*. Elsevier Ltd, 50, pp. 1–21. doi: 10.1016/j.marpetgeo.2013.10.015.
- Thiede, D. S. and Vasconcelos, P. M. (2010) 'Paraná flood basalts: Rapid extrusion hypothesis confirmed by new 40Ar/39Ar results', *Geology*, 38(8), pp. 747–750. doi: 10.1130/G30919.1.
- Thirlwall, M. F. (1981) 'Implications for Caledonian plate tectonic models of chemical data from volcanic rocks of the British Old Red Sandstone', *Journal of the Geological Society*, 138(2), pp. 123–138. doi: 10.1144/gsjgs.138.2.0123.
- Thirlwall, M. F. (1988) 'Geochronology of Late Caledonian magmatism in northern Britain', *Journal - Geological Society (London)*, 145(6), pp. 951–967. doi: 10.1144/gsjgs.145.6.0951.

Thompson, R. N. et al. (1986) 'Two contrasting styles of interaction between basic magmas and continental crust in the British Tertiary Volcanic Province', *Journal of Geophysical Research*, 91(B6), p. 5985. doi: 10.1029/jb091ib06p05985.

Umino, S. (2000) 'Subaqueous lava flow lobes , observed on ROV KAIKO dives off Hawaii', 7613(June). doi: 10.1130/0091-7613(2000)28<503.

Velev, S. and Nedialkov, R. (2011) 'Comparison of geological , textural and petrographic characteristics of the pillow lava flows from the areas of Malo Buchino , Babitsa and Nedelkovo villages (Western Srednogorie)', in Bulgarian Geological Society, Nacional Conference eith international participation 'Geosciences 2011', pp. 75–76.

Waichel, B. L. et al. (2007) 'Peperite formed by lava flows over sediments: An example from the central Paraná Continental Flood Basalts, Brazil', *Journal of Volcanology and Geothermal Research*, 159(4), pp. 343–354. doi: 10.1016/j.jvolgeores.2006.07.009.

Waichel, B. L. et al. (2012) 'Stratigraphy and volcanic facies architecture of the Torres Syncline, Southern Brazil, and its role in understanding the Paraná-Etendeka Continental Flood Basalt Province', *Journal of Volcanology and Geothermal Research*. Elsevier B.V., 215–216, pp. 74–82. doi: 10.1016/j.jvolgeores.2011.12.004.

Waichel, B. L., Lima, E. F. and Sommer, C. A. (2006) 'Tipos de Derrame e Reconhecimento de Estruturas nos Basaltos da Formação Serra Geral : Terminologia e Aspectos de Campo', *Pesquisas em Geociencias*, 33(2), pp. 123–133. Available at: <http://www.ufrgs.br/igeo/pesquisas/3302/11-3302.pdf>.

Walker, G. P. L. (1987) 'Pipe vesicles in Hawaiian basalt lavas: their origin and potential as paleoslope indicators', *Geology*, 15, pp. 84–87.

Walker, G. P. L. (1992) 'Morphometric study of pillow-size spectrum among pillow lavas', *Bulletin of Volcanology*, 54, pp. 459–474. doi: 10.1007/BF00301392.

Watton, T. J. et al. (2013) 'Three-dimensional lithofacies variations in hyaloclastite deposits', *Journal of Volcanology and Geothermal Research*. Elsevier B.V., 250, pp. 19–33. doi: 10.1016/j.jvolgeores.2012.10.011.

Watton, T. J. et al. (2014) 'The petrophysical and petrographical properties of hyaloclastite deposits: Implications for petroleum exploration', *AAPG Bulletin*, 98(3), pp. 449–463. doi: 10.1306/08141313029.

- White, J. D. L., Mcphie, J. and Skilling, I. (2000) 'Peperite: A useful genetic term', *Bulletin of Volcanology*, 62(1), pp. 65–66. doi: 10.1007/s004450050293.
- White, J. D. L., McPhie, J. and Soule, S. A. (2015) Submarine Lavas and Hyaloclastite. Second Edition, *The Encyclopedia of Volcanoes*. Second Edition. Elsevier Inc. doi: 10.1016/b978-0-12-385938-9.00019-5.
- White, R. and McKenzie, D. (1989) 'Magmatism at rift zones: The generation of volcanic continental margins and flood basalts', *Journal of Geophysical Research*, 94(B6), p. 7685. doi: 10.1029/JB094iB06p07685.
- Williamson, I. T. and Bell, B. R. (2012) 'The Staffa Lava formation: Graben-related volcanism, associated sedimentation and landscape character during the early development of the palaeogene Mull Lava field, NW Scotland', *Scottish Journal of Geology*, 48(1), pp. 1–46. doi: 10.1144/0036-9276/01-439.
- Wright, K. A. et al. (2012) 'Application of seismic and sequence stratigraphic concepts to a lava-fed delta system in the Faroe-Shetland Basin, UK and Faroes', *Basin Research*, 24(1), pp. 91–106. doi: 10.1111/j.1365-2117.2011.00513.x.
- Yamagishi, H. (1985) 'Growth of pillow lobes - evidence from pillow lavas of Hokkaido, Japan, and North Island, New Zealand.', *Geology*, 13, pp. 499–502.

Anexo A

Cartas de submissão dos artigos

Carta de resubmissão do artigo intitulado “*Lithostratigraphy of the Serra Geral Formation in the northern portion of the Paraná-Etendeka Igneous Province: a tool for tracking early Cretaceous paleoenvironmental changes*” submetido para o *Journal of Volcanology and Geothermal Research*.

Received revision VOLGEO_2020_15_R2

Journal of Volcanology and Geothermal Research <EviseSupport@elsevier.com>

21 de agosto de 2020

14:52

Responder a: volgeo-eo@elsevier.com

Para: natfamelli@gmail.com

This message was sent automatically.

Ref: VOLGEO_2020_15_R2

Title: LITHOSTRATIGRAPHY OF THE SERRA GERAL FORMATION IN THE NORTHERN PORTION OF THE PARANÁ-ETENDEKA IGNEOUS PROVINCE: A TOOL FOR TRACKING EARLY-CRETACEOUS PALEOENVIRONMENTAL CHANGES

Journal: Journal of Volcanology and Geothermal Research

Dear Miss. FAMELLI,

Thank you for submitting your revised manuscript for consideration for publication in Journal of Volcanology and Geothermal Research. Your revision was received in good order.

To track the status of your manuscript, please log into EVISE® http://www.evise.com/evise/faces/pages/navigation/NavController.jspx?JRNL_ACR=VOLGEO and locate the submission under the header 'My Submissions with Journal' on your 'My Author Tasks' view.

We appreciate your submitting your revision to this journal.

Kind regards,

Journal of Volcanology and Geothermal Research

Have questions or need assistance?

For further assistance, please visit our [Customer Support](#) site. Here you can search for solutions on a range of topics, find answers to frequently asked questions, and learn more about EVISE® via interactive tutorials. You can also talk 24/5 to our customer support team by phone and 24/7 by live chat and email.

Copyright © 2018 Elsevier B.V. | [Privacy Policy](#)

Elsevier B.V., Radarweg 29, 1043 NX Amsterdam, The Netherlands, Reg. No. 33156677.

Carta de resubmissão do artigo intitulado “*Characterizing the nature and importance of lava-sediment interactions in sedimentary basins with the aid of field outcrop analogues*” submetido para o *Journal of South American Earth Sciences*.

Confirming submission to Journal of South American Earth Sciences

Journal of South American Earth Sciences <em@editorialmanager.com>
Responder a: Journal of South American Earth Sciences <sames@elsevier.com>
Para: Natália Famelli <natfamelli@gmail.com>

21 de agosto de 2020 17:09

This is an automated message.

CHARACTERIZING THE NATURE AND IMPORTANCE OF LAVA-SEDIMENT INTERACTIONS IN SEDIMENTARY BASINS WITH THE AID OF FIELD OUTCROP ANALOGUES

Dear Ms. Famelli,

We have received the above referenced manuscript you submitted to Journal of South American Earth Sciences.

To track the status of your manuscript, please log in as an author at <https://www.editorialmanager.com/sames/>, and navigate to the "Submissions Being Processed" folder.

Thank you for submitting your work to this journal.

Kind regards,
Journal of South American Earth Sciences

More information and support

You will find information relevant for you as an author on Elsevier's Author Hub: <https://www.elsevier.com/authors>

FAQ: How can I reset a forgotten password?

https://service.elsevier.com/app/answers/detail/a_id/28452/supporthub/publishing/

For further assistance, please visit our customer service site: <https://service.elsevier.com/app/home/supporthub/publishing/>

Here you can search for solutions on a range of topics, find answers to frequently asked questions, and learn more about Editorial Manager via interactive tutorials. You can also talk 24/7 to our customer support team by phone and 24/7 by live chat and email

In compliance with data protection regulations, you may request that we remove your personal registration details at any time. (Use the following URL: <https://www.editorialmanager.com/sames/login.asp?a=r>). Please contact the publication office if you have any questions.

Carta de resubmissão do artigo intitulado “*Understanding the petrophysical properties, seismic responses and impacts of the basalt-sediment transition in prospective sedimentary basins.*” submetido para *AAPG Bulletin*.

Submission Confirmation for AAPG Bulletin BLTN20-158

1 mensagem

AAPG Bulletin <em@editorialmanager.com>
Responder a: AAPG Bulletin <bulletin@aapg.org>
Para: Natália Famelli <natfamelli@gmail.com>

18 de setembro de 2020 20:31

RE: BLTN20-158

Dear natfamelli,

Your submission, "UNDERSTANDING THE PETROPHYSICAL PROPERTIES, SEISMIC RESPONSES AND IMPACTS OF THE BASALT-SEDIMENT TRANSITION IN PROSPECTIVE SEDIMENTARY BASINS." has been received by journal AAPG Bulletin.

You will be able to check on the progress of your paper by logging on to Editorial Manager as an author. The URL is <https://www.editorialmanager.com/bltn/>. Please be aware that the review process can take up to 4 months to complete - this is mainly due to reviewer availability.

Please use the manuscript number BLTN20-158 when corresponding about your submission.

Thank you for submitting your work to this journal.

Kind regards,

AAPG Bulletin

In compliance with data protection regulations, you may request that we remove your personal registration details at any time. (Use the following URL: <https://www.editorialmanager.com/bltn/login.asp?a=r>). Please contact the publication office if you have any questions.

Anexo B

Localização dos perfis e afloramentos contemplados nas figuras do artigo intitulado “Lithostratigraphy of the Serra Geral Formation in the northern portion of the Paraná-Etendeka Igneous Province: a tool for tracking early Cretaceous paleoenvironmental changes”. Datum: WGS-84.

Log	East (X)	North (Y)	Zone	Band
Log A	781208	7910589	22	K
Log B	789942	7917506	22	K
Log C	790753	7925050	22	K
Log D	794464	7927119	22	K
Log E	804721	7938916	22	K

Figure	Picture code	East (X)	North (Y)	Zone	Band
Figure 3	A	792719	7926879	22	K
	B	792719	7926879	22	K
	C	790888	7929554	22	K
	D	791090	7929192	22	K
	E	791090	7929192	22	K
	F	791090	7929192	22	K
Figure 4	A	791090	7929192	22	K
	B	792334	7926823	22	K
	C	794071	7927168	22	K
	D	794335	7925957	22	K
	E	793951	7926948	22	K
	F	792579	7928645	22	K
Figure 5	A	794310	7925807	22	K
	B	794364	7925996	22	K
	C	793951	7926948	22	K
	D	794364	7925996	22	K
Figure 7	A	792948	7927881	22	K
	B	792719	7926879	22	K
	C	793033	7926987	22	K
	D	792948	7927881	22	K
Figure 9	A	794276	7925816	22	K
	B	793951	7926948	22	K
	C	794335	7925957	22	K
Figure 10	A	794364	7925996	22	K
	B	793951	7926948	22	K
	C	781208	7910589	22	K

Anexo C

*Dados das análises de difratometria de raios-x para as amostras da área de
Uberlândia e Araguari.*

IS – Interbedded sedimentary rocks; PP – Host sediment of peperitic domain; GB – Glassy-basaltic breccia; SP – Simple pahoehoe; PL – Pillow lavas; CP – Compound pahoehoe.

Whole rock mineralogical composition of the (%)																				
SAMPLE	MT	C+P	HEM	KFD	PLG	QTZ	OTI	PIR	PRX	ZEO	CAL	SID	APT	ANL	MAG	OLI	ANT	DOL	ANF	MHM
Sedimentary rocks																				
UB-01	IS	4	TR	6	3	87	-	-	-	-	-	-	-	-	-	-	-	-		
UB-03a	IS	12	-	8	5	74	-	-	-	1	-	-	-	-	-	-	-	-		
UB-17e	PP	9	-	18	7	66	-	PR	-	-	-	-	-	-	-	-	-	-		
UB-20a	PP	2	-	13	27	30	-	TR	17	11	-	-	-	-	-	-	-	-		
UB-21a	PP	17	-	10	8	65	?	-	-	-	-	-	-	-	-	-	-	-		
UB-27a	IS	19	-	26	10	45	-	TR	-	-	-	-	-	-	-	-	-	-		
UB-29a	IS	9	PR	5	2	84	-	-	-	-	-	-	-	-	-	-	-	-		
UB-32a	IS	27	-	6	10	34	?	-	-	-	23	-	-	-	-	-	-	-		
UB-32e	GB	21		6	-	69				4			-	-	-	-	-	-		
UB-32f	IS	7	-	11	3	79	-	-	-	-	-	-	-	-	-	-	-	-		
UB-32J	GB	37		7	3	40				9		4	-	-	-	-	-	-		
UB-32m	GB	67	-	2	6	-	3	PR	10	3	6				3	-	-	-		
UB-33a	GB	60		26	-	5			2	-		-	1	6	-					
UB-33e	GB	63		14	5	2		4		TR		8	-	-	4					
UB-33g	GB	8	-	6	3	81	-	-	-	2	-				-	-	-	-		
UB-40a	IS	2	-	7	2	89	-	-	-	-	?				-	-	-	-		
UB-51b	IS	7	PR	13	6	74	-	-	-	-	-				-	-	-	-		
UB-60a	PP	21	2	15	13	48	-	-	-	1	-				-	-	-	-		
UB-62a	IS	7	1	8	-	84	-	-	-	-	-				-	-	-	-		
UB-63a	IS	1	-	8	3	88	-	-	-	-	-				-	-	-	-		
UB-64a	GB	15	?	5	5	71	-	-	-	2	PR				-	2	-	-		
UB-68	IS	6	-	5	-	89	-	-	-	-	-				-	-	-	-		
UB-70a	GB	57	1	18	-	22	1	-	-	-	-				-	-	1			

Whole rock mineralogical composition of the (%)																				
SAMPLE	MT	C+P	HEM	KFD	PLG	QTZ	OTI	PIR	PRX	ZE0	CAL	SID	APT	ANL	MAG	OLI	ANT	DOL	ANF	MHM
UB-71a	IS	31	3	14	15	14	1	-	22	-	-	-	-	-	-	-	-	-	-	
UB-72a	IS	5	-	8	5	81	-	-	-	-	-	-	1	-	-	?	-	-	-	
UB-72b	IS	19	PR	5	5	33	-	-	-	-	-	-	36	-	PR	2	-	-	-	

Volcanic rocks

UB-16b	SP	17	-	6	42	TR	-	TR	35	-	-	-	-	TR	-	-	-	-
UB-16e	SP	4	-	3	44	TR	2	-	47	-	-	-	TR	-	-	-	-	-
UB-16g	SP	19	-	10	41	TR	1	TR	29	-	-	-	-	TR	-	-	-	-
UB-17d	SP	9	-	4	45	TR	5	TR	37	-	-	-	-	-	-	-	-	-
UB-18a	SP	9	-	1	46	TR	4	-	40	-	-	-	-	-	-	-	-	-
UB-20c	SP	13	-	2	43	TR	4	-	38	-	-	-	-	-	-	-	-	-
UB-20d	SP	3	-	3	47	TR	4	1	42	-	-	-	-	-	-	-	-	-
UB-25b	SP	TR	-	5	48	TR	3	-	44	-	-	-	-	-	-	-	-	-
UB-25d	SP	3	-	2	47	TR	3	-	45	-	-	-	-	-	-	-	-	-
UB-26b	SP	13	-	1	42	4	3	?	37	-	-	-	-	-	-	-	-	-
UB-27c	SP	TR	-	5	49	1	4	TR	41	-	-	-	-	TR	-	-	-	-
UB-27d	SP	3	-	3	46	TR	4	-	44	-	-	-	-	-	-	-	-	-
UB-28a	SP	16	-	2	42	?	2	-	38	-	-	-	-	-	-	-	-	-
UB-30a	SP	12	-	3	43	TR	5	TR	37	-	-	-	-	-	-	-	-	-
UB-32b	PL	19	-	13	37	TR	2	1	28	-	-	-	-	-	-	-	-	-
UB-32c	PL	14	-	15	39	-	-	5	27	-	-	-	-	-	-	-	-	-
UB-32d	PL	17	-	13	38	?	4	1	27	-	-	-	-	-	-	-	-	-
UB-32g	PL	15	-	5	41	TR	?	4	35	-	-	-	-	-	-	-	-	-
UB-32h	PL	15	-	7	37	?	5	1	35	-	-	-	-	-	-	-	-	-
UB-32i	PL	26	-	11	35	TR	4	TR	24	-	-	-	-	-	-	-	-	-
UB-32l	CP	12	-	8	43	?	?	5	32	-	-	-	-	-	-	-	-	-
UB-33d	PL	15	-	10	39	TR	2	1	33	-	-	-	-	-	-	-	-	-

Whole rock mineralogical composition of the (%)

SAMPLE	MT	C+P	HEM	KFD	PLG	QTZ	OTI	PIR	PRX	ZEO	CAL	SID	APT	ANL	MAG	OLI	ANT	DOL	ANF	MHM
UB-33f	SP	6	-	7	43	TR	4	-	40	-	-	-	-	-	-	-	-	-	-	
UB-34a	SP	4	-	5	40	TR	5	-	46	-	-	-	-	-	-	-	-	-	-	

MT= Morphology type; C+P=Clay minerals + phyllosilicates; HEM=Hematite; KFD=K-Feldspar; PLG=Plagioclase; QTZ=Quartz; OTI=Titanium Oxide; PIR=Pyrite; PRX=Pyroxene; ZEO=Zeolite; CAL=Calcite; SID=Siderite; APT=Apatite; ANL=Analcime; MAG=Magnesite; OLI=Olivine; ANT=Anatase; DOL=Dolomite; ANF=Amphibole; MHM=Maghemite.

Clay fraction mineral composition (%)

SAMPLE	MT	ILI	ISO	ESM	CAU	ISI	CLO	Observations
--------	----	-----	-----	-----	-----	-----	-----	--------------

Sedimentary rocks

UB-01a	IS	55	45	-	-	-	-	Presence of quartz.
UB-03a	IS	61	30	-	2	7	-	-
UB-17e	PP	42	5	-	45	8	-	Presence of quartz.
UB-20a	PP	5	-	-	?	94	1	Presence of quartz, k-feldspar and plagioclase.
UB-21a	PP	64	28	-	-	-	8	Presence of quartz.
UB-27a	IS	9	-	-	3	88	-	Presence of quartz.
UB-29a	IS	43	10	-	47	-	-	Presence of quartz.
UB-32a	IS	10	3	86	-	-	1	Presence of quartz and calcite.
UB-32e	GB	68	3	-		28	1	Presence of quartz, K-feldspar and calcite.
UB-32f	IS	72	28	-	-	-	-	Presence of quartz.
UB-32j	GB	70	6	-		22	2	Presence of quartz, K-feldspar and calcite.
UB-32m	GB	53	31	-	-	15	1	Presence of quartz.
UB-33a	GB	4	-	96		-	-	Presence of calcite.
UB-33e	GB	63	-	-		36	1	Presence of quartz.
UB-33g	GB	64	7	-	-	29	-	Presence of quartz and zeolite.
UB-40a	IS	8	4	87	1	-	-	Presence of quartz.

Clay fraction mineral composition (%)

SAMPLE	MT	ILI	ISO	ESM	CAU	ISI	CLO	Observations
UB-51b	IS	64	28	-	-	8	-	Presence of quartz and K-feldspar.
UB-60a	PP	7	-	-	-	93	-	Presence of quartz, k-feldspar, and plagioclase.
UB-62a	IS	4	2	-	-	85	9	Presence of quartz.
UB-63a	IS	5	5	-	1	88	1	Presence of quartz.
UB-64a	GB	50	15	-	-	30	5	Presence of quartz.
UB-68	IS	52	17	-	-	31	-	Presence of quartz.
UB-70a	GB	32	6	-	-	60	2	Presence of quartz.
UB-71a	IS	30	8	-	-	60	2	Presence of quartz.
UB-72a	IS	15	16	66	-	-	3	Presence of quartz and calcite.
UB-72b	IS	8	4	88	-	-	TR	Presence of quartz and calcite.

Volcanic rocks

UB-16b	SP	17	-	83	-	-	-	Presence of k-feldspar and plagioclase.
UB-16g	SP	7	-	93	-	-	-	Presence of quartz.
UB-17d	SP	5	-	-	-	95	-	Presence of plagioclase.
UB-18a	SP	1	-	99	-	-	-	Presence of non-identified organic components.
UB-20c	SP	4	-	-	-	96	-	Presence of quartz, k-feldspar, and plagioclase.
UB-20d	SP	2	-	-	-	98	-	Presence of k-feldspar and plagioclase.
UB-25b	SP	2	-	98	?	-	-	Presence of quartz and plagioclase.
UB-25d	SP	2	-	98	?	-	-	Presence of plagioclase.
UB-26b	SP	1	-	99	?	-	-	Presence of plagioclase.
UB-27c	SP	-	-	-	-	100	-	Presence of k-feldspar and plagioclase.
UB-27d	SP	2	-	-	-	98	-	Presence of k-feldspar and plagioclase.
UB-28a	SP	9	-	-	-	91	-	Presence of non-identified organic components, k-feldspar, and plagioclase.
UB-30a	SP	?	-	100	-	-	-	Presence of plagioclase.
UB-32b	PL	8	-	90	2	-	?	Presence of quartz, k-feldspar, and plagioclase.

Clay fraction mineral composition (%)

SAMPLE	MT	ILI	ISO	ESM	CAU	ISI	CLO	Observations
UB-32c	PL	4	-	94	2	-	?	Presence of quartz,k-feldspar, and plagioclase.
UB-32d	PL	3	-	95	1	-	1	Presence of quartz,k-feldspar, and plagioclase.
UB-32g	PL	3	-	96	?	-	1	Presence of quartz,k-feldspar, and plagioclase.
UB-32h	PL	2	-	97	?	-	1	Presence of quartz,k-feldspar, and plagioclase.
UB-32i	PL	9	-	90	1	-	?	Presence of quartz.
UB-32l	CP	3	-	93	3	-	1	Presence of quartz, k-feldspar, and plagioclase.
UB-33d	PL	3	-	-	-	96	1	Presence of quartz, k-feldspar, and plagioclase.
UB-33f	SP	1	-	-	-	99	-	Presence of plagioclase and possible tri-octahedral smectite.
UB-34a	SP	6	-	93	-	-	1	Presence of non-identified organic components and plagioclase.

MT= Morphology type; ILI=Ilite; ISO= Ilite-Smectite - ordered interstratified clay mineral; ESM=Smectite; CAU=Kaolinite; ISI= Ilite-Smectite - irregular interstratified clay mineral; CLO=Chlorite; ?= occurrence not confirmed, TR=Trace (<1%).

Anexo D

Geochemical data of basalts from Uberlândia-Araguari region-MG/Brazil.

CP - Compound pahoehoe lava flows; SP – Simple pahoehoe lava flows; PL – Pillow lavas.

Sample	D.Lim	A.Method	UB-08b	UB-6a	UB-16b	UB-16e	UB-17d	UB-18a	UB-20c	UB-20d	UB-23a	UB-23c	UB-23e	UB-25a	UB-25d	UB-26b	UB-26c	UB-27b	UB-27c
Morph. Type			CP	SP	SP	SP	SP	SP	SP	SP	SP	SP	SP	SP	SP	SP	SP	SP	
Major elements (wt%)																			
SiO ₂	0.01	FUS-ICP	49.49	48.77	50.21	50.15	50.49	49.53	50.79	50.72	50.47	50.61	50.51	50.39	50.29	48.95	50.52	50.71	51.05
TiO ₂	0.001	FUS-ICP	4.02	3.19	3.12	3.13	3.44	3.18	3.47	3.46	3.46	3.53	3.47	3.32	3.19	3.18	3.16	3.38	3.38
Al ₂ O ₃	0.01	FUS-ICP	12.17	13.03	12.76	13.04	13.04	13.88	12.70	12.99	12.54	13.24	12.99	13.52	13.28	13.16	13.19	13.07	12.51
Fe ₂ O ₃ (T)	0.01	FUS-ICP	15.63	14.30	14.64	14.63	14.21	13.81	14.19	14.41	14.80	14.76	14.26	14.08	13.75	14.36	14.44	15.00	14.35
MnO	0.001	FUS-ICP	0.23	0.23	0.21	0.19	0.19	0.19	0.19	0.20	0.20	0.21	0.20	0.20	0.20	0.19	0.20	0.20	0.19
MgO	0.01	FUS-ICP	4.38	5.26	5.46	5.32	4.82	5.14	4.63	4.74	4.95	5.01	4.92	5.28	5.20	5.38	5.20	4.76	4.65
CaO	0.01	FUS-ICP	8.60	9.69	9.72	9.71	9.15	10.02	9.30	9.19	9.15	9.37	9.16	9.91	9.85	10.04	9.95	9.18	9.09
Na ₂ O	0.01	FUS-ICP	2.58	2.33	2.36	2.50	2.49	2.29	2.63	2.70	2.65	2.71	2.60	2.52	2.39	2.25	2.51	2.56	2.57
K ₂ O	0.01	FUS-ICP	0.94	1.54	1.17	0.66	1.08	0.84	1.01	0.79	0.69	0.83	0.85	0.83	0.80	0.60	0.74	1.02	0.99
P ₂ O ₅	0.01	FUS-ICP	0.54	0.35	0.35	0.35	0.40	0.35	0.49	0.42	0.42	0.42	0.44	0.35	0.37	0.36	0.36	0.43	0.41
LOI		FUS-ICP	0.61	0.46	0.14	0.11	0.31	0.52	0.11	-0.16	-0.08	-0.23	1.26	-0.07	0.36	0.45	-0.20	-0.23	0.36
Total	0.01	FUS-ICP	99.18	99.14	100.10	99.81	99.62	99.76	99.50	99.44	99.25	100.50	100.70	100.30	99.67	98.92	100.10	100.10	99.55
Minor elements (ppm)																			
Ba	2	FUC-ICP	507	371	371	413	474	353	424	400	383	407	423	343	346	303	346	417	406
Co	1	FUC-MS	65	43	43	44	43	43	42	41	41	40	40	42	41	43	40	40	40
Ni	20	FUC-MS	70	100	90	90	90	100	80	80	80	80	50	90	90	90	90	90	80
Sc	1	FUC-ICP	30	33	33	33	32	33	32	32	32	32	32	33	33	33	33	32	32
Rb	1	FUC-MS	20	31	21	18	20	14	19	21	19	19	23	19	20	11	17	26	28
Sr	2	FUC-ICP	512	466	458	474	467	517	467	455	470	494	490	479	471	484	485	470	472
Ta	0.01	FUC-MS	1.56	1.28	1.26	1.32	1.49	1.33	1.52	1.48	1.45	1.39	1.25	1.29	1.30	1.32	1.37	1.47	1.44
Nb	0.2	FUC-MS	20	17	16	17	20	18	20	21	20	19	19	18	18	18	18	18	20
Th	0.05	FUC-MS	3.21	2.61	2.52	2.54	2.95	2.55	2.98	2.98	2.97	2.96	2.62	2.55	2.60	2.55	2.54	2.96	2.95
U	0.01	FUC-MS	0.67	0.58	0.51	0.53	0.60	0.55	0.61	0.65	0.59	0.65	0.65	0.52	0.56	0.53	0.51	0.63	0.59
V	5	FUC-ICP	482	481	469	467	470	479	492	492	483	494	458	478	467	475	480	480	480
Zr	1	FUC-ICP	244	187	190	192	221	193	228	226	219	222	238	198	197	192	194	220	227
Y	0.5	FUC-MS	40	29	29	30	33	30	35	35	33	33	34	30	30	30	30	33	34
Pb	5	FUC-MS	5						5	5	5	5			6	5	5	6	
Hf	0.1	FUC-MS	5.9	4.7	4.5	4.6	5.6	4.9	5.6	5.4	5.4	5.3	5.8	4.8	4.8	5.1	4.8	5.3	5.5
La	0.05	FUC-MS	32.3	25.1	24.4	25.5	29.0	25.7	30.1	29.9	29.3	29.4	30.5	25.9	26.0	26.1	26.5	30.8	29.8
Ce	0.05	FUC-MS	74.7	57.9	56.3	59.5	66.8	59.3	70.1	69.0	67.2	68.3	67.6	59.8	60.4	60.7	60.5	70.2	68.5
Pr	0.01	FUC-MS	9.99	7.51	7.32	7.67	8.68	7.62	9.01	9.01	8.63	8.73	8.44	7.73	7.78	7.79	7.78	9.06	8.77
Nd	0.05	FUC-MS	44.30	32.90	31.80	33.90	37.80	33.50	38.70	38.50	37.90	38.00	37.90	33.80	34.00	34.20	39.20	38.30	

Sample	D.Lim	A.Method	UB-08b	UB-6a	UB-16b	UB-16e	UB-17d	UB-18a	UB-20c	UB-20d	UB-23a	UB-23c	UB-23e	UB-25a	UB-25d	UB-26b	UB-26c	UB-27b	UB-27c
Morph. Type			CP	SP	SP	SP	SP	SP	SP	SP	SP	SP	SP	SP	SP	SP	SP	SP	SP
Sm	0.01	FUC-MS	10.70	7.49	7.50	7.95	8.45	7.92	8.96	8.95	8.72	8.84	8.06	7.73	8.01	7.90	7.86	9.11	8.90
Eu	0.005	FUC-MS	3.34	2.40	2.42	2.54	2.72	2.52	2.78	2.78	2.71	2.77	2.72	2.53	2.46	2.57	2.55	2.83	2.70
Gd	0.01	FUC-MS	9.94	6.94	6.77	7.37	8.20	7.26	8.12	8.34	8.08	8.11	7.26	7.35	7.33	7.41	7.17	8.44	8.17
Tb	0.01	FUC-MS	1.50	1.07	1.03	1.11	1.21	1.10	1.27	1.26	1.24	1.27	1.14	1.12	1.12	1.14	1.10	1.25	1.23
Dy	0.01	FUC-MS	7.96	6.02	5.86	6.31	6.89	6.29	7.00	7.15	6.87	7.10	6.43	6.13	6.24	6.31	6.35	7.09	6.97
Ho	0.01	FUC-MS	1.48	1.13	1.07	1.15	1.28	1.15	1.32	1.30	1.29	1.28	1.26	1.12	1.14	1.13	1.17	1.30	1.26
Er	0.01	FUC-MS	3.88	2.91	2.93	3.07	3.46	3.11	3.61	3.39	3.46	3.47	3.37	2.98	3.10	3.09	3.17	3.54	3.40
Tm	0.005	FUC-MS	0.55	0.41	0.40	0.41	0.49	0.41	0.49	0.48	0.48	0.47	0.45	0.42	0.42	0.45	0.44	0.50	0.46
Yb	0.01	FUC-MS	3.27	2.55	2.51	2.71	3.06	2.62	3.01	3.05	3.06	2.95	2.85	2.67	2.63	2.66	2.73	3.15	3.03
Lu	0.002	FUC-MS	0.47	0.37	0.37	0.37	0.43	0.38	0.44	0.44	0.44	0.43	0.43	0.40	0.38	0.39	0.41	0.45	0.43

Sample	D.Lim	A.Method	UB-27d	UB-28a	UB-30a	UB-32b	UB-32c	UB-32d	UB-32g	UB-32h	UB-32i	UB-32l	UB-33c	UB-33d	UB-33f	UB-34a	UB-40c	UB-48	UB-55b
Morph. Type			SP	SP	SP	PL	PL	PL	PL	PL	CP	PL	PL	SP	SP	SP	SP	SP	SP

Major elements (wt%)

SiO ₂	0.01	FUS-ICP	50.98	47.50	50.59	48.91	48.50	48.80	47.20	48.55	47.78	46.33	50.69	50.97	50.92	49.99	49.53	49.27	49.59
TiO ₂	0.001	FUS-ICP	3.42	3.50	3.86	3.47	3.92	3.92	3.55	3.49	3.67	3.66	4.03	3.86	3.20	3.06	3.17	3.16	3.03
Al ₂ O ₃	0.01	FUS-ICP	13.03	13.08	12.26	13.94	13.83	13.77	12.82	12.69	13.75	13.36	13.15	13.31	13.14	13.21	13.21	13.29	12.82
Fe ₂ O ₃ (T)	0.01	FUS-ICP	14.43	15.17	15.66	14.83	15.19	14.02	15.31	14.61	13.85	16.52	13.81	14.54	14.66	14.23	14.65	14.58	14.04
MnO	0.001	FUS-ICP	0.21	0.23	0.21	0.25	0.26	0.25	0.29	0.26	0.22	0.26	0.18	0.19	0.19	0.18	0.20	0.20	0.20
MgO	0.01	FUS-ICP	4.65	5.10	4.20	4.18	4.01	4.34	5.42	5.60	5.13	5.09	3.25	3.41	5.43	5.07	5.48	5.50	5.47
CaO	0.01	FUS-ICP	9.28	9.70	8.67	7.55	8.06	7.95	8.91	8.34	7.73	8.11	8.17	8.17	9.78	9.67	9.88	9.87	9.79
Na ₂ O	0.01	FUS-ICP	2.59	2.05	2.62	2.34	2.69	2.67	2.33	2.26	2.44	2.51	2.40	2.52	2.38	2.40	2.50	2.50	2.36
K ₂ O	0.01	FUS-ICP	0.91	0.86	0.99	3.07	2.64	2.55	1.12	1.50	2.36	1.45	1.25	1.50	0.95	0.81	0.85	0.82	0.83
P ₂ O ₅	0.01	FUS-ICP	0.42	0.40	0.53	0.49	0.53	0.51	0.41	0.43	0.46	0.43	0.70	0.57	0.34	0.35	0.38	0.37	0.34
LOI		FUS-ICP	0.17	1.36	-0.14	1.27	0.82	0.81	1.23	1.31	1.11	1.11	1.19	0.10	-0.41	-0.28	0.70	0.88	0.92
Total	0.01	FUS-ICP	100.10	98.95	99.45	100.30	100.40	99.60	98.60	99.05	98.50	98.83	98.82	99.14	100.60	98.68	100.60	100.40	99.38

Minor elements (ppm)

Ba	2	FUC-ICP	408	676	548	407	511	490	473	507	489	650	736	556	359	334	348	370	404
Co	1	FUC-MS	39	41	41	38	37	42	40	37	37	42	48	46	42	40	43	42	54
Ni	20	FUC-MS	80	90	50	50	50	50	60	50	50	60	50	60	110	100	70	70	90

Sample	D.Lim	A.Method	UB-27d	UB-28a	UB-30a	UB-32b	UB-32c	UB-32d	UB-32g	UB-32h	UB-32i	UB-32l	UB-33c	UB-33d	UB-33f	UB-34a	UB-40c	UB-48	UB-55b
Morph. Type			SP	SP	SP	PL	PL	PL	PL	PL	CP	PL	PL	SP	SP	SP	SP	SP	
Sc	1	FUC-ICP	32	32	29	28	31	32	28	28	29	29	31	29	33	32	33	33	32
Rb	1	FUC-MS	22	21	17	45	20	15	11	11	15	10	22	25	16	18	18	19	21
Sr	2	FUC-ICP	469	573	511	496	502	494	503	498	497	543	613	564	473	447	495	490	477
Ta	0.01	FUC-MS	1.44	1.42	1.52	1.70	1.90	1.88	1.75	1.76	1.73	1.77	2.30	2.08	1.34	1.28	1.08	1.07	1.10
Nb	0.2	FUC-MS	20	20	21	24	27	26	25	25	25	26	28	30	19	17	17	17	17
Th	0.05	FUC-MS	2.99	2.78	2.96	3.59	4.02	4.01	3.69	3.79	3.69	3.74	4.00	4.25	2.42	2.38	2.25	2.27	2.20
U	0.01	FUC-MS	0.61	0.45	0.60	1.31	1.10	1.57	1.40	1.56	1.16	1.23	0.80	0.87	0.52	0.50	0.54	0.57	0.50
V	5	FUC-ICP	479	510	477	426	482	466	511	503	457	542	435	431	470	459	449	444	445
Zr	1	FUC-ICP	226	217	246	277	320	315	285	275	295	298	329	304	194	189	210	206	202
Y	0.5	FUC-MS	34	36	36	42	45	45	39	39	40	41	44	43	29	28	29	30	30
Pb	5	FUC-MS	6	5	5	8	7	8	6	7	6	6	6	7					
Hf	0.1	FUC-MS	5.5	5.4	6.1	6.6	7.3	7.4	6.9	7.0	6.9	7.2	7.6	7.4	4.7	4.5	5.1	4.8	5.0
La	0.05	FUC-MS	30.3	26.6	32.0	38.8	40.3	39.8	37.1	38.4	38.3	37.5	45.2	44.0	26.0	25.8	26.2	26.0	25.7
Ce	0.05	FUC-MS	69.0	62.0	74.7	88.2	93.8	93.4	84.6	87.3	87.3	87.7	101.0	101.0	60.1	59.0	58.5	57.2	57.4
Pr	0.01	FUC-MS	8.90	8.24	9.84	11.30	11.80	11.90	10.80	11.10	11.10	11.10	12.90	12.70	7.60	7.56	7.25	7.23	7.14
Nd	0.05	FUC-MS	38.30	36.60	43.00	48.70	51.70	51.30	46.50	47.70	48.00	47.70	54.30	54.30	33.30	33.00	31.40	30.50	30.70
Sm	0.01	FUC-MS	8.80	8.37	10.10	11.00	11.70	11.80	10.80	10.70	10.80	10.80	11.60	12.20	7.72	7.63	7.01	7.12	7.02
Eu	0.005	FUC-MS	2.77	2.76	3.35	3.49	3.65	3.73	3.35	3.38	3.35	3.43	3.73	3.76	2.47	2.48	2.30	2.36	2.32
Gd	0.01	FUC-MS	8.22	8.02	9.49	10.00	11.00	10.90	10.10	9.80	10.00	10.10	11.20	11.10	7.19	7.05	6.46	6.81	6.22
Tb	0.01	FUC-MS	1.24	1.19	1.43	1.54	1.64	1.61	1.51	1.49	1.46	1.51	1.60	1.64	1.07	1.10	1.00	1.10	1.00
Dy	0.01	FUC-MS	6.84	6.64	7.79	8.72	9.10	9.06	8.30	8.32	8.24	8.44	8.90	9.07	6.09	6.12	5.85	5.89	5.81
Ho	0.01	FUC-MS	1.29	1.24	1.43	1.62	1.65	1.69	1.48	1.51	1.52	1.54	1.60	1.69	1.11	1.10	1.10	1.12	1.07
Er	0.01	FUC-MS	3.39	3.39	3.72	4.40	4.45	4.57	4.04	4.02	4.02	4.02	4.40	4.35	3.03	2.91	3.02	3.01	2.90
Tm	0.005	FUC-MS	0.47	0.47	0.51	0.60	0.62	0.64	0.56	0.55	0.57	0.57	0.58	0.60	0.42	0.40	0.41	0.40	0.41
Yb	0.01	FUC-MS	3.02	2.95	3.27	3.68	3.81	3.95	3.40	3.44	3.51	3.53	3.70	3.81	2.56	2.59	2.36	2.39	2.56
Lu	0.002	FUC-MS	0.46	0.45	0.48	0.53	0.54	0.56	0.50	0.48	0.51	0.50	0.52	0.55	0.37	0.37	0.38	0.38	0.38

Blank spaces correspond to values below detection limits.

Anexo E

Petrophysical data of basalts from the Parané-Etendeka Igneous Province.

Sample I.D.	Orientation	Lithology	Position within lava flow	Porosity (%)	Permeability (mD)	Grain Den. (g/cm³)	Rock Den. (g/cm³)
UB-01	Not oriented	Sandstone	-	16.6	72.2	2.62	2.17
UB-29a H	Horizontal	Sandstone	-	6.6	0.137	2.64	2.46
UB-29a V	Vertical	Sandstone	-	6.6	0.0041	2.64	2.46
UB-31a	Not oriented	Sandstone	-	3.5	-	2.58	2.47
UB-32f	Not oriented	Sandstone	-	9.4	0.011	2.64	2.38
UB-03a	Not oriented	Mudstone	-	7.4	0.0001	2.37	2.18
UB-32a H	Horizontal	Mudstone	-	14.6	0.011	2.61	2.23
UB-32a V	Vertical	Mudstone	-	13.2	0.001	2.62	2.27
UB-17a H	Horizontal	Peperite	-	13.5	0.017	2.61	2.24
UB-17a V	Vertical	Peperite	-	16.1	0.198	2.59	2.15
UB-20a	Not oriented	Peperite	-	19.3	0.062	2.74	2.21
UB-21a H	Horizontal	Peperite	-	9.2	0.149	2.62	2.38
UB-21a V	Vertical	Peperite	-	3.9	-	2.56	2.45
UB-27a	Not oriented	Peperite	-	18.0	0.201	2.64	2.15
UB-16a H	Horizontal	Basalt	Crust	0.3	0.0001	2.91	2.90
UB-16a V	Vertical	Basalt	Crust	0.4	0.0001	2.92	2.89
UB-16b H	Horizontal	Basalt	Crust	1.2	0.103	2.92	2.86
UB-16b V	Vertical	Basalt	Crust	0.3	-	2.94	2.91
UB-16g H	Horizontal	Basalt	Crust	24.7	0.020	2.84	2.05
UB-16g V	Vertical	Basalt	Crust	22.0	0.014	2.84	2.14
UB-18a H	Horizontal	Basalt	Crust	1.4	0.0001	2.86	2.82
UB-18a V	Vertical	Basalt	Crust	2.0	0.0001	2.87	2.80
UB-18b	Not oriented	Basalt	Crust	2.6	0.0003	2.90	2.82
UB-23b H	Horizontal	Basalt	Crust	0.3	0.0002	2.92	2.90
UB-23b V	Vertical	Basalt	Crust	0.3	0.0002	2.91	2.90
UB-26a H	Horizontal	Basalt	Crust	1.7	-	2.87	2.81
UB-26a V	Vertical	Basalt	Crust	1.6	0.0001	2.87	2.81
UB-26b H	Horizontal	Basalt	Crust	2.8	-	2.88	2.79
UB-26b V	Vertical	Basalt	Crust	2.3	0.0001	2.87	2.79

UB-28a H	Horizontal	Basalt	Crust	0.5	-	2.87	2.84
UB-28a V	Vertical	Basalt	Crust	1.0	0.0004	2.88	2.84
UB-28b	Not oriented	Basalt	Crust	1.5	0.0002	2.86	2.81
UB-32I	Not oriented	Basalt	Crust	11.5	0.0004	2.92	2.56
UB-08b	Not oriented	Basalt	Core	3.1	0.0003	2.88	2.79
UB-16c H	Horizontal	Basalt	Core	1.3	0.018	2.89	2.84
UB-16c V	Vertical	Basalt	Core	0.5	0.0013	2.90	2.88
UB-16d H	Horizontal	Basalt	Core	0.3	-	2.92	2.90
UB-16d V	Vertical	Basalt	Core	0.3	-	2.91	2.90
UB-16e H	Horizontal	Basalt	Core	0.5	-	2.92	2.90
UB-16e V	Vertical	Basalt	Core	0.5	-	2.92	2.90
UB-16f H	Horizontal	Basalt	Core	0.4	-	2.91	2.88
UB-16f V	Vertical	Basalt	Core	0.2	-	2.92	2.90
UB-17d H	Horizontal	Basalt	Core	0.9	0.0001	2.90	2.87
UB-17d V	Vertical	Basalt	Core	0.4	-	2.91	2.89
UB-18c H	Horizontal	Basalt	Core	1.4	0.0002	2.87	2.81
UB-18c V	Vertical	Basalt	Core	0.9	-	2.87	2.83
UB-20b H	Horizontal	Basalt	Core	0.5	-	2.91	2.89
UB-20b V	Vertical	Basalt	Core	0.3	-	2.91	2.89
UB-20c H	Horizontal	Basalt	Core	0.6	0.051	2.89	2.87
UB-20c V	Vertical	Basalt	Core	0.2	0.011	2.89	2.87
UB-20d H	Horizontal	Basalt	Core	0.1	-	2.92	2.91
UB-20d V	Vertical	Basalt	Core	0.2	-	2.93	2.92
UB-23a H	Horizontal	Basalt	Core	0.1	-	2.91	2.89
UB-23a V	Vertical	Basalt	Core	0.3	-	2.92	2.91
UB-23c H	Horizontal	Basalt	Core	0.1	0.0004	2.90	2.88
UB-23c V	Vertical	Basalt	Core	0.6	-	2.90	2.87
UB-23d H	Horizontal	Basalt	Core	0.7	0.087	2.90	2.87
UB-23d V	Vertical	Basalt	Core	0.7	-	2.91	2.88
UB-25a H	Horizontal	Basalt	Core	0.5	-	2.93	2.90
UB-25a V	Vertical	Basalt	Core	0.5	-	2.93	2.91

UB-25b H	Horizontal	Basalt	Core	0.4	-	2.92	2.91
UB-25b V	Vertical	Basalt	Core	0.2	-	2.92	2.91
UB-25c H	Horizontal	Basalt	Core	0.4	0.0086	2.92	2.90
UB-25c V	Vertical	Basalt	Core	0.3	-	2.92	2.90
UB-25d H	Horizontal	Basalt	Core	0.7	-	2.86	2.84
UB-25d V	Vertical	Basalt	Core	0.6	-	2.86	2.84
UB-26c	Not oriented	Basalt	Core	1.7	-	2.93	2.86
UB-27b H	Horizontal	Basalt	Core	0.4	-	2.92	2.90
UB-27b V	Vertical	Basalt	Core	0.2	-	2.92	2.91
UB-27c H	Horizontal	Basalt	Core	0.7	0.0001	2.89	2.86
UB-27c V	Vertical	Basalt	Core	0.6	-	2.89	2.87
UB-27d-1 H	Horizontal	Basalt	Core	0.5	-	2.90	2.88
UB-27d-1 V	Vertical	Basalt	Core	0.4	-	2.89	2.87
UB-27d-2 H	Horizontal	Basalt	Core	0.3	0.0001	2.87	2.85
UB-27d-2 V	Vertical	Basalt	Core	0.3	-	2.87	2.86
UB-30a H	Horizontal	Basalt	Core	0.5	-	2.89	2.86
UB-30a V	Vertical	Basalt	Core	0.4	0.0001	2.89	2.86
UB-33f H	Horizontal	Basalt	Core	0.2	0.0002	2.96	2.94
UB-33f V	Vertical	Basalt	Core	0.2	-	2.96	2.95
UB-34a H	Horizontal	Basalt	Core	0.1	-	2.94	2.92
UB-34a V	Vertical	Basalt	Core	0.1	-	2.95	2.93

Anexo F

Velocity data of basalts from the Parané-Etendeka Igneous Province.

Velocity data of basalts from the Parané-Etendeka Igneous Province.

Sample I.D.	Orientation	Lithology	Position		Porosity (%)	Perm. (mD)	Rock Den.	Pressure (psi)	Trajectory	Vp	Vs	Vp/Vs
			within lava flow									
UB-01	Not oriented	Sandstone	-	16.57	72.2	2.17	1000	Ascent	3.08	2.06	1.49	
UB-01	Not oriented	Sandstone	-	16.57	72.2	2.17	1500	Ascent	3.23	2.14	1.51	
UB-01	Not oriented	Sandstone	-	16.57	72.2	2.17	2000	Ascent	3.34	2.20	1.52	
UB-01	Not oriented	Sandstone	-	16.57	72.2	2.17	2500	Ascent	3.43	2.24	1.53	
UB-01	Not oriented	Sandstone	-	16.57	72.2	2.17	3000	Ascent	3.50	2.28	1.53	
UB-01	Not oriented	Sandstone	-	16.57	72.2	2.17	3500	Ascent	3.56	2.31	1.54	
UB-01	Not oriented	Sandstone	-	16.57	72.2	2.17	4000	Ascent	3.62	2.34	1.55	
UB-01	Not oriented	Sandstone	-	16.57	72.2	2.17	4500	Ascent	3.66	2.36	1.55	
UB-01	Not oriented	Sandstone	-	16.57	72.2	2.17	5000	-	3.71	2.38	1.56	
UB-01	Not oriented	Sandstone	-	16.57	72.2	2.17	4500	Descent	3.69	2.37	1.55	
UB-01	Not oriented	Sandstone	-	16.57	72.2	2.17	4000	Descent	3.66	2.36	1.55	
UB-01	Not oriented	Sandstone	-	16.57	72.2	2.17	3500	Descent	3.62	2.34	1.55	
UB-01	Not oriented	Sandstone	-	16.57	72.2	2.17	3000	Descent	3.58	2.32	1.54	
UB-01	Not oriented	Sandstone	-	16.57	72.2	2.17	2500	Descent	3.53	2.30	1.54	
UB-01	Not oriented	Sandstone	-	16.57	72.2	2.17	2000	Descent	3.46	2.26	1.53	
UB-01	Not oriented	Sandstone	-	16.57	72.2	2.17	1500	Descent	3.36	2.21	1.52	
UB-01	Not oriented	Sandstone	-	16.57	72.2	2.17	1000	Descent	3.23	2.13	1.51	
UB-03a	Not oriented	Mudstone	-	7.40	0.0001	2.18	1000	Ascent	4.62	3.00	1.54	
UB-03a	Not oriented	Mudstone	-	7.40	0.0001	2.18	1500	Ascent	4.69	3.01	1.56	
UB-03a	Not oriented	Mudstone	-	7.40	0.0001	2.18	2000	Ascent	4.75	3.03	1.57	
UB-03a	Not oriented	Mudstone	-	7.40	0.0001	2.18	2500	Ascent	4.79	3.04	1.58	
UB-03a	Not oriented	Mudstone	-	7.40	0.0001	2.18	3000	Ascent	4.84	3.05	1.59	
UB-03a	Not oriented	Mudstone	-	7.40	0.0001	2.18	3500	Ascent	4.88	3.06	1.60	
UB-03a	Not oriented	Mudstone	-	7.40	0.0001	2.18	4000	Ascent	4.92	3.07	1.61	

UB-03a	Not oriented	Mudstone	-	7.40	0.0001	2.18	4500	Ascent	4.97	3.07	1.62
UB-03a	Not oriented	Mudstone	-	7.40	0.0001	2.18	5000	-	4.99	3.07	1.62
UB-03a	Not oriented	Mudstone	-	7.40	0.0001	2.18	4500	Descent	4.97	3.07	1.62
UB-03a	Not oriented	Mudstone	-	7.40	0.0001	2.18	4000	Descent	4.94	3.07	1.61
UB-03a	Not oriented	Mudstone	-	7.40	0.0001	2.18	3500	Descent	4.91	3.07	1.60
UB-03a	Not oriented	Mudstone	-	7.40	0.0001	2.18	3000	Descent	4.87	3.07	1.59
UB-03a	Not oriented	Mudstone	-	7.40	0.0001	2.18	2500	Descent	4.83	3.07	1.58
UB-03a	Not oriented	Mudstone	-	7.40	0.0001	2.18	2000	Descent	4.81	3.06	1.57
UB-03a	Not oriented	Mudstone	-	7.40	0.0001	2.18	1500	Descent	4.79	3.05	1.57
UB-03a	Not oriented	Mudstone	-	7.40	0.0001	2.18	1000	Descent	4.77	3.04	1.57
UB-20a	Not oriented	Peperite	-	19.26	0.062	2.21	1000	Ascent	3.43	2.15	1.60
UB-20a	Not oriented	Peperite	-	19.26	0.062	2.21	1500	Ascent	3.45	2.17	1.59
UB-20a	Not oriented	Peperite	-	19.26	0.062	2.21	2000	Ascent	3.47	2.18	1.59
UB-20a	Not oriented	Peperite	-	19.26	0.062	2.21	2500	Ascent	3.48	2.19	1.59
UB-20a	Not oriented	Peperite	-	19.26	0.062	2.21	3000	Ascent	3.49	2.20	1.59
UB-20a	Not oriented	Peperite	-	19.26	0.062	2.21	3500	Ascent	3.50	2.20	1.59
UB-20a	Not oriented	Peperite	-	19.26	0.062	2.21	4000	Ascent	3.51	2.20	1.59
UB-20a	Not oriented	Peperite	-	19.26	0.062	2.21	4500	Ascent	3.51	2.21	1.59
UB-20a	Not oriented	Peperite	-	19.26	0.062	2.21	5000	-	3.52	2.21	1.59
UB-20a	Not oriented	Peperite	-	19.26	0.062	2.21	4500	Descent	3.51	2.21	1.59
UB-20a	Not oriented	Peperite	-	19.26	0.062	2.21	4000	Descent	3.51	2.21	1.59
UB-20a	Not oriented	Peperite	-	19.26	0.062	2.21	3500	Descent	3.51	2.20	1.59
UB-20a	Not oriented	Peperite	-	19.26	0.062	2.21	3000	Descent	3.50	2.20	1.59
UB-20a	Not oriented	Peperite	-	19.26	0.062	2.21	2500	Descent	3.50	2.20	1.59
UB-20a	Not oriented	Peperite	-	19.26	0.062	2.21	2000	Descent	3.49	2.20	1.59
UB-20a	Not oriented	Peperite	-	19.26	0.062	2.21	1500	Descent	3.48	2.19	1.59
UB-20a	Not oriented	Peperite	-	19.26	0.062	2.21	1000	Descent	3.47	2.17	1.60

UB-21aV	Vertical	Peperite	-	3.87	-	2.45	1000	Ascent	4.56	3.00	1.52
UB-21aV	Vertical	Peperite	-	3.87	-	2.45	1500	Ascent	4.61	3.01	1.53
UB-21aV	Vertical	Peperite	-	3.87	-	2.45	2000	Ascent	4.66	3.03	1.54
UB-21aV	Vertical	Peperite	-	3.87	-	2.45	2500	Ascent	4.70	3.04	1.55
UB-21aV	Vertical	Peperite	-	3.87	-	2.45	3000	Ascent	4.73	3.05	1.55
UB-21aV	Vertical	Peperite	-	3.87	-	2.45	3500	Ascent	4.76	3.06	1.56
UB-21aV	Vertical	Peperite	-	3.87	-	2.45	4000	Ascent	4.78	3.07	1.56
UB-21aV	Vertical	Peperite	-	3.87	-	2.45	4500	Ascent	4.80	3.07	1.56
UB-21aV	Vertical	Peperite	-	3.87	-	2.45	5000	-	4.82	3.08	1.56
UB-21aV	Vertical	Peperite	-	3.87	-	2.45	4500	Descent	4.81	3.08	1.56
UB-21aV	Vertical	Peperite	-	3.87	-	2.45	4000	Descent	4.80	3.07	1.56
UB-21aV	Vertical	Peperite	-	3.87	-	2.45	3500	Descent	4.79	3.07	1.56
UB-21aV	Vertical	Peperite	-	3.87	-	2.45	3000	Descent	4.77	3.07	1.56
UB-21aV	Vertical	Peperite	-	3.87	-	2.45	2500	Descent	4.75	3.06	1.55
UB-21aV	Vertical	Peperite	-	3.87	-	2.45	2000	Descent	4.72	3.05	1.54
UB-21aV	Vertical	Peperite	-	3.87	-	2.45	1500	Descent	4.65	3.04	1.53
UB-21aV	Vertical	Peperite	-	3.87	-	2.45	1000	Descent	4.53	2.92	1.55
UB-27a	Vertical	Peperite	-	18.03	0.201	2.15	1000	Ascent	2.65	1.74	1.52
UB-27a	Vertical	Peperite	-	18.03	0.201	2.15	1500	Ascent	2.78	1.81	1.54
UB-27a	Vertical	Peperite	-	18.03	0.201	2.15	2000	Ascent	2.90	1.87	1.55
UB-27a	Vertical	Peperite	-	18.03	0.201	2.15	2500	Ascent	3.00	1.92	1.56
UB-27a	Vertical	Peperite	-	18.03	0.201	2.15	3000	Ascent	3.08	1.97	1.57
UB-27a	Vertical	Peperite	-	18.03	0.201	2.15	3500	Ascent	3.16	2.01	1.57
UB-27a	Vertical	Peperite	-	18.03	0.201	2.15	4000	Ascent	3.23	2.05	1.58
UB-27a	Vertical	Peperite	-	18.03	0.201	2.15	4500	Ascent	3.29	2.08	1.58
UB-27a	Vertical	Peperite	-	18.03	0.201	2.15	5000	-	3.34	2.11	1.58
UB-27a	Vertical	Peperite	-	18.03	0.201	2.15	4500	Descent	3.33	2.10	1.58
UB-27a	Vertical	Peperite	-	18.03	0.201	2.15	4000	Descent	3.31	2.09	1.58

UB-27a	Vertical	Peperite	-	18.03	0.201	2.15	3500	Descent	3.27	2.07	1.58
UB-27a	Vertical	Peperite	-	18.03	0.201	2.15	3000	Descent	3.23	2.05	1.58
UB-27a	Vertical	Peperite	-	18.03	0.201	2.15	2500	Descent	3.18	2.02	1.57
UB-27a	Vertical	Peperite	-	18.03	0.201	2.15	2000	Descent	3.11	1.99	1.57
UB-27a	Vertical	Peperite	-	18.03	0.201	2.15	1500	Descent	3.03	1.94	1.56
UB-27a	Vertical	Peperite	-	18.03	0.201	2.15	1000	Descent	2.91	1.88	1.55
UB-16bH	Horizontal	Basalt	Crust	1.22	0.103	2.86	1000	Ascent	5.63	3.20	1.76
UB-16bH	Horizontal	Basalt	Crust	1.22	0.103	2.86	1500	Ascent	5.70	3.22	1.77
UB-16bH	Horizontal	Basalt	Crust	1.22	0.103	2.86	2000	Ascent	5.75	3.23	1.78
UB-16bH	Horizontal	Basalt	Crust	1.22	0.103	2.86	2500	Ascent	5.79	3.24	1.79
UB-16bH	Horizontal	Basalt	Crust	1.22	0.103	2.86	3000	Ascent	5.82	3.25	1.79
UB-16bH	Horizontal	Basalt	Crust	1.22	0.103	2.86	3500	Ascent	5.84	3.26	1.79
UB-16bH	Horizontal	Basalt	Crust	1.22	0.103	2.86	4000	Ascent	5.87	3.27	1.80
UB-16bH	Horizontal	Basalt	Crust	1.22	0.103	2.86	4500	Ascent	5.89	3.27	1.80
UB-16bH	Horizontal	Basalt	Crust	1.22	0.103	2.86	5000	-	5.91	3.28	1.80
UB-16bH	Horizontal	Basalt	Crust	1.22	0.103	2.86	4500	Descent	5.90	3.28	1.80
UB-16bH	Horizontal	Basalt	Crust	1.22	0.103	2.86	4000	Descent	5.89	3.27	1.80
UB-16bH	Horizontal	Basalt	Crust	1.22	0.103	2.86	3500	Descent	5.88	3.27	1.80
UB-16bH	Horizontal	Basalt	Crust	1.22	0.103	2.86	3000	Descent	5.87	3.27	1.80
UB-16bH	Horizontal	Basalt	Crust	1.22	0.103	2.86	2500	Descent	5.85	3.26	1.79
UB-16bH	Horizontal	Basalt	Crust	1.22	0.103	2.86	2000	Descent	5.83	3.26	1.79
UB-16bH	Horizontal	Basalt	Crust	1.22	0.103	2.86	1500	Descent	5.81	3.25	1.79
UB-16bH	Horizontal	Basalt	Crust	1.22	0.103	2.86	1000	Descent	5.79	3.24	1.78
UB-16bV	Vertical	Basalt	Crust	0.28	-	2.91	1000	Ascent	5.86	3.33	1.76
UB-16bV	Vertical	Basalt	Crust	0.28	-	2.91	1500	Ascent	5.92	3.35	1.77
UB-16bV	Vertical	Basalt	Crust	0.28	-	2.91	2000	Ascent	5.95	3.35	1.77
UB-16bV	Vertical	Basalt	Crust	0.28	-	2.91	2500	Ascent	5.98	3.36	1.78

UB-16bV	Vertical	Basalt	Crust	0.28	-	2.91	3000	Ascent	6.00	3.37	1.78
UB-16bV	Vertical	Basalt	Crust	0.28	-	2.91	3500	Ascent	6.02	3.37	1.79
UB-16bV	Vertical	Basalt	Crust	0.28	-	2.91	4000	Ascent	6.04	3.38	1.79
UB-16bV	Vertical	Basalt	Crust	0.28	-	2.91	4500	Ascent	6.05	3.38	1.79
UB-16bV	Vertical	Basalt	Crust	0.28	-	2.91	5000	-	6.07	3.38	1.79
UB-16bV	Vertical	Basalt	Crust	0.28	-	2.91	4500	Descent	6.06	3.38	1.79
UB-16bV	Vertical	Basalt	Crust	0.28	-	2.91	4000	Descent	6.05	3.38	1.79
UB-16bV	Vertical	Basalt	Crust	0.28	-	2.91	3500	Descent	6.04	3.38	1.79
UB-16bV	Vertical	Basalt	Crust	0.28	-	2.91	3000	Descent	6.04	3.38	1.79
UB-16bV	Vertical	Basalt	Crust	0.28	-	2.91	2500	Descent	6.03	3.37	1.79
UB-16bV	Vertical	Basalt	Crust	0.28	-	2.91	2000	Descent	6.02	3.37	1.79
UB-16bV	Vertical	Basalt	Crust	0.28	-	2.91	1500	Descent	6.01	3.37	1.78
UB-16bV	Vertical	Basalt	Crust	0.28	-	2.91	1000	Descent	6.00	3.37	1.78
UB-18aV	Vertical	Basalt	Crust	1.95	0.0001	2.80	1000	Ascent	5.25	3.09	1.70
UB-18aV	Vertical	Basalt	Crust	1.95	0.0001	2.80	1500	Ascent	5.30	3.11	1.71
UB-18aV	Vertical	Basalt	Crust	1.95	0.0001	2.80	2000	Ascent	5.34	3.11	1.71
UB-18aV	Vertical	Basalt	Crust	1.95	0.0001	2.80	2500	Ascent	5.37	3.12	1.72
UB-18aV	Vertical	Basalt	Crust	1.95	0.0001	2.80	3000	Ascent	5.40	3.13	1.72
UB-18aV	Vertical	Basalt	Crust	1.95	0.0001	2.80	3500	Ascent	5.44	3.14	1.73
UB-18aV	Vertical	Basalt	Crust	1.95	0.0001	2.80	4000	Ascent	5.46	3.15	1.74
UB-18aV	Vertical	Basalt	Crust	1.95	0.0001	2.80	4500	Ascent	5.49	3.16	1.74
UB-18aV	Vertical	Basalt	Crust	1.95	0.0001	2.80	5000	-	5.51	3.16	1.74
UB-18aV	Vertical	Basalt	Crust	1.95	0.0001	2.80	4500	Descent	5.50	3.16	1.74
UB-18aV	Vertical	Basalt	Crust	1.95	0.0001	2.80	4000	Descent	5.49	3.16	1.74
UB-18aV	Vertical	Basalt	Crust	1.95	0.0001	2.80	3500	Descent	5.47	3.15	1.74
UB-18aV	Vertical	Basalt	Crust	1.95	0.0001	2.80	3000	Descent	5.45	3.15	1.73
UB-18aV	Vertical	Basalt	Crust	1.95	0.0001	2.80	2500	Descent	5.42	3.14	1.73
UB-18aV	Vertical	Basalt	Crust	1.95	0.0001	2.80	2000	Descent	5.39	3.13	1.72

UB-18aV	Vertical	Basalt	Crust	1.95	0.0001	2.80	1500	Descent	5.36	3.12	1.72
UB-18aV	Vertical	Basalt	Crust	1.95	0.0001	2.80	1000	Descent	5.31	3.11	1.71
UB-26bV	Vertical	Basalt	Crust	2.33	0.0001	2.79	1000	Ascent	4.99	2.99	1.67
UB-26bV	Vertical	Basalt	Crust	2.33	0.0001	2.79	1500	Ascent	5.11	3.02	1.69
UB-26bV	Vertical	Basalt	Crust	2.33	0.0001	2.79	2000	Ascent	5.19	3.05	1.71
UB-26bV	Vertical	Basalt	Crust	2.33	0.0001	2.79	2500	Ascent	5.26	3.06	1.72
UB-26bV	Vertical	Basalt	Crust	2.33	0.0001	2.79	3000	Ascent	5.31	3.07	1.73
UB-26bV	Vertical	Basalt	Crust	2.33	0.0001	2.79	3500	Ascent	5.34	3.08	1.73
UB-26bV	Vertical	Basalt	Crust	2.33	0.0001	2.79	4000	Ascent	5.37	3.09	1.74
UB-26bV	Vertical	Basalt	Crust	2.33	0.0001	2.79	4500	Ascent	5.40	3.09	1.74
UB-26bV	Vertical	Basalt	Crust	2.33	0.0001	2.79	5000	-	5.42	3.10	1.75
UB-26bV	Vertical	Basalt	Crust	2.33	0.0001	2.79	4500	Descent	5.41	3.10	1.75
UB-26bV	Vertical	Basalt	Crust	2.33	0.0001	2.79	4000	Descent	5.40	3.10	1.74
UB-26bV	Vertical	Basalt	Crust	2.33	0.0001	2.79	3500	Descent	5.39	3.09	1.74
UB-26bV	Vertical	Basalt	Crust	2.33	0.0001	2.79	3000	Descent	5.37	3.09	1.74
UB-26bV	Vertical	Basalt	Crust	2.33	0.0001	2.79	2500	Descent	5.34	3.09	1.73
UB-26bV	Vertical	Basalt	Crust	2.33	0.0001	2.79	2000	Descent	5.30	3.08	1.72
UB-26bV	Vertical	Basalt	Crust	2.33	0.0001	2.79	1500	Descent	5.21	3.06	1.70
UB-26bV	Vertical	Basalt	Crust	2.33	0.0001	2.79	1000	Descent	5.07	3.01	1.68
UB-28aV	Vertical	Basalt	Crust	0.98	0.0004	2.84	1000	Ascent	5.34	3.06	1.74
UB-28aV	Vertical	Basalt	Crust	0.98	0.0004	2.84	1500	Ascent	5.45	3.11	1.75
UB-28aV	Vertical	Basalt	Crust	0.98	0.0004	2.84	2000	Ascent	5.54	3.15	1.76
UB-28aV	Vertical	Basalt	Crust	0.98	0.0004	2.84	2500	Ascent	5.60	3.17	1.76
UB-28aV	Vertical	Basalt	Crust	0.98	0.0004	2.84	3000	Ascent	5.65	3.19	1.77
UB-28aV	Vertical	Basalt	Crust	0.98	0.0004	2.84	3500	Ascent	5.68	3.20	1.78
UB-28aV	Vertical	Basalt	Crust	0.98	0.0004	2.84	4000	Ascent	5.72	3.21	1.78
UB-28aV	Vertical	Basalt	Crust	0.98	0.0004	2.84	4500	Ascent	5.75	3.22	1.79

UB-28aV	Vertical	Basalt	Crust	0.98	0.0004	2.84	5000	-	5.78	3.23	1.79
UB-28aV	Vertical	Basalt	Crust	0.98	0.0004	2.84	4500	Descent	5.76	3.22	1.79
UB-28aV	Vertical	Basalt	Crust	0.98	0.0004	2.84	4000	Descent	5.75	3.22	1.78
UB-28aV	Vertical	Basalt	Crust	0.98	0.0004	2.84	3500	Descent	5.72	3.22	1.78
UB-28aV	Vertical	Basalt	Crust	0.98	0.0004	2.84	3000	Descent	5.69	3.21	1.77
UB-28aV	Vertical	Basalt	Crust	0.98	0.0004	2.84	2500	Descent	5.65	3.19	1.77
UB-28aV	Vertical	Basalt	Crust	0.98	0.0004	2.84	2000	Descent	5.60	3.17	1.76
UB-28aV	Vertical	Basalt	Crust	0.98	0.0004	2.84	1500	Descent	5.52	3.12	1.77
UB-28aV	Vertical	Basalt	Crust	0.98	0.0004	2.84	1000	Descent	5.41	3.08	1.76
UB-32I	Not oriented	Basalt	Crust	11.52	0.0004	2.56	1000	Ascent	4.13	2.53	1.64
UB-32I	Not oriented	Basalt	Crust	11.52	0.0004	2.56	1500	Ascent	4.21	2.55	1.65
UB-32I	Not oriented	Basalt	Crust	11.52	0.0004	2.56	2000	Ascent	4.26	2.56	1.66
UB-32I	Not oriented	Basalt	Crust	11.52	0.0004	2.56	2500	Ascent	4.30	2.57	1.67
UB-32I	Not oriented	Basalt	Crust	11.52	0.0004	2.56	3000	Ascent	4.33	2.58	1.68
UB-32I	Not oriented	Basalt	Crust	11.52	0.0004	2.56	3500	Ascent	4.35	2.59	1.68
UB-32I	Not oriented	Basalt	Crust	11.52	0.0004	2.56	4000	Ascent	4.37	2.59	1.69
UB-32I	Not oriented	Basalt	Crust	11.52	0.0004	2.56	4500	Ascent	4.39	2.60	1.69
UB-32I	Not oriented	Basalt	Crust	11.52	0.0004	2.56	5000	-	4.41	2.60	1.69
UB-32I	Not oriented	Basalt	Crust	11.52	0.0004	2.56	4500	Descent	4.40	2.60	1.69
UB-32I	Not oriented	Basalt	Crust	11.52	0.0004	2.56	4000	Descent	4.39	2.60	1.69
UB-32I	Not oriented	Basalt	Crust	11.52	0.0004	2.56	3500	Descent	4.38	2.60	1.69
UB-32I	Not oriented	Basalt	Crust	11.52	0.0004	2.56	3000	Descent	4.37	2.59	1.68
UB-32I	Not oriented	Basalt	Crust	11.52	0.0004	2.56	2500	Descent	4.36	2.59	1.68
UB-32I	Not oriented	Basalt	Crust	11.52	0.0004	2.56	2000	Descent	4.35	2.59	1.68
UB-32I	Not oriented	Basalt	Crust	11.52	0.0004	2.56	1500	Descent	4.34	2.59	1.68
UB-32I	Not oriented	Basalt	Crust	11.52	0.0004	2.56	1000	Descent	4.33	2.59	1.67
UB-16eV	Vertical	Basalt	Core	0.50	-	2.90	1000	Ascent	6.22	3.48	1.79

UB-16eV	Vertical	Basalt	Core	0.50	-	2.90	1500	Ascent	6.26	3.49	1.80
UB-16eV	Vertical	Basalt	Core	0.50	-	2.90	2000	Ascent	6.30	3.49	1.80
UB-16eV	Vertical	Basalt	Core	0.50	-	2.90	2500	Ascent	6.33	3.50	1.81
UB-16eV	Vertical	Basalt	Core	0.50	-	2.90	3000	Ascent	6.37	3.51	1.82
UB-16eV	Vertical	Basalt	Core	0.50	-	2.90	3500	Ascent	6.40	3.52	1.82
UB-16eV	Vertical	Basalt	Core	0.50	-	2.90	4000	Ascent	6.41	3.52	1.82
UB-16eV	Vertical	Basalt	Core	0.50	-	2.90	4500	Ascent	6.44	3.53	1.83
UB-16eV	Vertical	Basalt	Core	0.50	-	2.90	5000	-	6.45	3.53	1.83
UB-16eV	Vertical	Basalt	Core	0.50	-	2.90	4500	Descent	6.45	3.53	1.83
UB-16eV	Vertical	Basalt	Core	0.50	-	2.90	4000	Descent	6.44	3.53	1.83
UB-16eV	Vertical	Basalt	Core	0.50	-	2.90	3500	Descent	6.43	3.52	1.83
UB-16eV	Vertical	Basalt	Core	0.50	-	2.90	3000	Descent	6.41	3.52	1.82
UB-16eV	Vertical	Basalt	Core	0.50	-	2.90	2500	Descent	6.39	3.51	1.82
UB-16eV	Vertical	Basalt	Core	0.50	-	2.90	2000	Descent	6.35	3.51	1.81
UB-16eV	Vertical	Basalt	Core	0.50	-	2.90	1500	Descent	6.32	3.51	1.80
UB-16eV	Vertical	Basalt	Core	0.50	-	2.90	1000	Descent	6.31	3.50	1.80
UB-17dV	Vertical	Basalt	Core	0.41	-	2.89	1000	Ascent	6.15	3.44	1.79
UB-17dV	Vertical	Basalt	Core	0.41	-	2.89	1500	Ascent	6.17	3.45	1.79
UB-17dV	Vertical	Basalt	Core	0.41	-	2.89	2000	Ascent	6.19	3.45	1.79
UB-17dV	Vertical	Basalt	Core	0.41	-	2.89	2500	Ascent	6.20	3.46	1.79
UB-17dV	Vertical	Basalt	Core	0.41	-	2.89	3000	Ascent	6.22	3.46	1.80
UB-17dV	Vertical	Basalt	Core	0.41	-	2.89	3500	Ascent	6.23	3.46	1.80
UB-17dV	Vertical	Basalt	Core	0.41	-	2.89	4000	Ascent	6.25	3.47	1.80
UB-17dV	Vertical	Basalt	Core	0.41	-	2.89	4500	Ascent	6.26	3.47	1.81
UB-17dV	Vertical	Basalt	Core	0.41	-	2.89	5000	-	6.27	3.47	1.81
UB-17dV	Vertical	Basalt	Core	0.41	-	2.89	4500	Descent	6.27	3.47	1.81
UB-17dV	Vertical	Basalt	Core	0.41	-	2.89	4000	Descent	6.26	3.47	1.81
UB-17dV	Vertical	Basalt	Core	0.41	-	2.89	3500	Descent	6.26	3.47	1.80

UB-17dV	Vertical	Basalt	Core	0.41	-	2.89	3000	Descent	6.25	3.47	1.80
UB-17dV	Vertical	Basalt	Core	0.41	-	2.89	2500	Descent	6.24	3.46	1.80
UB-17dV	Vertical	Basalt	Core	0.41	-	2.89	2000	Descent	6.23	3.46	1.80
UB-17dV	Vertical	Basalt	Core	0.41	-	2.89	1500	Descent	6.23	3.46	1.80
UB-17dV	Vertical	Basalt	Core	0.41	-	2.89	1000	Descent	6.21	3.46	1.80
UB-20cV	Vertical	Basalt	Core	0.22	0.011	2.87	1000	Ascent	5.85	3.29	1.78
UB-20cV	Vertical	Basalt	Core	0.22	0.011	2.87	1500	Ascent	5.91	3.32	1.78
UB-20cV	Vertical	Basalt	Core	0.22	0.011	2.87	2000	Ascent	5.96	3.34	1.78
UB-20cV	Vertical	Basalt	Core	0.22	0.011	2.87	2500	Ascent	5.99	3.36	1.79
UB-20cV	Vertical	Basalt	Core	0.22	0.011	2.87	3000	Ascent	6.02	3.37	1.79
UB-20cV	Vertical	Basalt	Core	0.22	0.011	2.87	3500	Ascent	6.06	3.38	1.79
UB-20cV	Vertical	Basalt	Core	0.22	0.011	2.87	4000	Ascent	6.08	3.39	1.79
UB-20cV	Vertical	Basalt	Core	0.22	0.011	2.87	4500	Ascent	6.10	3.40	1.79
UB-20cV	Vertical	Basalt	Core	0.22	0.011	2.87	5000	-	6.11	3.40	1.80
UB-20cV	Vertical	Basalt	Core	0.22	0.011	2.87	4500	Descent	6.11	3.40	1.80
UB-20cV	Vertical	Basalt	Core	0.22	0.011	2.87	4000	Descent	6.10	3.40	1.79
UB-20cV	Vertical	Basalt	Core	0.22	0.011	2.87	3500	Descent	6.10	3.40	1.80
UB-20cV	Vertical	Basalt	Core	0.22	0.011	2.87	3000	Descent	6.10	3.40	1.79
UB-20cV	Vertical	Basalt	Core	0.22	0.011	2.87	2500	Descent	6.08	3.39	1.79
UB-20cV	Vertical	Basalt	Core	0.22	0.011	2.87	2000	Descent	6.06	3.38	1.79
UB-20cV	Vertical	Basalt	Core	0.22	0.011	2.87	1500	Descent	6.04	3.37	1.79
UB-20cV	Vertical	Basalt	Core	0.22	0.011	2.87	1000	Descent	6.00	3.35	1.79
UB-20dV	Vertical	Basalt	Core	0.22	-	2.92	1000	Ascent	6.12	3.52	1.74
UB-20dV	Vertical	Basalt	Core	0.22	-	2.92	1500	Ascent	6.21	3.53	1.76
UB-20dV	Vertical	Basalt	Core	0.22	-	2.92	2000	Ascent	6.26	3.55	1.77
UB-20dV	Vertical	Basalt	Core	0.22	-	2.92	2500	Ascent	6.30	3.55	1.77
UB-20dV	Vertical	Basalt	Core	0.22	-	2.92	3000	Ascent	6.34	3.56	1.78

UB-20dV	Vertical	Basalt	Core	0.22	-	2.92	3500	Ascent	6.36	3.57	1.78
UB-20dV	Vertical	Basalt	Core	0.22	-	2.92	4000	Ascent	6.38	3.57	1.79
UB-20dV	Vertical	Basalt	Core	0.22	-	2.92	4500	Ascent	6.40	3.57	1.79
UB-20dV	Vertical	Basalt	Core	0.22	-	2.92	5000	-	6.41	3.57	1.79
UB-20dV	Vertical	Basalt	Core	0.22	-	2.92	4500	Descent	6.41	3.57	1.79
UB-20dV	Vertical	Basalt	Core	0.22	-	2.92	4000	Descent	6.40	3.57	1.79
UB-20dV	Vertical	Basalt	Core	0.22	-	2.92	3500	Descent	6.40	3.57	1.79
UB-20dV	Vertical	Basalt	Core	0.22	-	2.92	3000	Descent	6.40	3.57	1.79
UB-20dV	Vertical	Basalt	Core	0.22	-	2.92	2500	Descent	6.39	3.57	1.79
UB-20dV	Vertical	Basalt	Core	0.22	-	2.92	2000	Descent	6.36	3.57	1.78
UB-20dV	Vertical	Basalt	Core	0.22	-	2.92	1500	Descent	6.32	3.56	1.77
UB-20dV	Vertical	Basalt	Core	0.22	-	2.92	1000	Descent	6.25	3.55	1.76
UB-25bV	Vertical	Basalt	Core	0.23	-	2.91	1000	Ascent	6.05	3.42	1.77
UB-25bV	Vertical	Basalt	Core	0.23	-	2.91	1500	Ascent	6.14	3.44	1.78
UB-25bV	Vertical	Basalt	Core	0.23	-	2.91	2000	Ascent	6.20	3.46	1.79
UB-25bV	Vertical	Basalt	Core	0.23	-	2.91	2500	Ascent	6.23	3.47	1.80
UB-25bV	Vertical	Basalt	Core	0.23	-	2.91	3000	Ascent	6.25	3.47	1.80
UB-25bV	Vertical	Basalt	Core	0.23	-	2.91	3500	Ascent	6.26	3.47	1.80
UB-25bV	Vertical	Basalt	Core	0.23	-	2.91	4000	Ascent	6.28	3.48	1.81
UB-25bV	Vertical	Basalt	Core	0.23	-	2.91	4500	Ascent	6.29	3.48	1.81
UB-25bV	Vertical	Basalt	Core	0.23	-	2.91	5000	-	6.29	3.48	1.81
UB-25bV	Vertical	Basalt	Core	0.23	-	2.91	4500	Descent	6.29	3.48	1.81
UB-25bV	Vertical	Basalt	Core	0.23	-	2.91	4000	Descent	6.29	3.48	1.81
UB-25bV	Vertical	Basalt	Core	0.23	-	2.91	3500	Descent	6.29	3.48	1.81
UB-25bV	Vertical	Basalt	Core	0.23	-	2.91	3000	Descent	6.29	3.48	1.81
UB-25bV	Vertical	Basalt	Core	0.23	-	2.91	2500	Descent	6.29	3.48	1.81
UB-25bV	Vertical	Basalt	Core	0.23	-	2.91	2000	Descent	6.29	3.48	1.81
UB-25bV	Vertical	Basalt	Core	0.23	-	2.91	1500	Descent	6.26	3.47	1.80

UB-25bV	Vertical	Basalt	Core	0.23	-	2.91	1000	Descent	6.04	3.43	1.76
UB-25dV	Vertical	Basalt	Core	0.57	-	2.84	1000	Ascent	5.44	3.18	1.71
UB-25dV	Vertical	Basalt	Core	0.57	-	2.84	1500	Ascent	5.51	3.20	1.72
UB-25dV	Vertical	Basalt	Core	0.57	-	2.84	2000	Ascent	5.56	3.21	1.73
UB-25dV	Vertical	Basalt	Core	0.57	-	2.84	2500	Ascent	5.60	3.22	1.74
UB-25dV	Vertical	Basalt	Core	0.57	-	2.84	3000	Ascent	5.63	3.23	1.74
UB-25dV	Vertical	Basalt	Core	0.57	-	2.84	3500	Ascent	5.66	3.24	1.75
UB-25dV	Vertical	Basalt	Core	0.57	-	2.84	4000	Ascent	5.68	3.24	1.75
UB-25dV	Vertical	Basalt	Core	0.57	-	2.84	4500	Ascent	5.70	3.25	1.76
UB-25dV	Vertical	Basalt	Core	0.57	-	2.84	5000	-	5.72	3.25	1.76
UB-25dV	Vertical	Basalt	Core	0.57	-	2.84	4500	Descent	5.72	3.25	1.76
UB-25dV	Vertical	Basalt	Core	0.57	-	2.84	4000	Descent	5.71	3.25	1.76
UB-25dV	Vertical	Basalt	Core	0.57	-	2.84	3500	Descent	5.69	3.25	1.75
UB-25dV	Vertical	Basalt	Core	0.57	-	2.84	3000	Descent	5.67	3.24	1.75
UB-25dV	Vertical	Basalt	Core	0.57	-	2.84	2500	Descent	5.65	3.24	1.75
UB-25dV	Vertical	Basalt	Core	0.57	-	2.84	2000	Descent	5.62	3.23	1.74
UB-25dV	Vertical	Basalt	Core	0.57	-	2.84	1500	Descent	5.58	3.22	1.73
UB-25dV	Vertical	Basalt	Core	0.57	-	2.84	1000	Descent	5.53	3.21	1.72
UB-27cV	Vertical	Basalt	Core	0.57	-	2.87	1000	Ascent	5.84	3.35	1.75
UB-27cV	Vertical	Basalt	Core	0.57	-	2.87	1500	Ascent	5.90	3.36	1.76
UB-27cV	Vertical	Basalt	Core	0.57	-	2.87	2000	Ascent	5.94	3.36	1.76
UB-27cV	Vertical	Basalt	Core	0.57	-	2.87	2500	Ascent	5.96	3.37	1.77
UB-27cV	Vertical	Basalt	Core	0.57	-	2.87	3000	Ascent	5.99	3.38	1.78
UB-27cV	Vertical	Basalt	Core	0.57	-	2.87	3500	Ascent	6.02	3.38	1.78
UB-27cV	Vertical	Basalt	Core	0.57	-	2.87	4000	Ascent	6.04	3.39	1.78
UB-27cV	Vertical	Basalt	Core	0.57	-	2.87	4500	Ascent	6.06	3.39	1.78
UB-27cV	Vertical	Basalt	Core	0.57	-	2.87	5000	-	6.08	3.40	1.79

UB-27cV	Vertical	Basalt	Core	0.57	-	2.87	4500	Descent	6.08	3.40	1.79
UB-27cV	Vertical	Basalt	Core	0.57	-	2.87	4000	Descent	6.08	3.40	1.79
UB-27cV	Vertical	Basalt	Core	0.57	-	2.87	3500	Descent	6.07	3.39	1.79
UB-27cV	Vertical	Basalt	Core	0.57	-	2.87	3000	Descent	6.06	3.39	1.79
UB-27cV	Vertical	Basalt	Core	0.57	-	2.87	2500	Descent	6.06	3.39	1.79
UB-27cV	Vertical	Basalt	Core	0.57	-	2.87	2000	Descent	6.04	3.38	1.79
UB-27cV	Vertical	Basalt	Core	0.57	-	2.87	1500	Descent	6.01	3.38	1.78
UB-27cV	Vertical	Basalt	Core	0.57	-	2.87	1000	Descent	5.98	3.37	1.77
UB-27d-2V	Vertical	Basalt	Core	0.27	-	2.86	1000	Ascent	5.39	3.23	1.67
UB-27d-2V	Vertical	Basalt	Core	0.27	-	2.86	1500	Ascent	5.47	3.25	1.68
UB-27d-2V	Vertical	Basalt	Core	0.27	-	2.86	2000	Ascent	5.54	3.27	1.69
UB-27d-2V	Vertical	Basalt	Core	0.27	-	2.86	2500	Ascent	5.61	3.29	1.71
UB-27d-2V	Vertical	Basalt	Core	0.27	-	2.86	3000	Ascent	5.66	3.30	1.71
UB-27d-2V	Vertical	Basalt	Core	0.27	-	2.86	3500	Ascent	5.69	3.30	1.72
UB-27d-2V	Vertical	Basalt	Core	0.27	-	2.86	4000	Ascent	5.73	3.31	1.73
UB-27d-2V	Vertical	Basalt	Core	0.27	-	2.86	4500	Ascent	5.75	3.31	1.74
UB-27d-2V	Vertical	Basalt	Core	0.27	-	2.86	5000	-	5.78	3.32	1.74
UB-27d-2V	Vertical	Basalt	Core	0.27	-	2.86	4500	Descent	5.76	3.32	1.74
UB-27d-2V	Vertical	Basalt	Core	0.27	-	2.86	4000	Descent	5.74	3.32	1.73
UB-27d-2V	Vertical	Basalt	Core	0.27	-	2.86	3500	Descent	5.71	3.31	1.72
UB-27d-2V	Vertical	Basalt	Core	0.27	-	2.86	3000	Descent	5.67	3.31	1.71
UB-27d-2V	Vertical	Basalt	Core	0.27	-	2.86	2500	Descent	5.61	3.30	1.70
UB-27d-2V	Vertical	Basalt	Core	0.27	-	2.86	2000	Descent	5.55	3.28	1.69
UB-27d-2V	Vertical	Basalt	Core	0.27	-	2.86	1500	Descent	5.49	3.26	1.69
UB-27d-2V	Vertical	Basalt	Core	0.27	-	2.86	1000	Descent	5.44	3.23	1.68
UB-30aV	Vertical	Basalt	Core	0.44	0.0001	2.86	1000	Ascent	5.32	3.15	1.69
UB-30aV	Vertical	Basalt	Core	0.44	0.0001	2.86	1500	Ascent	5.42	3.19	1.70

UB-30aV	Vertical	Basalt	Core	0.44	0.0001	2.86	2000	Ascent	5.50	3.21	1.72
UB-30aV	Vertical	Basalt	Core	0.44	0.0001	2.86	2500	Ascent	5.57	3.23	1.73
UB-30aV	Vertical	Basalt	Core	0.44	0.0001	2.86	3000	Ascent	5.63	3.24	1.74
UB-30aV	Vertical	Basalt	Core	0.44	0.0001	2.86	3500	Ascent	5.68	3.25	1.75
UB-30aV	Vertical	Basalt	Core	0.44	0.0001	2.86	4000	Ascent	5.72	3.26	1.75
UB-30aV	Vertical	Basalt	Core	0.44	0.0001	2.86	4500	Ascent	5.75	3.27	1.76
UB-30aV	Vertical	Basalt	Core	0.44	0.0001	2.86	5000	-	5.79	3.28	1.76
UB-30aV	Vertical	Basalt	Core	0.44	0.0001	2.86	4500	Descent	5.78	3.28	1.76
UB-30aV	Vertical	Basalt	Core	0.44	0.0001	2.86	4000	Descent	5.76	3.27	1.76
UB-30aV	Vertical	Basalt	Core	0.44	0.0001	2.86	3500	Descent	5.74	3.27	1.76
UB-30aV	Vertical	Basalt	Core	0.44	0.0001	2.86	3000	Descent	5.72	3.27	1.75
UB-30aV	Vertical	Basalt	Core	0.44	0.0001	2.86	2500	Descent	5.67	3.25	1.74
UB-30aV	Vertical	Basalt	Core	0.44	0.0001	2.86	2000	Descent	5.61	3.24	1.73
UB-30aV	Vertical	Basalt	Core	0.44	0.0001	2.86	1500	Descent	5.52	3.22	1.71
UB-30aV	Vertical	Basalt	Core	0.44	0.0001	2.86	1000	Descent	5.40	3.18	1.70
UB-33fV	Vertical	Basalt	Core	0.17	-	2.95	1000	Ascent	5.80	3.45	1.68
UB-33fV	Vertical	Basalt	Core	0.17	-	2.95	1500	Ascent	5.96	3.47	1.72
UB-33fV	Vertical	Basalt	Core	0.17	-	2.95	2000	Ascent	6.06	3.48	1.74
UB-33fV	Vertical	Basalt	Core	0.17	-	2.95	2500	Ascent	6.14	3.49	1.76
UB-33fV	Vertical	Basalt	Core	0.17	-	2.95	3000	Ascent	6.21	3.50	1.77
UB-33fV	Vertical	Basalt	Core	0.17	-	2.95	3500	Ascent	6.25	3.51	1.78
UB-33fV	Vertical	Basalt	Core	0.17	-	2.95	4000	Ascent	6.28	3.51	1.79
UB-33fV	Vertical	Basalt	Core	0.17	-	2.95	4500	Ascent	6.31	3.52	1.79
UB-33fV	Vertical	Basalt	Core	0.17	-	2.95	5000	-	6.32	3.52	1.80
UB-33fV	Vertical	Basalt	Core	0.17	-	2.95	4500	Descent	6.32	3.52	1.80
UB-33fV	Vertical	Basalt	Core	0.17	-	2.95	4000	Descent	6.32	3.52	1.80
UB-33fV	Vertical	Basalt	Core	0.17	-	2.95	3500	Descent	6.32	3.52	1.80
UB-33fV	Vertical	Basalt	Core	0.17	-	2.95	3000	Descent	6.30	3.52	1.79

UB-33fV	Vertical	Basalt	Core	0.17	-	2.95	2500	Descent	6.28	3.52	1.78
UB-33fV	Vertical	Basalt	Core	0.17	-	2.95	2000	Descent	6.24	3.52	1.77
UB-33fV	Vertical	Basalt	Core	0.17	-	2.95	1500	Descent	6.17	3.52	1.76
UB-33fV	Vertical	Basalt	Core	0.17	-	2.95	1000	Descent	6.05	3.51	1.72
UB-34aV	Vertical	Basalt	Core	0.12	-	2.93	1000	Ascent	6.19	3.53	1.75
UB-34aV	Vertical	Basalt	Core	0.12	-	2.93	1500	Ascent	6.25	3.54	1.77
UB-34aV	Vertical	Basalt	Core	0.12	-	2.93	2000	Ascent	6.29	3.54	1.78
UB-34aV	Vertical	Basalt	Core	0.12	-	2.93	2500	Ascent	6.32	3.55	1.78
UB-34aV	Vertical	Basalt	Core	0.12	-	2.93	3000	Ascent	6.35	3.55	1.79
UB-34aV	Vertical	Basalt	Core	0.12	-	2.93	3500	Ascent	6.36	3.56	1.79
UB-34aV	Vertical	Basalt	Core	0.12	-	2.93	4000	Ascent	6.38	3.56	1.79
UB-34aV	Vertical	Basalt	Core	0.12	-	2.93	4500	Ascent	6.39	3.56	1.80
UB-34aV	Vertical	Basalt	Core	0.12	-	2.93	5000	-	6.40	3.56	1.80
UB-34aV	Vertical	Basalt	Core	0.12	-	2.93	4500	Descent	6.40	3.56	1.80
UB-34aV	Vertical	Basalt	Core	0.12	-	2.93	4000	Descent	6.40	3.56	1.80
UB-34aV	Vertical	Basalt	Core	0.12	-	2.93	3500	Descent	6.39	3.56	1.79
UB-34aV	Vertical	Basalt	Core	0.12	-	2.93	3000	Descent	6.39	3.56	1.79
UB-34aV	Vertical	Basalt	Core	0.12	-	2.93	2500	Descent	6.37	3.56	1.79
UB-34aV	Vertical	Basalt	Core	0.12	-	2.93	2000	Descent	6.35	3.56	1.79
UB-34aV	Vertical	Basalt	Core	0.12	-	2.93	1500	Descent	6.33	3.56	1.78
UB-34aV	Vertical	Basalt	Core	0.12	-	2.93	1000	Descent	6.30	3.55	1.77

ANEXO I

Título da Dissertação/Tese:

“ASSOCIAÇÃO DE LITOFAZIES, INTERAÇÃO LAVA-SEDIMENTO E CARACTERIZAÇÃO SÍSMICA DO MAGMATISMO SERRA GERAL NA REGIÃO DE UBERLÂNDIA E ARAGUARI (MG)”

Área de Concentração: Geoquímica

Autor: **Natália Famelli Pereira**

Orientador: Prof. Dr. Evandro Fernandes de Lima

Examinadora: Prof. Dr. Carlos Augusto Sommer

Data: 27/10/2020

Conceito: **A**

A tese de doutorado do Sra. Natália Famelli Pereira, intitulada “ASSOCIAÇÃO DE LITOFAZIES, INTERAÇÃO LAVA-SEDIMENTO E CARACTERIZAÇÃO SÍSMICA DO MAGMATISMO SERRA GERAL NA REGIÃO DE UBERLÂNDIA E ARAGUARI (MG)” tem como objetivos principais a caracterização das litofazies para a construção da arquitetura da sucessão vulcânica na região de Araguari (porção norte da Província Ígnea Paraná-Etendeka), assim como sua caracterização petrofísica e sua assinatura sísmica, de forma a avaliar seu potencial como reservatório de fluidos e definir uma assinatura sísmica para sucessões vulcânicas.

A tese está estruturada na forma de artigos científicos, seguindo as normas do PPGGEO desta Universidade, no qual três artigos foram submetidos e correspondem aos capítulos principais do trabalho. A obra é complementada por uma parte introdutória, constituída de Introdução, Contexto Geológico, Estado da Arte, Metodologia e uma parte final, composta pelas Síntese e Conclusões e Referências Bibliográficas.

Em termos formais, a tese está muito bem organizada. Apresenta uma redação correta e todas as figuras e tabelas são pertinentes e editadas com uma resolução adequada. Os capítulos introdutórios são claros e bem desenvolvidos e apresentam todas as informações requeridas formalmente para uma tese de doutorado. Isso permite uma leitura dinâmica e preparatória para os capítulos principais da tese que são os artigos científicos.

A **Introdução** apresenta a temática a ser desenvolvida na tese, bem como justificativas e os objetivos propostos e a organização do trabalho.

No **capítulo II**, a autora apresenta uma síntese sobre Grandes Províncias Ígneas e o contexto geológico da Província Ígnea Paraná-Etendeka e das outras áreas abrangidas pela temática da tese, como a Província do Atlântico Norte e a Bacia Midland Valley na Escócia.

O **Estado da Arte** apresenta uma revisão sobre os depósitos vulcânicos associados à Províncias Magmáticas Continentais. Neste capítulo é feita uma caracterização dos principais produtos relacionados a ambientes subaéreos, subaquosos e os originados a partir da interação lava-sedimento.

No capítulo de **Metodologia** são apresentadas todas as etapas de trabalho e métodos utilizados na execução do projeto. Está muito bem detalhado e ilustra a participação da autora em muitas e diversas atividades e métodos de ponta, bem como o intercâmbio envolvendo vários pesquisadores e instituições nacionais e internacionais.

A parte principal da tese envolve o capítulo 5, onde são apresentados os 3 artigos científicos, submetidos a revistas internacionais indexadas e de excelente qualidade. De uma forma geral, por ser uma tese no formato de 3 artigos, é natural que haja a repetição nos artigos de partes descritivas em termos de contexto geológico e geologia da área. O importante é o que os temas e as metodologias apresentados nos artigos se complementam e fomentam as discussões e considerações finais da tese. Todos os artigos têm muita qualidade e uma abundância de dados que garantem a futura publicação. O primeiro artigo tem um foco mais regional e envolve o estudo detalhado das sucessões vulcânicas e sedimentares da porção nordeste da PIPE apoiado no uso de litofácies e associação de litofácies, e geoquímica. Será uma excelente contribuição para a compreensão das questões paleoambientais relacionadas a deposição dos produtos vulcânicos do Grupo Serra Geral e da Bacia do Paraná, como um todo. Outros dois artigos complementam o capítulo de forma excelente. São artigos metodológicos e didáticos, envolvendo metodologias de ponta e modelagens, aplicadas em áreas geologicamente bem descritas, sendo por isso consideradas excelentes estudos de caso. O artigo 2 foca, principalmente, a origem e a importância da interação lava-sedimento em bacias sedimentares. O artigo 3, "Understanding the petrophysical properties, seismic responses and impacts of the basalt-sediment transition in prospective sedimentary basins" tem também um aspecto metodológico de ponta. Apresenta dados e modelagens muito interessantes, com um viés prospectivo para óleo/gás em bacias sedimentares, onde são abundantes os produtos vulcana-sedimentares e suas interações.

O capítulo de **síntese e conclusões** da tese são diretas e claras e sintetizam as principais conclusões apresentadas nos artigos científicos. Do meu modo de ver são corretas e coerentes com os objetivos propostos e metodologias utilizadas durante o desenvolvimento do trabalho.

As **referências bibliográficas** relacionadas ao corpo da tese estão concentradas no capítulo final e são pertinentes, atualizadas e apresentadas com formatação correta.

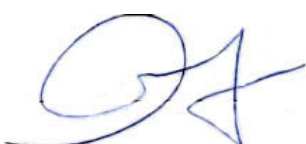
Algumas sugestões e discussões são sugeridas e incorporadas no arquivo pdf da tese.

Em resumo, pode-se constatar através desta obra científica que a Sra. Natália Famelli Pereira atingiu plenamente todos os objetivos propostos para uma tese de doutorado. A abordagem do tema foi muito bem desenvolvida e será uma excelente contribuição científica, possibilitando um avanço na compreensão sobre questões paleoambientais relacionados a PIPE e sobre a origem dos produtos gerados a partir da interação lava-sedimento desta província.

Face a esta análise, sou de parecer amplamente positivo e considero a tese plenamente aprovada com conceito excelente.

Assinatura:

Data: 27/10/2020



Ciente do Orientador:

Ciente do Aluno:

ANEXO I

Título da Dissertação/Tese:

"ASSOCIAÇÃO DE LITOFAZES, INTERAÇÃO LAVA-SEDIMENTO E CARACTERIZAÇÃO SÍSMICA DO MAGMATISMO SERRA GERAL NA REGIÃO DE UBERLÂNDIA E ARAGUARI (MG)"

Área de Concentração: Geoquímica

Autor: Natália Famelli Pereira

Orientador: Prof. Dr. Evandro Fernandes de Lima

Examinador: Dr. João Marinho de Moraes Neto

Data: 27 de outubro de 2020

Conceito: A

PARECER:

A tese sumariza um projeto de pesquisa muito bem estruturado, com base em extensivo trabalho de campo, detalhadas descrições petrográficas e diversos tratamentos analíticos laboratoriais, tendo a autora se mostrado apta para descrever, interpretar e propor inovações para o estudo das seqüências vulcânicas da Bacia do Paraná.

A candidata demonstrou grande capacidade de síntese ao lidar com assunto complexo e relativamente inédito na literatura nacional, incorporando o uso de modernas ferramentas de acesso remoto para descrição e apresentação de dados de campo, assim como demonstrou ser capaz de extrair ganhos de aprendizado e amadurecimento durante seu curto intercâmbio internacional.

A utilização de dados de afloramentos de outras bacias foi essencial para estabelecer analogias e incorporar padrões de ocorrência de rochas extrusivas, assim como serviu de *input* para a modelagem de modelos sintéticos.

A tese está muito bem escrita e com organização adequada. Os capítulos de introdução e revisão regional estão bem focados no tema da pesquisa, trazendo bibliografia atualizada e sem omitir os estudos pioneiros mais relevantes. Há raríssimos erros de ortografia e concordância, o que não compromete o conteúdo do volume final do trabalho.

Os três artigos científicos submetidos também estão adequadamente formatados, com conteúdo bem distribuído e organizados numa ordem que ajuda a compreensão dos capítulos subsequentes. Sabemos como é difícil e trabalhoso produzir um *paper*, e isso comprova a grande capacidade de foco da candidata, o que eu dificilmente teria. Outro ponto a destacar é a redação “limpa” no corpo da tese e o inglês correto e bem revisado nos artigos submetidos.

Considero este trabalho uma grande contribuição ao conhecimento do Magmatismo Serra Geral, que servirá de modelo para aplicação e detalhamento em outras áreas, não apenas em bacias terrestres, mas também nas seqüências vulcânicas amostradas por poços em bacias *offshore*, podendo se configurar numa importante ferramenta para amarração de poços exploratórios profundos e até mesmo para a identificação de fácies reservatórias potencialmente portadoras de hidrocarbonetos.

Assinatura: *João Marinho de Moraes Neto.*

Data: *27/10/2020*

Ciente do Orientador:

Ciente do Aluno:

ANEXO I

Título da Dissertação/Tese:

"ASSOCIAÇÃO DE LITOFAÇIES, INTERAÇÃO LAVA-SEDIMENTO E CARACTERIZAÇÃO SÍSMICA DO MAGMATISMO SERRA GERAL NA REGIÃO DE UBERLÂNDIA E ARAGUARI (MG)"

Área de Concentração: Geoquímica

Autor: **Natália Famelli Pereira**

Orientador: Prof. Dr. Evandro Fernandes de Lima

Examinadora: Prof. Dr. Breno Leitão Waichel

Data: 27/10/2020

Conceito: A

PARECER:

A tese está bem estruturada e contempla todos os tópicos necessários. O artigo 1 versa de maneira geral sobre a geologia da área de estudo, abordando a estratigrafia e divisão de litofácies. Considero que houve um exagero na criação de litofácies, estas podem ser diminuídas, o que facilitaria o entendimento do artigo. O artigo 2 faz uma comparação entre a área de estudo e 2 afloramentos clássicos na NAIP na Escócia, abordando os estudos destes para utilização como análogos para sequências vulcânicas off-shore. Os afloramentos estão bem descritos e a comparação entre eles atingiu o proposto. No entanto, senti falta de um tópico sobre peperitos e exemplos destes gerados no contato de intrusivas rasas e fluxos invasivos, que é o tópico central do artigo. O artigo 3 utiliza dados petrofísicos da área de estudo e um extenso afloramento na NAIP para fazer modelos sísmicos para avaliação do efeitos de rochas vulcânicas em bacias sedimentares. A ideia é interessante e os resultados obtidos satisfatórios. Penso que deveria ser utilizado dados petrofísicos do afloramento onde foi confeccionado o modelo 3D, desta forma teríamos dados mais realísticos, mas como a tese versa sobre a Província Paraná-Etendeka era necessário a utilização de dados desta província.

Assinatura:

Data: 27/10/2020

Ciente do Orientador:

Ciente do Aluno: